Resistance to Diagonal Tension Cracking in Pre-stressed Beams

SJ Kroeze

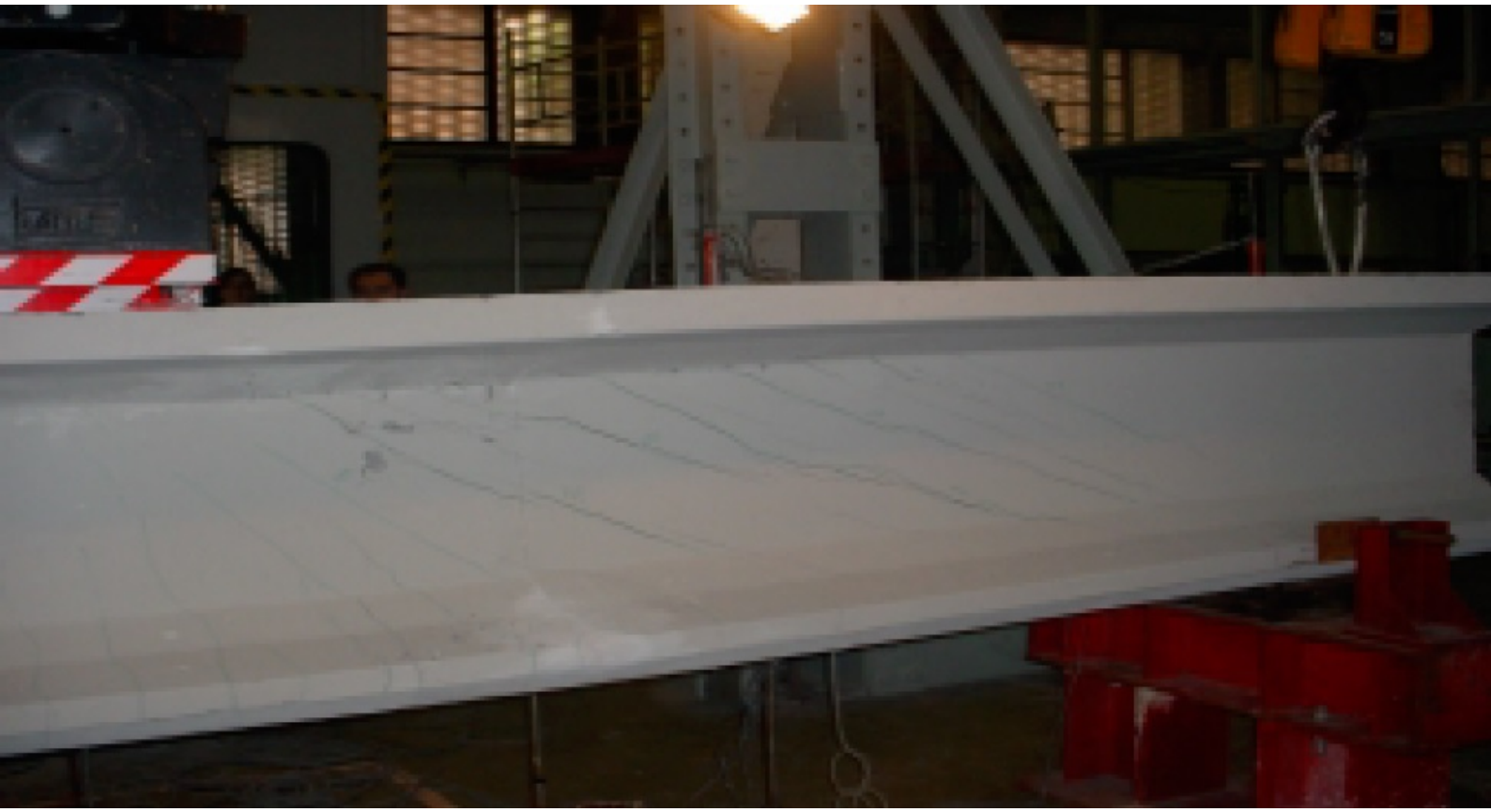

TU Delft

Resistance to Diagonal Tension Cracking in Prestressed Beams

by

SJ Kroeze

to obtain the degree of Master of Science
at the Delft University of Technology,
to be defended publicly on Friday 20 July 2018 at 13:30.

Student number:	4417046	
Project duration:	25 September 2017 – 20 July 2018	
Thesis committee:	Prof. dr. ir. D. A. Hordijk	TU Delft, supervisor
	Dr. ir. C. van der Veen	TU Delft
	Dr. ir. M. A. N. Hendriks	TU Delft
	Ir. M. A. Roosen	TU Delft
	Ir. L. J. M. Houben	TU Delft

An electronic version of this thesis is available at `http://repository.tudelft.nl/`.

TU Delft

Acknowledgements

Before you lies my master thesis, the final part of the master Civil Engineering at Delft University of Technology. After a period with sometimes difficult moments, including a second course, the thesis is finished. The past few years have been of great experience to me, as I expanded deeply my knowledge of several subjects in the Structural Engineering. In this context, I can certainly say that the Master's degree in Civil Engineering is a valuable addition to my Bachelor's degree at Hanze University of Applied Sciences Groningen. Further, I can gladly say that I finally can move back to my own home city Groningen.

I would like to thank the graduation committee. First of all, I would like to thank very much my direct supervisors Ir. M. A. Roosen and Dr. ir. C. van der Veen, for suggesting the research topic for the thesis. Further, I particularly liked philosophizing and discussing the results and follow-up steps. Further, I would like to thank also Prof. dr. ir. D. A. Hordijk and Dr. ir. M. A. N. Hendriks for their input and indispensable role in the coaching.

SJ Kroeze
Delft, 15 July 2018

Abstract

The bridges built in the 50's, 60's and 70's are reaching the end of their originally service life. Many bridges require reassessment. In 2009 the former ministry of "Volkshuisvesting, Ruimtelijke Ordening en Milieubeheer"(Housing, Spatial Planning and the Environment) carried out a study about the state of the bridges, following several incidents including for example the closure of the Sebastiaansbridge in Delft. The main conclusion from the research was that it is hard to prove that the structural safety of existing bridges and viaducts is sufficient. One of the main topics in the reassessment of the bridges was the shear capacity.

The aim of this study is first to investigate the present Eurocode approach to determine the shear tension capacity, secondly if there is a possibility to improve this Eurocode approach or to propose another model. The general main research question is: *What model determines the resistance with respect to the formation of shear tension cracks most accurate?* Practical experiments of the researchers Choulli[8] and Elzanaty[9] already carried out will serve as a basis to evaluate of different models in this thesis. The experiments consist of single-span prestressed I- and T-beams. The study focusses on two topics. In the first topic attention is paid to the comparison of the analytical stress distribution and the numerical stress distribution of the web of the single-span prestressed I- and T-beams. The analytical stress distribution is determined according to the Euler-Bernoulli beam theory, the vertical stress component σ_y is not taken into account. The current Eurocode model is based on the analytical stress distribution. The numerical stress distribution is determined with a linear elastic analysis in the finite element software program DIANA FEA. The following topic is about the choice of a consistent model that predicts the first shear crack in the web and the consideration of a strength criterion. In this study in total there are considered 6 models and 3 strength criterions. Model 1 is the Eurocode model and is considered with the analytical stress distribution. Model 2, the "LE-FEA" model is considered with the numerical stress distribution. Model 3, the "midheight" model around the neutral axis, is considered with the analytical stress distribution. Models 4, 5 and 6 respectively the 45°, the 35°and the 30°model, are considered with the analytical stress distribution. Each model consists of a single or a set points in the web of the prestressed beams to consider. For both the textual explanation and the graphical representation of the models, reference is made to sections 5.1.1 and 5.2.1. There are considered 3 strength criterions: the uniaxial tensile strength f_{ctm}, the biaxial tensile strength according to "Mohr-Coulomb" and the biaxial tensile strength according to "Huber". For each model, the set of points or the single point is divided by a value of a strength criterion. This is defined as "model uncertainty".

From the analysis it is found that the analytical stress distribution does not equal the numerical stress distribution at some parts of the prestressed beams. This is the case in the socalled "disturbed areas". These areas are located near concentrated loads, so around supports and external concentrated loads. After analysis it is found that the analytical stress distribution takes a too high principal tensile stress σ_1 into account, in the "disturbed areas". After analysis of the different stress components σ_x, σ_y and τ_{xy}, it is found that components σ_y and τ_{xy} are the cause of the deviant stress distribution in the "disturbed areas". The test set consists of in total 29 experiments: 12 experiments of Choulli and 17 experiments of Elzanaty. First the results per model, per strength criterion of the Choulli and Elzanaty experiments will be combined, from which the mean and the variation coefficient of the "model uncertainties" are determined.

The conclusion is based on one important feature: the conclusions are based on both the complete set of experiments and on the set of experiments where no flexural cracks have been observed. In case of the set of experiments where no flexural cracks have been observed, also the experiments where the calculated tensile stress in the ultimate fiber exceeds the uniaxial tensile strength f_{ctm} are left out. From the comparison of the analytical and the numerical stress distribution it can be concluded that stress distribution in the socalled "disturbed areas" is overestimated. Based on the complete set of experiments, model 3, the "midheight" around the neutral axis, is preferred. This model offers the best consistency. Concerning the strength criterion: there is a little difference in consistency between the model with uniaxial tensile strength and the model with the biaxial tensile strength(this holds true for both "Mohr-Coulomb" and "Huber"). Based on this it is preferable for practice to reduce the uniaxial tensile strength with 20%. Based on the set without the experiments which showed flexural cracks, it is found that the "means" of the models were lower and that the models are more consistent. Concerning the strength criterion: both the uniaxial tensile strength f_{ctm} and the tensile strength according to "Mohr-Coulomb" are overestimated. For future research it is recommended

to investigate the influence of present flexural cracks on the stress distribution, what will be the influence on the way of predicting diagonal tension cracking. From the results in this study it can be seen that the presence of flexural cracks can have significant influence on the consistency of the models. Further, it is also important for future research to consider distributed loads in addition to concentrated loads, because in practice there will be always present a significant distributed load.

Contents

List of Figures

List of Tables

1 Introduction

The Netherlands is traditionally known as a “water land”, because of the many rivers and other waters. Because of this phenomenon, the Netherlands has many bridges. These bridges are indispensable in the road network, as they connect the highways, the provincial and the local roads. After the second World War a lot of new bridges were built, because of reconstruction and as response to the hugh economic growth. Most major bridges are made of concrete. Of the 1092 bridges, managed by Rijkwaterstaat, 810 are made of concrete[1]. The bridges built in the 50’s, 60’s and 70’s are reaching the end of their originally service life. Many bridges require reassessment. In 2009 the former ministry of “Volkshuisvesting, Ruimtelijke Ordening en Milieubeheer”(Housing, Spatial Planning and the Environment) carried out a study about the state of the bridges, following several incidents including for example the closure of the Sebastiaansbridge in Delft, see figure 1.1. The main conclusion from the research was that the structural safety of existing bridges and viaducts

Figure 1.1: Sebastiaansbridge[2]

is insufficient. Another important aspects that need to be taken into account nowadays are the enormous increase in traffic in both number and load and of course the changing design standards. Bridges built in the 60s and 70s were designed according to the old Dutch standards: the GBV, RVB and the VB standards. Two important changes in the Eurocode compared to the old code is that the Eurocode prescribes a heavier live load model and the Eurocode prescribes a smaller shear capacity for shear stresses in the cross sections. All this together makes it of great importance to reassess existing bridges. Nowadays new bridges are designed in accordance with the Eurocode. For existing structures adapted rules are available, the Eurocode and the extra standards NEN8700 and NEN8701. In case for bridges, a guideline for the assessment is available. This guideline is called the “Richtlijnen Beoordeling Kunstwerken”(Guideline Assessment Bridges). The “Richtlijnen Beoordeling Kunstwerken” is intended to be used in addition to the Eurocode. In addition to the safety aspect there is an economical aspect. Economically, both directly and indirectly, it is a valuable operation to replace all bridges. Investigations also focus on possible so-called “hidden capacities”, in order to see whether rejection of a structure can be prevented. One of the main topics in the reassessment is the shear capacity.

1.1. Background information

In prestressed and/or reinforced concrete beams there are several possibilities of failure. The most commonly known mode of failure is flexural failure. In case the flexural failure cracks will envelop perpendicular to the beam axis, in other words perpendicular to the direction of the tensile stress. Before failure occurs the flexural cracks will develop into the compression zone, because of the yielding of the reinforcement. Failure in the end is caused by the crushing of the compression zone, see figure 1.4a. Other examples of failure mechanisms are the anchorage failure, the flexural shear failure, the shear tension failure, the web crushing failure and failure of the compression struts in the web.

In case of flexural shear failure the initiated flexural cracks will develop into inclined cracks in the web of the beam. These inclined cracks in the web will develop into the compression zone of the beam, failure again will be caused by crushing of the compression zone, see figure 1.4b.

In case of shear tension failure an inclined crack or cracks start developing in the web. These inclined cracks will have an angle of 30 to 45 degrees to the beam axis, this cracks can develop rapidly to the top and the bottom along the main reinforcement. In case there is no shear reinforcement cracks in the web will immediately lead to failure, see figure 1.2.

In case of failure of the compression struts the struts of the socalled “truss analogy” in slender beams will fail in compression. This type of failure often occurs in case of concentrated external forces close to the support, see figure 1.4c.

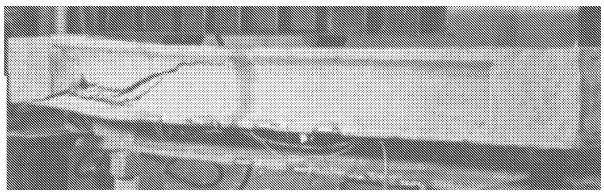

Figure 1.2: Shear Tension failure[4]

Another possible mechanism is crushing of the web. Again inclined crack(s) are initiated in the web, this will cause some redistribution of stresses in the web. After increasing of the external concentrated load, the web will fail in compression, see figure 1.3. In figure 1.4 a beam with the possible locations of the modes of failure. There exist different codes how to treat with flexural shear and shear tension. The Eurocode

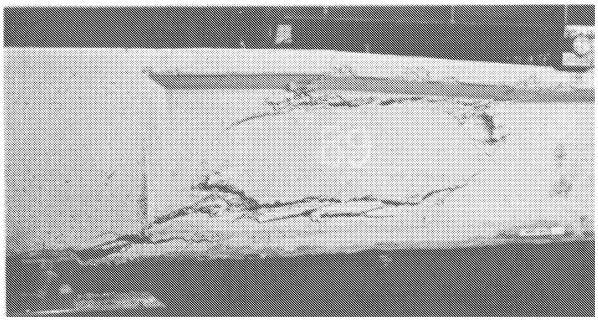

Figure 1.3: Web crushing[4]

indicates that the theory about shear tension is only applicable in case there are no cracks caused by flexure in the assessed cross-section, in this case formula 1.1 is applicable, this is formula 6.4 in EC2[17].

$$V_{Rd,c} = \frac{I \cdot b_w}{S} \sqrt{(f_{ctd})^2 + \alpha_l \sigma_{cp} f_{ctd}} \tag{1.1}$$

On the other hand the theory about flexural shear is applicable in case there is a combination of cracks caused by flexure and cracks in the web caused by shear. So this means according to the Eurocode that the theory about shear tension is not applicable in cross-sections, in case of cracks caused by flexure. The parts of a beam which show flexural cracks should be assessed to flexural shear, and the parts which show no flexural cracks should be assessed to shear tension, see figure 1.5. In case of flexural shear formulas 1.2 and 1.3 are

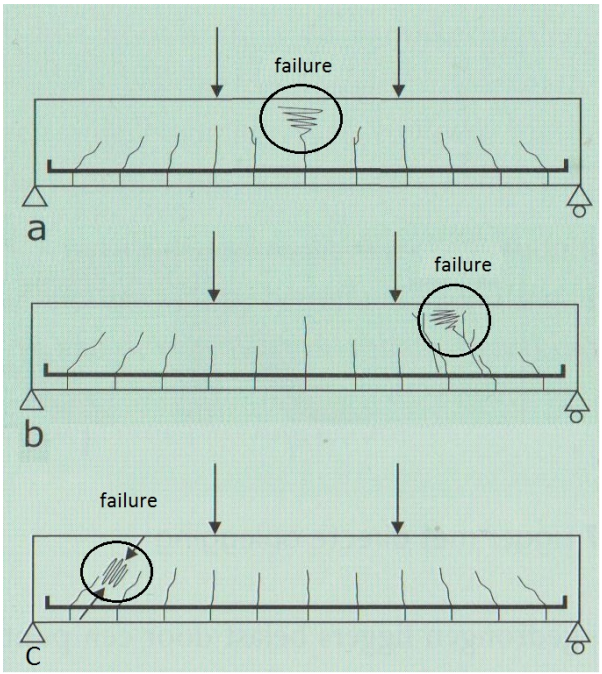

Figure 1.4: Failure modes: a)flexural failure b)flexural shear failure c)failure compression struts[7]

applicable, these are formulas 6.2a and 6.2b in EC2[17].

$$V_{Rd,c} = [C_{Rd,c}k(100\rho f_{ck})^{\frac{1}{3}} + k_1\sigma_{cp}]b_w d \tag{1.2}$$

With a minimum of

$$V_{Rd,c} = (v_{min} + k_1\sigma_{cp})b_w d \tag{1.3}$$

The theory about shear tension capacity as described in the Eurocode has a linear elastic approach. As described before, the Eurocode prescribes that the theory about shear tension(thus formula 1.1) can be used for parts that show no flexural cracks, while on the same time other parts could show flexural cracks. The influence of the parts that show flexural cracks on the parts that do not show these cracks is not described. In order to get more insight into the behavior of cracked concrete, a non-linear elastic analyses of experiments should be made.

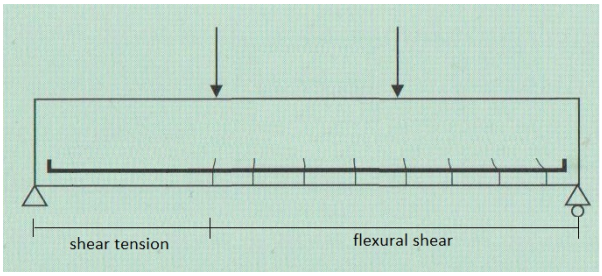

Figure 1.5: Zone of shear tension and flexural shear

1.2. Aim of study

As mentioned before the Eurocode is significantly changed in the way it treats shear, in comparison to the old Dutch codes. The Eurocode provides lower shear capacity than the former Dutch standards. Specific topic in this research is the shear tension capacity. The general main research question is;

What model determines the resistance with respect to the formation of shear tension cracks most accurate?

The aim is to investigate the current Eurocode approach of the shear tension capacity and whether there is a possibility to improve this Eurocode approach or to propose another model. According to calculations following the Eurocode procedure the Shear Tension capacity is often insufficient. In this context, consideration should be given to the possibility that capacity, unnecessarily, will not be used. The investigation may be important to see whether bridges are rightly or wrongly rejected. Practical experiments already carried out will serve as a basis for the models in this thesis. These experiments consist of prestressed single-span I- and T-beams. In this research both the analytical and numerical stress distribution of the practical experiments are determined, in this context all the geometrical conditions like as they were in the practical experiments are adopted(external load, supports, etc.). Only in this way it is possible to make comparisons between the experiments and the analytical and stress distributions. Important to note is that the magnitude of the external load is adopted at which the first Shear crack in the web appeared. It is assumed that the concrete behaves linearly elastically to this first Shear crack. The research focuses on two topics.

1.2.1. Accuracy of the analytical and numerical stress distribution

In this step there will be determined both a 2D analytical and a 2D numerical stress distribution of the web of the single-span prestressed I- and T-beams. The analytical stress distribution will be determined according to the Euler-Bernoulli beam theory. The different stress parameters will be calculated according to the formulas in section 2.4, formula 2.9(σ_x) and formula 2.11(τ_{xy}). The formula 2.7 will be used to determine the principal stresses σ_1 and σ_2(without accouting for σ_y). The current Eurocode model is based on the analytical stress distribution.

The numerical stress distribution is determined with a linear elastic analysis of a numerical model in the finite element software program DIANA FEA. This numerical stress distribution includes the vertical stress component σ_y. The purpose of this step is to compare the analytical and the numerical stress distribution. This will be done by analyzing the stress diagrams of the different stress components. Further by analyzing the analytical stress distribution it can be seen what the impact is of the σ_y and how this stress can be initiated. Another aspect is the phenomenon of the disturbed area caused by initiating of a concentrated load, so around an external concentrated load and the supports.

1.2.2. Suitability of the uniaxial tensile strength and accuracy of models

Two subjects are considered in this topic. Attention is paid to an accurate model which predicts the first Shear crack in the web. Furthermore, the strength criterion, to which the model is tested, will be considered. Based on specific reasons and choices, which will be explainded in chapter 5, points between de support and the external load are considered in the developed analytical and numerical models. In this points the stress parameter σ_1, which represents the principal tensile stress, is of interest. A model can consist of a collection of points or a single point. Take for example figure 1.6, in which the considered part of the Elzanaty beams is shown. This is on the interval of 0 mm to 380 + a mm, from start of the beam. The values on the right side show the height relative to the neutral axis. The figure shows the considered points of model 1. Concerning the strength criterion special attention will be paid to the phenomenon of the biaxial stress state. The influence of the principal stresses(σ_1 and σ_2) on the tensile strength of the concrete is considered. In the past, various studies have been conducted to the biaxial behavior of concrete, for example Kupfer, 1969. These studies showed that various factors influence biaxial behavior, like for example the concrete strength class. Given the fact that the external load is adopted at which the first Shear crack appeared in the web, verification will be given at this point between the experiments and the proposed models in this step. One of the considered models is the Eurocode model. The purpose of this step is to propose an accurate and consistent model in combination with an strength criterion.

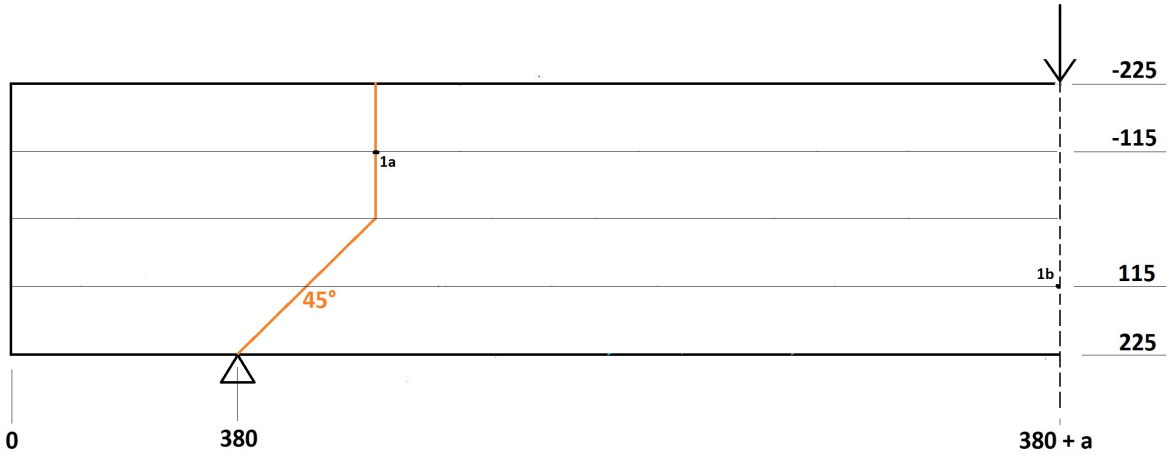

Figure 1.6: The considered points of model 1 of the Elzanaty beams, distance and height in mm

1.3. Outline and methodology of study

In this section the outline and the methodology of the study will be explained. In chapter 2 a literature study is included. In this chapter varying subjects will be discussed. In chapter 3 the used experiments will be discussed. In this research the practical experiments of Choulli and Elzanaty are used. In this chapter first the research goals of the Choulli and Elzanaty studies are explained. Then all the set-up conditions are explained, like concrete and reinforcement properties, test procedures, etc. The Choulli experiments consists of 12 indepent experiments and the Elzanaty experiments consists of 17 experiments, so totally there are available 29 experiments. In chapter 4 the first topic is discussed, as described in section 1.2 a comparison of the analytical and numerical stress distributions of the web of the prestressed beams will be made. For all 29 experiments there will be made both a 2D analytical and a 2D numerical model. The results of these models are processed in an excel sheet, it consists of the stress distributions in the web and the ultimate fiber of a beam. The chapter is divided in the consideration of the Choulli experiments and the Elzanaty experiments. Both the Choulli and the Elzanaty section starts with a pre-analysis which forms an outline for this section, further general things will be explained here. Then for both Choulli and Elzanaty there is made an analytical and a numerical analysis of one experiment. To compare the stress distribution of the analytical model with the numerical model, a verification has to be done between the models. For the verification the nondisturbed parts of the stress distribution are considered. In chapter 5 the second topic is discussed, as described in section 1.2. The suggested models consist of a collection of points or a single point. In this study there are considered 6 models and 3 strength criterions. The 6 models consist of 5 analytical models, of which one is the Eurocode model, and 1 numerical model. In order to say something about the models and strength criterions, the following procedure is taken. For each model, the set of points or the single point is divided by a value of a strength criterion. This is defined as “model uncertainty”. In case of a model consists of a collection of points, the point with the highest “model uncertainty” will be the representative point of that particular model. In case a model consists of one single point, of course this point will be the representative point. With the consideration of three strength criterions this means that each suggested model will have 3 “model uncertainty” factors. With the consideration of 29 experiments this means that per model, per strength criterion there are 29 independent values of the “model uncertainty”. It is possible to determine per model, per strength criterion a mean “model uncertainty” and a coefficient of variation. This coefficient of variation says something about the consistency of the model. The meaning of the “model uncertainty” can be explained as follows. In case of a “model uncertainty” of > 1.0, the considered strength criterion is underestimated and is conservative. In case of a “model uncertainty” of < 1.0, the considered strength criterion is overestimated, these values can be seen as dangerous values. In chapter 6 the conclusions and recommendations regarding future research will be discussed.

2

Literature study

In order to get a better understanding about the phenomenon shear tension a literature study is performed. In this study the mechanical background of shear tension will be explained. Further, attention will be paid to the general European code of practice: the Eurocode. The way the Eurocode deals with shear tension will be explained. From the mechanical background an addition can be given to the prescribed formulas in the theory as described in de Eurocode. Also there is research done to the biaxial tensile strength of concrete, special attention is paid to the influence of a combination of a tensile stress and a compressive stress.

2.1. Stresses

In statics, a distinction is made between a number of important principles: external loads, support reactions, equilibrium equations and the internal forces. The external loads can be quantified as surface forces and body forces. Direct contact between bodies will generate the surface forces, in all cases these surface forces will be distributed over the contact surface. In case this contact surface is rather small, the surface force can be idealized as one concentrated force. This concentrated force will act as a point load on the body. In case the contact surface is a strip-shaped surface, the surface force can be seen as a linear distributed force. A body force is generated by virtue of the position of a body within a force field such as a gravitational, electric, or magnetic field and is independent of contact with any other body. So there is no direct physical contact between the two bodies. The support reactions in the supports of a body are called the reactions. In general if a support blocks a translation or rotation in e certain direction, this will generate a force or a torque in that direction. The equilibrium equations describe the equilibrium of a body. The equilibrium of a body requires an equilibrium in both force and torque. The equilibrium equations can be expressed as two vector equations, see formula 2.1. If there is chosen for an x-y-z axial system, the two vector equations can be expressed as six scalar equations.

$$\begin{aligned} \Sigma \mathbf{F} &= \mathbf{0} \\ \Sigma \mathbf{M} &= \mathbf{0} \end{aligned} \tag{2.1}$$

One of the main targets of statics is to determine the resulting internal forces in a body. Take for example the body sketched in figure 2.1. There are acting four forces on de body, which is in equilibrium. In order to determine the internal forces on a certain surface, it's necessary to make an imaginary cut. The internal forces acting on this imaginary cut represent the part of the body that is taken off. Now it is possible to relate the external loads to the resulting internal forces, through the equilibrium equations. The next step it to decompose these internal forces in components perpendicular and in plane to/of the surface, in other words the normal and shear force. The third component is the internal bending moment caused by the external forces. The fourth component is the torsion moment. If the body is exposed to forces acting in one plane, the fourth component can be left out.
If the force is related to the surface on which it is acting, it is possible to speak about a stress. Take for example again an imaginary cut of a body, see figure 2.2. The force ΔF_z acting on the local surface Δ A represents the normal force, the forces Δ Fx and Δ Fy represent the shear forces. The definition of, for example, the normal stress is represented in formula 2.2 In the same way expressions can be derived of the shear stresses. If we consider a small cube, which is taken out of the body, a common three dimensional stress state can be

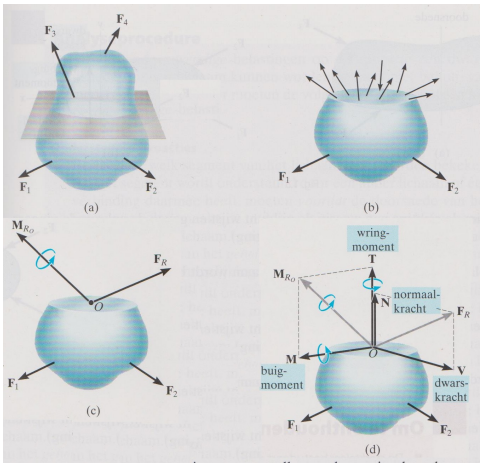

Figure 2.1: Forces on free body[15]

composed, see figure 2.3. On each side of the cube there will act three components, a normal stress and two components of the shear stress.

$$\sigma_z = \frac{\Delta F_z}{\Delta A} \tag{2.2}$$

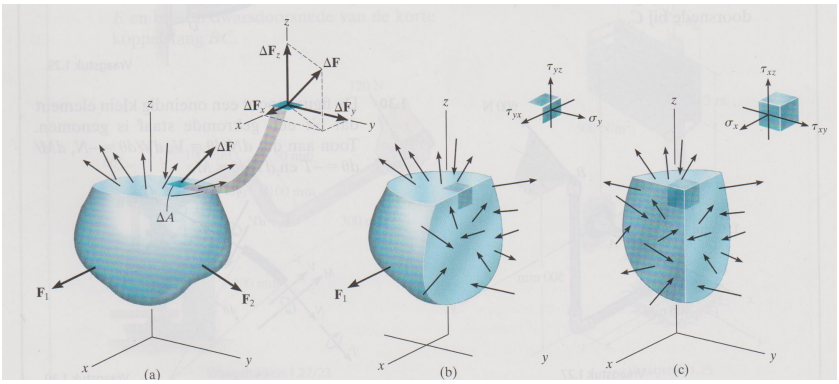

Figure 2.2: Relation forces and stresses[15]

In practice a two dimensional stress state is often considered, a plane stress state, see figure 2.4.
If the element in figure 2.4 gets another orientation, the three stress components will transform, see figure 2.5. The expressions of the new components can be derived as follows(see figure 2.6);

$$\begin{aligned}\Sigma F_{x'} = 0 : \sigma_{x'}\Delta A &- (\tau_{xy}\Delta A sin(\theta))cos(\theta)\\ &- (\sigma_y \Delta A sin(\theta))sin(\theta)\\ &- (\tau_{xy}\Delta A cos(\theta))sin(\theta)\\ &- (\sigma_x \Delta A cos(\theta))cos(\theta) = 0\end{aligned} \tag{2.3}$$

$$\begin{aligned}\Sigma F_{y'} = 0 : \tau_{x'y'}\Delta A &+ (\tau_{xy}\Delta A sin(\theta))sin(\theta)\\ &- (\sigma_y \Delta A sin(\theta))cos(\theta)\\ &- (\tau_{xy}\Delta A cos(\theta))cos(\theta)\\ &+ (\sigma_x \Delta A cos(\theta))sin(\theta) = 0\end{aligned} \tag{2.4}$$

After simplifying this will result in formulas 2.5 and 2.6

$$\sigma_{x'} = \frac{\sigma_x + \sigma_y}{2} + \frac{\sigma_x - \sigma_y}{2} cos(2\theta) + \tau_{xy} sin(2\theta) \tag{2.5}$$

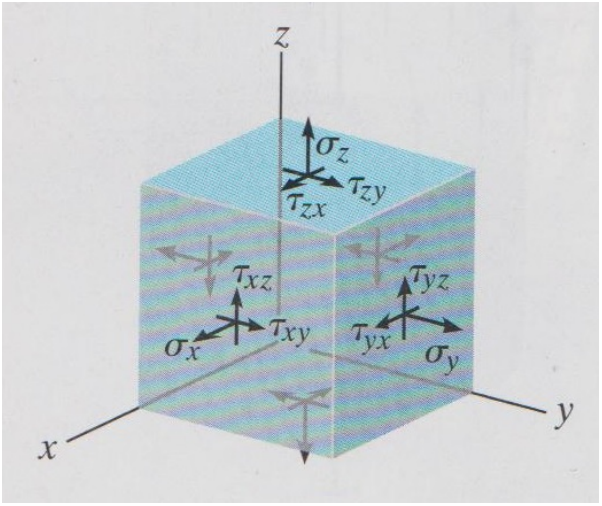

Figure 2.3: Three dimensional stress state[15]

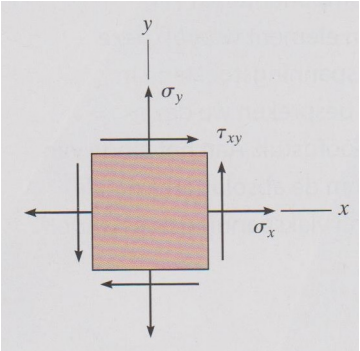

Figure 2.4: Plane stress state[15]

$$\tau_{x'y'} = -\frac{\sigma_x - \sigma_y}{2} sin(2\theta) + \tau_{xy} cos(2\theta) \tag{2.6}$$

In practice it is important to know the angle of inclination in which the normal stress has a maximum and a minimum. In this orientation it appears that the shear stresses equal zero. In order to determine these maximum and minimal stresses formula 2.5 should be differentiated to theta;

$$\frac{d\sigma_{x'}}{d\theta} = -\frac{\sigma_x - \sigma_y}{2}(2sin(2\theta)) + 2\tau_{xy} cos(2\theta) = 0 \tag{2.7}$$

With the help of goniometry this will result in the principal stresses σ_1 and σ_2, because it is possible to express the tangent component in a sine and a cosine component, see figure 2.7 the circle of Mohr. In a similar way it is possible to determine the orientation of the element which will result in a maximum shear stress. This will result in formula 2.8

$$\sigma_{1,2} = \frac{\sigma_x + \sigma_y}{2} \pm \sqrt{(\frac{\sigma_x - \sigma_y}{2})^2 + \tau_{xy}^2} \tag{2.8}$$

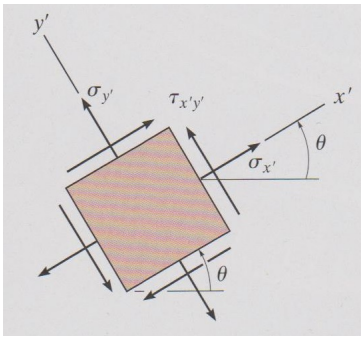

Figure 2.5: Stress transformation[15]

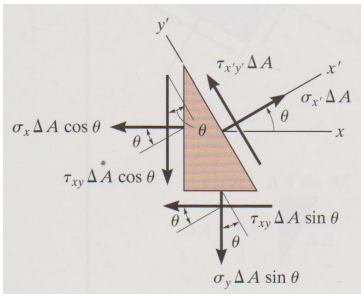

Figure 2.6: Stress equilibrium[15]

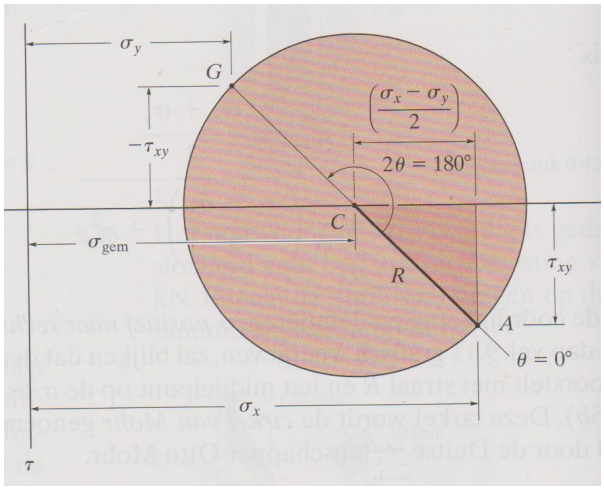

Figure 2.7: Circle of Mohr[15]

2.2. Principal stresses

With the expressions for the principal stresses it is possible to determine the maximum(=σ_1) and minimum(=σ_2) principal stress in construction elements at random locations. Take for example the prestressed slender beam, with straight prestressed cables, in figure 2.8. The σ_x in this beam represents a combination of the horizontal stresses caused by the prestress and the external force F_1. The σ_y represents the local vertical stress caused by external force F_1. The τ_{xy} represents the shear stress caused by the external force F_1. Based on the location something can be said about the composition of the principal stresses. At location 1,in the ultimate fiber, the shear stress and vertical stress equals zero, so the principal stresses are composed out of σ_x, so σ_1=σ_x At location 2, the transition point of flange and web, the shear stress does not equal zero. Also there is a horizontal stress present, consisting of a combination of horizontal stresses caused by the prestress and the external force F_1, so the principal stresses are composed out of σ_x and τ_{xy}. In practice the horizontal stress at location 1 would be the dominant factor if it comes to flexural cracks(σ_1=σ_x=$f_{ctm,fl}$).

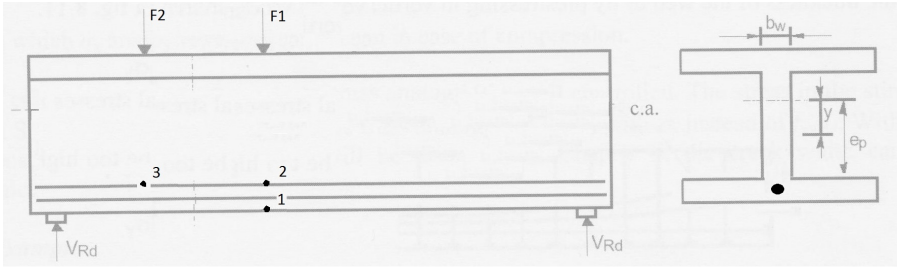

Figure 2.8: Prestressed slender beam

Now the external force F_1 becomes F_2 as presented in figure 2.8, the prestress and the magnitude of the external force stay the same. In a mechanical point of view the transformation of the external force F_1 into F_2 will cause an increase of the shear stress, because the shear force will increase, at location 3. At the same time the component of the horizontal stress caused by the external force F_2 will be lower, at location 3 and in the ultimate fiber straight down from location 3. This means that the total horizontal stress caused by the prestress and the external force F_1 will be lower as well. If the force F_2 would increase, the total horizontal stress would increase at location 3 and in the ultimate fiber straight down from location 3. Also the shear stress would increase at location 3. Theoretically compared to the situation of the original position of force F_1, the shear stress can be a dominant factor in causing cracks at location 3(and/or in other locations around location 3 in the web). So a crack could start in the web(σ_1=f_{ctm}).

2.3. Sensitivity components principal stresses

Another thing to realize is the impact of a changing parameter of formula 2.8 on the principal stresses. In figure 2.9 there are four circles of Mohr. The blue circle represents the standard circle in this case, formed out of the stresses σ_x, σ_y(=0) and τ_{xy}. The other colored circles represent circles in which one of the stresses σ_x, σ_y and τ_{xy} is changed. There are three lines drawn under the circles which represent the difference of principal stress σ_1 relative to the principal stress σ_1 of the standard circle. As mentioned the blue circle represents the circle which is formed out of the stresses σ_x, σ_y and τ_{xy}. The purple circle is formed by multiplying σ_x by a half, the other parameters remain the same, so the circle is formed out of the stresses 0,5σ_x, σ_y and τ_{xy}. The difference between $\sigma_{1;blue}$ and $\sigma_{1;purple}$ is represented as the purple line. The orange circle is formed by multiplying τ_{xy} by two, the other parameters remain the same, so the circle is formed out of the stresses σ_x, σ_y and 2τ_{xy}. The difference between $\sigma_{1;blue}$ and $\sigma_{1;orange}$ is represented as the orange line. The red circle is formed by adding a significant σ_y, the other parameters remain the same, so the circle is formed out of the stresses σ_x, σ_y and τ_{xy}. The difference between $\sigma_{1;blue}$ and $\sigma_{1;red}$ is represented as the red line.
As it can be seen a significant difference in σ_x does not give a big difference in σ_1 compared to difference that is caused by a significant change of τ_{xy}. Also adding a stress σ_y results significant difference. It comes down to the fact that in a situation in which there is a significant negative σ_x, like in a prestressed concrete beam, a change of τ_{xy}(shear stress) and σ_y(vertical stress) can result a significant change of the principal stress σ_1 compared to the change that is caused by a change of σ_x(horizontal stress). Certainly when paying attention to the generally low tensile strength of concrete, this can be important.

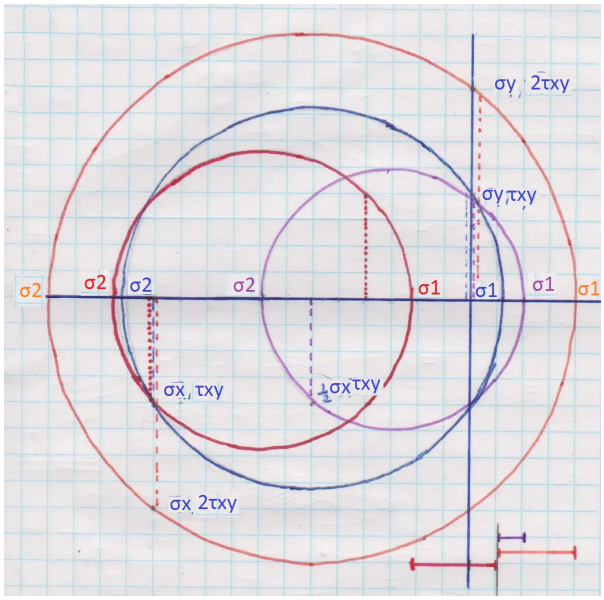

Figure 2.9: Circles of Mohr

2.4. Shear Tension: Mohr and Euler-Bernoulli

The stresses/parameters in formula 2.8 σ_x and τ_{xy} can be determined/approached in the following way. As mentioned before the σ_x is a combination of horizontal stresses caused by the prestress and the external force(s). Once the axial force, the shear force and the moment in a cross section is known, σ_x and τ_{xy} can be determined. The horizontal stress caused by the moment(formula 2.9)[15];

$$\sigma_x = \frac{MyE(y)}{\int y^2 E(y) dA} \tag{2.9}$$

where:

σ_x = the horizontal stress
M = the internally bending moment
y = a certain distance from the neutral axis
E = the modulus of elasticity

The horizontal stress caused by the axial force(formula 2.10);

$$\sigma_{x,y} = \frac{F}{A} \tag{2.10}$$

where:

$\sigma_{x,y}$ = the horizontal stress at a certain height y in de the cross-section
F = the force acting on the surface of the cross-section
A = the cross-section

The shear stress caused by the shear force(formula 2.11)[15];

$$\tau_{xy} = \frac{V \int yE(y) dA}{t \int y^2 E(y) dA} \tag{2.11}$$

where:

τ_{xy} = the shear stress
V = the internally shear force
y = a certain distance from the neutral axis
E = the modulus of elasticity
t = the width of the surface of the cross-section

The modulus of elasticity is processed in these formulas, in case a cross section consists of for example two materials. The stress σ_y, the vertical stress, is a result of the initiation of the external force and support reactions in the beam. There is no unambiguous way of determining the σ_y. As described in section 2.2 , if an external force is relative close to the support of a prestressed beam, the shear stress can be a dominant factor for cracks. The formula for the determination of the principal stresses can be used to determine the allowable shear stress. After substitution and rewriting of formula 2.11 in 2.8, it will result in formula 2.12. Now it is possible to determine the allowable shear force.

$$V = \frac{bI}{S}\sqrt{(f_{ctm} - \frac{\sigma_x + \sigma_y}{2})^2 - (\frac{\sigma_x - \sigma_y}{2})^2} \tag{2.12}$$

where:

τ_{xy} = the shear stress
V = the internally shear force
I = the moment of inertia
S = the static moment
b = the width of the surface of the cross-section
f_{ctm} = the mean concrete tensile strength
σ_x = the horizontal stress
σ_y = the vertical stress

Formula 2.12 could be simplified by leaving out σ_y, see formula 2.13.

$$V = \frac{bI}{S}\sqrt{(f_{ctm} - \frac{\sigma_x}{2})^2 - (\frac{\sigma_x}{2})^2} \tag{2.13}$$

where:

τ_{xy} = the shear stress
V = the internally shear force
I = the moment of inertia
S = the static moment
b = the width of the surface of the cross-section
f_{ctm} = the mean concrete tensile strength
σ_x = the horizontal stress

After rewriting formula 2.13, it looks familiar with the formula for shear tension as described in de Eurocode(formula 2.14). In this case σ_x=-$\sigma_{prestress}$ and in design calculations f_{ctm}=f_{ctd}, in experimental analyses the mean value of the tensile strength f_{ctm} will be used.

$$V = \frac{bI}{S}\sqrt{f_{ctm}^2 - \sigma_x f_{ctm}} \tag{2.14}$$

where:

τ_{xy} = the shear stress
V = the internally shear force
I = the moment of inertia
S = the static moment
b = the width of the surface of the cross-section
f_{ctm} = the mean concrete tensile strength
σ_x = the horizontal stress

2.5. Code of practice: Eurocode

This paragraph will explain how the Eurocode treats shear. Concerning shear there can be distinguished two types of structural prestressed elements: elements with and without shear reinforcement. First the elements without shear reinforcement will be discussed.

2.5.1. Elements without shear reinforcement

In figure 2.10 there is shown a cracked prestressed beam without shear reinforcement. Further there is included a stress diagram which indicates stress situation in the bottom part of the beam. In this beam there can be distinguished two areas, area 1 and 2.

Area 1

Area 1 shows no flexural cracks, however shear tension cracks may develop. In this area can occur shear tension failure(dutch: afschuiftrekbreuk). Also failure of the compression struts is possible(dutch: afschuifdrukbreuk). As indicated before in this area there is present a relative high shear force relative to the moment. The

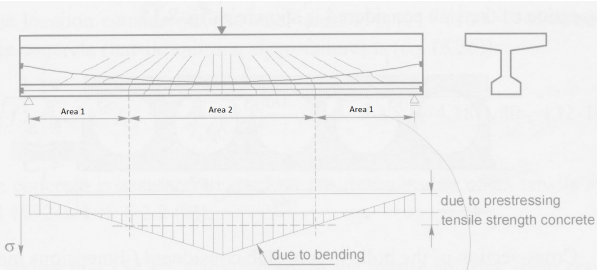

Figure 2.10: Crack pattern in prestressed beam[24]

cracks start developing in the web at the position where the principal tensile stress in the concrete reaches the concrete tensile strength. As mentioned before this principal tensile stress is composed of the horizontal stress caused by the external force and the prestress and the shear stress caused by the external force(in case the prestress cables are straight). In elements without shear reinforcement these cracks will lead to failure. This type of failure is called the tensile splitting shear failure. The Eurocode prescribes that areas which show no flexural cracks, the resistance to shear should be limited to the axial tensile strength of the concrete. The resistance to shear can be calculated according equation 6.4 of the Eurocode, see formula 2.14. The derivation of this formula is explained in section 2.4. There are some conditions set for this formula. First of all is that the tensile stress in the outer fiber should always be lower than $\frac{f_{ctk;0,05}}{\gamma}$.

Another thing is that the calculation of the shear force resistance according to equation formula 2.14 is not required for cross-sections which are closer to the support than the point that forms the point of intersection of the elastic centroidal axis and a line drawn at an angle of 45 degrees from the inner edge of the support, because in simple beams the combination of stresses will result in low principal stresses. This is caused by the fact that the moment caused by the external load equals almost zero near the support. The moment caused by curved prestress cables will also be low. In case of straight prestress cables theoretically this will cause a moment, this moment will cause a tensile stress in the upper part of the beam. As mentioned the moment caused by the the external load equals almost zero, so if the horizontal stress caused by the axial part of the prestress is not too high, then a reasonable tensile stress can occur. In practise the prestress is not fully initiated, so practically the impact of the prestress wil be low near the support.

Yet another thing for cross-sections in which the width varies over the height, the maximum principal stress may occur at a different axis than the center of gravity. In that case, the minimum value of the shear strength must be found by calculating $V_{Rd,c}$ on different axes in the cross-section.

Finally there is the situation that an external force is located close to the support, within the range: 0,5d < a_v < 2d of the edge of the support. For elements with external forces at the top within this range, the contribution of these forces to V_{Ed} may be multiplied by $\beta = \frac{a}{2d}$. This factor can only be used in combination with formula 2.15, it is not allowed to use it in combination with formula 2.14. This is only valid when the main reinforcement is fully anchored near the support. For a < 0,5d the value of $\frac{0,5d}{2d}$ should be used. Important to note is that the V_{Ed} should always meet the requirement Ved < 0,5 $b_w d \nu f_{cd}$, in which ν is the strength reduction factor for concrete. $\nu = 0,6(1 - \frac{f_{ck}}{250})$. This maximum V_{Ed} in order to prevent failure of the compression struts. It turns out to be that a part of the external force will go straight to the support, hence the factor β. Different tests showed that the capacity is not just calculated by applying the strut and tie model, because it takes into account the concrete strength(whether or not reduced) and the geometry. In this case the slenderness ratio a/d and the size effect(factor k) have a strong influence as well.

Area 2

Area 2 shows flexural cracks, in contrast to area 1 there is a larger moment present. In this area can occur flexural and flexural shear failure(dutch: afschuifbuigbreuk). The design value of the shear resistance, in an area which is cracked in flexure, according to the Eurocode can be calculated with formula 2.15. The background of this formula is partly based on many tests. There will be started with the formula present in 2.15, this is formula 6.2a in EC2[17].

$$V_{Rd,c} = (C_{Rd,c}k(100\rho_1 f_{ck})^{\frac{1}{3}} + k_1\sigma_{cp})b_w d \tag{2.15}$$

where:

$V_{Rd,c}$ = resistance value of the shear force
k = $1 + sqrt\frac{200}{d} < 2{,}0$ with d in mm
ρ_1 = $\frac{A_{sl}}{b_w d}$ <0,02
f_{ck} = characteristic cylindrical compressive strength
σ_{cp} = $\frac{N_{Ed}}{A_c}$
b_w = the smallest width of the cross-section
A_{sl} = the surface of the cross-section of the tensile reinforcement
N_{Ed} = the normal force in the cross-section caused by for example the prestress

This equation takes appropriate account of the most important factors like concrete strength, longitudinal reinforcement ratio, cross-sectional height and the prestress. The factor $C_{Rd,c}$ was determined after the analysis of shear tests. For $C_{Rd,c}$ can be taken $C_{Rd,c} = \frac{0{,}18}{\gamma}$. A disadvantage of formula 2.15 is that the shear capacity goes to zero when the longitudinal reinforcement ratio ρ_1 goes to zero. This would mean that in many slabs shear reinforcement would be required where it is actually not necessary. Therefore a minimum value for the shear resistance is derived, additional to formula 2.15. This is done in the following way. The most unfavorable position of an external force near to a support is at a distance a = 2,5d. For a < 2,5d the shear capacity increases as a result of arch action.

Many shear tests have been carried out with an external force in this position. Start with formula 2.16;

$$V_u = 0{,}15k(100\rho_1 f_{cm})^{\frac{1}{3}} b_w d \tag{2.16}$$

The corresponding bending moment is[24];

$$M_u = V_u 2{,}5d = 0{,}375k(100\rho_1 f_{cm})^{\frac{1}{3}} b_w d^2 \tag{2.17}$$

The yielding moment can be formulated by;

$$M_{uf} = 0{,}9d(\rho_1 bd)f_{yk} \tag{2.18}$$

Equating 2.17 and 2.18, and taking f_{yk} = 500 MPa gives for the value ρ_1 the expression(formula 2.19);

$$\rho_1 = 0{,}00024k^{\frac{3}{2}} f_{cm}^{\frac{1}{2}} (\frac{b_w}{b})^{\frac{3}{2}} \tag{2.19}$$

Substituting 2.19 in formula 2.16 gives formula 2.21.

$$\frac{V_u}{b_w d} = 0{,}035k^{\frac{3}{2}} f_{cm}^{\frac{1}{2}} (\frac{b_w}{b})^{\frac{1}{2}} \tag{2.20}$$

Replacing fcm by fck and taking bw/b = 1 for solid slabs the expression becomes;

$$\nu_{min} = 0{,}035k^{\frac{3}{2}} f_{ck}^{\frac{1}{2}} \tag{2.21}$$

Now the factor k_1 has to be determined, which determines the amount of prestress that can be added. The development of tensile cracks in an element is postponed by applying prestress. In the case shown in figure 2.11, the tensile zone is prestressed, which introduces an additional compressive stress in the outer tensile fibre.

$$\sigma_{cb} = -\frac{P_m}{A_c} - \frac{P_m e_p}{W_{cb}} \tag{2.22}$$

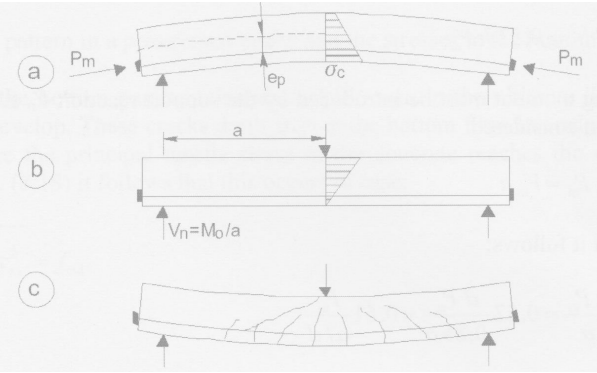

Figure 2.11: The additional compressive stress caused by the prestress[24]

$$M_0 = \sigma_{cb} W_{cb} = P_m(\frac{1}{6}h + e_p) \tag{2.23}$$

This stress is reduced to zero by applying a bending moment(formula 2.22), see figure 2.11. The moment M_0 is denoted as the compensating moment, see formula 2.23). The shear force at which the stress σ_c at the bottom side of the beam becomes zero is $V_n = \frac{M_0}{a}$. Assuming the beam has a rectangular cross-section with d = 0,85h and e_p = 0,35h. The concrete stress at the bottom fibre from prestressing(formula 2.24);

$$\sigma_{cb} = -\frac{P_m}{bh} - \frac{P_m \cdot 0,35h \cdot 0,5h}{\frac{1}{12}bh^3} = -3,1\frac{P_m}{bh} \tag{2.24}$$

The concrete stress is zero in case of an additional bending moment(formula 2.25);

$$M = \sigma_{cb}\frac{1}{6}bh^2 = 0,52hP_m \tag{2.25}$$

This bending moment must be introduced by the support reaction V_n at a distance a from the cross-section(formula 2.26);

$$M = 0,52hP_m = V_n a \tag{2.26}$$

From which it follows(formula 2.27);

$$V_n = 0,52\frac{hP_m}{a} = 0,52\frac{dP_m}{0,85a} = 0,61\frac{P_m}{\frac{a}{d}} \tag{2.27}$$

Many tests have been carried out for a ratio $\frac{a}{d}$ between 2,5 and 4,0. That means that V_n will vary between V_n = 0,24P_m and V_n = 0,15P_m. Research indicates that 0,15P_m is a conservative lower bound value. This value is used in EN 1992-1-1, the coefficient k_1 in formula 2.15 is now determined.

2.5.2. Elements with shear reinforcement

To complete the story about shear, a small explanation about elements with shear reinforcement will be given. If the design shear force is higher than the shear resistance of a member that contains no shear reinforcement, shear reinforcement has to be provided to increase the resistance. As a result of this, the behavior changes: the formation of an inclined crack does not result anymore in failure, a new load transfer mechanism can be described by a truss model. In this truss model the truss has to carry has to carry the shear force V_{Ed}. First the amount of shear reinforcement is calculated, closed stirrups are spaced at a distance s. In the truss model a number stirrups are represented by one tensile tie. A tensile tie is equivalent for the stirrups in the beam over a distance z($cot\theta + cot\alpha$), z is the distance from the tensile reinforcement to the resulting concrete compressive force. The cross section of the tensile bar has an area of A_{equi}, see formula 2.28.

$$A_{equi} = \frac{A_{sw}}{s} z(cot\theta + cot\alpha) \tag{2.28}$$

On basis of equilibrium it follows that in case of a full truss model, the tensile force N_t in a tensile tie is represented in formula 2.29

$$N_T = \frac{V_{Rd,s}}{sin\alpha} \tag{2.29}$$

Formula 2.28 and 2.29 can be combined to formula 2.30(this is formula 6.13 in EC2[17]), in which the steel stress is represented as the yield stress. In case the $\alpha = 90$ and $\theta = 45$ formula 2.30 transforms in formula 2.31.

$$V_{Rd,s} = \frac{A_{sw}}{s} z f_{ywd} (cot\theta + cot\alpha) sin\alpha \tag{2.30}$$

where:

A_{sw} = the total cross-sectional area of each stirrup
s = distance between the stirrups
z = distance from the tensile reinforcement to the resulting concrete compressive force $\frac{A_{sl}}{b_w d}$ <0,02
f_{ywd} = design yield stress reinforcement
θ = the angle of the compression struts
α = the angle of inclination of the tensile ties

In figure 2.12 the truss model.

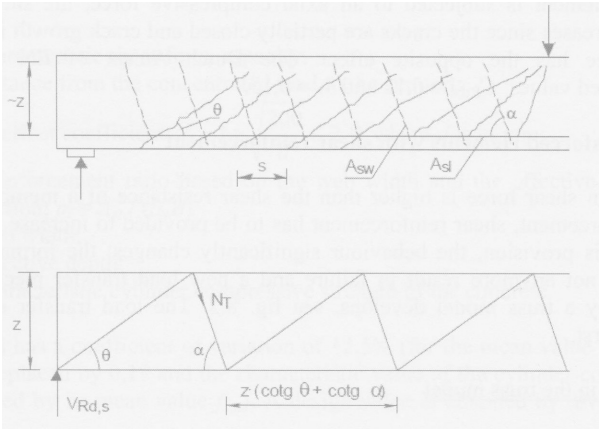

Figure 2.12: The truss model with compression struts at an angle of θ and inclined tensile ties at an angle α[24]

$$V_{Rd,s} = \frac{A_{sw}}{s} z f_{ywd} \tag{2.31}$$

In case there is chosen for vertical shear reinforcement ($\alpha = 90$) and the lower limit for $\theta = 21,8$, than formula 2.30 can written as formula 2.32(this is formula 6.8 in EC2[17]).

$$V_{Rd,s} = \frac{A_{sw}}{s} z f_{ywd} cot\theta \tag{2.32}$$

Tests showed that formula 2.30 might be conservative, because of a few aspects. The truss is a simple representation of the actual behavior, because the connections between the truss bars are not perfect hinges. Further the redundancy from dowel action of the longitudinal reinforcement should be considered. There might be still frictional forces in the cracks, this is called the aggregate interlock. The uncracked compression zone can also contribute to the shear force capacity. At last the direct load transfer to the support is not included.

The above described method is called the variable inclination method. In reality there is a redistribution of forces in the webs of shear reinforced concrete beams, this results in strut inclinations smaller than 45 degrees, see figure 2.13. In case of a smaller strut inclination, a larger number of stirrups is activated, in this way the shear capacity in increased. On the other side a smaller strut inclination causes larger stresses in the concrete struts. In this way an upper limit to the shear capacity can be defined. This method represents a more physical reality, in contrast to the in the past prescribed standard method. Further it a simple transparent equilibrium method. If the shear reinforcement yields, the truss can, by rotation of the compression struts to a lower inclination, activate more stirrups for the transmission of the shear force and extend the occurrence of failure.

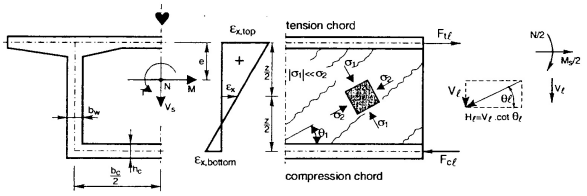

Figure 2.13: Redistribution of forces[23]

As mentioned before, due to the inclination the stress in the concrete struts increases. Rotation will continue until crushing of the concrete occurs. In order to prevent brittle failure of the struts a maximum amount of shear reinforcement is allowed. In formula 2.33 the expression of the maximum $V_{Rd,c}$.

$$V_{Rd,c} = b_w z(cot\theta + cot\alpha)sin^2\theta\sigma_{cd} = b_w z\sigma_{cd}\frac{cot\theta + cot\alpha}{1+cot^2\theta} \tag{2.33}$$

An important thing to note is that the compressive struts cannot be loaded up to the uniaxial concrete compressive strength, because the stirrups that cross the concrete diagonal struts in the web are loaded in tension. The tensile forces perpendicular to the direction of the struts are transferred by bond. As a result the strength in the struts will be reduced. Another thing to notice, from experiments it turns out that the maximum stress does not proportionally increase with the concrete strength class. In figure 2.14 the reduction of the concrete compressive strength due to transverse tension from bond forces introduced by the shear reinforcement. The expression in formula 2.34 takes the described effects into account.

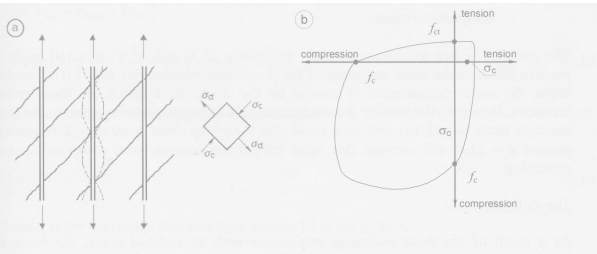

Figure 2.14: Reduction of the concrete compressive strength due to transverse tension from bond forces[24]

$$\sigma_{cd} = \alpha_{cw}\nu_1 f_{cd} \tag{2.34}$$

where:

α_{cw} = a coefficient taking into account the state of stress in the compression strut
ν_1 = a strength reduction factor for concrete cracked in shear

If formula 2.30 equals formula 2.33, the maximum possible shear force and the corresponding angle θ are found. In figure 2.15 the development of the formulas. In formulas 2.35[23] and 2.36[23] the expressions for the ultimate nominal shear strength corresponding value of θ.

$$\frac{\upsilon_{ultimate}}{\nu_1 f_{cd}} = \sqrt{\Psi(1-\Psi)} \tag{2.35}$$

and

$$tan\theta = \sqrt{\frac{\Psi}{1-\Psi}} \tag{2.36}$$

where:

$\upsilon_{ultimate} = \frac{V_{ultimate}}{b_w \cdot 0{,}9d}$
$\Psi = \frac{\rho_{sw} f_{yw}}{\nu_1 f_{cd}}$

In figure 2.16 there is a graphical impression of formula 2.35.

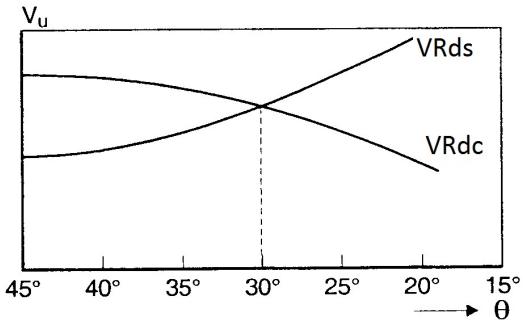

Figure 2.15: Dependence of $V_{Rd,s}$ and $V_{Rd,c}$ on the strut inclination θ[23]

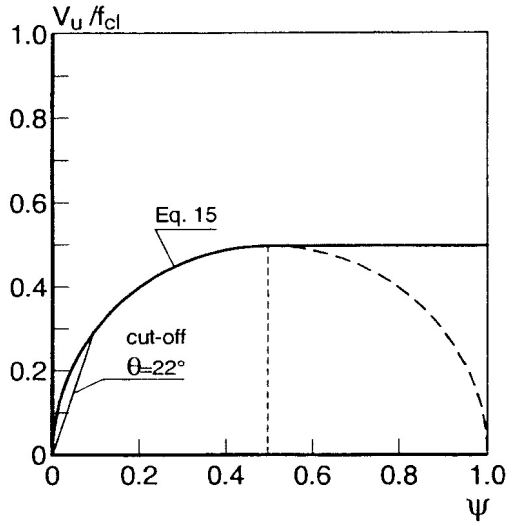

Figure 2.16: Graphical representation of formula 2.35, with cut-off for cotθ[23]

2.6. Poisson's ratio

An important aspect of a material is the Poisson's ratio, also called the contraction coefficient. When a deformable body elongates through an axial tensile force, in addition it will contract laterally. Also when a compressive force is acting on a body, it will contract in the direction of this force and expands laterally. The most common and well known example of a material in which this phenomenon can be seen is rubber. In formula 2.37 the mathematical expression of the Poisson's ratio ν.

$$\nu = -\frac{\epsilon_{lat}}{\epsilon_{long}} \tag{2.37}$$

where:

ϵ_{lat} = the lateral strain
ϵ_{long} = the longitudinal strain

The negative sign is used since longitudinal elongation causes lateral contraction. There exist materials in which a longitudinal elongation causes a lateral elongation. Further the Poisson's ratio is dimensionless. In order to see the influence of the Poisson's ratio on the mechanical behavior of a concrete beam there will be made a start with the generalization of the beam theory: the homogeneous isotropic plate. There are some basic assumptions in the thick plate theory. No membrane forces will occur due to support constraints. It is assumed that a straight line normal to the mid-plane of the plate in an unloaded state, stays a straight line after application of the load. However, it needs not be a normal to the mid-plane of the plate anymore. Sometimes it is called 'the needle hypotheses'. The stress σ_{zz} is negligibly small and is assumed zero. There are three kinds of basic equations: the kinematic equations, the constitutive equations and the equilibrium equations. The kinematic equations are presented in formula 2.38[6].

$$\begin{aligned}
\kappa_{xx} &= \frac{\partial \varphi_x}{\partial x} \\
\kappa_{yy} &= \frac{\partial \varphi_y}{\partial y} \\
\rho_{xy} &= \frac{\partial \varphi_x}{\partial y} + \frac{\partial \varphi_y}{\partial x} \\
\gamma_{xz} &= \varphi_x + \frac{\partial w}{\partial x} \\
\gamma_{yz} &= \varphi_y + \frac{\partial w}{\partial y}
\end{aligned} \tag{2.38}$$

where:

κ_{xx} = the curvature in x-plane in x-direction
κ_{yy} = the curvature in y-plane in y-direction
φ_x = the rotation in x-plane in x-direction
φ_y = the rotation in y-plane in y-direction
φ_x = the rotation in x-plane in x-direction
ρ_{xy} = the curvature in x-plane in y-direction
γ_{xz} = the strain in x-plane in z-direction
γ_{yz} = the strain in x-plane in z-direction
w = the displacement in z-direction

The constitutive equations are presented in formula 2.39[6].

$$\begin{aligned}
m_{xx} &= \frac{Et^3}{12(1-\nu^2)}(\kappa_{xx} + \nu\kappa_{yy}) \\
m_{yy} &= \frac{Et^3}{12(1-\nu^2)}(\kappa_{yy} + \nu\kappa_{xx}) \\
m_{xy} &= \frac{1}{2}\frac{Et^3}{12(1-\nu^2)}(1-\nu)\rho_{xy} \\
v_x &= \frac{E}{2(1+\nu)}\frac{t}{\eta}\gamma_x \\
v_y &= \frac{E}{2(1+\nu)}\frac{t}{\eta}\gamma_y
\end{aligned} \tag{2.39}$$

where:

m_{xx} = the moment in x-plane in x-direction, per unit length
m_{yy} = the moment in y-plane in y-direction, per unit length
m_{xy} = the moment in x-plane in y-direction, per unit length
v_x = the shear force in x-plane, per unit length
v_y = the shear force in y-plane, per unit length
E = the modulus of elasticity
t = the thickness of the plate
ν = the poisson's ratio
η = $\frac{6}{5}$ (value of shape factor for rectangle)

The equilibrium equations are presented in formula 2.40[6].

$$\begin{aligned}
&\frac{\partial v_x}{\partial x} + \frac{\partial v_y}{\partial y} + p = 0 \\
&\frac{\partial m_{xx}}{\partial x} + \frac{\partial m_{yx}}{\partial y} - v_x + q_x = 0 \\
&\frac{\partial m_{yy}}{\partial y} + \frac{\partial m_{xy}}{\partial x} - v_y + q_y = 0
\end{aligned} \tag{2.40}$$

where:

p = the external force, per unit of area
q_x = the externally distributed moment in x-direction, per unit length
q_y = the externally distributed moment in y-direction, per unit length

In formula 2.41 the end result after substitution of the kinematic equations, the constitutive equations and the equilibrium equations. In figure 2.17 the stress resultant and deformation due to bending in a plate with lateral contraction. In case there are no constraints in the y-direction, the plate can freely deform in the y-direction as a consequence of the effect of the poisson's ratio. In this case there will be no horizontal stresses(σ_{yy}) in the y-direction. In practice there are always certain forms of constraints, for example constraints that prevent vertical displacement or rotation of a plate. I this case a horizontal stress σ_y can occur as a consequence of the poissoin's ratio.

$$
\begin{aligned}
&-D_\gamma\left(\frac{\partial^2}{\partial x^2}+\frac{\partial^2}{\partial y^2}\right)w - D_\gamma\frac{\partial \varphi_x}{\partial x} - D_\gamma\frac{\partial \varphi_y}{\partial y} = p \\
&D_\gamma\frac{\partial w}{\partial x} + \left(D_\gamma - D\frac{\partial^2}{\partial x^2} - \frac{1}{2}(1-\nu)D\frac{\partial^2}{\partial y^2}\right)\varphi_x - \frac{1}{2}(1+\nu)D\frac{\partial^2 \varphi_y}{\partial x \partial y} = q_x \\
&D_\gamma\frac{\partial w}{\partial y} - \frac{1}{2}(1+\nu)D\frac{\partial^2 \varphi_x}{\partial x \partial y} + \left(D_\gamma - \frac{1}{2}(1-\nu)D\frac{\partial^2}{\partial x^2} - D\frac{\partial^2}{\partial y^2}\right)\varphi_y = q_y
\end{aligned}
\tag{2.41}
$$

where:

$D = \frac{Et^3}{12(1-\nu^2)}$
$D_\gamma = \frac{E}{2(1+\nu)}\frac{t}{\eta}$

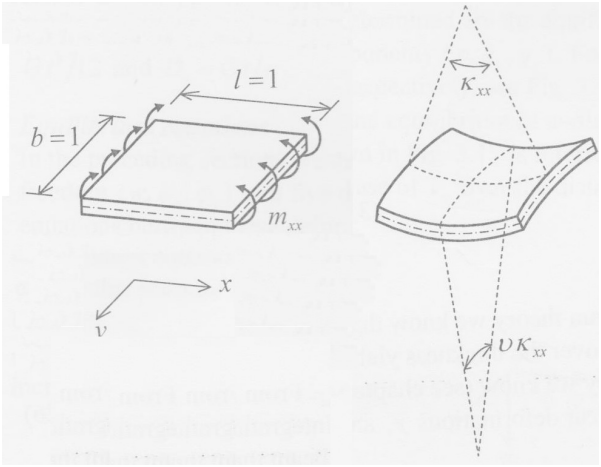

Figure 2.17: Stress resultants and deformations due to bending in a plate with lateral contraction[6]

If there is assumed that w and φ_x are constant in the y-direction and φ_y is zero, then $\frac{\partial v_y}{\partial y}$ and $\frac{\partial m_{yx}}{\partial y}$ are cancelled out. If further q_x and q_y are set to zero, then the expressions of formula 2.41 will transform into the expressions of formula 2.42. All force components are forces per unit length. After correction the well-known expressions according to the Timoshenko beam theory appear. Furthermore if the slenderness meets the requirements, then the Euler-Bernoulli beam theory is applicable. In that case the shear deformation can be neglected. Theoretically the contribution of the Poisson's ratio on the mechanical behavior of slender beams is as good as negligible, especially for small poisson's ratios.

$$
\begin{aligned}
&\frac{-EI}{1-\nu^2}\frac{\partial^2 \varphi}{\partial x^2} + GA_s\left(\varphi_x + \frac{\partial w}{\partial x}\right) = 0 \\
&-GA_s\left(\frac{\partial \varphi}{\partial x} + \frac{\partial^2 w}{\partial x^2}\right) = q
\end{aligned}
\tag{2.42}
$$

where:

GA_s = the shear stiffness
EI = the bending stiffness
ν = the poisson's ratio
q = the equal distributed external force in x-direction, per unit length

In case of slender beams the Poisson's ratio of course still effects the mechanical behavior in the y- and z-direction, so $\epsilon_y = -\nu\epsilon_x$ and $\epsilon_z = -\nu\epsilon_x$. In simple slender beams there are only constraints at the ends of the beam, these constraints prevent the vertical displacement(z-direction) and, depending on the type of constraint, the rotation in the x-direction. In these beams the external force will only be pointed towards the constraints in x-direction. The external force will cause a curvature κ_{xx}, as a consequence of the Possoin's ratio a curvature will occur in the y-direction($\nu\kappa_{xx}$). This curvature will cause an elongation at the topside of the beam and a shortening at the downside of the beam. This elongation and shortening will not be constrained, so through this theoretical way it is assumed no stress σ_{yy} will occur, see figure 2.18. In the same way it can be argued that no σ_{zz} will occur. At the location of the external concentrated force there will be present a σ_{zz} locally, as a result of initiating this force. The load plate could prevent a part of the elongation of the beam in z-direction at the topside of the beam, this could cause a σ_{zz} locally. For small Poisson's ratios this can be quantified as neglectable. In practice slender beams often modelled in a two dimensional way, a two dimensional stress state is then considered. As described in section 2.1, the stress state of an element in a beam can be considered as a plane stress state, see figure 2.4. Another possibility of modelling in a two dimensional way is to consider a plane strain state. Important is to realise that if a Poisson's ratio is cosidered, a plane stress state does not necessarily cause a plane strain state or vice versa. It can be concluded that the Poissoin's ratio has a small influence on the stress state of slender beams.

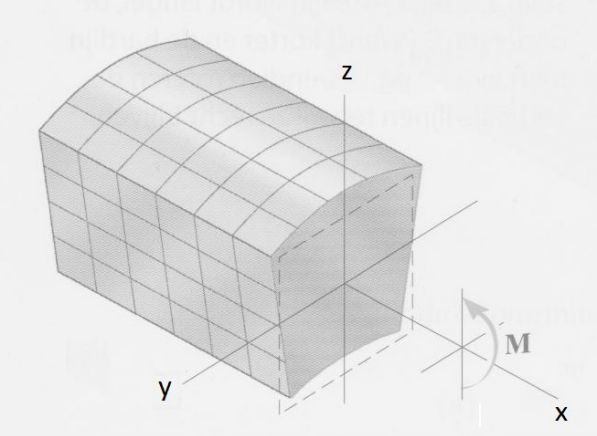

Figure 2.18: Effect of Poisson's ratio on a slender beam[14]

2.7. Biaxial behavior

An important aspect in structures is the multiaxial state of stress, because in practice a uniaxial state of stress hardly occurs. Knowledge about concrete under multiaxial stress states is essential to develop a failure criterion for example concrete. One can think of various types of concrete structures, for example the biaxial stress state in shells, plates and the shear region in beams. This failure criterion exists of certain stress limits. If a stress situation exceeds a limit we speak of failure of the material or structure. Actually the limit state is a model too. Important for a model is the description of the stress state which has to be tested to any limit or failure criteria. Most models are models based on principal stresses. From this point a definition of a failure model could be: Any combination of principal stresses that exceeds a certain limit function or value will initiate failure. Most models are based on plasticity, for example commonly known models are Von Mises, Tresca, Mohr-Coulomb and Drucker-Prager. In the past decades, however there are several failure criterions developed specifically for the material concrete, based on tests and experiments. Well known examples of failure criterions are Kupfer et all(1969)[19], Nelissen(1972)[21]. In Jena(1972)[18] the Griffith's theory and a parabolic form of Mohr-Coulomb criterion is included. More recent work are articles of Lee et al(2004)[20] and Huber(2016)[16].

2.7.1. Von Mises

The principal stress tensor can be split up in to an isotropic and a deviatoric part. Von Mises assumed that failure occurs when the deviatoric stress exceeds a limit value. This assumption was based on the observation that many materials are not sensitive to changes in the isotropic part of the stress but very sensitive to any change in the deviatoric part of the stress. In formula 2.43 the expression of the Von Mises yield criterion. In figure 2.19 the Von Mises criterion in plane stress situation.

$$(\sigma_1 - \sigma_2)^2 + (\sigma_2 - \sigma_3)^2 + (\sigma_3 - \sigma_1)^2 < 2f_y^2 \tag{2.43}$$

where:

f_y = the yield stress
$\sigma_{1,2,3}$ = the principal stresses in the three directions

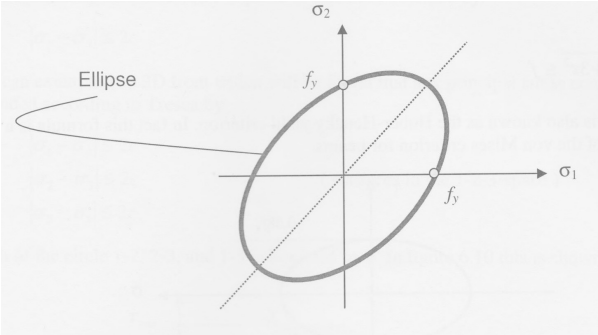

Figure 2.19: Von Mises criterion in plane stress situation[13]

The Drucker-Prager criterion is similar to the von Mises yield criterion, with provisions for handling materials with differing tensile and compressive yield strengths. The Drucker-Prager criterion is is suitable for concrete, because of the different yield stress for compression and tension.

2.7.2. Tresca

Tresca assumed failure if the maximum shear stress in the material exceeds a certain limit denoted with c. In case of a plane stress situation the maximum shear stress can be found with Mohr's stress circle. In formula 2.44 the expression of the Tresca yield criterion. In figure 2.20 the Tresca criterion in plane stress situation.

$$max(\sigma_1 - \sigma_2, \sigma_2 - \sigma_3, \sigma_3 - \sigma_1) < 2c \tag{2.44}$$

where:

c = $\frac{1}{2} f_y$
f_y = the yield stress
$\sigma_{1,2,3}$ = the principal stresses in the three directions

The Mohr-Coulomb criterion is similar to the Tresca criterion, with additional provisions for materials with different tensile and compressive yield strengths. The Mohr-Coulomb criterion is is suitable for concrete, because of the different yield stress for compression and tension.

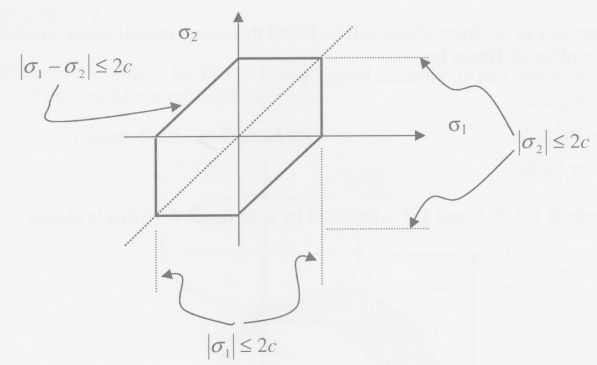

Figure 2.20: Tresca's criterion in the 1-2-principal stress plane[13]

2.7.3. Kupfer

In Kupfer et all(1969)[19] several experiments were done with concrete mixtures different in quality. The reason for the eperimental research in Kupfer et all(1969)[19] was the deviation of the test results obtained from previous conducted experiments by numerous scientists. Kupfer stated that a possible reason for this deviation could be the difficulty of applying a stable and uniform biaxial stress state in the specimen. Another reason for this research was that most studies and researches have been limited to tests in the range of biaxial compression, so no data on the behavior of concrete under biaxial tension and biaxial compressin/tension was available. The test apparatus used by Kupfer covers the entire range of stress combinations from biaxial compression to biaxial tension.

In figure 2.21 the hydraulic system used by Kupfer to apply a constant stress state in a specimen. The ratio of certain applied stresses σ_1 and σ_2 can be maintained constant throughout the load distributing frame. The hydraulic jack(number 1, figure 2.21) which is connected to a pump applies a load to a beam which is supported by two additional hydraulic jacks (number 2, figure 2.21) and (number 3, figure 2.21). Pressure lines connect the jacks (number 2, figure 2.21) and (number 3, figure 2.21) with the hydraulic jacks in the main testing machine. The position of the hydraulic jack(number 1) is adjustable along the beam and controls the ratio of the applied stresses σ_1 and σ_2. The platens used for loading the specimens in the experiments are brush bearing platens. These platens are used to lower the restraint of the specimen, so then it is possible that strains will occur in the concrete at a certain stress level. Kupfer tested the effectiveness and reliability of the brush bearing platens. Different prisms with various height to side length ratios including cubes as well as concrete plates were loaded in uniaxial compression with and without brush bearing platens. If brush bearing platens were used, the strength of the specimens was independent of the shape. This indicates that end restraint of concrete specimens can be eliminated by brush bearing platens.

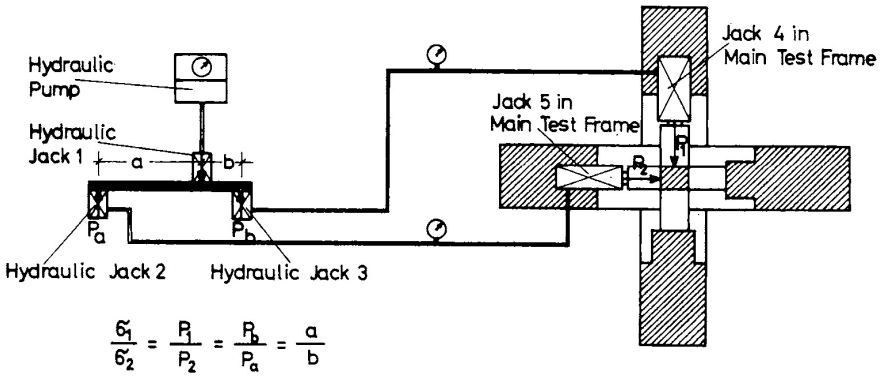

Figure 2.21: The hydraulic system[19]

Kupfer reported the obtained strength data as fractions of the uniaxial compressive strength β_p, this uniaxial compressive stresses followed from tests with 5x5x20 cm prismas. Three types of concrete with an uniaxial compressive strength of β_p=190, 315 and 590 kg/cm^2 were tested at 28 days. In each region of stress combinations four different stress ratios $\frac{\sigma_1}{\sigma_2}$ were chosen. In figure 2.22 the relationship between the princi-

pal stresses at failure $\frac{\sigma_1}{\beta_p}$ and $\frac{\sigma_2}{\beta_p}$ is given. In figure 2.23 the relationship for the range compression/tension and biaxial tension. In figure 2.22 it can be seen that the strength of concrete under biaxial compression is larger than under uniaxial compression. In the range of compression/tension and biaxial tension the relative strength decreases as the uniaxial strength increases. Also it can be seen that the ratio of uniaxial tensile strength to the prism strength of the concrete is variable. The strength of concrete under biaxial tension is almost independent of the stress ratio $\frac{\sigma_1}{\sigma_2}$ and almost equal to the uniaxial tensile strength. The highest relative strength was obtained for a stress ratio $\frac{\sigma_1}{\sigma_2} = \frac{1}{0,5}$ where $\frac{\sigma_1}{\beta_p} = 1,27$. For equal compression in both principal directions a strength of $1,16\beta_p$ was observed. It is important to realise that figure 2.22 and 2.23 are composed of the obtained data following from the described experiments, that means that there is a certain uncertainty in the areas $\frac{\sigma_2}{\beta_p} < 0,2$ and $\frac{\sigma_2}{\beta_p} > 0,9$. Kupfer also did experiments with solid bearing plates, to demonstrate the restraining effect of these plates. In figure 2.24 the strength of concrete under biaxial compression, it is a comparison of the restraint and unrestrained situation.

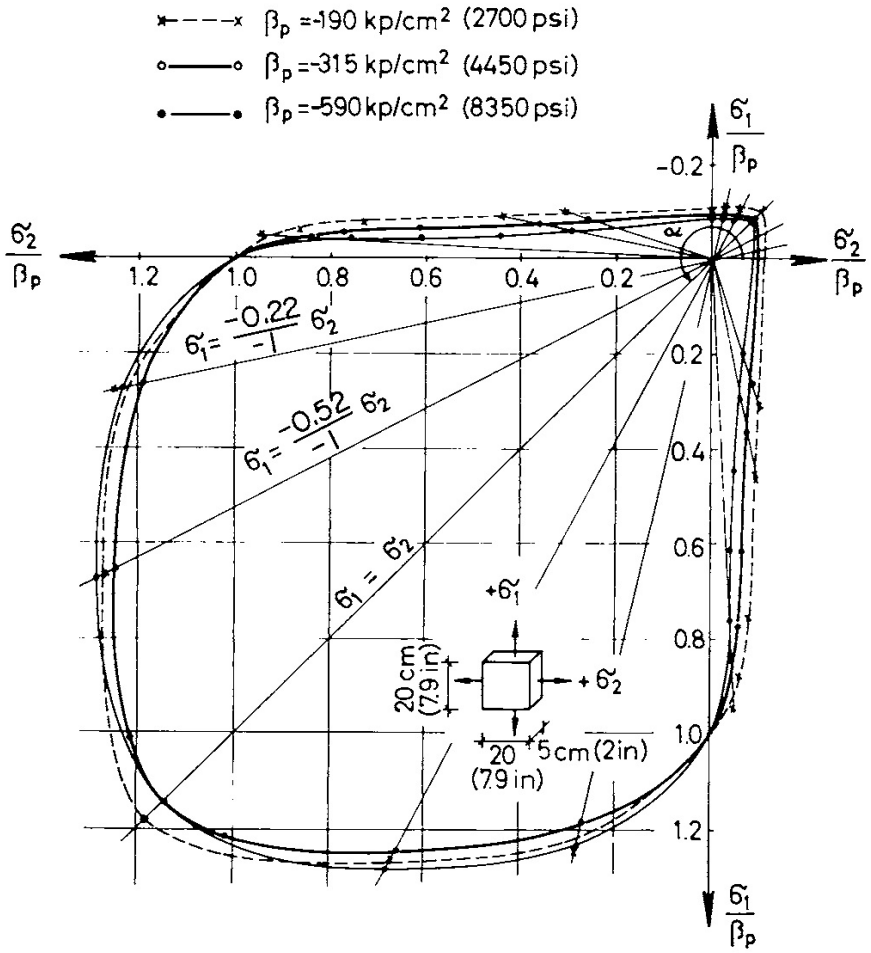

Figure 2.22: Biaxial strength concrete[19]

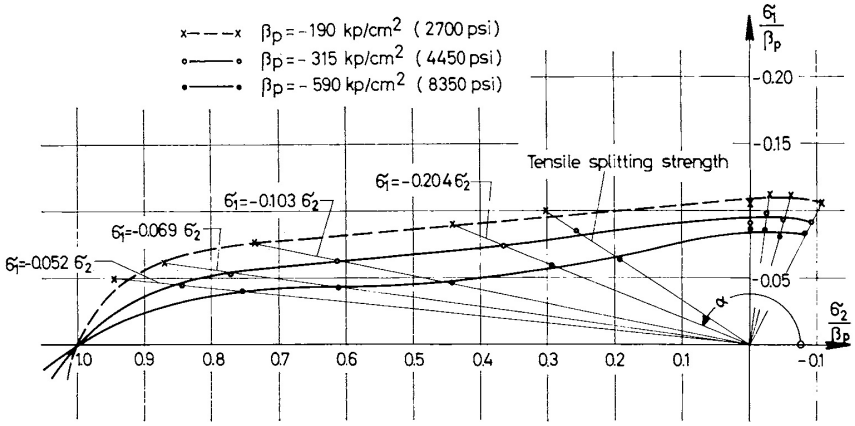

Figure 2.23: Compression/tension and biaxial tension[19]

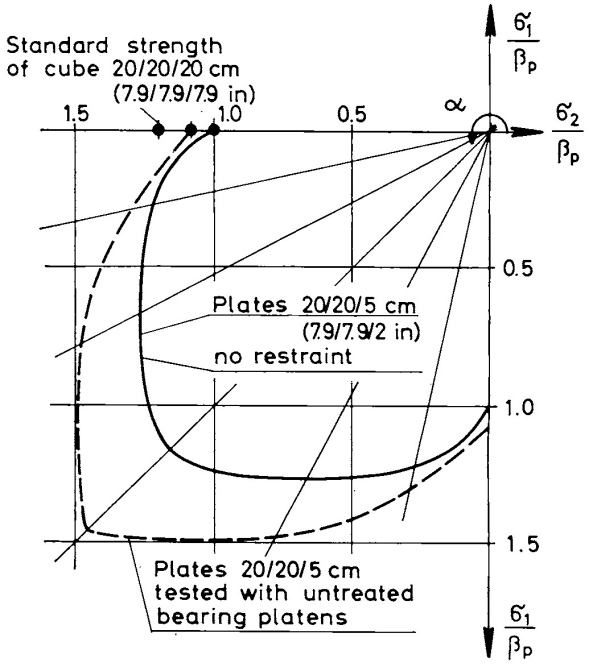

Figure 2.24: Comparision restrained and unrestrained specimen[19]

2.7.4. Lee

The main reason for the experimental research in Lee et all(1969)[20] was to obtain data of biaxial behavior of specific concrete mixtures. Lee remarked that most engineering designers use material models not developed from failure behavior tests on applied materials for every case but based on some existing experimental results for similar materials with slightly different physical properties. He added that it is not unreasonable to use existing nonlinear material models in the analyses of concrete structures, but more reliable and accurate analyses will be achieved based on experimentally verified data from real concrete structures. This idea consists with the fact that in some particular situations a more reliable analyses is needed. Such a specific situation is the containment building of a nuclear power plant, because it serves as the final barrier to the release of fission products to the outside environment. This specific situation was the reason for Lee to do his experimental analyses. Lee used a same sort of test apparatus as Kupfer, a hydraulic system that applies a constant stress state in the specimen. In order to lower the restraint of the specimen the solid loading platens were equiped with teflon pads. In the experiments all the three regions were considered: biaxial compression, biaxial tension and compression/tension.

Lee reported the obtained strength data as fractions of the uniaxial compressive strength, $\frac{f_1}{f_c}$ and $\frac{f_2}{f_c}$, this uniaxial compressive stresses followed from tests with 20x20x6 cm prismas. Two different concrete mixtures were considered, with uniaxial compressive strength of 39,0 MPa and 30,3 MPa. In each region of stress combinations four different stress ratios $\alpha = \frac{f_2}{f_1}$ were chosen. In figure 2.25 the relationship between the principal stresses at failure $\frac{f_1}{f_c}$ and $\frac{f_2}{f_c}$ is given. Again it can be seen that the strength of concrete under biaxial compres-

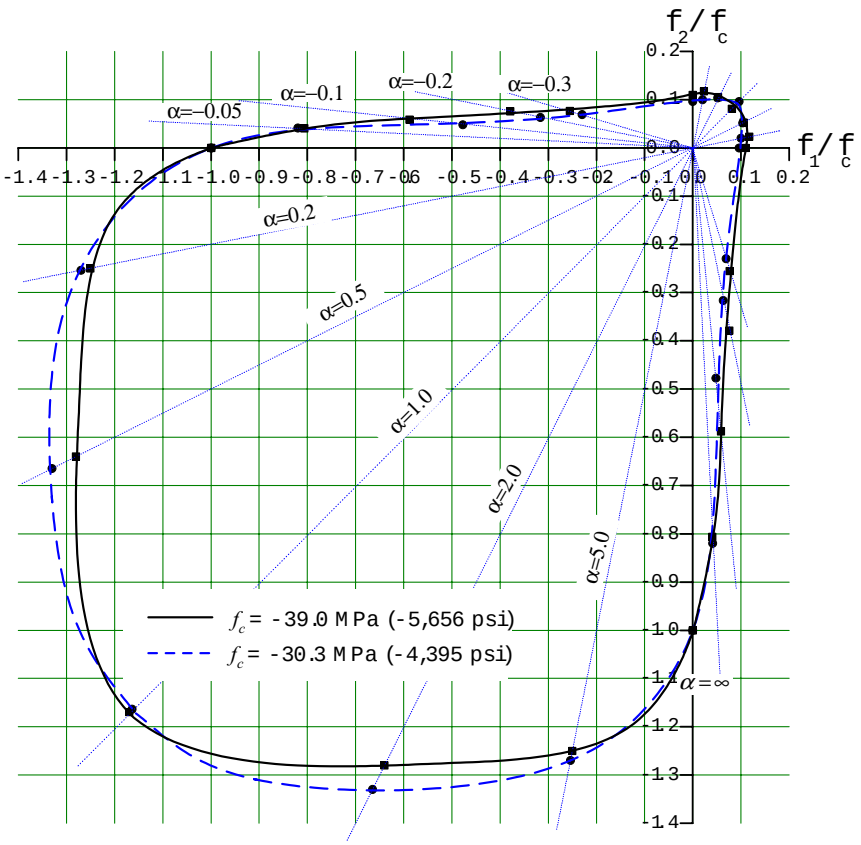

Figure 2.25: Biaxial strength envelopes[20]

sion is larger than under uniaxial compression. The maximum biaxial strength occurs at a biaxial stress ratio $\alpha = \frac{f_2}{f_1} = \frac{1}{2}$. At this stress ratio, a strength increase of respectively 28%(f_c = 39,0 MPa) and 33%(f_c = 30,3 MPa) is found. At equal biaxial compression $\alpha = \frac{f_2}{f_1}$ = 1,0 the relative strength increase is 17%(f_c = 39,0 MPa) and 16,4%(f_c = 30,3 MPa). In the range of compression/tension the relative strength decrease is almost identical for f_c = 30,3 MPa and f_c = 39,0 MPa, the concrete strengths are close to each other. On this basis it is difficult to make statements about the influence of the factor concrete strength. The strength of concrete under

under biaxial tension is almost independent of the stress ratio α and equals more or less the uniaxial tensile strength. The trends are in good agreement with the trend reported by Kupfer et all(1969)[19].

2.7.5. Huber

This article has been written with the purpose of proposing a method to determine the shear resistance of cross-sections with a low amount of transverse reinforcement. In the Eurocode there is described the commonly known method of the "truss model" with varying angle of compression struts θ see section 2.5. A more refined method is required for the assessment of beams with low amount of transverse reinforcement, ultimately with the aim of assessing existing reinforced/prestressed concrete bridges. In the article Huber described different possible areas in a concrete beam, see figure 2.26. For now, only the area "UN" is of importance, because in this area the principal stress $\sigma_1 < f_{ctd;eff}$. In the area "ST" the principal stress $\sigma_1 > f_{ctd;eff}$, the shear resistance is determined on basis of shear reinforcement. Analyses in the area "UN" is done on the basis of principal stresses, also the biaxial behavior of concrete is taken into account. Also Huber remarked, based on Kupfer and Hussein, that the biaxial behavior of concrete strongly dependents on the concrete quality. The experimentally observed reduction in the tensile strength due to compressive stress can be described with sufficient accuracy for all concrete types tested in the test series with a linear relationship. In formula 2.45 the developed failure model for the compression/tension region. Important to note is that formula 2.45 only is applicable for -0,9 < $\frac{\sigma_{2;Ed}}{f_{ck}}$ < -0,1, because for $\frac{\sigma_{2;Ed}}{f_{ck}}$ < -0,9 and $\frac{\sigma_{2;Ed}}{f_{ck}}$ > -0,1 there is no unambiguously (linear) relation. In figure 2.27 the graphical representation of the biaxial failure criterion in formula 2.45. In figure 2.27c it can be seen that the developed model approaches the experimental data of Kupfer and Hussein for certain concrete qualities. About cracks in the web Huber stated on the basis of experiments in Leonhardt et al, that in the presence of prestress cables shear cracks in the web often starts or propagates near/to the side by side cables.

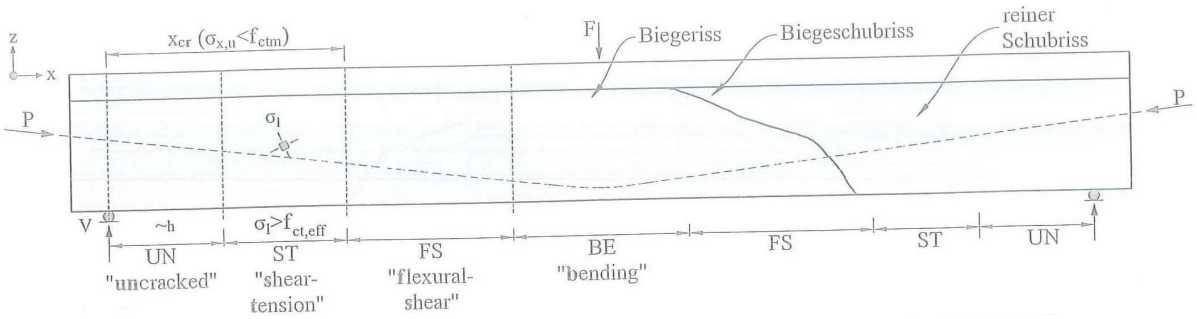

Figure 2.26: Subdivision in different areas[16]

$$f_{ctd;eff} = \left(1,6 - 0,2 f_{ck}^{\frac{1}{3}} + 0,6\frac{\sigma_{2;Ed}}{f_{ck}}\right) f_{ctd} < f_{ctd} \tag{2.45}$$

where:

$f_{ctd;eff}$ = the effective design value of the tensile strength
f_{ctd} = the design value of the tensile strength
f_{ck} = the characteristic value of the compressive strength
$\sigma_{2;Ed}$ = the principal compressive stress

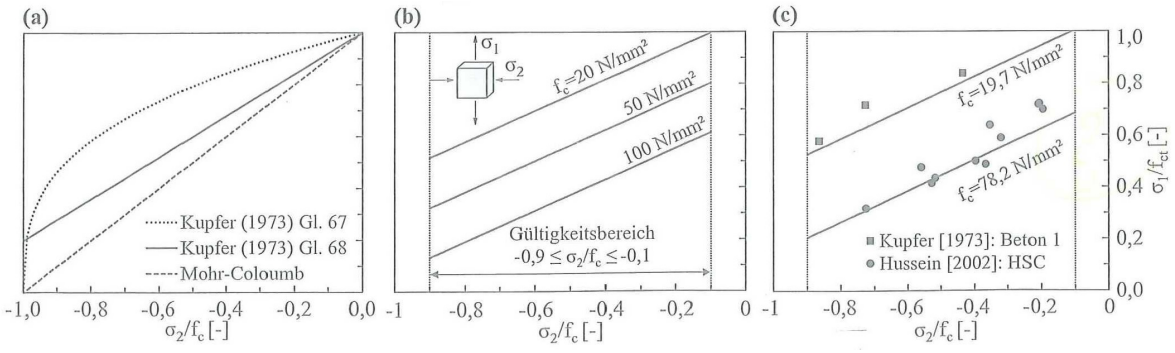

Figure 2.27: The biaxial failure criterion for compression/tension: a)existing models b)analysis of the proposed material model for different compression strength f_c c)comparison of the approach with test results out of literature[16]

3

Background of experiments

This chapter discusses the background of the studies/experiments used in this thesis. In the chapter the main purpose of the studies will be explained. Further, attention will be paid to the set-up of the experiments in the studies, including all the properties of the used specimen. The important observations of the experiments, that are important for this thesis, will be discussed.

3.1. Choulli

Reason for this study was the remarkable change in the construction environment in that time, if it comes to the development of Self-Compacting Concrete(SCC). This development made a huge step towards improved efficiency and working conditions on construction sites and in the precast industry. As a result of the mix design, some properties of the hardened concrete could be different for the Self-Compacting Concrete, if it was compared to the Conventional Vibrated Concrete(CVC). Therefore it was important to determine all mechanical properties of Self-Compacting Concrete. The investigated properties in this study were related to the shear behavior.

3.1.1. The main purpose

Much research had been carried out with respect to shear in reinforced concrete beams, but only few tests had treated the structural behavior of prestressed Self-Compacting Concrete elements. The general purpose of this study was to investigate and to improve the understanding of the shear behaviour of prestressed I-beams made with Self-Compacting Concrete. In order to reach this purpose, among other things were considered: the beams were made of CVC and SCC and there were both I-beams with and without vertical reinforcement.

3.1.2. Set-up and conditions of experiments

In the study there was made use of 6 I-beams, each 10 meters long, these beams were tested at both ends. This resulted in 12 experiments. The tests were carried at the Structural Technology Laboratory of the Technical University of Catalonia (UPC). The beams were fabricated with the support of the Spanish prefabrication company ALVISA. The following parameters were considered in order to study their influence: the type of concrete, level of prestressing, amount of longitudinal reinforcement in the web and the presence of vertical reinforcement. Four beams were made of Self-Compacting Concrete and 2 were made of Conventional Vibrated Concrete. The concrete beams were named: HAP1, HAP2, HAP1T, HAP2T, HCP1T and HCP2T. These beams were designed in such a way that web shear cracking was ensured under combined shear and bending. The beams HCP1T and HCP2T were made of Conventional Vibrated Concrete, the others were made of Self-Compacting Concrete. HAP1 and HAP2 did not contain vertical reinforcement, but had a different prestress reinforcement ratio. All the beams had the same cross-section dimensions, see figure 3.1.

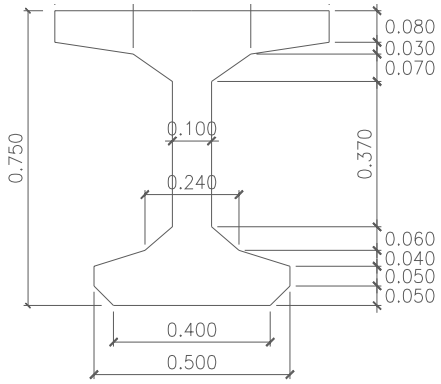

Figure 3.1: Cross-section(m)[8]

Concrete properties

The concrete used in the I-Beams was mixed in the prefabrication plant of ALVISA in Huesca (Spain). A maximum aggregate size of 12 mm was used throughout the beams. Standard 150×300 mm cylinders were cast for the 6 I-beams to obtain the compressive strength and elastic modulus. To obtain the flexural strength of each concrete mix, prismatic specimens with 150×150×450 mm nominal dimensions were cast for each beam specimen. In table 3.1 the concrete compressive and flexural tensile strength.

Beam	**Compressive strength(f_{cm})(MPa)**	**Flexural strength(MPa)(f_{ctf})**	**Modulus of elasticity**
HAP1	99	5,37	39788
HAP2	96	5,54	42409
HCP2T	90	5,93	39788
HAP2T	96	5,20	39569
HAP1T	91	5,04	39855
HCP1T	81	5,86	33675

Table 3.1: Concrete compressive and flexural strength properties[8]

Reinforcement and prestress properties

The vertical reinforcement was made from the Spanish standard B500S reinforcing bars, with a characteristic yielding stress of 500 MPa. The yielding stress, f_y, obtained in the test was equal to 525 MPa and the ultimate strength, f_u, was 660,6 MPa.

The longitudinal reinforcement was made from the Spanish standard B500SD. The yielding stress, f_y, obtained in the test was equal to 581 MPa and the ultimate strength, f_u, was 691 MPa.

The prestressing strands used in the I-Beams consisted of 0.5" diameter Y1860S7 with 99mm^2 of sectional area. The prestressing strands were tested following UNE 36.094-97. The yielding stress (f_{py}) and the ultimate stress (f_{pu}) were equal to 1776 and 1941.4 MPa, respectively. The prestress strands were placed in two ways. In the three beams HAP2, HAP2T and HCP2T were placed 10 strands, see figure 3.2. The average concrete stress in these beams, without accounting for prestress losses, was σ_{cp} = 7,11 MPa. In the other three beams HAP1, HAP1T and HCP1T were placed 16 strands, see figure 3.3. The average concrete stress in these beams, without accounting for prestress losses, was σ_{cp} = 11,37 MPa. Each of the strands was initially stressed to 1396.60 MPa. The prestressing force was transferred by straight strands in a long line process. Each of the strands was initially stressed to 1396.60 MPa. The prestressing force was transferred by straight strands in a long line process. After accounting for prestress losses the average concrete stress for the 10 strands serie was σ_{cp} = 6,3 MPa and for the 16 strands serie σ_{cp} = 9,56 MPa. All data is summarized in table 3.2.

Beam	Amount of strands	σ_{cp} excluding losses(MPa)	σ_{cp} including losses(MPa)
HAP1	16	11,37	9,56
HAP2	10	7,11	6,3
HCP2T	10	7,11	6,3
HAP2T	10	7,11	6,3
HAP1T	16	11,37	9,56
HCP1T	16	11,37	9,56

Table 3.2: Details prestress[8]

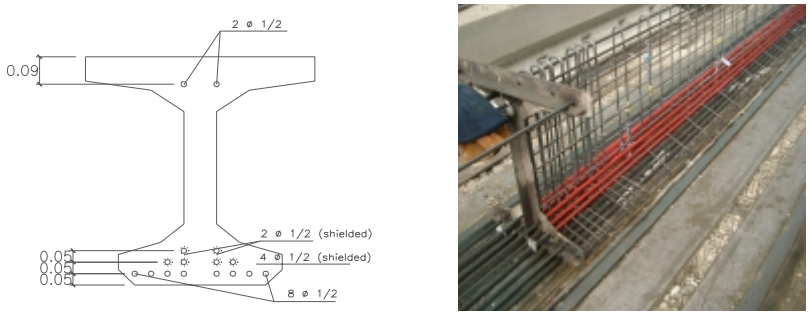

Figure 3.2: Cross-section with details strands[8]

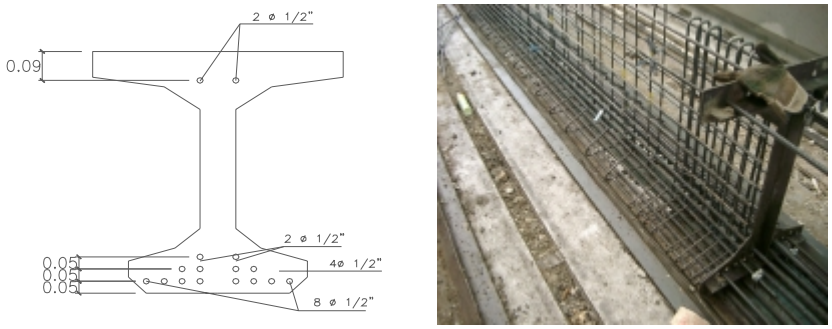

Figure 3.3: Cross-section with details strands[8]

Test procedure

As mentioned before each beam is tested twice. In the first phase the “East” side of the beam is tested and in the second phase the “West” side of beam. In figure 3.4 a sketch of the situation. During the test all sort

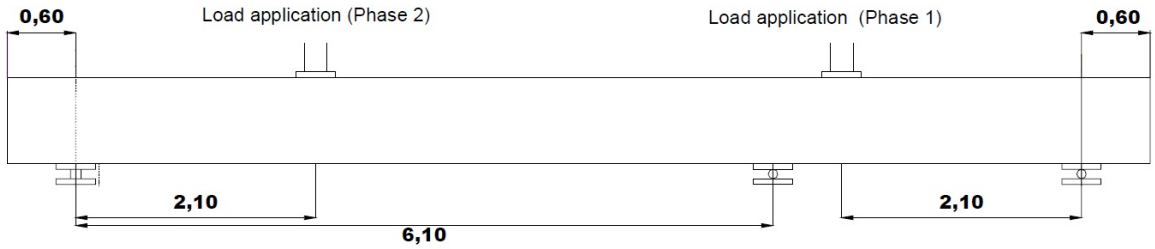

Figure 3.4: Phases of testing(m) [8]

of data was recorded: time, load increment, deflections and steel and concrete strains. All beams were tested under single point loading with a shear span-to-depth ratio of $\frac{a}{d}$ = 3,0 and $\frac{a}{d}$ = 3,13, see table 3.3. All the

Beam	Shear span-to-depth ratio $\frac{a}{d}$
HAP1	3,13
HAP2	3,0
HCP2T	3,0
HAP2T	3,0
HAP1T	3,13
HCP1T	3,13

Table 3.3: Shear span-to-depth ratio $\frac{a}{d}$ [8]

beams were simply supported, having a fixed pin bearing near the applied load, and a sliding pin bearing on the opposite side. In order to ensure the anchorage of the pretensioned strands and that of the longitudinal reinforcement, the distance from the end beam to the center of the support was taken equal to 0,60 m. The beams were loaded monotonically to failure, using displacement control and under a load placed with a constant length of shear span equal to 2.10 m, see figure 3.4. Load was applied by a hydraulic jack. At testing the west side of each of the beams HAP1T and HCP1T, the length of the cantilever had to be reduced from 3.30 m to 2.64 m in order to reach the ultimate failure. This reduction produced a higher shear force for the same load and therefore the failure could be reached taking into account the maximum load of the hydraulic jack. Before proceeding to record test data, a load of about 30 kN was applied to stabilize all the test system.

Analyses and observations

In this section the analyses and observations will be discussed shortly. The results are limited to the first observable shear crack, because that is important in this research. In table 3.4 an overview of all the tested beams, including the load that leaded to the first shear crack(excluding the 30kN), the load that leaded to the first shear crack(including the 30kN) and the present shear force. Important to note is that the test configuration of HAP1TW and HCP1TW was adapted, the length of the cantilever had to be reduced from 3.30 m (see figure 3.4) to 2.64 m in order to reach the ultimate failure.

HAP1E

The first major shear crack appeared at 518.68 kN load application which corresponded to 416 kN of the shear load, with an angle of 32 degrees to the horizontal. According to the measuring equipment, the first crack started in the mid-height of the web and propagated immediately throughout the depth of the web. The first shear crack had a shallower angle through the flange and cross the interface of flange and the web and reach the compression zone of the beam. Further there were no flexural cracks formed. In figure 3.5 the crack pattern at failure.

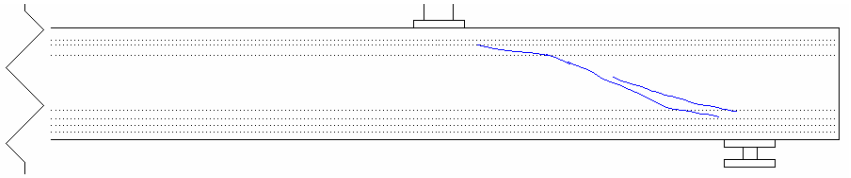

Figure 3.5: Crack pattern HAP1E[8]

HAP1W
The first major shear crack appeared at 603 kN load application which corresponded to 419 kN of the shear load, with an angle of 22 degrees to the horizontal. According to the measuring equipment, the first crack started in the mid-height of the web and propagated immediately throughout the depth of the web. Further there were no flexural cracks formed. In figure 3.6 the crack pattern at failure.

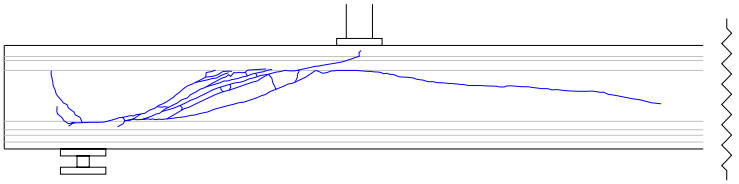

Figure 3.6: Crack pattern HAP1W[8]

HAP2E
The first major shear crack appeared at 418 kN load application which corresponded to 340 kN of the shear load, with an angle of about 25 degrees to the horizontal. This formed crack propagated immediately throughout the depth of the web to points on the web–flange intersection where they ran horizontally to the loading point at the top and to the support at the bottom, see figure 3.7. Further there were no flexural cracks formed.

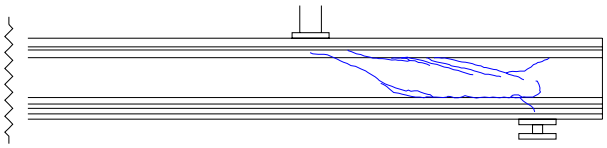

Figure 3.7: Crack pattern HAP2E[8]

HAP2W
The first major shear crack appeared at 514 kN load application which corresponded to 361 kN of the shear load, with an angle of about 32 degrees to the horizontal. According to the measuring equipment, the first crack propagated immediately from the mid-height of the web and propagated throughout the depth of the web, see figure 3.8. Further there were no flexural cracks formed.

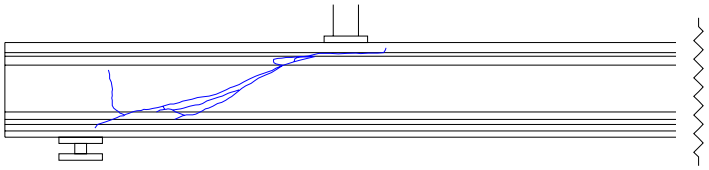

Figure 3.8: Crack pattern HAP2W[8]

HCP2TE
The first major shear crack appeared at 463 kN shear load, with an angle of 30 degrees to the horizontal. Flexural cracking occurred above the theoretically predicted value, before formation at center span of the first shear diagonal crack. In figure 3.9 the crack pattern of the beam at failure. According to the strain gages of the web reinforcement the first shear crack appeared between 8400 and 8600 mm from start of the beam.

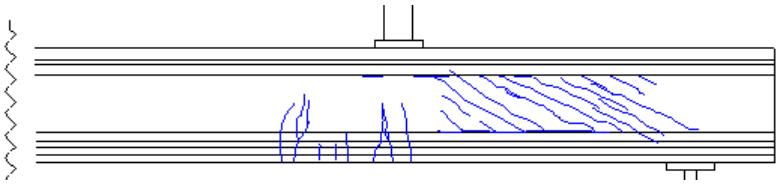

Figure 3.9: Crack pattern HCP2TE[8]

HCP2TW
The first major crack, was a diagonal shear crack which appeared at 404 kN shear load, with an angle of 26 degrees to the horizontal. Flexural cracking occurred above the theoretically predicted value, after formation at center span of the first shear diagonal crack. In figure 3.10 the crack pattern of the beam at failure. According to the strain gages of the web reinforcement the first shear crack appeared between 1400 and 1600 mm from start of the beam.

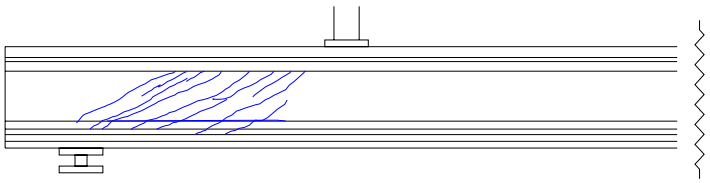

Figure 3.10: Crack pattern HCP2TW[8]

HAP2TE
The first major shear crack appeared at 359 kN shear load, with an angle of 24 degrees to the horizontal. Flexural cracking occurred above the theoretically predicted value, before formation of the shear diagonal cracks, at center span. In figure 3.11 the crack pattern of the beam at failure. According to the strain gages of the web reinforcement the first shear crack appeared between 8400 and 8600 mm from start of the beam.

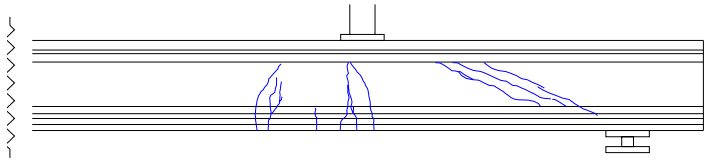

Figure 3.11: Crack pattern HAP2TE[8]

HAP2TW
The first major shear crack appeared at 368 kN shear load, with an angle of 32 degrees to the horizontal. Flexural cracking occurred above the theoretically predicted value, before formation of shear diagonal cracks at center span. In figure 3.12 the crack pattern of the beam at failure. According to the strain gages of the web reinforcement the first shear crack appeared between 800 and 1400 mm from start of the beam.

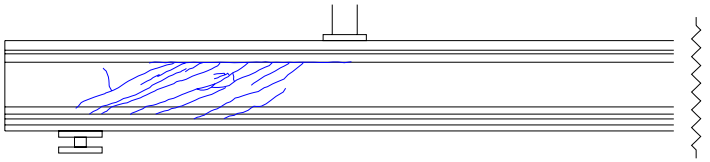

Figure 3.12: Crack pattern HAP2TW[8]

HAP1TE
The first major crack, was a diagonal shear crack which appeared at 409 kN shear load, with an angle of 26 degrees to the horizontal. Flexural cracking occurred above the theoretically predicted value, after formation of shear diagonal cracks at center span. In figure 3.13 the crack pattern of the beam at failure. According to the strain gages of the web reinforcement the first shear crack appeared between 8400 and 8600 mm from start of the beam.

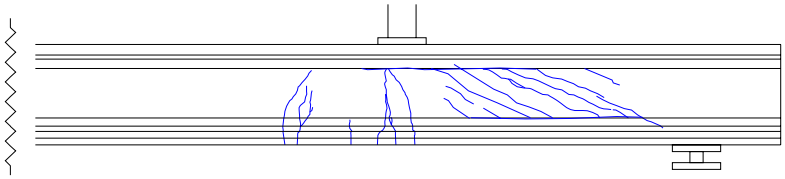

Figure 3.13: Crack pattern HAP1TE[8]

HAP1TW
The first major crack, was a diagonal shear crack which appeared at 438 kN shear load, with an angle of 25 degrees to the horizontal. As described in this section the test configuration of this beam should have been adapted, but after a checking calculation it appears that the configuration is not adapted. The first crack appeared at 438 kN shear load. That means, according to the original configuration(see figure 3.4), that the load applied load equals $\frac{438kN \cdot 6,1m}{4,0m} = 667kN$(including 30 kN). Flexural cracking occurred above the theoretically predicted value, before formation of shear diagonal cracks at center span. In figure 3.14 the crack pattern of the beam at failure. According to the strain gages of the web reinforcement the first shear crack appeared between 1400 and 1600 mm from start of the beam.

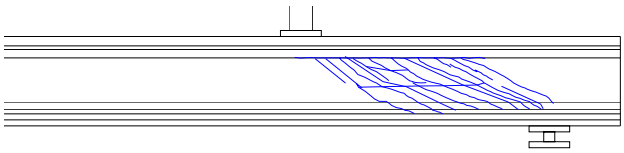

Figure 3.14: Crack pattern HAP1TW[8]

HCP1TE
The first major crack, was a diagonal shear crack which appeared at 502 kN shear load, with an angle of 28 degrees to the horizontal. Flexural cracking occurred above the theoretically predicted value, before formation of shear diagonal cracks at center span. In figure 3.15 the crack pattern of the beam at failure. According to the strain gages of the web reinforcement the first shear crack appeared between 8400 and 8600 mm from start of the beam.

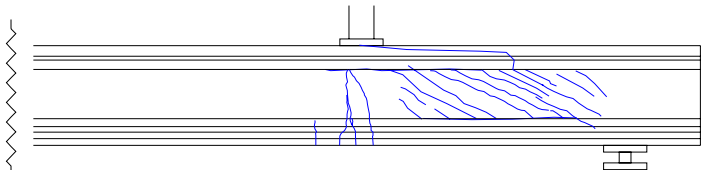

Figure 3.15: Crack pattern HCP1TE[8]

HCP1TW
The first major crack, was a diagonal shear crack which appeared at 421 kN shear load, with an angle of 30 degrees to the horizontal. Flexural cracking occurred above the theoretically predicted value, before formation of shear diagonal cracks at center span. In figure 3.16 the crack pattern of the beam at failure. According to the strain gages of the web reinforcement the first shear crack appeared between 1400 and 1600 mm from start of the beam.

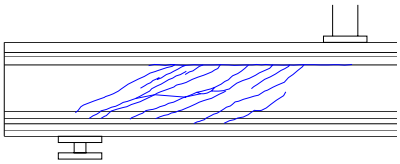

Figure 3.16: Crack pattern HCP1TW[8]

Beam	Applied load(kN)(excluding 30kN)	Applied load(kN)(including 30kN)	Shear force(kN)
HAP1E	519	549	416
HAP1W	603	633	419
HAP2E	418	448	340
HAP2W	514	544	361
HCP2TE	578	608	463
HCP2TW	580	610	404
HAP2TE	441	471	359
HAP2TW	529	559	368
HAP1TE	508	538	409
HAP1TW*	635	665	438
HCP1TE	629	659	502
HCP1TW	579	609	421

* As described in this section the test configuration of this beam should have been adapted, but after a checking calculation it appears that the configuration is not adapted, see the observations of HAP1TW

Table 3.4: Loads and shear forces [8]

3.2. Elzanaty

This study was done at a time when much research has been done on high-strength concrete. Specifications in that time, such as the ACI code, contain many empirically derived criteria that were based on tests of members having concrete strengths below certain strengths. Design of higher strengths was based on extrapolation. Doubts were expressed by many researchers about this extrapolation, following many investugations to the poperties of high-strength concrete.

3.2.1. The main purpose

The purpose of this investigation was to study the effect of using high-strength concrete on shear strength of reinforced and prestressed concrete beams, and to compare test results with the current design code provisions.

3.2.2. Set-up and conditions of experiments

A total of 53 beams was tested in two main groups. In the first group, 19 rectangular reinforced concrete beams were tested. The effects of concrete strength, longitudinal reinforcement ratio , shear span-to-depth ratio, and amount of shear reinforcement on shear strength were studied. In the second group, 34 prestressed concrete beams were tested. The same parameters were studied, and in addition the influence of varying the amount of prestress force and the prestressed steel ratio was investigated. The group of 34 prestressed concrete beams was again divided in two groups, based on two cross-sections. In figure 3.17 the cross-sections of the Elzanaty beams. The CW series consisted out of CW1 up till CW17 and the CI series out of CI1 up till CI17. CW/CI10, CW/CI11, CW/CI12, CW/CI13, CW/CI14, CW/CI15, CW/CI16, CW/CI17 had vertical reinforcement. All the other beams of the CW and CI series had no vertical reinforcement.

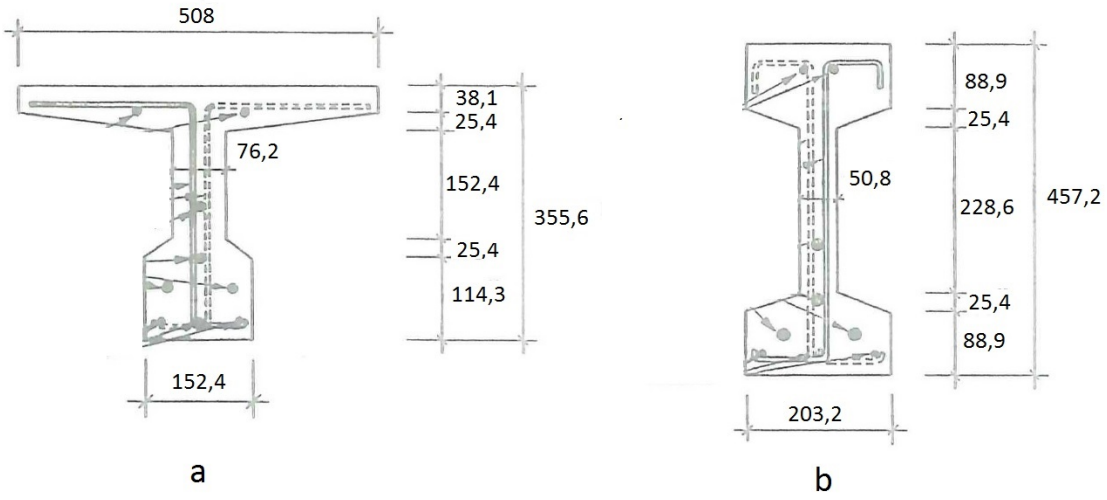

Figure 3.17: Cross-sections(mm): a)CI series b)CW series[9]

Concrete properties

The cement used was ASTM Type II portland cement. Sand was from a glacial alluvial deposit near Ithaca, N.Y., and consisted mainly of quartz and (particularly in the larger particles) of shale, sandstone, and limestone. Coarse aggregate was crushed limestone from a local quarry, with maximum size of 12,7 mm. A high-range water-reducing admixture (superplasticizer) with retarder, ASTM C 494 Type F, was used. In table 3.5 the concrete compressive and flexural strength.

Beam	**Compressive strength(f_{cm})(MPa)**	**Tensile strength(MPa)(f_{ctm})**	**Modulus of elasticity**
CW1	76,55	4,65	
CW2	76,55	4,65	
CW3	76,55	4,65	
CW4	78,60		
CW5	77,93	4,68	
CW6	77,93	4,68	
CW7	77,59	4,67	
CW8	41,38	3,38	
CW9	61,03	4,29	
CW10	73,08		
CW11	55,85		
CW12	39,99		
CW13	72,39		
CW14	73,77		
CW15	70,32		
CW16	73,08		
CW17	69,64		

Table 3.5: Concrete compressive and flexural strength properties[9][10]

Reinforcement and prestress properties

The prestressed reinforcement was made up of lowrelaxation seven-wire Grade 270 strands. Two diameters were used: 0.6 and 0.5 in. (15,4 and 12,7 mm), the area of the cross-section of 15,4 mm equals 142 mm^2 and the area of the cross-section of 12,7 mm equals 99 mm^2. The stress at 1 percent extension was 255 ksi (1760 MPa) and the ultimate elongation in 24 inch. (610 mm) was about 5.3 percent. The stress loss due to relaxation under 70 percent of uhimate stress was about 1 percent in three years. The amount of strands was equal for all the beams, 4 strands. In table 3.6 the data of the prestress(all losses included, so the effective prestress). In figure 3.18 the orientation of the strands.

Beam	Strands(mm)	Area prestress(mm^2)	Effective σ_{cp}(MPa)
CW1	15,4	568	11,20
CW2	15,4	568	11,13
CW3	15,4	568	11,01
CW4	15,4	568	11,6
CW5	15,4	568	11,18
CW6	15,4	568	8,40
CW7	12,7	395	8,19
CW8	15,4	568	8,33
CW9	15,4	568	8,25
CW10	15,4	568	8,4
CW11	15,4	568	8,2
CW12	15,4	568	8,2
CW13	15,4	568	11,5
CW14	15,4	568	11,6
CW15	12,7	395	8,2
CW16	15,4	568	11,6
CW17	15,4	568	11,6

Table 3.6: Details prestress[9][10]

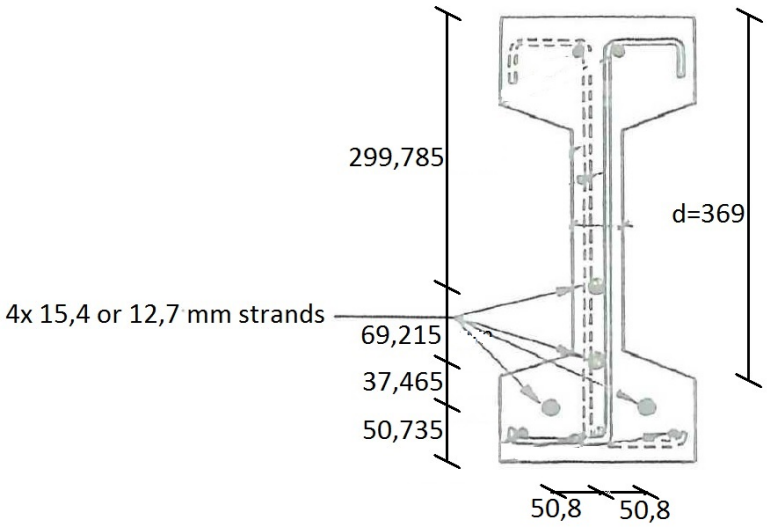

Figure 3.18: Orientation of strands(mm)[9]

Test procedure

In figure 3.19 the dimensions of the beam, the distance depends on the ratio $\frac{a}{d}$. In the CW beams d = 369 mm. All the beams were simply supported, having a fixed pin bearing near the applied load, and a sliding pin bearing on the opposite side. The load was applied incrementally to failure . For beams without stirrups, the load was applied in increments of 22,2 kN, until failure for CW series, and until flexural cracking for CI series. For beams with stirrups, the load increment was 22,2 kN until failure was approached, then a smaller increment was used. In table 3.7 the shear span-to-depth ratios.

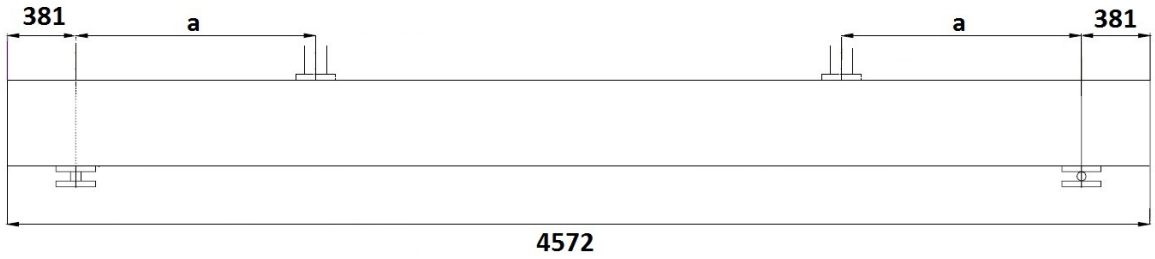

Figure 3.19: Dimensions of the CW beam(mm)[9]

Beam	Shear span-to-depth ratio $\frac{a}{d}$	a(mm)
CW1	2,90	1070
CW2	3,75	1384
CW3	5,00	1845
CW4	3,75	1384
CW5	3,75	1384
CW6	3,75	1384
CW7	3,75	1384
CW8	3,75	1384
CW9	3,75	1384
CW10	3,8	1402
CW11	3,8	1402
CW12	3,8	1402
CW13	3,8	1402
CW14	3,8	1402
CW15	3,8	1402
CW16	3,8	1402
CW17	3,8	1402

Table 3.7: Shear span-to-depth ratio $\frac{a}{d}$ [10]

Analyses and observations

In this section the analyses and observations will be discussed shortly. The results are limited to the first observable shear crack, because that is important in this research. In table 3.8 an overview of all the tested beams, including the load that leaded to the first shear crack and the present shear force. Crack patterns and behavior of beams of CW series were completely different from those of CI series. In all beams of CW series, diagonal cracks formed suddenly. The diagonal cracks always propagated immediately throughout the depth of the web, usually to points on the web-flange intersection, where they ran horizontally to the loading point at the top and to the support at the bottom. The slope of the diagonal cracks was from 15 to 30 deg. For all beams without stirrups except CWI the formation of the first diagonal crack represented the ultimate shear capacity. All the beams without stirrups were free of flexural cracks with the exception of CW6. Beam CW6 had single flexural cracks. In figure 3.20 the crack pattern of beam CW1. In figure 3.21 the crack pattern of beam CW3. In figure 3.22 the crack pattern of beam CW6. In figure 3.23 the crack pattern of beam CW7. In figure 3.24 the crack pattern of beam CW8. In figure 3.25 the crack pattern of beam CW17.

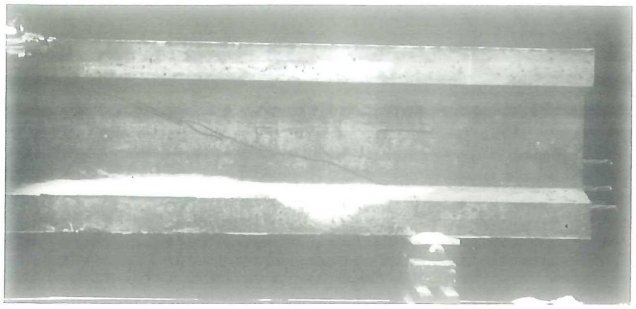

Figure 3.20: Crack pattern CW1[9]

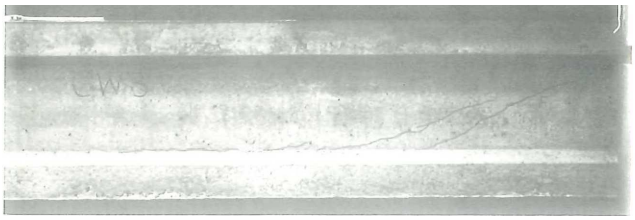

Figure 3.21: Crack pattern CW3[9]

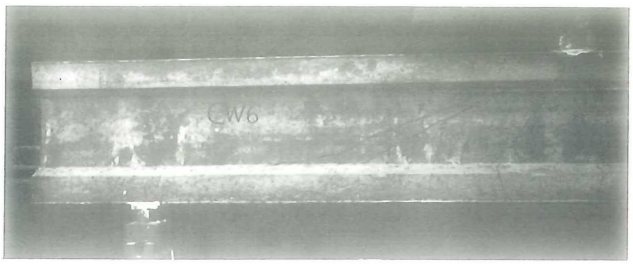

Figure 3.22: Crack pattern CW6[9]

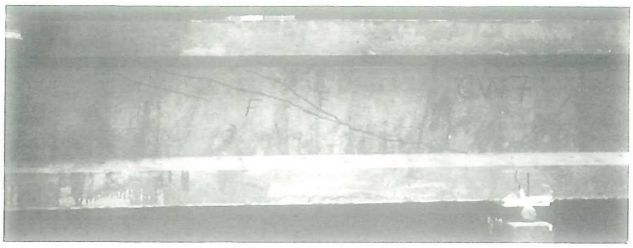

Figure 3.23: Crack pattern CW7[9]

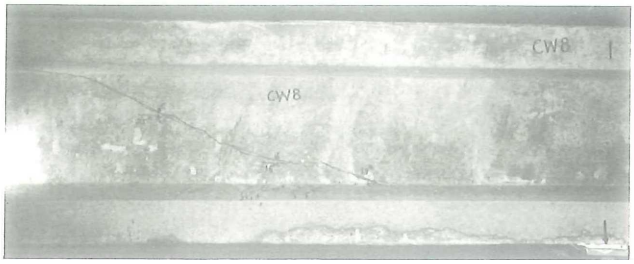

Figure 3.24: Crack pattern CW8[9]

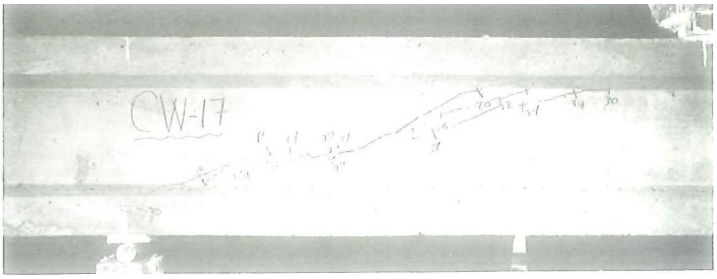

Figure 3.25: Crack pattern CW17[9]

Beam	Applied load(kN)	Shear force(kN)
CW1	138,33	138,33
CW2	124,55	124,55
CW3	117,43	117,43
CW4	127,22	127,22
CW5	124,11	124,11
CW6	112,10	112,10
CW7	105,87	105,87
CW8	89,85	89,85
CW9	100,97	100,97
CW10	108,54	108,54
CW11	95,64	95,64
CW12	85,41	85,41
CW13	122,77	122,77
CW14	123,66	123,66
CW15	100,53	100,53
CW16	122,33	122,33
CW17	123,22	123,22

Table 3.8: Loads and shear forces[9]

4

Accuracy of the analytical and numerical stress distribution

In this chapter the first topic “Accuracy of the analytical and numerical stress distribution” will be discussed. This is done for Choulli and Elzanaty separately.

4.1. Choulli

4.1.1. Pre-analysis

The coming paragraphs will form a short introduction and outline of the analytical analysis and numerical analysis, in which some things will be explained. In the last paragraph some general input/information concerning all beams will be discussed.

Analytical analysis

The analytical analysis is based on the Euler-Bernoulli theory. The stress distribution of the web of the beams(section 3.1) is determined in an analytical way. The dimensions are based on figure 3.1 and 3.4, the prestress based on table 3.2 and the applied loads on table 3.4. There are made excel sheets including all stresses like the horizontal and the shear stresses of the web of each beam. In appendix “Choulli: Analytical results” of the appendix report the analytical results of the Choulli beams. Prior to the results there is added a general informative sheet. This appendix exists out of 4 tables: σ_{xx}, τ_{xy}, σ_1 and σ_2. The phrase “Con” means that the results have been achieved with the cross-sectional properties, like the moment of inertia and the statical moment without the influence of the prestressing steel. The colomn “Rela. to n” refers to the location in the height in the web relative to the neutral axis, with the exception of the upper en bottom line, this is the distance to the ultimate fiber. The colomn “S” refers to the statical moment on that specific height. The tables of the “East” beams are on the interval of 7300 mm to 9400 mm, from the start of the beam. The tables of the “West” beams are on the interval of 600 mm to 2700 mm, from the start of the beam. The grey area of figure 4.1 represents the coverage of the tables of the “East” beams. The grey area of figure 4.2 represents the coverage of the tables of the “West” beams. The height as well as the length of the web is divided in pieces of 25 mm, so a sort of fine mesh is created. In this way it is possible to determine the stress in many points in the web. The formulas used to determine the different stress components are described in section 2.4, see formulas 2.9, 2.10 and 2.11. Formula 2.8 is used to determine the principal stresses. Subsequently stress diagrams can be made for each beam, so for σ_{xx} and τ_{xy}. The stress f_{ctm} is assumed as the stress at which the first crack in the web will occur. The stress $f_{ctm,fl}$ is assumed as the stress at which the first crack in the ultimate fiber will occur.

Numerical analysis

The numerical computational program used for the numerical analysis is DIANA. The dimensions again are based on figure 3.1 and 3.4, the prestress based on table 3.2 and the applied loads on table 3.4. In DIANA the analysis of the two dimensional model is linear elastic, there is made use of the hexa/quad mesher type, the mesh order is linear. For the element class there is chosen for the regular plane stress elements. The elements have a size of 25 mm. For the material concrete there is chosen for a linear elastic isotropic model. For the

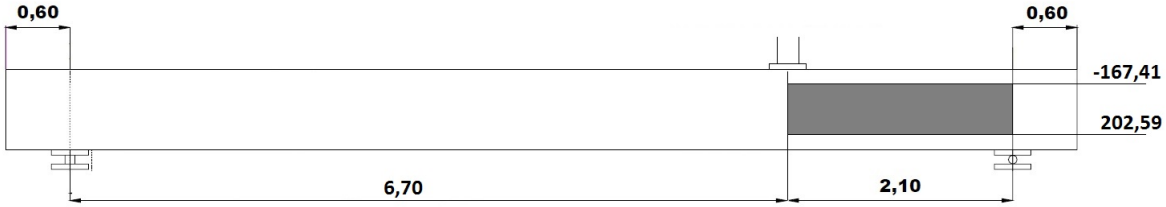

Figure 4.1: Area coverage of tables of "East" beams, distance in m and height in mm

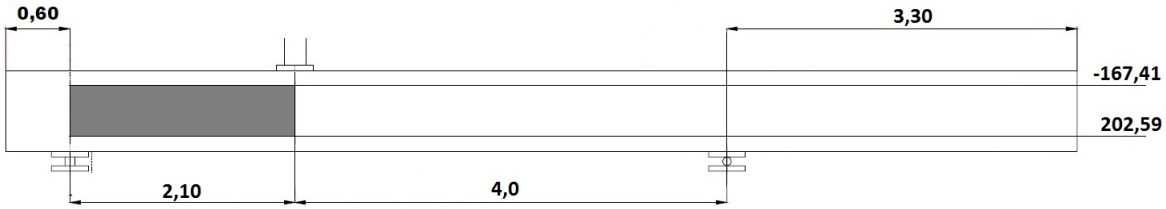

Figure 4.2: Area coverage of tables of "West" beams, distance in m and height in mm

steel plates there is also chosen for a linear isotropic model. Further, to model the width of the beam there is made use of a thickness function. The material model of the prestress strands is Von Mises plasticity. The prestress is modeled as embedded reinforcement, where the cables are bonded to the concrete. It has to be taken into account that DIANA calculates losses due to elastic deformation, on beforehand this should be compensated for. For HAP1E the numerical model is worked out. The analysis results will be exported to an excel sheet, with a Python script it is possible to present the results in such a way, that it is possible to compare these results with the obtained analytical results. In appendix "Choulli: Numerical results" of the appendix report the numerical results of the Choulli beams. This appendix exists out of 12(some 13) tables: σ_{xx}, τ_{xy}, σ_{yy}, σ_1(excluding component σ_{yy}), σ_1, σ_2(excluding component σ_{yy}), σ_2, the fraction $\frac{\sigma_{xx,Analytical}}{\sigma_{xx,Numerical}}$, the fraction $\frac{\tau_{xy,Analytical}}{\tau_{xy,Numerical}}$, the fraction $\frac{\sigma_{1,Analytical}}{\sigma_{1,Numerical,excl.\sigma_{yy}}}$, the fraction $\frac{\sigma_{1,Analytical}}{\sigma_{1,Numerical}}$ and the fraction $\frac{\sigma_{1;Poisson0,2}}{\sigma_{1;Poisson0,0}}$. For some experiments there is added a thirteenth table: θ_p. This table gives from certain values of σ_1 the angles of the principal stresses. Further, in the analyses there is taken into account the influence of the Poisson's ratio, by making an analysis with and without the Poisson's ratio. The interpretation of the numerical results will be discussed in the section "Numerical analysis".

General valid input

In this section the input for all beams will be discussed, in this case the cross-sectional properties. Further the way of determining assumed parameters of materials will be discussed, for example f_{ctm}.

Cross-sectional properties

The cross-section is the same for all the Choulli beams, there are only differences in the prestress strands. In figure 4.3 once again the cross-section of the Choulli beams. In table 4.1 all the cros-sectional properties. It is possible to determine the fraction of $I_{concrete}$, $I_{concrete+holestrands}$ and $EI_{concrete+10/16strands}$, then something can be said about the influence on the stress state, because the I is an important property in the determination of the σ_x and τ_{xy}. So $\frac{I_{concrete}}{I_{concrete+holestrands}} = 1,01$, $\frac{EI_{concrete}}{EI_{concrete+16strands}} = 0,96$ and $\frac{EI_{concrete}}{EI_{concrete+10strands}} = 0,97$. It can be seen from here that the prestressing steel has a low influence on the moment of inertia I.

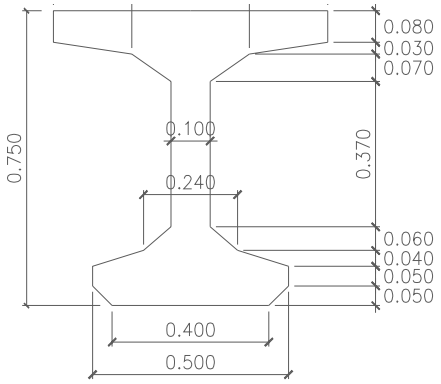

Figure 4.3: Cross-section(m)[8]

Condition	Parameter	Value
Concrete	A[mm^2]	194500
	a_{bottom}[mm]	402,59
	a_{top}[mm]	347,41
	I[mm^4]	15002572458
Concrete + hole strands	A[mm^2]	192916
	a_{bottom}[mm]	404,65
	a_{top}[mm]	345,35
	I[mm^4]	14841268661
Concrete + 16 strands	EA[$^N/_{mm^2} \cdot mm^2$]*	8008381808
	a_{bottom}[mm]	394,13
	a_{top}[mm]	355,87
	EI[$^N/_{mm^2} \cdot mm^4$]*	6,24·10^{14}
Concrete + 10 strands	EA[$^N/_{mm^2} \cdot mm^2$]*	7907275880
	a_{bottom}[mm]	397,67
	a_{top}[mm]	352,33
	EI[$^N/_{mm^2} \cdot mm^4$]*	6,16·10^{14}

* E based on concrete mixture of HAP1

Table 4.1: Cross-sectional properties

Material properties
A number of parameters are known from the experiments. From these known parameters the unknown parameters are calculated, according to the Eurocode. In this case it is only about concrete properties. The property f_{cm} can be calculated according formula 4.1.

$$f_{cm} = f_{ck} + 4N/mm^2 \tag{4.1}$$

where:

f_{cm} = the mean concrete compressive strength
f_{ck} = the characteristic concrete compressive strength

In formula 4.2 the expression to calculate f_{ctm}. This expression is only valid for concrete mixtures >C50/60.

$$f_{ctm} = 2,12ln\left(1 + \frac{f_{cm}}{10}\right) \tag{4.2}$$

where:

f_{ctm} = the mean concrete tensile strength
f_{cm} = the mean concrete cylindrical compressive strength

In formula 4.3 the expression to calculate f_{ctm}. This expression is only valid for concrete mixtures <C50/60.

$$f_{ctm} = 0,30 f_{ck}^{\frac{2}{3}} \tag{4.3}$$

where:

f_{ctm} = the mean concrete tensile strength
f_{ck} = the characteristic concrete compressive strength

In formula 4.4 the expression to calculate f_{ctk}.

$$f_{ctk} = 0,7 f_{ctm} \tag{4.4}$$

where:

f_{ctk} = the characteristic concrete tensile strength
f_{cm} = the mean concrete tensile strength

In formula 4.5 the expression to calculate $f_{ctm,fl}$.

$$f_{ctm,fl} = max\{\left(1,6 - \frac{h}{1000}\right) f_{ctm}; f_{ctm}\} \tag{4.5}$$

where:

h = the height of the element, in mm
f_{ctm} = the mean concrete tensile strength
$f_{ctm,fl}$ = the mean concrete flexural tensile strength

4.1.2. Analytical analysis

In this section the analytical results per beam will be discussed. In each coming section first the scheme and other conditions are given, then attention is paid to the stress states in the web.

HAP1E

In figure 4.4 the load scheme of HAP1E is schematized. In table 4.2 an overview of the applicable concrete parameters, the present external loads and the present prestress. The f_{cm} = 99 N/mm^2 was already known

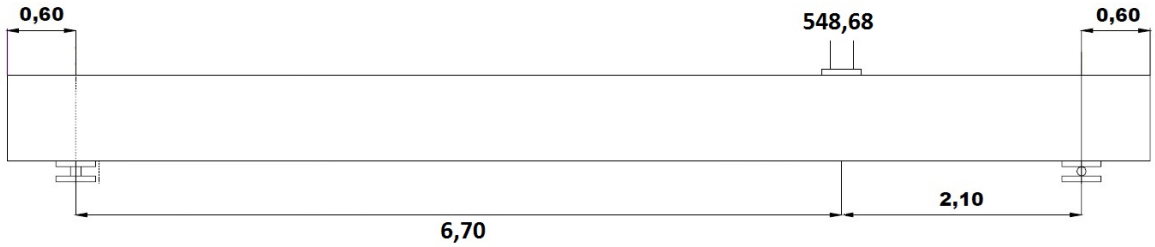

Figure 4.4: The load scheme HAP1E, dimensions in m and force in kN

from the Choulli study, see section 3.1. As described in the previous section, the parameter f_{ctm} can be calculated out of f_{cm}, $f_{ctm} = 2,12 ln\left(1 + \frac{99}{10}\right)$ = 5,06 N/mm^2. The q_{weight} = 25·0,1945 = 4,8625 kN/m. The F_{prestr} = 9,56·194500·10^{-3} = 1859 kN, $F_{prestr/strand}$ = 1859/16 = 116 kN and $\sigma_{p,strand}$ = 116·10^3 / 99 = 1173,88 N/mm^2. The $f_{ctm,fl}$ = max $\{\left(1,6 - \frac{750}{1000}\right) \cdot 5,06; 5,06\}$ = 5,06 N/mm^2.

Type parameter	Parameter	Value
Concrete property	$\rho_{density}[^{kN}/_{m^3}]$	25
	$f_{cm}[^{N}/_{mm^2}]^{*}$	99
	$f_{ctm,fl}[^{N}/_{mm^2}]^{**}$	5,06
	$f_{ctm}[^{N}/_{mm^2}]^{**}$	5,06
Loads	F_1[kN]*	548,68
	q_{weight}[kN/m]**	4,8625
Prestress	$\sigma_{cp}[^{N}/_{mm^2}]^{*}$	9,56
	A_{strand}[mm^2]*	99
	F_{prestr}[kN]**	1859
	$F_{prestr/strand}$[kN]**	116
	$\sigma_{p,strand}[^{N}/_{mm^2}]^{**}$	1173,88

* based on obtained data, see section 3.1
** based on calculated data

Table 4.2: Applicable concrete parameters, external loads and present prestress HAP1E

Results
In this part the results will be discussed. In appendix "Choulli: Shear forces and Moments" of the appendix report there is added the distribution of the shear force and the moment, caused by the loads of table 4.2. This is on the interval of 7300 mm to 9400 mm, from the start of the beam, see figure 4.4. In appendix "Choulli: Analytical results" of the appendix report there is added an excel sheet, containing data of σ_{xx}, τ_{xy} and σ_1 and σ_2. The σ_{xx} consists of the loads and the prestress, the τ_{xy} of the loads. The colomn "Rela. to n" refers to the location in the height in the web relative to the neutral axis, with the exception of the upper en bottom line, this is the distance to the ultimate fiber. The colomn "S" refers to the statical moment on that specific height. This is again on the interval of 7300 mm to 9400 mm, from the start of the beam. The red color in the σ_1 colomn represent values > f_{ctm}, the yellow color values > 0,9f_{ctm}. From this sheet it can be seen that the analytical solution gives the highest principal stress at the transition point of flage-web at 7300 mm from the start of the beam, so below the external load. In figure 4.5 the distribution of the σ_{xx} and τ_{xy} at 8350 mm from start of the beam over the height of the beam, it can be seen that the highest τ_{xy} and the mean effective σ_{cp} is around the neutral axis.

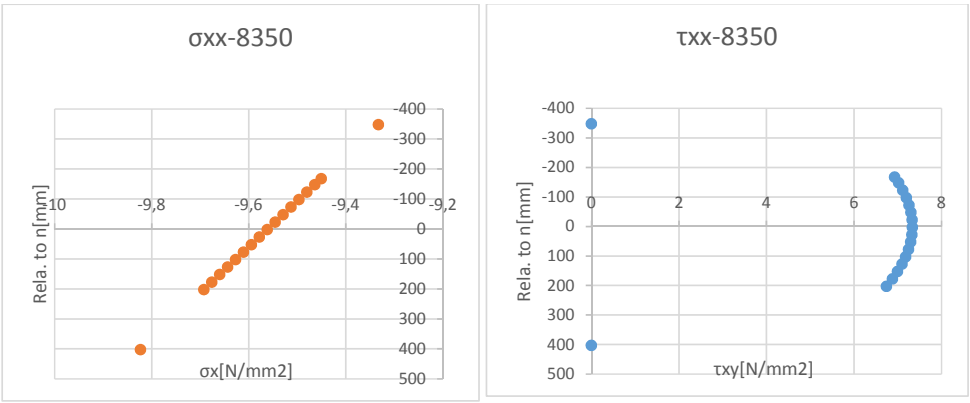

Figure 4.5: Chart of the σ_{xx} and τ_{xy} of HAP1E

A handcalculation of the transition point of flange-web at 7300 mm from the start of the beam. The σ_{xx} caused by the loads;

$$\frac{910,59 \cdot 10^6 \cdot 202,59}{15002572458} = 12,30 N/mm^2$$

The τ_{xy} caused by the loads;

$$\frac{428,929 \cdot 10^3 \cdot 23295951,2}{100 \cdot 15002572458} = 6,66 N/mm^2$$

The eccentrical moment caused by the prestress;

$$-116 \cdot 8 \cdot (0,402 - 0,050) - 116 \cdot 4 \cdot (0,402 - 0,1) - 116 \cdot 2 \cdot (0,402 - 0,15) + 116 \cdot 2 \cdot (0,347 - 0,090) = -467 kNm$$

The σ_{xx} caused by the eccentrical moment;

$$\frac{-467 \cdot 10^6 \cdot 202,59}{15002572458} = -6,30 N/mm^2$$

The mean effective σ_{cp} = -9,56 N/mm^2. So the principal tensile stress σ_1 will be;

$$\frac{12,30 - 6,30 - 9,56}{2} + \sqrt{\left(\frac{12,30 - 6,30 - 9,56}{2}\right)^2 + (6,66)^2} = 5,07 N/mm^2$$

So the principal compressive stress σ_2 will be;

$$\frac{12,30 - 6,30 - 9,56}{2} - \sqrt{\left(\frac{12,30 - 6,30 - 9,56}{2}\right)^2 + (6,66)^2} = -8,8 N/mm^2$$

According to the stress distribution of the analytical model this would be the critical point.

4.1.3. Numerical analysis

In this section the numerical results per beam will be discussed. The schemes and other conditions are the same as in the analytical analysis. First the specific input for the model is mentioned, then the results will be discussed per beam. In every point in the mesh 4 nodes of 4 elements come together, in case the width of the cross-section does not change, the values of these nodes do not differ much from each other. By the abrubt widening of the cross-section, the values of nodes can differ significantly, because a part of the elements can be in the wider zone. These elements will disturb the results. In table 4.3 an overview of the prestress as applied in DIANA. The values in the column "σ_p incl. losses" is the applied prestress in the strands.

Type prestress	**Layer**	**Strands[-]**	σ_p **excl. losses[N/mm^2]**	σ_p **incl. losses[N/mm^2]**
16 strands	1	8	1173	1273
	2	4	1173	1269
	3	2	1173	1264
	4	2	1173	1186
10 strands	1	8	1237	1314
	4	2	1237	1246

Table 4.3: Prestress as aplied in DIANA

HAP1E

First the numerical model in DIANA will be discussed. In figure 4.6 the meshed model of HAP1E, in figure 4.7 a more detailed figure of the right support and the plate of the external force. The elements can be seen clearly. The elements of the concrete are 25mm×25mm and the elements of the steel plates are 25mm×20mm. Further the prestress cables can be seen clearly. In table 4.4 all parameters used in the model, this table forms an addition to the already known parameters.

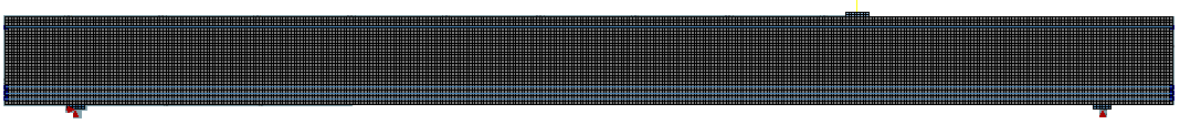

Figure 4.6: The meshed beam HAP1E

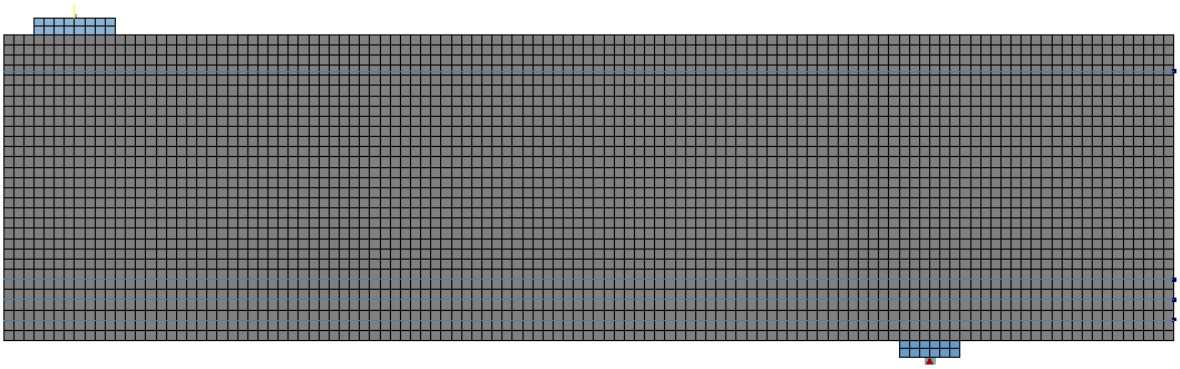

Figure 4.7: Detail of meshed beam HAP1E

Object	Parameter	Value
Concrete beam	E[$^N/_{mm^2}$]	39788
	h_{beam}[mm]	750
	l_{beam}[mm]	10000
	b_{beam}[m]	variable
	$\nu_{concrete}$[-]	0,2
Steel plate support	E[$^N/_{mm^2}$]	210000
	h_{plate}[mm]	40
	l_{plate}[mm]	150
	b_{plate}[mm]	150
	$\rho_{density}$[$^{kN}/_{m^3}$]	78,5
	ν_{steel}[-]	0,3
Steel plate force	E[$^N/_{mm^2}$]	210000
	h_{plate}[mm]	40
	l_{plate}[mm]	200
	b_{plate}[mm]	200
	$\rho_{density}$[$^{kN}/_{m^3}$]	78,5
	ν_{steel}[-]	0,3
Prestress cables	E[$^N/_{mm^2}$]	195000
	Yield stress[$^N/_{mm^2}$]	1522

Table 4.4: Parameters HAP1E used in DIANA

As described before to compare the numerical results with the analytical results, the numerical results have to be exported in a way it is possible to compare it with the analytical results. In every point in the mesh 4 nodes of 4 elements come together, this means 4 results per node. In case of a constant width of the cross-section the results of the different stresses almost equal each other. In this case the average has been taken, see figure 4.8. In case of a abrupt widening of the cross-section, around the transion of web to flange, the results of τ_{xy} differ significantly. In this case the nodes are located at the transition of web to flange. In figure 4.9 an example of an element row around the lower transition of web to flange. The green elements are located in the web, while the red elements are located in the widened. The results of the elements of τ_{xy} located in the widened part were significantly lower(20 to 30%), for the sake of realism this results of these elements are left out.

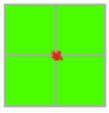

Figure 4.8: Coming together of 4 nodes of 4 elements

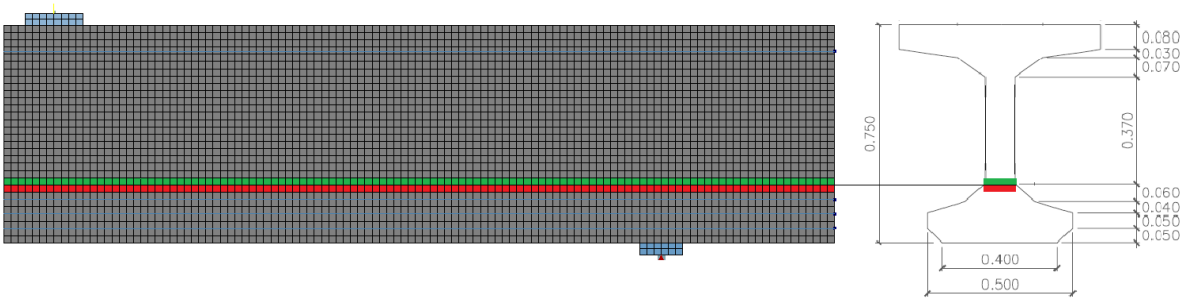

Figure 4.9: Elements around transition web to flange HAP1E

On large scale, a Python script is used to export the numerical results in an excel sheet. In this way it is possible to compare the numerical results with the analytical results.

Verification

In order to link the analytical model to the numerical model a verification is done. This verification is done by comparing different results, like σ_{xx}, τ_{xy} and the principal stress σ_1. Good use can be made of the different fractions as described in section 4.1.1. In figure 4.10 the results of the fraction of $\frac{\tau_{xy,Analytical}}{\tau_{xy,Numerical}}$, in figure 4.11 the results of the fraction $\frac{\sigma_{1,Analytical}}{\sigma_{1,Numerical}}$. These tables are on the interval of 8275 mm to 8675 mm, from the start of the beam. Again the colomn "Plaats n" refers to the location of the height in the web relative to the neutral axis, with the exception of the upper en bottom line, this is the distance to the ultimate fiber.

	Plaats n	8275	8300	8325	8350	8375	8400	8425	8450	8475	8500	8525	8550	8575	8600	8625	8650	8675
τxy(Con.) Analytical τxy Numerical	-347,41	0	0	0	0	0	0	0	0	0	0	0	0	0	0	0	0	0
	-167,41	1,078297	1,075526	1,072744	1,069963	1,067196	1,064454	1,061749	1,059094	1,056504	1,053996	1,051594	1,049324	1,047218	1,045318	1,043669	1,042328	1,041361
	-147,41	1,048469	1,046075	1,043663	1,041246	1,038837	1,036447	1,034088	1,031772	1,029514	1,027333	1,025247	1,023284	1,021474	1,019854	1,018467	1,017366	1,016612
	-122,41	1,012086	1,010107	1,008103	1,006087	1,004074	1,002072	1,000095	0,998155	0,996267	0,994446	0,992712	0,99109	0,989608	0,988298	0,987202	0,986366	0,985847
	-97,412	1,010415	1,008783	1,007123	1,005447	1,003766	1,002092	1,000436	0,998811	0,997228	0,995704	0,994258	0,99291	0,991686	0,990617	0,98974	0,989098	0,988742
	-72,412	1,008613	1,007335	1,006027	1,004699	1,003363	1,002028	1,000704	0,999401	0,998132	0,99691	0,99575	0,994671	0,993696	0,992852	0,992169	0,991687	0,99145
	-47,412	1,006698	1,005775	1,004823	1,00385	1,002865	1,001876	1,000892	0,999919	0,998968	0,99805	0,997177	0,996364	0,995629	0,994995	0,994487	0,994137	0,993982
	-22,412	1,00468	1,004111	1,003516	1,002901	1,002272	1,001634	1,000994	1,000356	0,999727	0,999115	0,998529	0,99798	0,997481	0,997047	0,996699	0,99646	0,996361
	2,58783	1,002565	1,002348	1,002109	1,001853	1,001581	1,001297	1,001004	1,000704	1,000401	1,000099	0,999802	0,999516	0,99925	0,999012	0,998815	0,998676	0,998614
	27,5878	1,000354	1,000484	1,0006	1,000701	1,000787	1,000858	1,000914	1,000956	1,000982	1,000992	1,000988	1,000969	1,000938	1,000897	1,00085	1,000805	1,000772
	52,5878	0,998043	0,998517	0,998984	0,99944	0,999882	1,000309	1,000716	1,001101	1,001459	1,001787	1,00208	1,002334	1,002544	1,002705	1,002815	1,002869	1,002869
	77,5878	0,995628	0,99644	0,997253	0,998061	0,998857	0,999638	1,000396	1,001125	1,001819	1,002469	1,003067	1,003602	1,004063	1,00444	1,004718	1,004887	1,004934
	102,587	0,9931	0,994244	0,995398	0,996552	0,997698	0,998829	0,999936	1,001011	1,002043	1,00302	1,003931	1,004758	1,005486	1,006095	1,006563	1,00687	1,00699
	127,587	0,990449	0,991919	0,993406	0,994899	0,996388	0,997863	0,999316	1,000734	1,002106	1,003416	1,004647	1,00578	1,006791	1,007655	1,008341	1,008818	1,00905
	152,587	0,987667	0,989453	0,991262	0,993082	0,994904	0,996716	0,998507	1,000265	1,001975	1,00362	1,00518	1,006631	1,007945	1,00909	1,010028	1,010718	1,011111
	177,587	0,984742	0,98683	0,988948	0,991082	0,993222	0,995356	0,997475	0,999563	1,001607	1,003586	1,005481	1,007262	1,008899	1,010354	1,011583	1,012533	1,013147
	202,587	0,972656	0,974869	0,977113	0,979376	0,981647	0,983916	0,986171	0,9884	0,990586	0,992711	0,994753	0,996683	0,998469	1,000071	1,001441	1,002525	1,00326
	402,587	0	0	0	0	0	0	0	0	0	0	0	0	0	0	0	0	0

Figure 4.10: Fraction $\frac{\tau_{xy,Analytical}}{\tau_{xy,Numerical}}$ of HAP1E

		8275	8300	8325	8350	8375	8400	8425	8450	8475	8500	8525	8550	8575	8600	8625	8650	8675
σ1(Con.) Analytical σ1 Numerical(σxx τxy σyy)	-347,41	0	0	0	0	0	0	0	0	0	0	0	0	0	0	0	0	0
	-167,41	1,101014	1,096358	1,091814	1,087387	1,083086	1,078931	1,074953	1,07119	1,067691	1,064519	1,061744	1,059453	1,057745	1,056737	1,05656	1,057366	1,05933
	-147,41	1,050768	1,046923	1,043196	1,039586	1,036101	1,032762	1,029597	1,026646	1,023961	1,021603	1,019649	1,018186	1,017317	1,017163	1,017859	1,019564	1,022458
	-122,41	0,995865	0,992748	0,989756	0,986887	0,984148	0,981558	0,979145	0,976945	0,975009	0,973397	0,97218	0,971446	0,971292	0,971837	0,973212	0,975573	0,979096
	-97,412	0,994917	0,992177	0,989578	0,987115	0,984795	0,982634	0,980659	0,978907	0,977429	0,976285	0,975548	0,975308	0,975665	0,97674	0,978671	0,981617	0,985764
	-72,412	0,993887	0,991524	0,989318	0,987261	0,985358	0,983621	0,982077	0,980762	0,979725	0,979027	0,978742	0,978959	0,979782	0,981332	0,983752	0,987206	0,991884
	-47,412	0,992782	0,990794	0,988979	0,987326	0,985834	0,984515	0,983392	0,982501	0,981887	0,981612	0,981749	0,982386	0,983628	0,985599	0,988442	0,992326	0,997447
	-22,412	0,991602	0,989989	0,988563	0,987309	0,986223	0,985313	0,984601	0,984118	0,983909	0,984033	0,984562	0,985583	0,9872	0,989538	0,992742	0,996981	1,002456
	2,58783	0,990346	0,989107	0,988068	0,987209	0,986523	0,986014	0,985701	0,985612	0,985789	0,986289	0,987181	0,988551	0,990501	0,993156	0,996659	1,001183	1,006928
	27,5878	0,98901	0,988146	0,987492	0,987025	0,986733	0,986617	0,986692	0,986983	0,987529	0,988382	0,98961	0,991296	0,993541	0,996465	1,000211	1,004952	1,010888
	52,5878	0,987586	0,987101	0,986832	0,986754	0,986851	0,987121	0,987573	0,988231	0,989128	0,990315	0,991855	0,993828	0,996331	0,999481	1,00342	1,008316	1,014369
	77,5878	0,986071	0,985967	0,986085	0,986394	0,986875	0,987523	0,988343	0,989355	0,99059	0,992092	0,993922	0,996156	0,998885	1,002224	1,00631	1,011307	1,017413
	102,587	0,98446	0,984743	0,985247	0,98594	0,986801	0,987819	0,988998	0,990353	0,991911	0,993713	0,995815	0,998286	1,001216	1,004713	1,008907	1,01396	1,020061
	127,587	0,98275	0,983423	0,984315	0,985389	0,986623	0,988004	0,989531	0,991218	0,993086	0,995173	0,99753	1,000221	1,00333	1,006959	1,011233	1,016304	1,022357
	152,587	0,980941	0,982007	0,983283	0,984733	0,986332	0,988065	0,98993	0,991936	0,994101	0,99646	0,999058	1,001954	1,005227	1,008971	1,013303	1,018368	1,024341
	177,587	0,979037	0,980493	0,982148	0,983964	0,985915	0,987987	0,990174	0,992484	0,994932	0,997549	1,000375	1,003466	1,006891	1,01074	1,015121	1,020168	1,026047
	202,587	0,966838	0,968441	0,97022	0,972143	0,974184	0,976326	0,978564	0,980897	0,983336	0,9859	0,988617	0,991525	0,994674	0,998126	1,001961	1,006275	1,011189
	402,587	0	0	0	0	0	0	0	0	0	0	0	0	0	0	0	0	0

Figure 4.11: Fraction $\frac{\sigma_{1,Analytical}}{\sigma_{1,Numerical}}$ of HAP1E

σxx(Con.) Analytical σxx Numerical	8275	8300	8325	8350	8375	8400	8425	8450	8475	8500	8525	8550	8575	8600	8625	8650	8675
-347,41	1,030938	1,030515	1,030293	1,030283	1,0305	1,030961	1,031689	1,032709	1,034054	1,035761	1,037874	1,040445	1,043535	1,047214	1,051565	1,056685	1,062685
-167,41	0,995397	0,995946	0,99633	0,996546	0,996591	0,99646	0,996148	0,995646	0,994948	0,994042	0,992918	0,991566	0,989972	0,988125	0,986013	0,983624	0,980948
-147,41	0,989669	0,990306	0,990756	0,991017	0,991084	0,990953	0,990619	0,990076	0,989318	0,988337	0,987127	0,985682	0,983994	0,982058	0,979871	0,977429	0,974733
-122,41	0,982395	0,983137	0,983673	0,983999	0,984112	0,984008	0,983682	0,983131	0,982353	0,981344	0,980102	0,978628	0,976923	0,974991	0,972836	0,97047	0,967904
-97,412	0,975543	0,976397	0,977031	0,977442	0,977625	0,977577	0,977296	0,97678	0,976029	0,975045	0,973831	0,972392	0,970736	0,968874	0,966821	0,964595	0,962219
-72,412	0,969223	0,970197	0,970943	0,971456	0,971731	0,971766	0,97156	0,971114	0,970431	0,969515	0,968373	0,967015	0,965455	0,963708	0,961797	0,959747	0,957589
-47,412	0,963449	0,964554	0,965423	0,966053	0,966438	0,966579	0,966475	0,966128	0,965543	0,964728	0,963692	0,962449	0,961017	0,959415	0,95767	0,955814	0,953882
-22,412	0,958229	0,959473	0,960477	0,961237	0,96175	0,962015	0,962032	0,961807	0,961346	0,960657	0,959752	0,958649	0,957366	0,955927	0,954361	0,952704	0,950995
2,58783	0,953564	0,954955	0,956104	0,957007	0,95766	0,958064	0,958221	0,958136	0,957817	0,957273	0,956519	0,955571	0,954452	0,953186	0,951804	0,950344	0,948845
27,5878	0,949448	0,950995	0,952298	0,953353	0,954158	0,954714	0,955025	0,955095	0,954932	0,954549	0,953959	0,953179	0,952233	0,951145	0,949946	0,948674	0,947371
52,5878	0,945873	0,947581	0,949045	0,950261	0,951227	0,951946	0,952421	0,952659	0,952666	0,952455	0,95204	0,951438	0,95067	0,949762	0,948744	0,947652	0,946526
77,5878	0,942825	0,9447	0,946329	0,947712	0,948848	0,949738	0,950387	0,950802	0,95099	0,950962	0,950731	0,950315	0,949732	0,949006	0,948166	0,947245	0,946281
102,587	0,940287	0,94233	0,944129	0,945683	0,946993	0,948062	0,948894	0,949495	0,949873	0,950038	0,950002	0,949779	0,949387	0,948848	0,948185	0,94743	0,946616
127,587	0,938236	0,940447	0,942416	0,944144	0,945633	0,946886	0,947909	0,948706	0,949284	0,949653	0,949821	0,949802	0,94961	0,949263	0,948782	0,948192	0,947524
152,587	0,936644	0,93902	0,941158	0,94306	0,944731	0,946174	0,947394	0,948396	0,949185	0,949769	0,950156	0,950353	0,950374	0,950231	0,94994	0,949523	0,949002
177,587	0,935478	0,938012	0,940315	0,942391	0,944245	0,945882	0,947306	0,948523	0,949536	0,950349	0,950969	0,9514	0,951651	0,951729	0,951646	0,951416	0,951055
202,587	0,934403	0,937088	0,939552	0,941802	0,943843	0,945682	0,947322	0,948767	0,95002	0,951085	0,951962	0,952656	0,953169	0,953505	0,95367	0,953672	0,953521
402,587	0,912773	0,91664	0,920504	0,924365	0,928226	0,932092	0,935966	0,939854	0,94376	0,947689	0,951649	0,955643	0,959677	0,963754	0,967877	0,972046	0,976258

Figure 4.12: Fraction $\frac{\sigma_{xx,Analytical}}{\sigma_{xx,Numerical}}$ of HAP1E

From figures 4.10 and 4.11 it can be seen that in this part of the beam the results of the analytical analysis correspond to the results of the numerical analysis. All parts had a similar result, except around the disturbed areas around the external force, the supports and the anchoring of the prestress. From figure 4.12 it can be seen that there is a little deviation in the results of the σ_{xx}. After analysis it appears that this deviation is not caused by the prestress part, because the fraction $\frac{\sigma_{xx;Analytical;pre}}{\sigma_{xx;Numerical;pre}} < 1\%$. It appears that the deviation is caused by the part of the external force. There is also checked wether the Poisson's ratio had a significant influence on the deviation, this was not the case. For this beam it comes down to a difference of 5%, so <0,9 N/mm^2.

Results

From the numerical results it can be seen that the component σ_{yy} has a local significant effect on the stress state in a beam, this effect is limited to the location of the external load and the support reaction respectively. In figure 4.13 the the results of σ_{yy}, around the external force. The σ_{yy} has influence from 7300 mm(location external load) up till 7900 mm, from start of the beam. The influence is low in the bottom part the of the web, at 202,58 mm relative to the neutral axis. In figure 4.15 the contour plot of σ_{yy}.

σyy Load+ Weight+ Prestress	Plaats n	7300	7300	7325	7350	7375	7400	7425	7450	7475	7500	7525	7550	7575	7600	7625	7650	7675	7700
-347,412	-31,1171	-31,1171	-10,6177	1,833525	-3,11038	-17,6952	-1,62795	-0,74827	-0,21891	-0,17797	-0,1188	-0,09303	-0,07137	-0,05622	-0,04477	-0,03639	-0,03023	-0,02576
-167,412	-6,33824	-6,33824	-6,37543	-6,45577	-6,52256	-6,49992	-6,32418	-5,97115	-5,46563	-4,86662	-4,23842	-3,63142	-3,07385	-2,5774	-2,14334	-1,76828	-1,44688	-1,17324
-147,412	-7,07486	-7,07486	-7,09563	-7,13337	-7,14283	-7,06733	-6,85942	-6,50006	-6,00497	-5,41599	-4,78471	-4,15624	-3,56212	-3,01949	-2,5352	-2,10963	-1,73982	-1,4212
-122,412	-6,87905	-6,87905	-6,88236	-6,87633	-6,83379	-6,72068	-6,50879	-6,18608	-5,76079	-5,25807	-4,7114	-4,15382	-3,61174	-3,10304	-2,63773	-2,21999	-1,85016	-1,52631
-97,4122	-6,41736	-6,41736	-6,41048	-6,38006	-6,31045	-6,18222	-5,97916	-5,6943	-5,33249	-4,90913	-4,44602	-3,96631	-3,49051	-3,03434	-2,60831	-2,2184	-1,86716	-1,55474
-72,4122	-5,95931	-5,95931	-5,94727	-5,90496	-5,8235	-5,69182	-5,50082	-5,24678	-4,93313	-4,57003	-4,17227	-3,75638	-3,33807	-2,93046	-2,54334	-2,18322	-1,8538	-1,55663
-47,4122	-5,51201	-5,51201	-5,49767	-5,45064	-5,36592	-5,23738	-5,06009	-4,83243	-4,55723	-4,2417	-3,89632	-3,53318	-3,16435	-2,80054	-2,45039	-2,12023	-1,81421	-1,53467
-22,4122	-5,07879	-5,07879	-5,06376	-5,01605	-4,9329	-4,81105	-4,64809	-4,4437	-4,20043	-3,92373	-3,62135	-3,30239	-2,97622	-2,65153	-2,33573	-2,03465	-1,75247	-1,4919
2,587832	-4,66079	-4,66079	-4,646	-4,59983	-4,52085	-4,4075	-4,25883	-4,07532	-3,85934	-3,61523	-3,34896	-3,06757	-2,77842	-2,4886	-2,20438	-1,93096	-1,67233	-1,43129
27,58783	-4,25796	-4,25796	-4,24391	-4,20046	-4,12699	-4,02289	-3,88808	-3,7235	-3,53136	-3,31525	-3,07992	-2,83095	-2,57424	-2,31559	-2,0603	-1,81294	-1,57715	-1,3557
52,58783	-3,86958	-3,86958	-3,85652	-3,81639	-3,749	-3,65432	-3,53276	-3,38545	-3,21448	-3,02289	-2,81455	-2,59399	-2,36601	-2,13539	-1,90664	-1,68369	-1,46986	-1,26773
77,58783	-3,49455	-3,49455	-3,4826	-3,44602	-3,3849	-3,29948	-3,19045	-3,05902	-2,90711	-2,73733	-2,55293	-2,35762	-2,15538	-1,9502	-1,74586	-1,54581	-1,35298	-1,16975
102,5878	-3,13154	-3,13154	-3,12074	-3,08779	-3,03287	-2,95642	-2,85922	-2,74247	-2,60793	-2,45787	-2,29502	-2,12249	-1,94359	-1,76169	-1,58	-1,40148	-1,22873	-1,0639
127,5878	-2,77913	-2,77913	-2,76949	-2,74011	-2,69126	-2,62343	-2,53741	-2,43435	-2,31584	-2,18384	-2,04069	-1,889	-1,73156	-1,57121	-1,41069	-1,25255	-1,09906	-0,95214
152,5878	-2,43579	-2,43579	-2,42729	-2,40142	-2,35846	-2,29891	-2,22352	-2,13337	-2,02984	-1,91465	-1,78978	-1,65746	-1,52002	-1,37988	-1,23936	-1,10065	-0,96572	-0,83626
177,5878	-2,09992	-2,09992	-2,09254	-2,07011	-2,03288	-1,98133	-1,91615	-1,83831	-1,749	-1,6497	-1,54209	-1,42805	-1,30956	-1,18863	-1,06724	-0,94725	-0,83034	-0,71799
202,5878	-1,59971	-1,59971	-1,59403	-1,57682	-1,54829	-1,50881	-1,45895	-1,39945	-1,33123	-1,25542	-1,17329	-1,08624	-0,99577	-0,90339	-0,81059	-0,71877	-0,62922	-0,54307
402,5878	0,099771	0,099771	0,099001	0,097992	0,096748	0,095274	0,093578	0,091672	0,089565	0,087273	0,084811	0,082194	0,079439	0,076565	0,07359	0,070531	0,067407	0,064236

Figure 4.13: Numerical σ_{yy} of HAP1E

From the results it also can be seen that τ_{xy} is disturbed around the external load and the support reaction, the disturbance around the external load runs from 7300 mm up till around 7750 mm. In figure 4.14 the results of the fraction $\frac{\tau_{xy,Analytical}}{\tau_{xy,Numerical}}$ around the external load. In figure 4.16 the contour plot of τ_{xy}.

τxy(Con.) Analytical τxy Numerical	Plaats n	7300	7300	7325	7350	7375	7400	7425	7450	7475	7500	7525	7550	7575	7600	7625	7650	7675	7700
	-347,412	0	0	0	0	0	0	0	0	0	0	0	0	0	0	0	0	0	0
	-167,412	-0,8317	2,979007	2,511602	2,137466	1,822144	1,562041	1,358459	1,208204	1,103656	1,035548	0,994971	0,974293	0,967407	0,96967	0,977708	0,989135	1,002288	1,016011
	-147,412	-0,8089	2,897358	2,441134	2,08589	1,794304	1,556199	1,368531	1,227231	1,125861	1,056842	1,012756	0,987104	0,974588	0,971111	0,973637	0,979968	0,988536	0,99822
	-122,412	-0,78107	2,797655	2,355334	2,021899	1,757607	1,545631	1,377811	1,248299	1,151418	1,081428	1,03286	1,00083	0,981208	0,970647	0,966529	0,966853	0,97012	0,97521
	-97,4122	-0,78027	2,7948	2,36079	2,03752	1,78558	1,585496	1,426651	1,302075	1,206197	1,13407	1,081222	1,043687	1,018062	1,001507	0,991717	0,986866	0,985523	0,986587
	-72,4122	-0,77953	2,792129	2,370965	2,057656	1,815023	1,623102	1,470306	1,34911	1,253954	1,180304	1,124274	1,082496	1,052079	1,030578	1,015964	1,006583	1,001105	0,998472
	-47,4122	-0,77878	2,789461	2,382795	2,079011	1,843842	1,657853	1,509274	1,390393	1,295682	1,220845	1,162356	1,117238	1,082958	1,05737	1,038672	1,025368	1,016231	1,010263
	-22,4122	-0,77801	2,786685	2,394588	2,099726	1,870809	1,689362	1,543837	1,426558	1,332071	1,256245	1,195789	1,147987	1,110559	1,081583	1,059435	1,042757	1,030416	1,021479
	2,587832	-0,77718	2,783728	2,405408	2,118745	1,895195	1,717378	1,574151	1,458001	1,363585	1,286905	1,224835	1,174841	1,134825	1,103029	1,077971	1,058405	1,043283	1,031733
	27,58783	-0,77629	2,780536	2,414736	2,135458	1,91656	1,741728	1,600293	1,48496	1,390521	1,313097	1,249684	1,197883	1,155726	1,12158	1,094073	1,07205	1,054536	1,040712
	52,58783	-0,77532	2,777064	2,422278	2,149507	1,934626	1,762286	1,622284	1,507561	1,413052	1,334983	1,270451	1,217155	1,173229	1,137131	1,107575	1,083479	1,06393	1,048154
	77,58783	-0,77426	2,773272	2,427859	2,160663	1,949197	1,778933	1,640091	1,52584	1,431246	1,352632	1,287177	1,232656	1,187279	1,149576	1,118327	1,092507	1,071252	1,053832
	102,5878	-0,7731	2,769119	2,431355	2,168752	1,960101	1,791537	1,653632	1,539753	1,445083	1,366028	1,299832	1,24433	1,197788	1,158793	1,126174	1,098954	1,076308	1,057538
	127,5878	-0,77183	2,764562	2,432651	2,17361	1,967158	1,799928	1,662762	1,54918	1,454461	1,375074	1,308313	1,252059	1,204622	1,164629	1,130947	1,102635	1,0789	1,059072
	152,5878	-0,77043	2,759555	2,431618	2,175046	1,97015	1,803883	1,667267	1,553923	1,459193	1,37959	1,312444	1,255666	1,207596	1,166891	1,132447	1,103348	1,078827	1,058232
	177,5878	-0,76889	2,754043	2,428092	2,172823	1,968799	1,803111	1,666855	1,553697	1,459006	1,379315	1,31197	1,254901	1,206467	1,165341	1,130439	1,100865	1,075865	1,054806
	202,5878	-0,75982	2,721542	2,399571	2,147393	1,945821	1,782104	1,647445	1,535585	1,441947	1,363102	1,296431	1,239891	1,191864	1,151045	1,116369	1,086955	1,062066	1,04108
	402,5878	0	0	0	0	0	0	0	0	0	0	0	0	0	0	0	0	0	0

Figure 4.14: Fraction $\frac{\tau_{xy,Analytical}}{\tau_{xy,Numerical}}$ of HAP1E

The maximum τ_{xy} = 7,31 N/mm^2(8350 mm), around the neutral axis, this falls back to 3,01 N/mm^2(7325 mm), see also appendix “Choulli: Numerical results” of the appendix report.

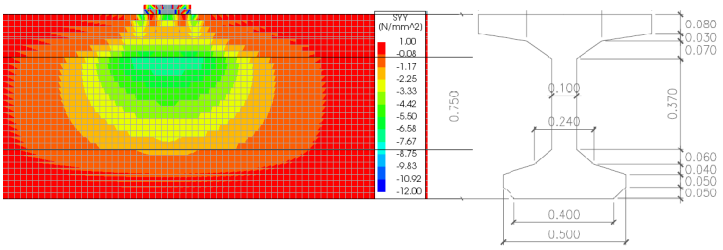

Figure 4.15: Contour plot σ_{yy} of HAP1E

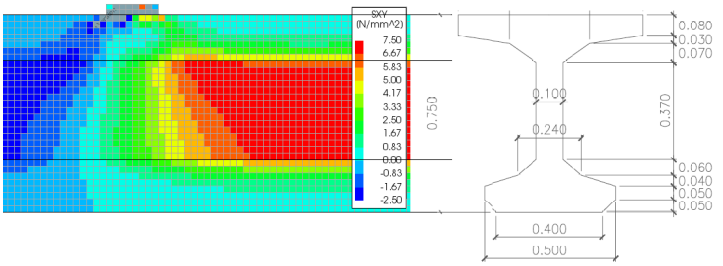

Figure 4.16: Contour plot τ_{xy} of HAP1E

In figure 4.17 the fraction $\frac{\sigma_{xx,Analytical}}{\sigma_{xx,Numerical}}$, it can be seen that there is also a deviation of σ_{xx} around the external load. As described before the σ_{xx} consists out of the contributions of the external load, the weight and the prestress. After analysis it appears that the deviation is caused by the external load part. This can be seen in figure 4.17, in the part below the neutral axis the value of the fraction drops towards 0,60-0,70 and in the part above the neutral axis the value of the fraction rises towards 1,25-1,30. The drop to 0,60-0,70 means that the value of $\sigma_{xx,Analytical}$ related to $\sigma_{xx,Numerical}$ is too high, this is caused by the tensional part of $\sigma_{xx,Analytical}$. The rise to 1,25-1,30 means that the value of $\sigma_{xx,Analytical}$ related to $\sigma_{xx,Numerical}$ is too low, this is caused by the compressional part of $\sigma_{xx,Analytical}$. This means that the part of $\sigma_{xx,Analytical}$ that is caused by the external force is too high.

σxx(Con.) Analytical σxx Numerical	Plaats n	7300	7300	7325	7350	7375	7400	7425	7450	7475	7500	7525	7550	7575	7600	7625	7650	7675	7700
	-347,412	0,678901	0,678901	0,654616	0,530416	0,408807	0,381476	0,618801	0,802361	0,882245	0,928493	0,963804	0,991396	1,01321	1,030086	1,042819	1,052099	1,05855	1,06272
	-167,412	1,338209	1,338209	1,335102	1,334465	1,331056	1,318562	1,292544	1,253187	1,20527	1,155458	1,109427	1,070305	1,038989	1,014923	0,996993	0,983996	0,974872	0,968753
	-147,412	1,298503	1,298503	1,294432	1,290741	1,284222	1,27103	1,248584	1,216929	1,178809	1,138405	1,099651	1,065243	1,036404	1,013265	0,995318	0,981806	0,971945	0,965028
	-122,412	1,263131	1,263131	1,258677	1,253184	1,244845	1,231575	1,211988	1,186141	1,155609	1,122902	1,090632	1,060847	1,034779	1,012904	0,995166	0,981204	0,970529	0,962634
	-97,4122	1,231109	1,231109	1,226874	1,220892	1,212149	1,19949	1,182181	1,160321	1,134913	1,107586	1,080135	1,054115	1,030611	1,010211	0,993089	0,979136	0,968082	0,959586
	-72,4122	1,196509	1,196509	1,19286	1,187158	1,178843	1,167298	1,152164	1,13358	1,112242	1,089257	1,065893	1,043324	1,022458	1,003879	0,987867	0,974467	0,963562	0,954945
	-47,4122	1,159349	1,159349	1,156551	1,151618	1,144255	1,134152	1,121167	1,105467	1,087569	1,068261	1,048466	1,029076	1,010834	0,994272	0,979706	0,967264	0,956934	0,948606
	-22,4122	1,119503	1,119503	1,117764	1,113938	1,107879	1,099453	1,088639	1,075618	1,060791	1,044748	1,028177	1,011764	0,996113	0,981689	0,968806	0,957632	0,948219	0,940528
	2,587832	1,076739	1,076739	1,076247	1,073785	1,069293	1,062732	1,054146	1,043715	1,031765	1,018747	1,005188	0,991626	0,978549	0,966356	0,95534	0,945682	0,937471	0,930715
	27,58783	1,030741	1,030741	1,03168	1,030806	1,028102	1,023578	1,01731	1,009465	1,000311	0,990205	0,979556	0,96879	0,958302	0,948432	0,939442	0,931514	0,924751	0,919195
	52,58783	0,981112	0,981112	0,983681	0,98461	0,983903	0,981594	0,977766	0,972568	0,966221	0,959009	0,951254	0,943295	0,935453	0,928014	0,921208	0,915207	0,910121	0,906006
	77,58783	0,927374	0,927374	0,931793	0,934754	0,936266	0,936368	0,935139	0,932706	0,929249	0,924991	0,920188	0,915109	0,910016	0,905144	0,900694	0,89682	0,893631	0,891193
	102,5878	0,868954	0,868954	0,875479	0,880726	0,884704	0,887446	0,889017	0,889522	0,889101	0,887928	0,886204	0,88414	0,881946	0,879814	0,877914	0,876383	0,875322	0,874797
	127,5878	0,805177	0,805177	0,814107	0,821935	0,828662	0,834311	0,838933	0,842603	0,845428	0,847538	0,849085	0,850232	0,851141	0,851967	0,852849	0,853902	0,855216	0,856856
	152,5878	0,735245	0,735245	0,746935	0,757687	0,767495	0,776371	0,784344	0,791467	0,797811	0,803468	0,808546	0,813163	0,81744	0,821494	0,825434	0,829351	0,833321	0,8374
	177,5878	0,658221	0,658221	0,673094	0,687176	0,700456	0,712932	0,724619	0,735542	0,745744	0,755281	0,764221	0,772639	0,780616	0,788231	0,795561	0,802673	0,809621	0,816452
	202,5878	0,576159	0,576159	0,594785	0,612709	0,629916	0,6464	0,662159	0,677203	0,69155	0,705225	0,718264	0,730705	0,742593	0,753972	0,764887	0,775377	0,78548	0,795223
	402,5878	4,4928	4,4928	4,936211	6,02163	9,664994	-250,868	-5,02287	-1,65064	-0,55641	-0,03774	0,252831	0,431704	0,548664	0,628426	0,684558	0,725063	0,754926	0,777381

Figure 4.17: Fraction $\frac{\sigma_{xx,Analytical}}{\sigma_{xx,Numerical}}$ of HAP1E

Both σ_{yy} and τ_{xy} have a big influence on the principal stresses σ_1 and σ_2. In order to say something about the parameters a few points will be pointed out. The point at 7350 mm from start of the beam and 2,5878 mm relative to the neutral axis of the beam has a σ_{xx} = -8,83535 N/mm^2, σ_{yy} = -4,59983 N/mm^2 and τ_{xy} = 3,4224 N/mm^2, the analytical value at this point $\tau_{xy,Anal}$ = 7,286064 N/mm^2. The calculation of σ_1 without changed parameters;

$$\sigma_1 = \frac{-8,83535}{2} + \sqrt{\left(\frac{-8,83535}{2}\right)^2 + 7,286064^2} = 4,10 N/mm^2$$

The calculation of σ_1 with addition of σ_{yy};

$$\sigma_1 = \frac{-8,83535 - 4,59983}{2} + \sqrt{\left(\frac{-8,83535 + 4,59983}{2}\right)^2 + 7,286064^2} = 0,87 N/mm^2$$

The calculation of σ_1 with changed of τ_{xy};

$$\sigma_1 = \frac{-8,83535}{2} + \sqrt{\left(\frac{-8,83535}{2}\right)^2 + 3,422359^2} = 1,17056 N/mm^2$$

The point at 7575 mm from start of the beam and 202,5878 mm relative to the neutral axis of the beam has a σ_{xx} = -6,96189 N/mm^2, σ_{yy} = -0,99577 N/mm^2 and τ_{xy} = 5,605637 N/mm^2, the analytical value at this point $\tau_{xy,Anal}$ = 7,015 N/mm^2. The calculation of σ_1 without changed parameters;

$$\sigma_1 = \frac{-6,96189}{2} + \sqrt{\left(\frac{-6,96189}{2}\right)^2 + 7,015^2} = 4,3502 N/mm^2$$

The calculation of σ_1 with addition of σ_{yy};

$$\sigma_1 = \frac{-6,96189 - 0,99577}{2} + \sqrt{\left(\frac{-6,96189 + 0,99577}{2}\right)^2 + 7,015^2} = 3,644 N/mm^2$$

The calculation of σ_1 with changed of τ_{xy};

$$\sigma_1 = \frac{-6,96189}{2} + \sqrt{\left(\frac{-6,96189}{2}\right)^2 + 5,605637^2} = 3,11756 N/mm^2$$

The point at 7700 mm from start of the beam and 52,5878 mm relative to the neutral axis of the beam has a σ_{xx} = -9,50223 N/mm^2, σ_{yy} = -1,26773 N/mm^2 and τ_{xy} = 6,907612 N/mm^2, the analytical value at this point $\tau_{xy,Anal}$ = 7,309 N/mm^2. The calculation of σ_1 without changed parameters;

$$\sigma_1 = \frac{-9,50223}{2} + \sqrt{\left(\frac{-9,50223}{2}\right)^2 + 7,309^2} = 3,9664 N/mm^2$$

The calculation of σ_1 with addition of σ_{yy};

$$\sigma_1 = \frac{-9,50223 - 1,26773}{2} + \sqrt{\left(\frac{-9,50223 + 1,26773}{2}\right)^2 + 7,309^2} = 3,0 N/mm^2$$

The calculation of σ_1 with changed of τ_{xy};

$$\sigma_1 = \frac{-9,50223}{2} + \sqrt{\left(\frac{-9,50223}{2}\right)^2 + 6,907612^2} = 3,633 N/mm^2$$

The σ_{xx} has influence on the σ_1 as well. The point at 7900 mm from start of the beam and -47,4122 mm relative to the neutral axis of the beam has a σ_{xx} = -10,8848 N/mm^2, σ_{yy} = -0,19711 N/mm^2 and τ_{xy} = 7,205051 N/mm^2, the analytical value at this point $\sigma_{xx,Anal}$ = -10,1447 N/mm^2. The calculation of σ_1 without changed parameters;

$$\sigma_1 = \frac{-10,1447 - 0,19711}{2} + \sqrt{\left(\frac{-10,1447 + 0,19711}{2}\right)^2 + 7,205051^2} = 3,58417 N/mm^2$$

The calculation of σ_1 with changed of σ_{xx};

$$\sigma_1 = \frac{-10,8848 - 0,19711}{2} + \sqrt{\left(\frac{-10,8848 + 0,19711}{2}\right)^2 + 7,205051^2} = 3,4295 N/mm^2$$

The above examples show that the stress parameter τ_{xy} is more sensitive to changes, this is reflected in σ_1. Further it can be seen that a significant change of σ_{xx} will not lead to a significant change of σ_1, relative to σ_{yy} and τ_{xy}. The above analysis is in consistents with the theoretical analysis of section 2.3. Further the influence of the Poisson's ratio is considered, it can be seen that it has no significant influence on the stress state. The deviation of σ_{xx}, σ_{yy} and τ_{xy} has a significant influence on the σ_1, the numerical results show an influence up to 8000 mm from start of the beam.

HAP2E

First the numerical model in DIANA will be discussed. The elements of the concrete are 25mm×25mm and the elements of the steel plates are 25mm×20mm. In table 4.5 all parameters used in the model, this table forms an addition to the already known parameters.

Object	Parameter	Value
Concrete beam	E[$^N/_{mm^2}$]	42409
	h_{beam}[mm]	750
	l_{beam}[mm]	10000
	b_{beam}[m]	variable
	$\nu_{concrete}$[-]	0,2
Steel plate support	E[$^N/_{mm^2}$]	210000
	h_{plate}[mm]	40
	l_{plate}[mm]	150
	b_{plate}[mm]	150
	$\rho_{density}$[$^{kN}/_{m^3}$]	78,5
	ν_{steel}[-]	0,3
Steel plate force	E[$^N/_{mm^2}$]	210000
	h_{plate}[mm]	40
	l_{plate}[mm]	200
	b_{plate}[mm]	200
	$\rho_{density}$[$^{kN}/_{m^3}$]	78,5
	ν_{steel}[-]	0,3
Prestress cables	E[$^N/_{mm^2}$]	195000
	Yield stress[$^N/_{mm^2}$]	1522

Table 4.5: Parameters HAP2E used in DIANA

Verification

In order to link the analytical model to the numerical model a verification is done. This verification is done by comparing different results, like σ_{xx}, τ_{xy} and the principal stress σ_1. Good use can be made of the different fractions as described in section 4.1.1. In figure 4.18 the results of the fraction of $\frac{\tau_{xy,Analytical}}{\tau_{xy,Numerical}}$, in figure 4.19 the results of the fraction $\frac{\sigma_{1,Analytical}}{\sigma_{1,Numerical}}$. These tables are on the interval of 8275 mm to 8675 mm, from the start of the beam. Again the colomn "Plaats n" refers to the location of the height in the web relative to the neutral axis, with the exception of the upper en bottom line, this is the distance to the ultimate fiber.

τxy(Con.) Analytical / τxy Numerical	Plaats n	8275	8300	8325	8350	8375	8400	8425	8450	8475	8500	8525	8550	8575	8600	8625	8650	8675
	-347,41	0	0	0	0	0	0	0	0	0	0	0	0	0	0	0	0	0
	-167,41	1,078638	1,075865	1,073063	1,070246	1,067427	1,064618	1,06183	1,059076	1,056372	1,053734	1,051184	1,048751	1,046466	1,04437	1,042509	1,04094	1,039729
	-147,41	1,048942	1,046546	1,044118	1,04167	1,039216	1,036766	1,034334	1,03193	1,029571	1,027273	1,025057	1,022949	1,020978	1,019183	1,017607	1,016302	1,015329
	-122,41	1,012699	1,010719	1,008702	1,006661	1,004609	1,002557	1,000518	0,998503	0,996527	0,994606	0,99276	0,991013	0,989392	0,987931	0,986671	0,985658	0,984949
	-97,412	1,011215	1,009584	1,007914	1,006217	1,004504	1,002788	1,001079	0,99939	0,997733	0,996123	0,99458	0,993124	0,991781	0,990581	0,989561	0,988763	0,98824
	-72,412	1,009631	1,008355	1,007039	1,005696	1,004336	1,002967	1,0016	1,000247	0,998917	0,997625	0,996386	0,995218	0,994144	0,993189	0,992387	0,991773	0,991393
	-47,412	1,007961	1,007042	1,006086	1,005103	1,004102	1,003089	1,002073	1,001063	1,000067	0,999096	0,998162	0,997281	0,996469	0,995748	0,995145	0,994688	0,994417
	-22,412	1,006216	1,005652	1,005057	1,004438	1,0038	1,003149	1,00249	1,001828	1,001171	1,000525	0,999899	0,999303	0,99875	0,998255	0,997837	0,99752	0,997331
	2,58783	1,004398	1,004188	1,003954	1,003699	1,003428	1,003141	1,002843	1,002535	1,002221	1,001904	1,001588	1,00128	1,000985	1,000713	1,000474	1,000284	1,000162
	27,5878	1,002508	1,002647	1,002772	1,002882	1,002978	1,003058	1,003123	1,003173	1,003206	1,003223	1,003223	1,003206	1,003173	1,003125	1,003066	1,003002	1,00294
	52,5878	1,000541	1,001027	1,001508	1,001981	1,002442	1,00289	1,003321	1,00373	1,004115	1,004471	1,004793	1,005074	1,005311	1,005496	1,005625	1,005693	1,005697
	77,5878	0,998492	0,999319	1,000152	1,000984	1,001811	1,002625	1,003421	1,004194	1,004934	1,005635	1,006286	1,006876	1,007394	1,007826	1,008158	1,008375	1,008463
	102,587	0,996352	0,997515	0,998695	0,999882	1,001069	1,002247	1,003408	1,004544	1,005643	1,006694	1,007684	1,008595	1,009411	1,010109	1,010667	1,011059	1,01126
	127,587	0,994112	0,995605	0,997124	0,998659	1,0002	1,001736	1,003259	1,004757	1,006217	1,007624	1,008961	1,010208	1,011339	1,012327	1,013141	1,013745	1,0141
	152,587	0,991763	0,993577	0,995426	0,997298	0,999183	1,00107	1,002947	1,004803	1,006623	1,008389	1,010082	1,011677	1,013145	1,014451	1,015556	1,016416	1,016978
	177,587	0,989297	0,99142	0,993585	0,99578	0,997994	1,000217	1,002438	1,004643	1,006818	1,008943	1,010997	1,012953	1,014777	1,016431	1,017868	1,019035	1,019869
	202,587	0,977398	0,979648	0,981943	0,984271	0,986622	0,988985	0,99135	0,993702	0,996029	0,99831	1,000524	1,002642	1,00463	1,006448	1,008046	1,009367	1,010345
	402,587	0	0	0	0	0	0	0	0	0	0	0	0	0	0	0	0	0

Figure 4.18: Fraction $\frac{\tau_{xy,Analytical}}{\tau_{xy,Numerical}}$ of HAP2E

σ1(Con.) Analytical σ1 Numerical(σxx τxy σyy)	8275	8300	8325	8350	8375	8400	8425	8450	8475	8500	8525	8550	8575	8600	8625	8650	8675
-347,41	0	0	0	0	0	0	0	0	0	0	0	0	0	0	0	0	0
-167,41	1,097729	1,092985	1,088341	1,083801	1,079373	1,075077	1,07094	1,067001	1,063305	1,059912	1,056891	1,054325	1,05231	1,050959	1,050401	1,050782	1,052273
-147,41	1,048882	1,044942	1,041111	1,037388	1,033781	1,030308	1,026996	1,023882	1,021014	1,018452	1,016267	1,014544	1,01338	1,012891	1,013208	1,014481	1,016884
-122,41	0,995715	0,992524	0,989453	0,986498	0,983666	0,980974	0,978446	0,97612	0,974038	0,972259	0,97085	0,969891	0,969477	0,969717	0,970737	0,972683	0,975723
-97,412	0,995586	0,992775	0,990102	0,98756	0,985155	0,982903	0,980826	0,978959	0,977349	0,97605	0,97513	0,974671	0,974767	0,975529	0,977085	0,979583	0,983195
-72,412	0,995497	0,993065	0,990788	0,988657	0,986676	0,984855	0,983219	0,9818	0,980641	0,979797	0,979335	0,979335	0,979892	0,981115	0,983135	0,9861	0,990183
-47,412	0,995432	0,993377	0,991493	0,989768	0,988203	0,986807	0,985599	0,984611	0,983884	0,98347	0,983434	0,983854	0,984824	0,986453	0,988868	0,992218	0,996678
-22,412	0,995372	0,993691	0,992196	0,990872	0,989716	0,988734	0,987944	0,987372	0,987057	0,987048	0,987408	0,988212	0,989551	0,991532	0,994279	0,997941	1,002689
2,58783	0,9953	0,99399	0,99288	0,991951	0,991197	0,99062	0,990234	0,990063	0,990142	0,990516	0,991245	0,9924	0,994069	0,996353	0,999376	1,003281	1,008238
27,5878	0,995195	0,994256	0,993527	0,992988	0,992628	0,992447	0,992454	0,992671	0,993126	0,993864	0,994937	0,996414	0,998377	1,000924	1,004173	1,008263	1,013358
52,5878	0,99504	0,99447	0,99412	0,993965	0,993993	0,994199	0,994589	0,99518	0,995998	0,997081	0,998478	1,000253	1,002481	1,005256	1,008689	1,012913	1,018086
77,5878	0,994819	0,994618	0,994643	0,994868	0,995276	0,99586	0,996623	0,997577	0,998744	1,000157	1,001861	1,003913	1,006384	1,009359	1,012943	1,017261	1,022464
102,587	0,994518	0,994684	0,995081	0,99568	0,996461	0,997414	0,998539	0,999845	1,001348	1,003079	1,005076	1,00739	1,010085	1,01324	1,016952	1,021337	1,026535
127,587	0,994126	0,994658	0,995421	0,996385	0,997529	0,998841	1,000317	1,001962	1,003791	1,005827	1,008104	1,010669	1,013576	1,016899	1,020724	1,025159	1,030332
152,587	0,993636	0,994527	0,995648	0,996967	0,998462	1,000118	1,001931	1,003902	1,006042	1,008371	1,010919	1,013725	1,016838	1,020323	1,024257	1,028736	1,033879
177,587	0,993045	0,994287	0,995752	0,99741	0,999237	1,001219	1,003349	1,005627	1,008062	1,010671	1,013477	1,016516	1,019831	1,023478	1,027525	1,032058	1,037181
202,587	0,982272	0,98362	0,985176	0,986911	0,988803	0,990837	0,993006	0,995305	0,997738	1,000314	1,003048	1,00596	1,009077	1,012436	1,01608	1,020064	1,024455
402,587	0	0	0	0	0	0	0	0	0	0	0	0	0	0	0	0	0

Figure 4.19: Fraction $\frac{\sigma_{1,Analytical}}{\sigma_{1,Numerical}}$ of HAP2E

σxx(Con.) Analytical σxx Numerical	8275	8300	8325	8350	8375	8400	8425	8450	8475	8500	8525	8550	8575	8600	8625	8650	8675
-347,41	1,029175	1,028716	1,028437	1,02835	1,028466	1,0288	1,02937	1,030199	1,031312	1,032741	1,034521	1,036694	1,039308	1,042418	1,046087	1,050388	1,055401
-167,41	1,001075	1,001645	1,002037	1,002247	1,00227	1,002101	1,001731	1,001151	1,000351	0,999318	0,998039	0,996501	0,994687	0,992582	0,990172	0,987441	0,984376
-147,41	0,995307	0,995955	0,996398	0,996631	0,996648	0,996444	0,99601	0,995338	0,994419	0,993245	0,991805	0,990089	0,988089	0,985796	0,983203	0,980305	0,977101
-122,41	0,987682	0,98842	0,988927	0,989197	0,989222	0,988997	0,988515	0,98777	0,986757	0,98547	0,983905	0,98206	0,979935	0,97753	0,974851	0,971906	0,968709
-97,412	0,980181	0,981022	0,981611	0,98194	0,982002	0,981792	0,981304	0,980536	0,979483	0,978147	0,976528	0,97463	0,972461	0,970031	0,967356	0,964455	0,961355
-72,412	0,972935	0,973897	0,974589	0,975004	0,975135	0,974977	0,974525	0,97378	0,972741	0,971412	0,9698	0,967914	0,965767	0,963379	0,960773	0,957978	0,95503
-47,412	0,965983	0,967087	0,967908	0,968437	0,968668	0,968597	0,968222	0,967543	0,966565	0,965294	0,963741	0,96192	0,95985	0,957556	0,955067	0,95242	0,949658
-22,412	0,959356	0,960627	0,961603	0,962276	0,962639	0,962691	0,96243	0,961859	0,960984	0,959816	0,958367	0,956656	0,954706	0,952545	0,950209	0,947739	0,945183
2,58783	0,953078	0,954544	0,955704	0,956552	0,95708	0,957289	0,957178	0,956753	0,956021	0,954995	0,95369	0,952128	0,950333	0,948338	0,94618	0,943903	0,941561
27,5878	0,94717	0,948861	0,950237	0,95129	0,952016	0,952415	0,95249	0,952247	0,951695	0,950848	0,949722	0,948342	0,946732	0,944927	0,942966	0,940894	0,938764
52,5878	0,941647	0,943595	0,945218	0,946509	0,947466	0,94809	0,948385	0,948358	0,94802	0,947385	0,946472	0,945304	0,943906	0,942313	0,940563	0,938701	0,936781
77,5878	0,936519	0,938759	0,940661	0,942223	0,943443	0,944325	0,944873	0,945097	0,945007	0,944618	0,943948	0,94302	0,94186	0,940498	0,938973	0,937327	0,935612
102,587	0,931792	0,934357	0,936572	0,938437	0,939954	0,941126	0,941962	0,94247	0,942661	0,942551	0,942156	0,941498	0,9406	0,939491	0,938206	0,936784	0,935272
127,587	0,927465	0,93039	0,932951	0,935152	0,936997	0,938494	0,93965	0,940476	0,940984	0,941186	0,941099	0,940741	0,940134	0,939303	0,938277	0,93709	0,935785
152,587	0,923531	0,926849	0,929788	0,932357	0,934563	0,936417	0,937929	0,939108	0,939967	0,940518	0,940775	0,940753	0,940469	0,939944	0,939203	0,938272	0,937187
177,587	0,919972	0,923715	0,927064	0,930032	0,932631	0,934876	0,936778	0,938348	0,939597	0,940536	0,941176	0,941529	0,941607	0,941427	0,941004	0,94036	0,939519
202,587	0,916266	0,920471	0,924265	0,927669	0,930701	0,933377	0,935711	0,937717	0,939403	0,94078	0,941858	0,942643	0,943144	0,943371	0,943335	0,943049	0,94253
402,587	0,846409	0,857907	0,868495	0,878332	0,887546	0,89624	0,9045	0,912398	0,919994	0,927343	0,934489	0,941472	0,948326	0,95508	0,961757	0,968375	0,974946

Figure 4.20: Fraction $\frac{\sigma_{xx,Analytical}}{\sigma_{xx,Numerical}}$ of HAP2E

From figures 4.18 and 4.19 it can be seen that in this part of the beam the results of the analytical analysis correspond to the results of the numerical analysis. All parts had a similar result, except around the disturbed areas around the external force, the supports and the anchoring of the prestress. From figure 4.20 it can be seen that there is a little deviation in the results of the σ_{xx}. After analysis it appears that this deviation is not caused by the prestress part, because the fraction $\frac{\sigma_{xx;Analytical;pre}}{\sigma_{xx;Numerical;pre}} < 1\%$. It appears that the deviation is caused by the part of the external force. There is also checked wether the Poisson's ratio had a significant influence on the deviation, this was not the case. For this beam it comes down to a difference of 5-7%, so <0,7-1,0 N/mm^2.

Results

From the numerical results it can be seen that the component σ_{yy} has a local significant effect on the stress state in a beam, this effect is limited to the location of the external load and the support reaction respectively. In figure 4.21 the the results of σ_{yy}, around The σ_{yy} has influence from 7300 mm(location external load) up till 7750 mm, from start of the beam. The influence is low in the bottom part the of the web, at 202,58 mm relative to the neutral axis.

σyy Load+ Weight+ Prestress	Plaats n	7300	7300	7325	7350	7375	7400	7425	7450	7475	7500	7525	7550	7575	7600	7625	7650	7675	7700
	-347,412	-24,563	-24,563	-8,18647	1,487487	-3,35839	-15,6864	-1,53479	-0,6945	-0,21351	-0,17589	-0,12316	-0,1005	-0,08143	-0,06807	-0,05793	-0,05046	-0,04495	-0,04091
	-167,412	-4,82513	-4,82513	-4,87668	-5,00031	-5,13673	-5,20667	-5,14215	-4,91328	-4,53774	-4,06705	-3,55944	-3,06149	-2,60003	-2,18686	-1,82418	-1,50986	-1,23982	-1,0094
	-147,412	-5,43601	-5,43601	-5,47118	-5,55231	-5,63207	-5,65045	-5,55555	-5,32266	-4,96088	-4,50538	-4,00196	-3,49169	-3,00394	-2,55521	-2,15266	-1,79756	-1,48801	-1,22059
	-122,412	-5,33239	-5,33239	-5,34816	-5,37965	-5,39801	-5,36644	-5,253	-5,04102	-4,73353	-4,35043	-3,92056	-3,47333	-3,03284	-2,61575	-2,23175	-1,88532	-1,57742	-1,30691
	-97,4122	-5,00718	-5,00718	-5,0108	-5,01191	-4,99353	-4,93403	-4,81423	-4,62351	-4,36271	-4,04315	-3,68294	-3,30216	-2,91912	-2,54814	-2,19905	-1,8777	-1,58688	-1,32718
	-72,4122	-4,6727	-4,6727	-4,66957	-4,65396	-4,61591	-4,54259	-4,42252	-4,2491	-4,02259	-3,74995	-3,44294	-3,11555	-2,78146	-2,45239	-2,13726	-1,84221	-1,57088	-1,32502
	-47,4122	-4,33835	-4,33835	-4,33161	-4,30733	-4,25964	-4,18097	-4,06449	-3,90628	-3,70665	-3,47021	-3,20499	-2,92092	-2,62827	-2,33641	-2,05306	-1,78401	-1,53321	-1,30298
	-22,4122	-4,00923	-4,00923	-4,00072	-3,9725	-3,92111	-3,84212	-3,73158	-3,58732	-3,40984	-3,20249	-2,971	-2,72263	-2,46518	-2,20608	-1,95185	-1,7077	-1,47747	-1,26376
	2,587832	-3,68792	-3,68792	-3,67874	-3,64935	-3,59774	-3,5214	-3,41811	-3,28687	-3,12836	-2,9452	-2,74168	-2,52326	-2,29594	-2,06568	-1,83788	-1,61711	-1,40695	-1,21
	27,58783	-3,37554	-3,37554	-3,36633	-3,33739	-3,28759	-3,21556	-3,12019	-3,00118	-2,85936	-2,69689	-2,51712	-2,32427	-2,12307	-1,91829	-1,71444	-1,51543	-1,32452	-1,14419
	52,58783	-3,07232	-3,07232	-3,06346	-3,0359	-2,98905	-2,92224	-2,83502	-2,72752	-2,60067	-2,45631	-2,29714	-2,12653	-1,94824	-1,76617	-1,58405	-1,40525	-1,23264	-1,06853
	77,58783	-2,77799	-2,77799	-2,76968	-2,74402	-2,70074	-2,63959	-2,5605	-2,46387	-2,35064	-2,22244	-2,08149	-1,93053	-1,77263	-1,61098	-1,4487	-1,28867	-1,13341	-0,98501
	102,5878	-2,49194	-2,49194	-2,48431	-2,46083	-2,42143	-2,36608	-2,29498	-2,20863	-2,10796	-1,99441	-1,86985	-1,73654	-1,59703	-1,45395	-1,30993	-1,16742	-1,02861	-0,89538
	127,5878	-2,21339	-2,21339	-2,20649	-2,18533	-2,14993	-2,10042	-2,03709	-1,9605	-1,87155	-1,77148	-1,66191	-1,54472	-1,42204	-1,29606	-1,169	-1,04295	-0,91981	-0,80124
	152,5878	-1,9414	-1,9414	-1,93526	-1,91648	-1,88512	-1,84139	-1,78562	-1,71837	-1,64047	-1,55301	-1,45737	-1,35514	-1,24809	-1,13807	-1,02695	-0,91651	-0,80838	-0,70402
	177,5878	-1,67494	-1,67494	-1,66958	-1,6532	-1,62589	-1,58786	-1,53946	-1,48123	-1,4139	-1,33841	-1,25593	-1,16781	-1,07552	-0,98063	-0,88469	-0,78921	-0,69559	-0,60507
	202,5878	-1,27773	-1,27773	-1,27358	-1,26096	-1,23995	-1,21073	-1,17361	-1,129	-1,07748	-1,01978	-0,95678	-0,88949	-0,81902	-0,74653	-0,67319	-0,60014	-0,52844	-0,45904
	402,5878	0,100027	0,100027	0,09939	0,098566	0,097558	0,096369	0,095007	0,093478	0,091792	0,089958	0,087988	0,085894	0,083688	0,081385	0,078997	0,07654	0,074026	0,071469

Figure 4.21: Numerical σ_{yy} of HAP2E

From the results it also can be seen that τ_{xy} is disturbed around the external load and the support reaction, the disturbance around the external load runs from 7300 mm up till around 7750 mm. In figure 4.22 the results of the fraction $\frac{\tau_{xy,Analytical}}{\tau_{xy,Numerical}}$ around the external load.

τxy(Con.) Analytical / τxy Numerical	Plaats n	7300	7300	7325	7350	7375	7400	7425	7450	7475	7500	7525	7550	7575	7600	7625	7650	7675	7700
	-347,412	0	0	0	0	0	0	0	0	0	0	0	0	0	0	0	0	0	0
	-167,412	-0,80181	2,950723	2,590301	2,256831	1,938018	1,654022	1,423584	1,251296	1,130915	1,052075	1,004376	0,978981	0,968954	0,969114	0,975748	0,986257	0,998844	1,012261
	-147,412	-0,77992	2,870167	2,499603	2,178345	1,887463	1,633629	1,426223	1,267482	1,152786	1,074259	1,023589	0,993416	0,97779	0,972166	0,973211	0,978532	0,986435	0,995711
	-122,412	-0,75318	2,771748	2,392206	2,085329	1,825348	1,605864	1,426178	1,284768	1,17781	1,099967	1,045535	1,009215	0,986481	0,973672	0,967934	0,967103	0,96956	0,974104
	-97,4122	-0,75253	2,76936	2,384796	2,08381	1,837813	1,634554	1,46841	1,33552	1,231928	1,153313	1,095293	1,053759	1,025091	1,006243	0,99474	0,988618	0,986346	0,986746
	-72,4122	-0,75195	2,767229	2,386213	2,092074	1,856058	1,663494	1,506357	1,379415	1,278441	1,199552	1,139099	1,093727	1,060455	1,036721	1,020379	1,009675	1,003194	0,999815
	-47,4122	-0,75139	2,765168	2,391903	2,104903	1,876544	1,691436	1,540476	1,417699	1,318658	1,239663	1,177473	1,12921	1,092333	1,064643	1,044266	1,029638	1,019467	1,012703
	-22,4122	-0,75082	2,763068	2,399321	2,119351	1,897188	1,717553	1,570969	1,451133	1,353474	1,274394	1,210894	1,160395	1,120659	1,089753	1,066019	1,048054	1,034682	1,024927
	2,587832	-0,75022	2,760854	2,407013	2,133706	1,916728	1,741287	1,597906	1,480175	1,383481	1,30429	1,23975	1,187478	1,145446	1,111913	1,085387	1,0646	1,048474	1,036108
	27,58783	-0,74957	2,758475	2,414133	2,146948	1,934377	1,762255	1,621286	1,505087	1,409059	1,329723	1,26433	1,210628	1,166732	1,131045	1,102202	1,079038	1,060565	1,045942
	52,58783	-0,74887	2,755892	2,420177	2,158446	1,949622	1,780177	1,641066	1,526	1,430429	1,350929	1,284824	1,229957	1,184544	1,147092	1,116332	1,091184	1,070728	1,054181
	77,58783	-0,74811	2,753069	2,424828	2,167791	1,962109	1,794827	1,657164	1,542948	1,447694	1,368029	1,301334	1,24552	1,198879	1,159991	1,127661	1,100876	1,078772	1,060611
	102,5878	-0,74726	2,749973	2,427869	2,174693	1,971562	1,806001	1,669461	1,555889	1,460859	1,381045	1,313875	1,257308	1,209689	1,169656	1,136068	1,107962	1,084518	1,06504
	127,5878	-0,74634	2,746572	2,42913	2,178911	1,977733	1,813483	1,677795	1,564705	1,469842	1,389915	1,322384	1,265244	1,21688	1,175968	1,141409	1,112277	1,08779	1,06728
	152,5878	-0,74532	2,742827	2,428452	2,180214	1,980371	1,817032	1,681946	1,569208	1,474479	1,394488	1,326717	1,269183	1,220297	1,178763	1,143509	1,11364	1,088398	1,067139
	177,5878	-0,7442	2,738697	2,425663	2,178356	1,979192	1,816358	1,681637	1,569138	1,474525	1,394534	1,326652	1,268907	1,219723	1,177822	1,142151	1,111834	1,08613	1,064413
	202,5878	-0,73561	2,707083	2,397633	2,153175	1,956321	1,795387	1,662238	1,55104	1,457501	1,378388	1,311214	1,254031	1,205285	1,163717	1,128293	1,098152	1,07257	1,050933
	402,5878	0	0	0	0	0	0	0	0	0	0	0	0	0	0	0	0	0	0

Figure 4.22: Fraction $\frac{\tau_{xy,Analytical}}{\tau_{xy,Numerical}}$ of HAP2E

The maximum τ_{xy} = 6,01 N/mm^2(8350 mm), around the neutral axis, this falls back to 2,47 N/mm^2(7325 mm), see appendix "Choulli: Numerical results" of the appendix report. In figure 4.23 the fraction $\frac{\sigma_{xx,Analytical}}{\sigma_{xx,Numerical}}$, it can be seen that there is also a deviation of σ_{xx} around the external load. As described before the σ_{xx} consists out of the contributions of the external load, the weight and the prestress. After analysis it appears that the deviation is caused by the external load part. This can be seen in figure 4.23, in the part below the neutral axis the value of the fraction drops towards 0,50-0,70 and in the part above the neutral axis the value of the fraction rises towards 1,25-1,30. The drop to 0,50-0,70 means that the value of $\sigma_{xx,Analytical}$ related to $\sigma_{xx,Numerical}$ is too high, this is caused by the tensional part of $\sigma_{xx,Analytical}$. The rise to 1,25-1,30 means that the value of $\sigma_{xx,Analytical}$ related to $\sigma_{xx,Numerical}$ is too low, this is caused by the compressional part of $\sigma_{xx,Analytical}$. This means that the part of $\sigma_{xx,Analytical}$ that is caused by the external force is too high.

σxx(Con.) Analytical / σxx Numerical	Plaats n	7300	7300	7325	7350	7375	7400	7425	7450	7475	7500	7525	7550	7575	7600	7625	7650	7675	7700
	-347,412	0,679683	0,679683	0,639141	0,503839	0,3816	0,359612	0,606844	0,794561	0,875928	0,922318	0,957556	0,98508	1,006902	1,023866	1,036755	1,046243	1,052941	1,057384
	-167,412	1,344632	1,344632	1,343809	1,349764	1,355486	1,351948	1,331915	1,294092	1,243706	1,189071	1,137558	1,093343	1,05776	1,030297	1,009729	0,994701	0,984021	0,976714
	-147,412	1,314377	1,314377	1,311829	1,312702	1,312488	1,305447	1,28714	1,256555	1,216544	1,172249	1,128757	1,089649	1,056624	1,029981	1,009198	0,993436	0,981808	0,973515
	-122,412	1,288732	1,288732	1,285132	1,282503	1,278126	1,268659	1,251512	1,226017	1,193716	1,157646	1,121168	1,086999	1,056818	1,031324	1,010529	0,994048	0,981334	0,971807
	-97,4122	1,264601	1,264601	1,260769	1,256499	1,250141	1,239676	1,223553	1,201356	1,17402	1,143486	1,112058	1,0818	1,054188	1,030045	1,009652	0,992924	0,979561	0,969175
	-72,4122	1,235945	1,235945	1,232388	1,227573	1,220499	1,209957	1,195026	1,175489	1,151971	1,125779	1,098541	1,071817	1,046845	1,024433	1,004989	0,988606	0,975167	0,964435
	-47,4122	1,202464	1,202464	1,19958	1,194974	1,188047	1,178085	1,164564	1,147407	1,12708	1,104512	1,080887	1,057399	1,035066	1,014624	0,99652	0,980948	0,967913	0,957295
	-22,4122	1,163477	1,163477	1,161618	1,157797	1,151661	1,142803	1,13095	1,11612	1,098689	1,079356	1,05901	1,03858	1,018895	1,000606	0,984154	0,969782	0,957571	0,947484
	2,587832	1,117895	1,117895	1,117423	1,114887	1,11009	1,102813	1,092938	1,080545	1,065957	1,04972	1,032525	1,015105	0,998141	0,982197	0,967686	0,954868	0,94387	0,934712
	27,58783	1,064123	1,064123	1,065456	1,064717	1,061798	1,056599	1,049093	1,039396	1,027793	1,014724	1,000739	0,986429	0,972356	0,959003	0,946747	0,935848	0,926457	0,918631
	52,58783	0,99987	0,99987	1,003541	1,005191	1,004766	1,002229	0,997607	0,991029	0,982747	0,973123	0,962604	0,951669	0,940785	0,930367	0,920753	0,91219	0,90484	0,898786
	77,58783	0,921815	0,921815	0,928551	0,933356	0,936201	0,937081	0,936046	0,933224	0,928829	0,923162	0,916587	0,909495	0,902276	0,895283	0,888817	0,88311	0,878323	0,874556
	102,5878	0,825019	0,825019	0,835866	0,844894	0,852078	0,857422	0,860973	0,862842	0,863208	0,862314	0,860452	0,857942	0,855106	0,852247	0,849627	0,847459	0,845902	0,845064
	127,5878	0,701864	0,701864	0,718415	0,733255	0,746347	0,757681	0,767289	0,775251	0,781702	0,786831	0,790867	0,794065	0,796689	0,798994	0,801207	0,803524	0,806099	0,809041
	152,5878	0,540016	0,540016	0,564844	0,588013	0,609458	0,629143	0,647068	0,663275	0,677854	0,690936	0,702693	0,71332	0,72303	0,732034	0,740528	0,748691	0,756668	0,764575
	177,5878	0,318197	0,318197	0,355776	0,391554	0,425433	0,457346	0,487259	0,515178	0,541147	0,56525	0,587607	0,608366	0,627692	0,645759	0,662738	0,678792	0,694062	0,70867
	202,5878	-0,00364	-0,00364	0,056064	0,11315	0,167507	0,219059	0,267771	0,313644	0,356717	0,397066	0,434797	0,470043	0,502959	0,533709	0,562462	0,589385	0,614635	0,638353
	402,5878	1,259768	1,259768	1,233962	1,210734	1,190004	1,171706	1,155792	1,142231	1,131014	1,122156	1,115707	1,111756	1,110449	1,112008	1,116763	1,125205	1,138072	1,156492

Figure 4.23: Fraction $\frac{\sigma_{xx,Analytical}}{\sigma_{xx,Numerical}}$ of HAP2E

Further the influence of the Poisson's ratio is considered, it can be seen that it has no significant influence on the stress state. The deviation of σ_{xx}, σ_{yy} and τ_{xy} has a significant influence on the σ_1, the numerical results show an influence up to 7950-8000 mm from start of the beam.

HAP2E,pres

In this section the prestress level of the original HAP2E beam is adapted. The original mean prestress level of the HAP2E beam was σ_{cp} = 6,3 N/mm^2, in this fictional beam the mean prestress is σ_{cp} = 10,26 N/mm^2. The prestress as aplied in DIANA is presented in table 4.6. Further the cross-sectional area of the strands is A$_p$ = 160 mm^2. Further all the conditions and parameters equals HAP2E.

Type prestress	**Layer**	**Strands**[-]	σ_p **excl. losses**[N/mm^2]	σ_p **incl. losses**[N/mm^2]
10 strands	1	8	1339	1220
	4	2	1246	1232

Table 4.6: Prestress as aplied in DIANA HAP2E,pres

Verification

In order to link the analytical model to the numerical model a verification is done. This verification is done by comparing different results, like σ_{xx}, τ_{xy} and the principal stress σ_1. Good use can be made of the different fractions as described in section 4.1.1. In figure 4.24 the results of the fraction of $\frac{\tau_{xy,Analytical}}{\tau_{xy,Numerical}}$, in figure 4.25 the results of the fraction $\frac{\sigma_{1,Analytical}}{\sigma_{1,Numerical}}$. These tables are on the interval of 8275 mm to 8675 mm, from the start of the beam. Again the colomn "Plaats n" refers to the location of the height in the web relative to the neutral axis, with the exception of the upper en bottom line, this is the distance to the ultimate fiber.

τxy(Con.) Analytical / τxy Numerical	Plaats n	8275	8300	8325	8350	8375	8400	8425	8450	8475	8500	8525	8550	8575	8600	8625	8650	8675
	-347,41	0	0	0	0	0	0	0	0	0	0	0	0	0	0	0	0	0
	-167,41	1,081431	1,078519	1,075576	1,07262	1,069664	1,066722	1,063808	1,060938	1,058131	1,055407	1,052795	1,050326	1,048039	1,045981	1,044206	1,04278	1,041779
	-147,41	1,051664	1,049147	1,046596	1,044027	1,041453	1,038888	1,036347	1,033845	1,0314	1,029032	1,026767	1,024635	1,022673	1,020923	1,019437	1,018275	1,017508
	-122,41	1,015334	1,013251	1,011131	1,008989	1,006837	1,004691	1,002563	1,000468	0,998424	0,996451	0,994572	0,992814	0,991212	0,989805	0,988639	0,987769	0,987261
	-97,412	1,013815	1,012097	1,01034	1,008557	1,006761	1,004966	1,003183	1,001429	0,999717	0,998068	0,996501	0,995044	0,993726	0,992582	0,991657	0,990999	0,990667
	-72,412	1,012156	1,010809	1,009423	1,00801	1,006581	1,005148	1,003723	1,002317	1,000944	0,999622	0,998367	0,997203	0,996155	0,995255	0,994539	0,994052	0,993846
	-47,412	1,010372	1,009397	1,008387	1,007349	1,006295	1,005232	1,00417	1,00312	1,002091	1,001097	1,000153	0,999276	0,998488	0,997814	0,997284	0,996935	0,99681
	-22,412	1,008468	1,007865	1,007231	1,006573	1,005897	1,00521	1,004517	1,003827	1,003145	1,002482	1,001848	1,001256	1,00072	1,00026	0,999898	0,999662	0,999586
	2,58783	1,006446	1,006212	1,005955	1,005677	1,005382	1,005073	1,004753	1,004426	1,004096	1,003767	1,003445	1,003137	1,00285	1,002598	1,002393	1,002254	1,002205
	27,5878	1,004302	1,004434	1,004551	1,004653	1,004739	1,004811	1,004867	1,004907	1,004932	1,004941	1,004935	1,004913	1,004879	1,004835	1,004785	1,004738	1,004705
	52,5878	1,002029	1,002523	1,003011	1,003491	1,003958	1,004411	1,004844	1,005255	1,005639	1,005991	1,006307	1,00658	1,006805	1,006976	1,007088	1,007139	1,007126
	77,5878	0,999616	1,000466	1,001322	1,002176	1,003023	1,003855	1,004667	1,005451	1,006199	1,006901	1,007548	1,008126	1,008622	1,009024	1,009314	1,009479	1,009503
	102,587	0,997048	0,99825	0,999467	1,000691	1,001913	1,003124	1,004314	1,005473	1,006589	1,007649	1,008636	1,009533	1,010319	1,010972	1,011466	1,011773	1,011866
	127,587	0,994311	0,995857	0,997429	0,999016	1,000606	1,00219	1,003756	1,00529	1,006778	1,008202	1,009542	1,010774	1,011872	1,012804	1,013534	1,014025	1,014232
	152,587	0,991387	0,993268	0,995184	0,997123	0,999073	1,001023	1,002958	1,004864	1,006724	1,008518	1,010222	1,011808	1,013242	1,014486	1,015495	1,016219	1,016601
	177,587	0,988259	0,990461	0,992707	0,994984	0,997279	0,999581	1,001875	1,004146	1,006376	1,008543	1,01062	1,012576	1,014373	1,015965	1,0173	1,018316	1,018946
	202,587	0,976017	0,978353	0,980735	0,983151	0,985589	0,988038	0,990483	0,992909	0,995298	0,997628	0,999871	1,001996	1,003961	1,005719	1,007215	1,008384	1,009151
	402,587	0	0	0	0	0	0	0	0	0	0	0	0	0	0	0	0	0

Figure 4.24: Fraction $\frac{\tau_{xy,Analytical}}{\tau_{xy,Numerical}}$ of HAP2E,pres

σ1(Con.) Analytical / σ1 Numerical(σxx τxy σyy)		8275	8300	8325	8350	8375	8400	8425	8450	8475	8500	8525	8550	8575	8600	8625	8650	8675
	-347,41	0	0	0	0	0	0	0	0	0	0	0	0	0	0	0	0	0
	-167,41	1,098222	1,093153	1,08818	1,083308	1,078553	1,073942	1,069513	1,065318	1,06142	1,057896	1,054839	1,052356	1,050573	1,049637	1,049715	1,051	1,053716
	-147,41	1,045082	1,040827	1,036681	1,032643	1,028727	1,024959	1,021378	1,018035	1,014997	1,012342	1,010167	1,008585	1,007725	1,007741	1,008807	1,011127	1,014937
	-122,41	0,987423	0,983919	0,980537	0,977276	0,974147	0,971175	0,968396	0,965859	0,963629	0,961782	0,960412	0,959629	0,95956	0,960355	0,962188	0,96526	0,969804
	-97,412	0,985413	0,982303	0,979338	0,976514	0,973839	0,971336	0,969041	0,967005	0,965292	0,963982	0,96317	0,96297	0,963517	0,964966	0,9675	0,971331	0,976708
	-72,412	0,983307	0,980593	0,978045	0,975657	0,973434	0,971396	0,969578	0,968029	0,966815	0,966015	0,965728	0,96607	0,96718	0,96922	0,972378	0,976879	0,982983
	-47,412	0,981114	0,978794	0,976664	0,974709	0,972933	0,971352	0,969999	0,968923	0,968186	0,967869	0,968071	0,968911	0,97053	0,973094	0,9768	0,981878	0,988602
	-22,412	0,978833	0,97691	0,975195	0,973671	0,972336	0,971204	0,970304	0,969682	0,9694	0,969537	0,970193	0,971486	0,973559	0,976582	0,980755	0,986317	0,993551
	2,58783	0,976461	0,974938	0,973639	0,972543	0,971643	0,970951	0,970491	0,970306	0,970456	0,971019	0,972092	0,973794	0,976268	0,979685	0,984249	0,990203	0,997837
	27,5878	0,973993	0,972874	0,971993	0,971324	0,970855	0,970594	0,970562	0,970798	0,971359	0,97232	0,973776	0,975845	0,978668	0,982416	0,987296	0,993551	1,001478
	52,5878	0,971421	0,970715	0,970256	0,970013	0,969972	0,970135	0,97052	0,971163	0,972115	0,973449	0,975256	0,977652	0,980776	0,984797	0,989921	0,996392	1,004508
	77,5878	0,968738	0,968454	0,968423	0,968609	0,968994	0,969576	0,970369	0,971404	0,972729	0,974414	0,976544	0,979232	0,982614	0,986855	0,992158	0,998765	1,006974
	102,587	0,965939	0,966089	0,966492	0,96711	0,967919	0,968916	0,970108	0,971525	0,973209	0,975225	0,977655	0,980605	0,984207	0,988622	0,994046	1,000719	1,008932
	127,587	0,96302	0,963617	0,964461	0,965513	0,966746	0,968153	0,969739	0,971527	0,973557	0,975888	0,978598	0,981786	0,985578	0,990129	0,995629	1,002308	1,010451
	152,587	0,959981	0,961035	0,962326	0,963813	0,965469	0,967281	0,969254	0,971405	0,973771	0,976406	0,97938	0,982789	0,98675	0,99141	0,99695	1,003591	1,011607
	177,587	0,956826	0,958344	0,960085	0,962006	0,964078	0,96629	0,96864	0,971146	0,973839	0,976768	0,979998	0,983617	0,987735	0,99249	0,998051	1,004629	1,012481
	202,587	0,944079	0,945862	0,94784	0,949976	0,952241	0,954621	0,957112	0,959723	0,962473	0,965398	0,968546	0,971978	0,975777	0,980045	0,984908	0,990523	0,997083
	402,587	0	0	0	0	0	0	0	0	0	0	0	0	0	0	0	0	0

Figure 4.25: Fraction $\frac{\sigma_{1,Analytical}}{\sigma_{1,Numerical}}$ of HAP2E,pres

σxx(Con.) Analytical σxx Numerical	8275	8300	8325	8350	8375	8400	8425	8450	8475	8500	8525	8550	8575	8600	8625	8650	8675
-347,41	1,039095	1,038579	1,038258	1,038144	1,038251	1,038596	1,039202	1,040093	1,041299	1,042855	1,044802	1,047187	1,050066	1,0535	1,057561	1,06233	1,067903
-167,41	1,007126	1,007585	1,007891	1,008042	1,008035	1,007866	1,007528	1,007015	1,006319	1,005432	1,004345	1,003046	1,001527	0,999776	0,997785	0,995543	0,993044
-147,41	1,002336	1,002865	1,003224	1,00341	1,003419	1,003247	1,00289	1,002341	1,001596	1,000648	0,999491	0,998119	0,996528	0,994713	0,992673	0,990405	0,987911
-122,41	0,996364	0,996972	0,997395	0,99763	0,997672	0,997518	0,997165	0,996609	0,995847	0,994877	0,993699	0,992313	0,99072	0,988924	0,986932	0,984754	0,982402
-97,412	0,990893	0,991582	0,992078	0,992374	0,992468	0,992356	0,992035	0,991506	0,990768	0,989822	0,988671	0,987321	0,98578	0,984057	0,982167	0,980128	0,977962
-72,412	0,986001	0,986777	0,987352	0,987723	0,987884	0,987834	0,987572	0,987098	0,986414	0,985525	0,984437	0,98316	0,981705	0,980089	0,97833	0,976454	0,974489
-47,412	0,981684	0,98255	0,983213	0,983668	0,98391	0,983938	0,983752	0,983355	0,98275	0,981943	0,980943	0,979763	0,978419	0,976928	0,975316	0,973611	0,971847
-22,412	0,97793	0,978891	0,979648	0,980194	0,980528	0,980647	0,980553	0,980249	0,979739	0,979032	0,978139	0,977073	0,975852	0,974498	0,973038	0,971503	0,969929
2,58783	0,974724	0,975783	0,976638	0,977284	0,977717	0,977938	0,977946	0,977747	0,977347	0,976753	0,975978	0,975037	0,973948	0,972735	0,971425	0,970051	0,968652
27,5878	0,972046	0,973207	0,974164	0,974914	0,975453	0,975783	0,975903	0,975819	0,975537	0,975067	0,974419	0,973609	0,972657	0,971584	0,97042	0,969197	0,967953
52,5878	0,969874	0,971138	0,9722	0,973058	0,973709	0,974153	0,974392	0,974431	0,974276	0,973936	0,973422	0,972749	0,971935	0,971003	0,969978	0,968894	0,967787
77,5878	0,968184	0,969551	0,97072	0,971688	0,972454	0,973018	0,973382	0,97355	0,973529	0,973326	0,972952	0,97242	0,971747	0,970954	0,970065	0,96911	0,968123
102,587	0,966947	0,968416	0,969692	0,970772	0,971655	0,972343	0,972837	0,973141	0,97326	0,973201	0,972973	0,972589	0,972061	0,971409	0,970653	0,969821	0,968942
127,587	0,966135	0,967703	0,969084	0,970276	0,971279	0,972094	0,972722	0,973168	0,973435	0,973528	0,973454	0,973224	0,972849	0,972342	0,971722	0,971011	0,970236
152,587	0,965713	0,967376	0,968858	0,970161	0,971285	0,97223	0,972998	0,973592	0,974015	0,974269	0,974361	0,974296	0,974083	0,973731	0,973256	0,972672	0,972001
177,587	0,965646	0,967396	0,968975	0,970387	0,971631	0,972709	0,973623	0,974373	0,974961	0,975388	0,975658	0,975772	0,975737	0,975556	0,975239	0,974797	0,974242
202,587	0,965667	0,967495	0,969166	0,970683	0,972049	0,973263	0,974328	0,975244	0,97601	0,976627	0,977094	0,977411	0,97758	0,977601	0,977478	0,977217	0,976824
402,587	0,956567	0,958707	0,960917	0,963195	0,965538	0,967947	0,970423	0,972967	0,97558	0,978265	0,981024	0,98386	0,986775	0,989772	0,99285	0,996008	0,999244

Figure 4.26: Fraction $\frac{\sigma_{xx,Analytical}}{\sigma_{xx,Numerical}}$ of HAP2E,pres

From figures 4.24 and 4.25 it can be seen that in this part of the beam the results of the analytical analysis correspond to the results of the numerical analysis. All parts had a similar result, except around the disturbed areas around the external force, the supports and the anchoring of the prestress. From figure 4.26 it can be seen that there is a little deviation in the results of the σ_{xx}. After analysis it appears that this deviation is not caused by the prestress part, because the fraction $\frac{\sigma_{xx;Analytical;pre}}{\sigma_{xx;Numerical;pre}} < 1\%$. It appears that the deviation is caused by the part of the external force. There is also checked wether the Poisson's ratio had a significant influence on the deviation, this was not the case. For this beam it comes down to a difference of 3-4%, so <0,6 N/mm^2.

Results

The tables 4.27, 4.28 and 4.29 are on the interval of 8275 mm to 8675 mm, from the start of the beam.In figure 4.27 the σ_{xx}, it can be seen that the mean prestress level σ_{cp} is increased. In figure 4.28 and 4.29 respectively the results of σ_1 and σ_2, it can be seen that σ_1 decreased with 22% and σ_2 increased with 32%. The percentages are relative to the σ_1 and σ_2 of HAP2E.

σxx Load+ Weight+ Prestress	Plaats n	8275	8300	8325	8350	8375	8400	8425	8450	8475	8500	8525	8550	8575	8600	8625	8650	8675
	-347,41	-8,62198	-8,42723	-8,23066	-8,03231	-7,83217	-7,63026	-7,42655	-7,22103	-7,01368	-6,80445	-6,59331	-6,38021	-6,16512	-5,948	-5,72883	-5,50759	-5,28429
	-167,41	-9,52473	-9,42153	-9,3198	-9,21951	-9,12065	-9,02322	-8,9272	-8,83263	-8,73951	-8,64787	-8,55775	-8,46918	-8,38219	-8,29683	-8,21311	-8,13106	-8,0507
	-147,41	-9,64048	-9,54793	-9,45705	-9,36782	-9,28023	-9,19427	-9,10994	-9,02723	-8,94617	-8,86675	-8,78899	-8,71289	-8,63845	-8,56567	-8,49453	-8,42499	-8,35701
	-122,41	-9,78657	-9,70754	-9,63037	-9,55504	-9,48156	-9,4099	-9,34007	-9,27204	-9,20582	-9,14138	-9,07869	-9,01772	-8,95843	-8,90074	-8,84457	-8,78982	-8,73634
	-97,412	-9,92941	-9,86405	-9,80068	-9,7393	-9,67992	-9,62253	-9,56711	-9,51363	-9,46208	-9,4124	-9,36455	-9,31845	-9,27401	-9,2311	-9,18959	-9,14928	-9,10997
	-72,412	-10,0679	-10,0163	-9,96684	-9,91945	-9,87417	-9,83099	-9,7899	-9,75086	-9,71384	-9,67876	-9,64555	-9,61411	-9,5843	-9,55597	-9,52891	-9,50288	-9,4776
	-47,412	-10,2018	-10,1641	-10,1286	-10,0952	-10,064	-10,035	-10,0082	-9,98346	-9,96083	-9,94021	-9,92149	-9,90455	-9,88922	-9,87531	-9,86258	-9,85073	-9,83944
	-22,412	-10,331	-10,3072	-10,2856	-10,2663	-10,2492	-10,2343	-10,2217	-10,2112	-10,2029	-10,1966	-10,1922	-10,1896	-10,1887	-10,1891	-10,1906	-10,1929	-10,1956
	2,58783	-10,4552	-10,4454	-10,4379	-10,4326	-10,4295	-10,4287	-10,4302	-10,4339	-10,4398	-10,4477	-10,4576	-10,4693	-10,4826	-10,4972	-10,513	-10,5294	-10,5463
	27,5878	-10,5745	-10,5788	-10,5853	-10,594	-10,605	-10,6182	-10,6338	-10,6515	-10,6715	-10,6935	-10,7175	-10,7433	-10,7708	-10,7997	-10,8296	-10,8603	-10,8913
	52,5878	-10,6889	-10,7073	-10,7278	-10,7505	-10,7755	-10,8027	-10,8322	-10,864	-10,8979	-10,9339	-10,9719	-11,0118	-11,0533	-11,0963	-11,1404	-11,1853	-11,2306
	77,5878	-10,7985	-10,8309	-10,8654	-10,9021	-10,9411	-10,9822	-11,0256	-11,0713	-11,119	-11,1689	-11,2208	-11,2746	-11,3301	-11,3871	-11,4453	-11,5045	-11,5641
	102,587	-10,9033	-10,9498	-10,9984	-11,0491	-11,1019	-11,1569	-11,2141	-11,2734	-11,3349	-11,3985	-11,4641	-11,5316	-11,6009	-11,6718	-11,7441	-11,8174	-11,8914
	127,587	-11,0035	-11,0642	-11,1268	-11,1914	-11,2581	-11,3268	-11,3977	-11,4707	-11,5457	-11,6228	-11,7019	-11,7829	-11,8658	-11,9504	-12,0365	-12,1238	-12,2122
	152,587	-11,0995	-11,1742	-11,2509	-11,3294	-11,4099	-11,4923	-11,5767	-11,6631	-11,7515	-11,8419	-11,9342	-12,0285	-12,1247	-12,2227	-12,3224	-12,4236	-12,526
	177,587	-11,1914	-11,2804	-11,3711	-11,4635	-11,5577	-11,6536	-11,7514	-11,851	-11,9525	-12,0559	-12,1612	-12,2685	-12,3776	-12,4887	-12,6016	-12,7162	-12,8325
	202,587	-11,2822	-11,3855	-11,4903	-11,5966	-11,7045	-11,8139	-11,9249	-12,0376	-12,1519	-12,268	-12,3859	-12,5056	-12,6272	-12,7508	-12,8762	-13,0036	-13,1329
	402,587	-12,1255	-12,3483	-12,5692	-12,7884	-13,0057	-13,2212	-13,4347	-13,6463	-13,8559	-14,0634	-14,2688	-14,4719	-14,6728	-14,8714	-15,0677	-15,2616	-15,4531

Figure 4.27: Numerical σ_{xx} of HAP2E,pres

σ1 σxx τxy σyy	Plaats n	8275	8300	8325	8350	8375	8400	8425	8450	8475	8500	8525	8550	8575	8600	8625	8650	8675
	-347,41	0,013319	0,014661	0,016059	0,017513	0,019022	0,020586	0,022206	0,023884	0,025621	0,027418	0,02928	0,031207	0,033204	0,035273	0,037418	0,03964	0,041943
	-167,41	2,414885	2,443761	2,472885	2,502247	2,531805	2,561492	2,591205	2,620809	2,650125	2,678933	2,706964	2,733895	2,759347	2,782878	2,803981	2,822077	2,836519
	-147,41	2,580559	2,60773	2,635012	2,662397	2,689846	2,717283	2,744593	2,771622	2,798169	2,823984	2,848764	2,872148	2,893715	2,912976	2,929374	2,942278	2,950981
	-122,41	2,777644	2,802476	2,827254	2,851972	2,876588	2,90102	2,925145	2,948795	2,971755	2,993757	3,01448	3,033539	3,05049	3,064819	3,075941	3,083197	3,08585
	-97,412	2,818229	2,839412	2,860383	2,881147	2,901664	2,921858	2,941603	2,960733	2,97903	2,996223	3,011987	3,025936	3,037622	3,046527	3,052067	3,053581	3,050334
	-72,412	2,847629	2,865052	2,882122	2,898855	2,915221	2,931149	2,946521	2,961173	2,974891	2,987408	2,9984	3,007486	3,01422	3,018089	3,018511	3,014832	3,006322
	-47,412	2,865765	2,879353	2,892466	2,905134	2,917339	2,92902	2,94007	2,950331	2,959598	2,967613	2,974059	2,978562	2,980686	2,979928	2,975714	2,967401	2,954268
	-22,412	2,872605	2,882313	2,891448	2,900053	2,908126	2,915618	2,922434	2,928429	2,93341	2,937128	2,939282	2,939509	2,937385	2,932422	2,924062	2,911674	2,894552
	2,58783	2,868156	2,873968	2,879133	2,883711	2,887714	2,891108	2,893814	2,8957	2,896586	2,896242	2,894378	2,890651	2,884653	2,875914	2,863895	2,847983	2,827492
	27,5878	2,852464	2,854389	2,855622	2,856237	2,856263	2,855682	2,854429	2,852389	2,849398	2,845243	2,839654	2,832305	2,822811	2,810723	2,795523	2,776624	2,75336
	52,5878	2,825604	2,82368	2,821046	2,817792	2,813964	2,809557	2,804523	2,798763	2,792132	2,784435	2,775421	2,764789	2,752175	2,737156	2,71924	2,697866	2,672396
	77,5878	2,787684	2,781974	2,775568	2,768569	2,761037	2,752981	2,744369	2,735117	2,7251	2,71414	2,702011	2,688433	2,673069	2,655523	2,635333	2,611968	2,584822
	102,587	2,738839	2,729438	2,719386	2,708797	2,697741	2,686241	2,674276	2,661782	2,648647	2,634716	2,619783	2,603594	2,585839	2,566152	2,544103	2,519196	2,49086
	127,587	2,679233	2,666273	2,652736	2,638745	2,624377	2,609665	2,5946	2,57913	2,563163	2,546559	2,529137	2,510666	2,490866	2,469401	2,445877	2,419835	2,390744
	152,587	2,609062	2,592716	2,575896	2,558729	2,541295	2,523634	2,505747	2,487593	2,469091	2,450123	2,430527	2,410096	2,38858	2,365675	2,341025	2,314209	2,284741
	177,587	2,528561	2,509048	2,489192	2,469116	2,448902	2,428591	2,408189	2,387662	2,366943	2,345927	2,324472	2,302396	2,279476	2,255442	2,229975	2,202697	2,173169
	202,587	2,462491	2,440331	2,41798	2,395547	2,373108	2,350707	2,328357	2,306041	2,283714	2,261304	2,23871	2,215801	2,192416	2,168358	2,143391	2,117236	2,089565
	402,587	-0,01014	-0,01177	-0,01335	-0,01487	-0,01635	-0,01777	-0,01914	-0,02045	-0,0217	-0,0229	-0,02403	-0,0251	-0,02609	-0,02702	-0,02787	-0,02865	-0,02936

Figure 4.28: Numerical σ_1 of HAP2E,pres

		8275	8300	8325	8350	8375	8400	8425	8450	8475	8500	8525	8550	8575	8600	8625	8650	8675
	-347,41	-8,62302	-8,42831	-8,23179	-8,03348	-7,8334	-7,63153	-7,42788	-7,22243	-7,01514	-6,80598	-6,59491	-6,3819	-6,16689	-5,94987	-5,7308	-5,50968	-5,2865
	-167,41	-11,8504	-11,776	-11,7034	-11,6324	-11,563	-11,4951	-11,4286	-11,3636	-11,2999	-11,2375	-11,1764	-11,1164	-11,0575	-10,9995	-10,9422	-10,8855	-10,829
	-147,41	-12,1066	-12,0409	-11,9771	-11,9151	-11,8547	-11,7959	-11,7387	-11,683	-11,6288	-11,5759	-11,5244	-11,474	-11,4248	-11,3765	-11,329	-11,282	-11,2353
	-122,41	-12,4321	-12,3773	-12,3245	-12,2735	-12,2243	-12,1768	-12,131	-12,0867	-12,044	-12,0027	-11,9628	-11,9241	-11,8865	-11,8497	-11,8137	-11,7781	-11,7426
	-97,412	-12,6035	-12,5584	-12,5153	-12,4741	-12,4349	-12,3974	-12,3617	-12,3277	-12,2952	-12,2643	-12,2348	-12,2066	-12,1795	-12,1533	-12,1278	-12,1028	-12,0778
	-72,412	-12,7613	-12,7259	-12,6925	-12,6612	-12,6318	-12,6043	-12,5786	-12,5546	-12,5324	-12,5117	-12,4926	-12,4748	-12,4582	-12,4426	-12,4278	-12,4135	-12,3993
	-47,412	-12,9052	-12,8796	-12,8561	-12,8345	-12,815	-12,7973	-12,7816	-12,7677	-12,7556	-12,7452	-12,7363	-12,729	-12,7229	-12,718	-12,714	-12,7106	-12,7074
σ2	-22,412	-13,0353	-13,0195	-13,0057	-12,994	-12,9843	-12,9766	-12,9708	-12,9669	-12,9649	-12,9647	-12,9662	-12,9693	-12,9738	-12,9797	-12,9866	-12,9943	-13,0024
σxx	2,58783	-13,1512	-13,1454	-13,1415	-13,1397	-13,1399	-13,1421	-13,1463	-13,1524	-13,1606	-13,1706	-13,1824	-13,196	-13,2112	-13,2279	-13,2458	-13,2648	-13,2845
τxy	27,5878	-13,2532	-13,2574	-13,2635	-13,2716	-13,2818	-13,294	-13,3082	-13,3244	-13,3427	-13,363	-13,3852	-13,4093	-13,4352	-13,4629	-13,492	-13,5224	-13,5539
σyy	52,5878	-13,3412	-13,3555	-13,3717	-13,3899	-13,4102	-13,4324	-13,4567	-13,4831	-13,5116	-13,5422	-13,5748	-13,6095	-13,6462	-13,6848	-13,7252	-13,7672	-13,8107
	77,5878	-13,4154	-13,44	-13,4665	-13,4949	-13,5253	-13,5577	-13,5922	-13,6288	-13,6675	-13,7085	-13,7516	-13,7969	-13,8444	-13,894	-13,9457	-13,9994	-14,0549
	102,587	-13,476	-13,5111	-13,548	-13,5868	-13,6275	-13,6702	-13,715	-13,7619	-13,8109	-13,8622	-13,9158	-13,9718	-14,0301	-14,0907	-14,1537	-14,2191	-14,2867
	127,587	-13,5233	-13,5691	-13,6166	-13,666	-13,7172	-13,7703	-13,8255	-13,8828	-13,9422	-14,004	-14,0681	-14,1346	-14,2037	-14,2753	-14,3496	-14,4265	-14,5062
	152,587	-13,5577	-13,6144	-13,6728	-13,7329	-13,7948	-13,8586	-13,9243	-13,9921	-14,0621	-14,1343	-14,2089	-14,286	-14,3657	-14,4482	-14,5336	-14,622	-14,7135
	177,587	-13,5795	-13,6475	-13,717	-13,7882	-13,861	-13,9356	-14,0121	-14,0905	-14,171	-14,2538	-14,3389	-14,4265	-14,5168	-14,61	-14,7063	-14,8058	-14,9088
	202,587	-13,6295	-13,7094	-13,7908	-13,8736	-13,958	-14,044	-14,1317	-14,2213	-14,3128	-14,4064	-14,5022	-14,6006	-14,7016	-14,8054	-14,9125	-15,0229	-15,137
	402,587	-12,1264	-12,3492	-12,5701	-12,7893	-13,0065	-13,222	-13,4355	-13,647	-13,8566	-14,0641	-14,2694	-14,4726	-14,6735	-14,8721	-15,0683	-15,2621	-15,4536

Figure 4.29: Numerical σ_2 of HAP2E,pres

	Plaats n	7300	7300	7325	7350	7375	7400	7425	7450	7475	7500	7525	7550	7575	7600	7625	7650	7675	7700
	-347,412	-25,2425	-25,2425	-26,4784	-33,0409	-42,7808	-44,5317	-26,0217	-19,6229	-17,5619	-16,4524	-15,6301	-14,9833	-14,4537	-14,0136	-13,642	-13,3235	-13,0458	-12,7993
	-167,412	-10,4228	-10,4228	-10,3583	-10,257	-10,1611	-10,1218	-10,1806	-10,351	-10,614	-10,9279	-11,2446	-11,5266	-11,752	-11,9145	-12,0175	-12,0686	-12,0768	-12,0504
	-147,412	-10,3927	-10,3927	-10,3451	-10,2798	-10,2236	-10,2096	-10,2642	-10,3973	-10,5987	-10,8427	-11,0977	-11,3353	-11,5363	-11,6912	-11,7986	-11,8617	-11,8862	-11,8781
	-122,412	-10,259	-10,259	-10,2264	-10,1903	-10,1662	-10,1733	-10,2271	-10,3341	-10,489	-10,6773	-10,8792	-11,0755	-11,2507	-11,3955	-11,5055	-11,5806	-11,6232	-11,637
	-97,4122	-10,0969	-10,0969	-10,0748	-10,0568	-10,0521	-10,072	-10,1259	-10,2177	-10,3448	-10,498	-10,6648	-10,8317	-10,9869	-11,122	-11,2318	-11,3146	-11,3707	-11,4018
	-72,4122	-9,94143	-9,94143	-9,92724	-9,92131	-9,92898	-9,95692	-10,0107	-10,0927	-10,2012	-10,3305	-10,472	-10,6163	-10,7546	-10,8796	-10,9866	-11,0728	-11,1375	-11,1812
	-47,4122	-9,78971	-9,78971	-9,78205	-9,78458	-9,80045	-9,83353	-9,8871	-9,96245	-10,0583	-10,1708	-10,294	-10,4211	-10,5455	-10,6613	-10,7642	-10,8514	-10,9215	-10,9741
σxx	-22,4122	-9,64015	-9,64015	-9,63819	-9,64709	-9,66869	-9,70523	-9,75853	-9,82919	-9,91615	-10,0166	-10,1263	-10,2404	-10,3536	-10,4614	-10,5601	-10,6469	-10,7203	-10,7794
Load+	2,587832	-9,49188	-9,49188	-9,4951	-9,50914	-9,53504	-9,57405	-9,62711	-9,69438	-9,77491	-9,86657	-9,96626	-10,0703	-10,1747	-10,2758	-10,3704	-10,4562	-10,5315	-10,5953
Weight+	27,58783	-9,34441	-9,34441	-9,35253	-9,37098	-9,40034	-9,44125	-9,49415	-9,55892	-9,63468	-9,71978	-9,81186	-9,90808	-10,0054	-10,1009	-10,1919	-10,2764	-10,3528	-10,4201
Prestress	52,58783	-9,19755	-9,19755	-9,21039	-9,23282	-9,26515	-9,30767	-9,36049	-9,42336	-9,4955	-9,57556	-9,66172	-9,75179	-9,84338	-9,93415	-10,022	-10,1051	-10,182	-10,2518
	77,58783	-9,0513	-9,0513	-9,06875	-9,09491	-9,12991	-9,17385	-9,22668	-9,28807	-9,35733	-9,43339	-9,5148	-9,59985	-9,68669	-9,77344	-9,85839	-9,94002	-10,0171	-10,0888
	102,5878	-8,9058	-8,9058	-8,9278	-8,95752	-8,99501	-9,04024	-9,09311	-9,15328	-9,22015	-9,29286	-9,37027	-9,45107	-9,53379	-9,61698	-9,69926	-9,77939	-9,85636	-9,9294
	127,5878	-8,76134	-8,76134	-8,78784	-8,82101	-8,86083	-8,90726	-8,96014	-9,01919	-9,08391	-9,15363	-9,22748	-9,30444	-9,38341	-9,46326	-9,54293	-9,62142	-9,69795	-9,77186
	152,5878	-8,61833	-8,61833	-8,6493	-8,68581	-8,72783	-8,77532	-8,82813	-8,88602	-8,94864	-9,01548	-9,08589	-9,15915	-9,23444	-9,31095	-9,38788	-9,46451	-9,54023	-9,61454
	177,5878	-8,47734	-8,47734	-8,51273	-8,55248	-8,59656	-8,64492	-8,69747	-8,75405	-8,81441	-8,87823	-8,94508	-9,01448	-9,08591	-9,15884	-9,23272	-9,3071	-9,38155	-9,45576
	202,5878	-8,31136	-8,31136	-8,35124	-8,3944	-8,44082	-8,49048	-8,54332	-8,59926	-8,65817	-8,71987	-8,78414	-8,85074	-8,91939	-8,98981	-9,06172	-9,13488	-9,20906	-9,28411
	402,5878	-3,84232	-3,84232	-3,92753	-4,02641	-4,1388	-4,26444	-4,40298	-4,55397	-4,71686	-4,89103	-5,07579	-5,27038	-5,474	-5,68581	-5,90495	-6,13054	-6,36172	-6,59765

Figure 4.30: Numerical σ_{xx} of HAP2E,pres

4.2. Elzanaty

4.2.1. Pre-analysis

The coming paragraphs will form a short introduction and outline of the analytical analysis and numerical analysis of the Elzanaty beams, in which some things will be explained. In the last paragraph some general input/information concerning all beams will be discussed.

Analytical analysis

The analytical analysis is based on the Euler-Bernoulli theory. The stress distribution of the web of the beams(section 3.2) is determined in an analytical way. The dimensions are based on figure 3.17 and 3.19, the prestress based on table 3.6 and the applied loads on table 3.8. There are made excel sheets including all stresses like the horizontal and the shear stresses of the web of each beam. In appendix "Elzanaty: Analytical results" of the appendix report the analytical results of the Elzanaty beams. Prior to the results there is added a general informative sheet. This appendix exists out of 4 tables: σ_{xx}, τ_{xy}, σ_1 and σ_2. The phrase "Con" means that the results have been achieved with the cross-sectional properties, like the moment of inertia and the statical moment without the influence of the prestressing steel. The colomn "Rela. to n" refers to the location in the height in the web relative to the neutral axis, with the exception of the upper en bottom line, this is the distance to the ultimate fiber. The colomn "S" refers to the statical moment on that specific height. The tables are on the interval of 380 mm to 380+a mm, from the start of the beam. The grey area of figure 4.31 represents the coverage of the tables of the CW beams. The height of the web is divided in pieces of 20 mm, the length is divided in pieces of 10 mm, so a sort of fine mesh is created. In this way it is possible to determine the stress in many points in the web. The formulas used to determine the different stress components are described in section 2.4, see formulas 2.9, 2.10 and 2.11. Formula 2.8 is used to determine the principal stresses. Subsequently stress diagrams can be made for each beam, so for σ_{xx} and τ_{xy}. The stress f_{ctm} is assumed as the stress at which the first crack in the web will occur. The stress $f_{ctm,fl}$ is assumed as the stress at which the first crack in the ultimate fiber will occur.

Numerical analysis

The numerical computational program used for the numerical analysis is DIANA. The dimensions again are based on figure 3.17 and 3.19, the prestress based on table 3.6 and the applied loads on table 3.8. In DIANA

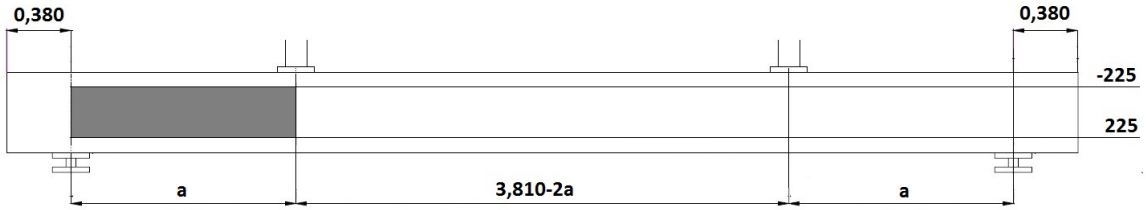

Figure 4.31: Area coverage of tables of the CW beams, distance in m and height in mm

the analysis of the two dimensional model is linear elastic, there is made use of the hexa/quad mesher type, the mesh order is linear. For the element class there is chosen for the regular plane stress elements. The elements have a size of 10 mm. For the material concrete there is chosen for a linear elastic isotropic model. For the steel plates there is also chosen for a linear isotropic model. Further, to model the width of the beam there is made use of a thickness function. The material model of the prestress strands is Von Mises plasticity. The prestress is modeled as embedded reinforcement, where the cables are bonded to the concrete. It has to be taken into account that DIANA calculates losses due to elastic deformation, on beforehand this should be compensated for. For CW1 the numerical model is worked out. The analysis results will be exported to an excel sheet, with a Python script it is possible to present the results in such a way, that it is possible to compare these results with the obtained analytical results. In appendix "Elzanaty: Numerical results" of the appendix report the numerical results of the Elzanaty beams. This appendix exists out of 12(some 13) tables: σ_{xx}, τ_{xy}, σ_{yy}, σ_1(excluding component σ_{yy}), σ_1, σ_2(excluding component σ_{yy}), σ_2, the fraction $\frac{\sigma_{xx,Analytical}}{\sigma_{xx,Numerical}}$, the fraction $\frac{\tau_{xy,Analytical}}{\tau_{xy,Numerical}}$, the fraction $\frac{\sigma_{1,Analytical}}{\sigma_{1,Numerical,excl.\sigma_{yy}}}$, the fraction $\frac{\sigma_{1,Analytical}}{\sigma_{1,Numerical}}$ and the fraction $\frac{\sigma_{1;Poisson0,2}}{\sigma_{1;Poisson0,0}}$. For some experiments there is added a thirteenth table: θ_p. This table gives from certain values of σ_1 the angles of the principal stresses. Further, in the analyses there is taken into account the influence of the Poisson's ratio, by making an analysis with and without the Poisson's ratio. The interpretation of the numerical results will be discussed in the section "Numerical analysis".

General valid input

In this section the input for all beams will be discussed, in this case the cross-sectional properties. Further the way of determining assumed parameters of materials will be discussed, for example f_{ctm}.

Cross-sectional properties

The cross-section is the same for all the Elzanaty beams, there are only differences in the prestress strands. In figure 4.32 once again the cross-section of the Elzanaty beams. In table 4.7 all the cros-sectional properties. It is possible to determine the fraction of $I_{concrete}$, $I_{concrete+holestrands}$ and $EI_{concrete+4(142mm^2)/4(99mm^2)strands}$, then something can be said about the influence on the stress state, because the I is an important property in the determination of the σ_x and τ_{xy}. So $\frac{I_{concrete}}{I_{concrete+holestrands}} = 1,009$, $\frac{EI_{concrete}}{EI_{concrete+4strands(142mm^2)}} = 0,96$ and $\frac{EI_{concrete}}{EI_{concrete+4strands(99mm^2)}} = 0,98$. It can be seen from here that the prestressing steel has a low influence on the moment of inertia I.

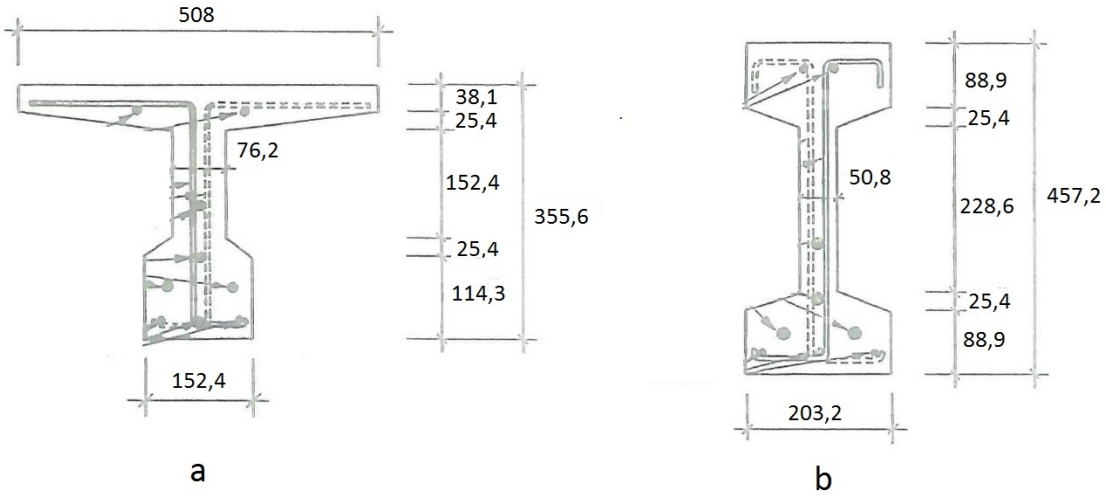

Figure 4.32: Cross-sections(mm): a)CI series b)CW series[9]

Condition	Parameter	Value
Concrete	A[mm^2]	52500
	a_{bottom}[mm]	225
	a_{top}[mm]	225
	I[mm^4]	1322187500
Concrete + hole strands	A[mm^2]	51932
	a_{bottom}[mm]	226,5
	a_{top}[mm]	223,5
	I[mm^4]	1310131745
Concrete + 4 strands(142 mm^2)	EA[$^N/_{mm^2} \cdot mm^2$]*	2185550416
	a_{bottom}[mm]	218,9
	a_{top}[mm]	231,1
	EI[$^N/_{mm^2} \cdot mm^4$]*	5,46·10^{13}
Concrete + 4 strands(99 mm^2)	EA[$^N/_{mm^2} \cdot mm^2$]*	2150333952
	a_{bottom}[mm]	221
	a_{top}[mm]	229
	EI[$^N/_{mm^2} \cdot mm^4$]*	5,39·10^{13}

* E based on concrete mixture of CW1

Table 4.7: Cross-sectional properties

Material properties
A number of parameters are known from the experiments. From these known parameters the unknown parameters are calculated, according to the Eurocode. In this case it is only about concrete properties. The property f_{cm} can be calculated according formula 4.6.

$$f_{cm} = f_{ck} + 4N/mm^2 \tag{4.6}$$

where:

f_{cm} = the mean concrete compressive strength
f_{ck} = the characteristic concrete compressive strength

In formula 4.7 the expression to calculate f_{ctm}. This expression is only valid for concrete mixtures <C50/60.

$$f_{ctm} = 0,30 f_{ck}^{\frac{2}{3}} \tag{4.7}$$

where:

f_{ctm} = the mean concrete tensile strength
f_{ck} = the characteristic concrete cylindrical compressive strength

In formula 4.8 the expression to calculate f_{ctm}. This expression is only valid for concrete mixtures >C50/60.

$$f_{ctm} = 2,12 ln\left(1 + \frac{f_{cm}}{10}\right) \tag{4.8}$$

where:

f_{ctm} = the mean concrete tensile strength
f_{cm} = the mean concrete cylindrical compressive strength

In formula 4.9 the expression to calculate f_{ctk}.

$$f_{ctk} = 0,7 f_{ctm} \tag{4.9}$$

where:

f_{ctk} = the characteristic concrete tensile strength
f_{cm} = the mean concrete tensile strength

In formula 4.10 the expression to calculate $f_{ctm,fl}$.

$$f_{ctm,fl} = max\{\left(1,6 - \frac{h}{1000}\right) f_{ctm}; f_{ctm}\} \tag{4.10}$$

where:

h = the height of the element, in mm
f_{ctm} = the mean concrete tensile strength
$f_{ctm,fl}$ = the mean concrete flexural tensile strength

4.2.2. Analytical analysis

In this section the analytical results per beam will be discussed. In each coming section first the scheme and other conditions are given, then attention is paid to the stress states in the web. Further the approach and interpretation of the Eurocode will be discussed.

CW1

In figure 4.33 the load scheme of CW1 is schematized. In table 4.8 an overview of the applicable concrete parameters, the present external loads and the present prestress. The f_{cm} = 76,55 N/mm^2 was already known from the Elzanaty study, see section 3.2. As described in the previous section, the parameter f_{ctm} can be calculated out of f_{cm}, $f_{ctm} = 2,12 ln\left(1 + \frac{76,55}{10}\right)$ = 4,6 N/mm^2. The q_{weight} = 25·0,0525 = 1,3125 kN/m. The F_{prestr} = 11,20·52500·10^{-3} = 588 kN, $F_{prestr/strand}$ = 588/4 = 147 kN and $\sigma_{p,strand}$ = 147·10^3 / 142 = 1035,21 N/mm^2. The $f_{ctm,fl}$ = max $\{\left(1,6 - \frac{450}{1000}\right) \cdot 4,6; 4,6\}$ = 5,3 N/mm^2.

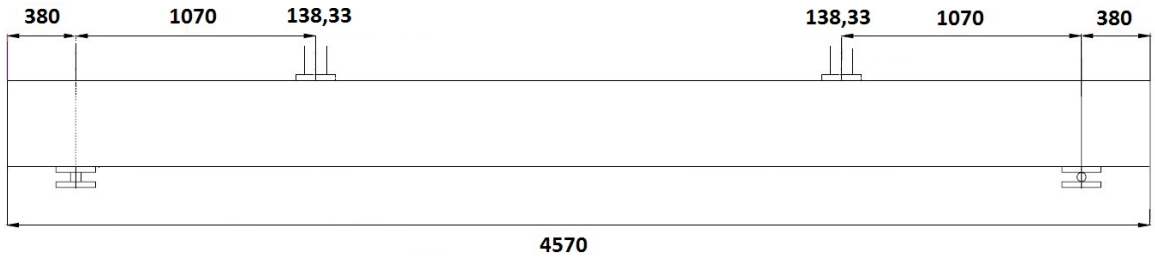

Figure 4.33: The load scheme CW1, dimensions in mm and force in kN

Type parameter	Parameter	Value
Concrete property	$\rho_{density}[^{kN}/_{m^3}]$	25
	$f_{cm}[^{N}/_{mm^2}]^{*}$	76,55
	$f_{ctm,fl}[^{N}/_{mm^2}]^{**}$	5,3
	$f_{ctm}[^{N}/_{mm^2}]^{**}$	4,6
Loads	F_1[kN]*	138,33
	q_{weight}[kN/m]**	1,3125
Prestress	$\sigma_{cp}[^{N}/_{mm^2}]^{*}$	11,20
	A_{strand}[mm^2]*	142
	F_{prestr}[kN]**	588
	$F_{prestr/strand}$[kN]**	147
	$\sigma_{p,strand}[^{N}/_{mm^2}]^{**}$	1035

* based on obtained data, see section 3.2
** based on calculated data

Table 4.8: Applicable concrete parameters, external loads and present prestress CW1

Results
In this part the results will be discussed. In appendix “Elzanaty: Shear forces and Moments” of the appendix report there is added the distribution of the shear force and the moment, caused by the loads of table 4.8. This is on the interval of 380 mm to 1450 mm, from the start of the beam, see figure 4.33. In appendix “Elzanaty: Analytical results” of the appendix report there is added an excel sheet, containing data of σ_{xx}, τ_{xy} and σ_1 and σ_2. The σ_{xx} consists of the loads and the prestress, the τ_{xy} of the loads. The colomn “Rela. to n” refers to the location in the height in the web relative to the neutral axis, with the exception of the upper en bottom line, this is the distance to the ultimate fiber. The colomn “S” refers to the statical moment on that specific height. This is again on the interval of 380 mm to 1450 mm, from the start of the beam. The red color in the σ_1 colomn represent values > f_{ctm}, the yellow color values > 0,9f_{ctm}. From this sheet it can be seen that the analytical solution gives the highest principal stress at the transition point of flage-web at 380 mm from the start of the beam, so above the external load. In figure 4.34 the distribution of the σ_{xx} and τ_{xy} at 920 mm from start of the beam over the height of the beam, it can be seen that the highest τ_{xy} and the mean effective σ_{cp} is around the neutral axis.

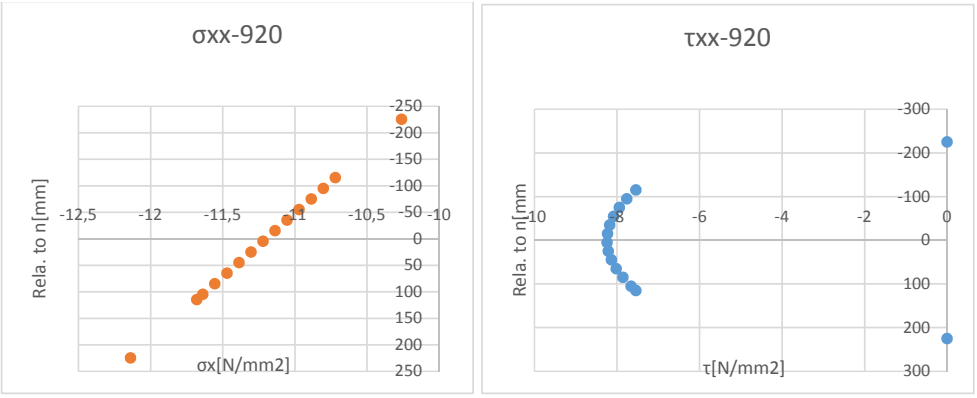

Figure 4.34: Chart of the σ_{xx} and τ_{xy} of CW1

A handcalculation of the transition point of flange-web at 380 mm from the start of the beam. The σ_{xx} caused by the loads;

$$\frac{-0,09476 \cdot 10^6 \cdot -115}{1322187500} = 8,24 \cdot 10^{-3} N/mm^2$$

The τ_{xy} caused by the loads;

$$\frac{140,8303 \cdot 10^3 \cdot 3557500}{50 \cdot 1322187500} = 7,57841 N/mm^2$$

The eccentrical moment caused by the prestress;

$$-147 \cdot 2 \cdot (0,225 - 0,050735) - 147 \cdot 1 \cdot (0,225 - 0,0882) - 147 \cdot 1 \cdot (0,225 - 0,1574) = -81,28 kNm$$

The σ_{xx} caused by the eccentrical moment;

$$\frac{-81,28 \cdot 10^6 \cdot -115}{1322187500} = 7,069 N/mm^2$$

The mean effective σ_{cp} = -11,20 N/mm^2. So the principal tensile stress σ_1 will be;

$$\frac{8,24 \cdot 10^{-3} + 7,069 - 11,20}{2} + \sqrt{\left(\frac{8,24 \cdot 10^{-3} + 7,069 - 11,20}{2}\right)^2 + (7,57841)^2} = 5,792 N/mm^2$$

So the principal compressive stress σ_2 will be;

$$\frac{8,24 \cdot 10^{-3} + 7,069 - 11,20}{2} - \sqrt{\left(\frac{8,24 \cdot 10^{-3} + 7,069 - 11,20}{2}\right)^2 + (7,57841)^2} = -9,915 N/mm^2$$

According to the stress distribution of the analytical model this would be the critical point.

4.2.3. Numerical analysis

In this section the numerical results per beam will be discussed. The schemes and other conditions are the same as in the analytical analysis. First the specific input for the model is mentioned, then the numerical results will be verified with the analytical results. Finally the results will be discussed.

CW1

First the numerical model in DIANA will be discussed. In table 4.9 an overview of the prestress as applied in of CW1 in DIANA. The values in the column "σ_p incl. losses" is the applied prestress in the strands. In figure 4.35 the meshed model of CW1, in figure 4.36 a more detailed figure of the right support and the plate of the external force. The elements can be seen clearly. The elements of the concrete are 10mm×10mm and the elements of the steel plates are 10mm×10mm. Further the prestress cables can be seen clearly. In table 4.10 all parameters used in the model, this table forms an addition to the already known parameters.

Type prestress	**Layer**	**Strands[-]**	σ_p **excl. losses[N/mm^2]**	σ_p **incl. losses[N/mm^2]**
4 strands(142 mm^2)	1	2	1035	1135
	2	1	1035	1125
	3	1	1035	1106

Table 4.9: Prestress of CW1 as aplied in DIANA

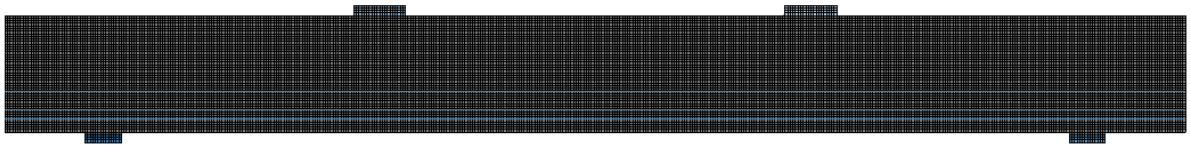

Figure 4.35: The meshed beam CW1

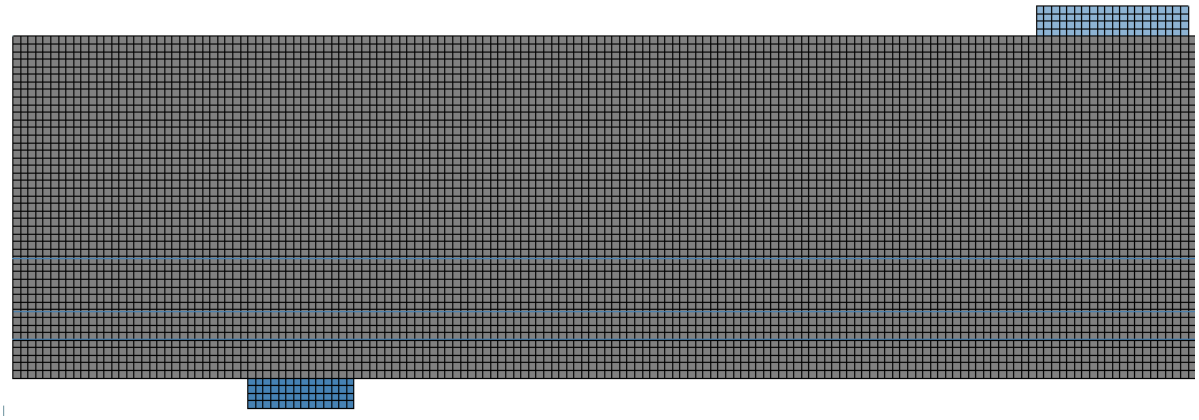

Figure 4.36: Detail of meshed beam CW1

Object	**Parameter**	**Value**
Concrete beam	E[$^N/_{mm^2}$]	39788
	h$_{beam}$[mm]	450
	l$_{beam}$[mm]	4570
	b$_{beam}$[m]	variable
	$\nu_{concrete}$[-]	0,2
Steel plate support	E[$^N/_{mm^2}$]	210000
	h$_{plate}$[mm]	40
	l$_{plate}$[mm]	140
	b$_{plate}$[mm]	140
	$\rho_{density}$[$^{kN}/_{m^3}$]	78,5
	ν_{steel}[-]	0,3
Steel plate force	E[$^N/_{mm^2}$]	210000
	h$_{plate}$[mm]	40
	l$_{plate}$[mm]	200
	b$_{plate}$[mm]	200
	$\rho_{density}$[$^{kN}/_{m^3}$]	78,5
	ν_{steel}[-]	0,3
Prestress cables	E[$^N/_{mm^2}$]	195000
	Yield stress[$^N/_{mm^2}$]	1522

Table 4.10: Parameters CW1 used in DIANA

As described before to compare the numerical results with the analytical results, the numerical results have to be exported in a way it is possible to compare it with the analytical results. In every point in the mesh 4 nodes of 4 elements come together, this means 4 results per node. In case of a constant width of the cross-section the results of the different stresses almost equal each other. In this case the average has been taken(see figure 4.8, section 4.1.3). In case of a abrupt widening of the cross-section, around the transion of web to flange, the results of τ_{xy} differ significantly. In this case the nodes are located at the at the transition of web to flange. The results of the elements of τ_{xy} located in the widened part were significantly lower(20 to 30%), for the sake of realism this results of these elements are left out. On large scale, a Python script is used to export the numerical results in an excel sheet. In this way it is possible to compare the numerical results with the analytical results.

Verification

In order to link the analytical model to the numerical model a verification is done. This verification is done by comparing different results, like σ_{xx}, τ_{xy} and the principal stress σ_1. Good use can be made of the different fractions as described in section 4.2.1. In figure 4.37 the results of the fraction of $\frac{\tau_{xy,Analytical}}{\tau_{xy,Numerical}}$, in figure 4.38 the results of the fraction $\frac{\sigma_{1,Analytical}}{\sigma_{1,Numerical}}$. These tables are on the interval of 810 mm to 970 mm, from the start of the beam. Again the colomn "Plaats n" refers to the location of the height in the web relative to the neutral axis, with the exception of the upper en bottom line, this is the distance to the ultimate fiber.

	Plaats n	810	820	830	840	850	860	870	880	890	900	910	920	930	940	950	960	970
	-225	0	0	0	0	0	0	0	0	0	0	0	0	0	0	0	0	0
	-115	0,991671	0,991288	0,99109	0,991052	0,991146	0,991348	0,991632	0,991974	0,99235	0,992735	0,993108	0,993443	0,993718	0,993908	0,993991	0,993943	0,993739
	-95	1,000585	1,000043	0,999681	0,999471	0,99939	0,999414	0,999518	0,99968	0,999877	1,000088	1,00029	1,000464	1,000588	1,00064	1,000602	1,000453	1,000173
	-75	1,001043	1,00038	0,999882	0,999524	0,999285	0,999142	0,999075	0,999064	0,999089	0,999133	0,999177	0,999205	0,999199	0,999143	0,999023	0,998824	0,998532
	-55	1,000721	1,000026	0,999478	0,999054	0,998734	0,998501	0,998337	0,998226	0,998152	0,998101	0,998058	0,998012	0,99795	0,997862	0,997737	0,997567	0,997343
	-35	0,99974	0,999088	0,998559	0,998135	0,997799	0,997537	0,997335	0,997181	0,997063	0,996972	0,996898	0,996833	0,99677	0,996704	0,996629	0,996542	0,996441
τxy(Con.)	-15	0,998221	0,997669	0,997213	0,996838	0,996533	0,996286	0,996089	0,995932	0,995811	0,995717	0,995649	0,9956	0,995571	0,99556	0,995566	0,995593	0,995644
Analytical	5	0,996279	0,995867	0,995519	0,995227	0,994982	0,994778	0,99461	0,994475	0,994371	0,994296	0,99425	0,994236	0,994254	0,99431	0,994409	0,994557	0,994763
τxy Numerical	25	0,994027	0,993774	0,993552	0,993357	0,993184	0,993033	0,992903	0,992796	0,992712	0,992657	0,992635	0,992652	0,992715	0,992831	0,993012	0,993267	0,99361
	45	0,991565	0,991474	0,991377	0,991275	0,991169	0,991063	0,990961	0,990869	0,990794	0,990745	0,990729	0,990758	0,990842	0,990994	0,991227	0,991557	0,992
	65	0,992601	0,992736	0,992812	0,992838	0,992822	0,992775	0,992707	0,99263	0,992557	0,992503	0,99248	0,992505	0,992593	0,992762	0,993031	0,993417	0,993941
	85	0,996486	0,996855	0,997103	0,997246	0,997301	0,997286	0,99722	0,997122	0,997012	0,99691	0,996836	0,996811	0,996857	0,996996	0,99725	0,997645	0,998203
	105	0,994562	0,994918	0,995116	0,995179	0,995128	0,994987	0,994778	0,994525	0,994251	0,993979	0,993734	0,993538	0,993416	0,993392	0,993492	0,993741	0,994166
	115	0,986163	0,986498	0,986668	0,986696	0,986606	0,986422	0,986167	0,985865	0,98554	0,985217	0,984919	0,98467	0,984495	0,984418	0,984466	0,984664	0,985039
	225	0	0	0	0	0	0	0	0	0	0	0	0	0	0	0	0	0

Figure 4.37: Fraction $\frac{\tau_{xy,Analytical}}{\tau_{xy,Numerical}}$ of CW1

	810	820	830	840	850	860	870	880	890	900	910	920	930	940	950	960	970
-225	0	0	0	0	0	0	0	0	0	0	0	0	0	0	0	0	0
-115	0,994611	0,991835	0,989633	0,987963	0,986788	0,986074	0,985791	0,98591	0,986408	0,987265	0,988462	0,989986	0,991827	0,993979	0,996439	0,99921	1,002299
-95	1,012027	1,008219	1,005101	1,002628	1,000762	0,999467	0,998715	0,99848	0,998743	0,999488	1,000706	1,002391	1,004546	1,007177	1,010297	1,013928	1,018099
-75	1,018147	1,013816	1,010214	1,007294	1,005016	1,003345	1,002252	1,001712	1,001707	1,002223	1,003253	1,004794	1,006851	1,009434	1,012559	1,016253	1,020548
-55	1,022482	1,01777	1,013821	1,010585	1,008021	1,006095	1,004776	1,004041	1,003874	1,004262	1,005199	1,006686	1,00873	1,011345	1,01455	1,018374	1,022856
σ1(Con.)	-35	1,025118	1,020151	1,015974	1,012536	1,009794	1,007712	1,006262	1,005421	1,005173	1,005508	1,006422	1,007917	1,010004	1,012699	1,016025	1,020013	1,024704
Analytical	-15	1,026143	1,021031	1,016728	1,013183	1,01035	1,008194	1,006687	1,005805	1,005535	1,005868	1,006802	1,008343	1,0105	1,013294	1,01675	1,020902	1,025793
σ1	5	1,025644	1,020482	1,016141	1,012565	1,009711	1,007541	1,006028	1,005151	1,004895	1,005254	1,006227	1,007822	1,010052	1,012937	1,016505	1,020792	1,025841
Numerical(σxx	25	1,023712	1,01858	1,014269	1,010723	1,007897	1,005755	1,004269	1,003418	1,00319	1,00358	1,00459	1,006226	1,008505	1,011447	1,015083	1,019449	1,024589
τxy σyy)	45	1,020442	1,015402	1,011173	1,007699	1,004933	1,00284	1,001392	1,000571	1,000365	1,000771	1,00179	1,003432	1,005714	1,008659	1,012296	1,016662	1,021801
	65	1,02187	1,017052	1,013007	1,00968	1,007029	1,005023	1,003637	1,002857	1,002675	1,00309	1,004108	1,005742	1,008012	1,010942	1,014566	1,018922	1,024056
	85	1,027035	1,02251	1,018692	1,015535	1,013002	1,011069	1,009718	1,00894	1,008731	1,009098	1,010051	1,011607	1,01379	1,016631	1,020164	1,024432	1,029484
	105	1,021236	1,016863	1,013144	1,010034	1,007501	1,00552	1,004077	1,003164	1,002781	1,002934	1,003636	1,004905	1,006766	1,009248	1,012387	1,016224	1,020807
	115	1,005095	1,002076	0,999483	0,997294	0,995497	0,994086	0,99306	0,992423	0,992186	0,992362	0,992971	0,994035	0,995583	0,997644	1,000256	1,003459	1,007296
225	0	0	0	0	0	0	0	0	0	0	0	0	0	0	0	0	0	0

Figure 4.38: Fraction $\frac{\sigma_{1,Analytical}}{\sigma_{1,Numerical}}$ of CW1

σxx(Con.) Analytical σxx Numerical	810	820	830	840	850	860	870	880	890	900	910	920	930	940	950	960	970
-225	1,055216	1,052422	1,049948	1,047771	1,045872	1,044229	1,042824	1,041638	1,040655	1,039857	1,039227	1,038748	1,038404	1,038178	1,038053	1,03801	1,038031
-115	0,975728	0,976625	0,977397	0,978047	0,978581	0,979002	0,979313	0,979521	0,979629	0,979643	0,979568	0,97941	0,979176	0,978872	0,978506	0,978087	0,977624
-95	0,96809	0,968709	0,969246	0,969701	0,970074	0,970367	0,97058	0,970715	0,970775	0,970763	0,970685	0,970544	0,970347	0,970101	0,969815	0,969496	0,969156
-75	0,962157	0,962451	0,962707	0,962921	0,96309	0,963213	0,963288	0,963316	0,963297	0,963234	0,96313	0,96299	0,962819	0,962625	0,962416	0,962202	0,961994
-55	0,95779	0,957778	0,957762	0,957737	0,957696	0,957637	0,957557	0,957454	0,957329	0,957182	0,957016	0,956835	0,956646	0,956454	0,956268	0,956098	0,955956
-35	0,954711	0,954425	0,954161	0,953911	0,953668	0,953428	0,953185	0,952939	0,952687	0,952431	0,952172	0,951913	0,951661	0,951421	0,951202	0,951013	0,950867
-15	0,952709	0,952191	0,951711	0,95126	0,950831	0,950417	0,950014	0,949617	0,949226	0,94884	0,948461	0,948092	0,947736	0,9474	0,947092	0,946821	0,946598
5	0,951632	0,950928	0,95027	0,949648	0,949054	0,948481	0,947922	0,947375	0,946837	0,946307	0,945785	0,945275	0,944779	0,944303	0,943853	0,943439	0,94307
25	0,951381	0,950539	0,949743	0,948982	0,948248	0,947533	0,94683	0,946135	0,945446	0,944761	0,944079	0,943403	0,942735	0,94208	0,941442	0,94083	0,940251
45	0,951904	0,950971	0,950076	0,949209	0,948361	0,947522	0,946688	0,945852	0,945012	0,944166	0,943312	0,942451	0,941585	0,940717	0,939852	0,938994	0,938151
65	0,953196	0,952215	0,951257	0,950314	0,949375	0,948432	0,947479	0,946511	0,945523	0,944513	0,943479	0,942421	0,941338	0,940234	0,93911	0,93797	0,936819
85	0,954719	0,953812	0,9529	0,951973	0,951021	0,950038	0,949018	0,947954	0,946844	0,945684	0,944472	0,943206	0,941887	0,940514	0,939088	0,937612	0,936087
105	0,957094	0,956293	0,955453	0,954564	0,953619	0,952612	0,951538	0,95039	0,949165	0,94786	0,946471	0,944997	0,943435	0,941784	0,940043	0,938212	0,93629
115	0,958687	0,957878	0,957022	0,956108	0,95513	0,95408	0,952955	0,951747	0,950454	0,949071	0,947594	0,94602	0,944347	0,942573	0,940695	0,938711	0,93662
225	0,983764	0,981886	0,979985	0,978072	0,976153	0,974237	0,972331	0,970438	0,968562	0,966707	0,964875	0,963067	0,961282	0,959519	0,957776	0,956051	0,954338

Figure 4.39: Fraction $\frac{\sigma_{xx,Analytical}}{\sigma_{xx,Numerical}}$ of CW1

From figures 4.37 and 4.38 it can be seen that in this part of the beam the results of the analytical analysis correspond to the results of the numerical analysis. All parts had a similar result, except around the disturbed areas around the external force, the supports and the anchoring of the prestress. From figure 4.39 it can be seen that there is a little deviation in the results of the σ_{xx}. After analysis it appears that this deviation is not caused by the prestress part, because the fraction $\frac{\sigma_{xx;Analytical;pre}}{\sigma_{xx;Numerical;pre}} < 1\%$. It appears that the deviation is caused by the part of the external force. There is also checked wether the Poisson's ratio had a significant influence on the deviation, this was not the case. For this beam it comes down to a difference of 5%, so <0,9 N/mm^2.

Results

From the numerical results it can be seen that the component σ_{yy} has a local significant effect on the stress state in a beam, this effect is limited to the location of the external load and the support reaction respectively. In figure 4.40 the the results of σ_{yy}, around the support. The σ_{yy} has influence from 380 mm(location external load) up till 780 mm, from start of the beam. The influence is low in the upper part the of the web, at -115 mm relative to the neutral axis. In figure 4.42 the contour plot of σ_{yy}.

σyy Load+ Weight+ Prestress	Plaats n	380	380	390	400	410	420	430	440	450	460	470	480	490	500	510	520	530	540
-225	0,073734	0,073734	0,073172	0,072561	0,071903	0,071199	0,070451	0,069661	0,068828	0,067954	0,067038	0,066083	0,065087	0,064053	0,06298	0,061871	0,060725	0,059544
-115	-0,74023	-0,74023	-0,73983	-0,74043	-0,74159	-0,7429	-0,7439	-0,74417	-0,74332	-0,74097	-0,73679	-0,7305	-0,72188	-0,71078	-0,69712	-0,68088	-0,66211	-0,64091
-95	-1,15848	-1,15848	-1,16176	-1,16611	-1,17092	-1,17555	-1,17935	-1,18167	-1,18189	-1,17944	-1,1738	-1,16455	-1,15137	-1,13403	-1,11244	-1,08659	-1,05661	-1,02269
-75	-1,40631	-1,40631	-1,41486	-1,42424	-1,43376	-1,44268	-1,45022	-1,45557	-1,45798	-1,45671	-1,45115	-1,44076	-1,42516	-1,4041	-1,3775	-1,3454	-1,30801	-1,26563
-55	-1,65452	-1,65452	-1,66978	-1,6857	-1,70154	-1,7164	-1,7293	-1,73924	-1,74522	-1,74632	-1,74172	-1,73075	-1,71294	-1,68804	-1,65596	-1,61686	-1,57105	-1,51902
-35	-1,90323	-1,90323	-1,92666	-1,95091	-1,9751	-1,99811	-2,01866	-2,03541	-2,04698	-2,05212	-2,04972	-2,03892	-2,01913	-1,99005	-1,9517	-1,90435	-1,84855	-1,78503
-15	-2,15263	-2,15263	-2,18557	-2,22014	-2,25524	-2,28936	-2,32072	-2,34736	-2,36734	-2,37884	-2,38032	-2,37061	-2,34894	-2,31503	-2,26902	-2,21146	-2,14325	-2,06553
5	-2,40214	-2,40214	-2,44567	-2,49286	-2,54222	-2,59155	-2,63819	-2,67917	-2,71157	-2,73267	-2,74024	-2,73263	-2,70891	-2,66885	-2,61288	-2,54203	-2,45778	-2,36191
25	-2,64907	-2,64907	-2,70401	-2,76678	-2,83513	-2,90568	-2,97419	-3,03605	-3,08667	-3,12191	-3,13844	-3,13398	-3,10741	-3,05874	-2,98899	-2,90005	-2,79434	-2,67468
45	-2,8872	-2,8872	-2,95435	-3,03688	-3,13128	-3,23207	-3,33242	-3,42489	-3,50218	-3,55789	-3,58703	-3,58647	-3,55502	-3,49333	-3,40358	-3,28913	-3,15404	-3,0027
65	-3,09858	-3,09858	-3,1794	-3,28963	-3,42333	-3,57123	-3,72181	-3,86257	-3,98144	-4,06811	-4,11503	-4,11801	-4,07627	-3,99212	-3,87024	-3,7168	-3,53873	-3,3429
85	-3,22991	-3,22991	-3,32884	-3,48547	-3,68896	-3,92246	-4,16484	-4,39321	-4,58576	-4,72449	-4,79732	-4,79909	-4,73138	-4,60125	-4,41941	-4,19823	-3,95007	-3,68606
105	-3,21758	-3,21758	-3,34291	-3,57465	-3,89436	-4,27244	-4,67072	-5,04681	-5,36007	-5,57796	-5,68096	-5,66457	-5,53798	-5,32017	-5,03486	-4,70601	-4,35463	-3,99733
115	-2,46643	-2,46643	-2,57616	-2,79134	-3,09477	-3,45809	-3,84342	-4,20755	-4,50848	-4,71286	-4,80187	-4,77343	-4,64021	-4,42446	-4,152	-3,84716	-3,52984	-3,21453
225	-7,48453	-7,48453	-6,5134	-4,6615	-3,33402	-3,33687	-5,25161	-9,12796	-18,307	-4,30588	-1,64528	-0,40164	-0,28312	-0,16176	-0,12478	-0,0993	-0,08531	-0,07529

Figure 4.40: Numerical σ_{yy} of CW1

From the results it also can be seen that τ_{xy} is disturbed around the external load and the support reaction, the disturbance around the support runs from 380 mm up till around 710 mm. In figure 4.41 the results of the fraction $\frac{\tau_{xy,Analytical}}{\tau_{xy,Numerical}}$ around the external load. In figure 4.43 the contour plot of τ_{xy}.

τxy(Con.) Analytical τxy Numerical	Plaats n	380	380	390	400	410	420	430	440	450	460	470	480	490	500	510	520	530	540
-225	0	0	0	0	0	0	0	0	0	0	0	0	0	0	0	0	0	0	0
-115	1,780502	1,819244	1,766478	1,715957	1,667601	1,621345	1,577135	1,534931	1,494699	1,456413	1,420049	1,385586	1,353001	1,322267	1,293354	1,266225	1,240839	1,217148
-95	1,796458	1,835547	1,783072	1,732644	1,684221	1,637766	1,593255	1,550669	1,509999	1,471237	1,43438	1,399422	1,366354	1,33516	1,30582	1,278303	1,252571	1,228578
-75	1,802315	1,841532	1,78965	1,739498	1,691075	1,644388	1,599451	1,556285	1,51492	1,475391	1,437731	1,401969	1,368126	1,336214	1,306228	1,278153	1,251958	1,227599
-55	1,812894	1,852341	1,800506	1,750084	1,7011	1,653587	1,607597	1,563198	1,520473	1,479512	1,440402	1,403227	1,36805	1,33492	1,303859	1,274869	1,247927	1,222989
-35	1,828721	1,868512	1,816092	1,764802	1,714645	1,665659	1,617923	1,57156	1,526721	1,483576	1,442295	1,403033	1,36592	1,331053	1,298489	1,268247	1,24031	1,214629
-15	1,850389	1,890652	1,837045	1,784318	1,732376	1,681219	1,630947	1,581749	1,53388	1,487631	1,443294	1,401139	1,361387	1,324201	1,28968	1,257859	1,228716	1,202184
5	1,878296	1,919165	1,864012	1,809469	1,755225	1,701183	1,647454	1,594337	1,542256	1,491704	1,443174	1,397108	1,353864	1,313691	1,276732	1,243025	1,212526	1,185119
25	1,912404	1,954016	1,89754	1,841248	1,784429	1,726804	1,668515	1,610058	1,55217	1,495693	1,441456	1,390177	1,342403	1,298492	1,258617	1,222789	1,190897	1,162735
45	1,952006	1,994479	1,937946	1,880759	1,821524	1,759669	1,695424	1,629684	1,563763	1,499135	1,437188	1,37906	1,325556	1,277138	1,233962	1,195945	1,162829	1,134247
65	2,02018	2,064137	2,013596	1,959629	1,899081	1,830667	1,755012	1,674299	1,591605	1,510172	1,432814	1,361593	1,297736	1,241736	1,19352	1,152639	1,118425	1,090115
85	2,111229	2,157168	2,130229	2,093027	2,037838	1,961337	1,865337	1,755894	1,641122	1,528808	1,424839	1,33271	1,253809	1,18802	1,134333	1,091313	1,057398	1,031086
105	2,15221	2,19904	2,225949	2,233324	2,202999	2,125052	2,002586	1,850528	1,688668	1,534119	1,39754	1,283296	1,191432	1,119708	1,065021	1,024205	0,994399	0,973185
115	2,143988	2,190639	2,237505	2,262814	2,243829	2,167114	2,035864	1,868887	1,691074	1,523169	1,377217	1,257388	1,16288	1,090537	1,036503	0,997066	0,968997	0,949641
225	0	0	0	0	0	0	0	0	0	0	0	0	0	0	0	0	0	0	0

Figure 4.41: Fraction $\frac{\tau_{xy,Analytical}}{\tau_{xy,Numerical}}$ of CW1

The maximum τ_{xy} = -8,287 N/mm^2(920 mm), around the neutral axis, this falls back to -4,315 N/mm^2(380 mm), see also appendix "Elzanaty: Numerical results" of the appendix report. In figure 4.44 the fraction

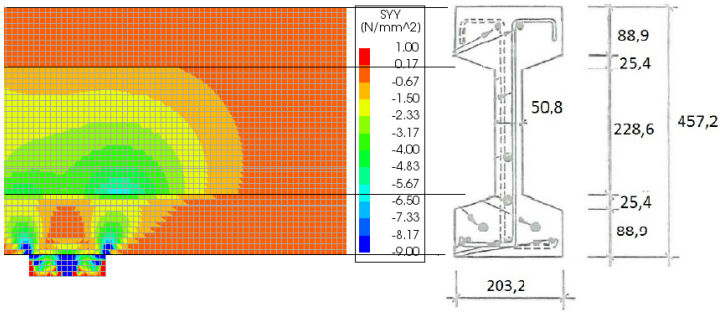

Figure 4.42: Contour plot σ_{yy} of CW1

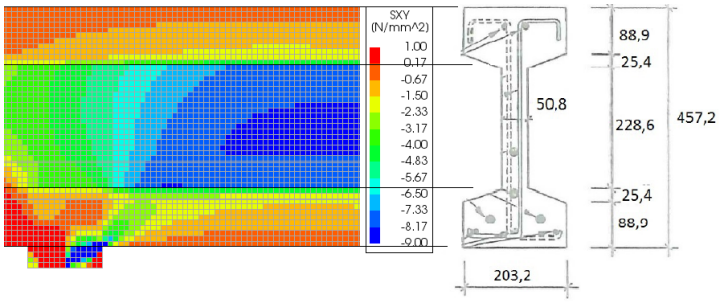

Figure 4.43: Contour plot τ_{xy} of CW1

$\frac{\sigma_{xx,Analytical}}{\sigma_{xx,Numerical}}$, it can be seen that there is also a deviation of σ_{xx} around the external load. As described before the σ_{xx} consists out of the contributions of the external load, the weight and the prestress. After analysis it appears that the deviation is caused by the external load part. This can be seen in figure 4.44, in the part below the neutral axis the value of the fraction drops towards 0,60-0,70 and in the part above the neutral axis the value of the fraction rises towards 1,25-1,30. The drop to 0,60-0,70 means that the value of $\sigma_{xx,Analytical}$ related to $\sigma_{xx,Numerical}$ is too high, this is caused by the tensional part of $\sigma_{xx,Analytical}$. The rise to 1,25-1,30 means that the value of $\sigma_{xx,Analytical}$ related to $\sigma_{xx,Numerical}$ is too low, this is caused by the compressional part of $\sigma_{xx,Analytical}$. This means that the part of $\sigma_{xx,Analytical}$ that is caused by the external force is too high.

σxx(Con.) / Analytical / σxx Numerical	1300	1310	1320	1330	1340	1350	1360	1370	1380	1390	1400	1410	1420	1430	1440	1450	1450
-225	0,805747	0,761819	0,70001	0,592336	0,391572	0,419295	0,606723	0,775959	0,887511	0,957722	1,033159	1,148565	1,34322	1,663038	2,075254	2,291882	2,291882
-115	1,262398	1,29843	1,328874	1,350096	1,359549	1,356726	1,343425	1,323122	1,299846	1,277128	1,257408	1,241943	1,231032	1,224391	1,221519	1,222009	1,222009
-95	1,208595	1,229489	1,246312	1,257715	1,262906	1,261876	1,255425	1,244975	1,232253	1,218951	1,206484	1,195872	1,187748	1,182437	1,180072	1,180696	1,180696
-75	1,176089	1,189473	1,199732	1,20627	1,208813	1,207477	1,202765	1,19548	1,186597	1,177127	1,16799	1,159953	1,153598	1,149332	1,147415	1,147996	1,147996
-55	1,141226	1,149883	1,156203	1,159921	1,160964	1,159471	1,155783	1,150406	1,143946	1,137047	1,130328	1,124338	1,119533	1,116262	1,114774	1,115217	1,115217
-35	1,105272	1,110787	1,114566	1,116498	1,116588	1,114967	1,111879	1,107663	1,102721	1,097482	1,092368	1,087769	1,08402	1,081391	1,080079	1,080208	1,080208
-15	1,068585	1,07186	1,073845	1,074502	1,073867	1,072049	1,069228	1,065641	1,061563	1,057287	1,053107	1,049296	1,046097	1,043706	1,042271	1,041885	1,041885
5	1,031084	1,032618	1,033192	1,032801	1,031487	1,02934	1,026492	1,023111	1,019389	1,01553	1,011737	1,008202	1,005097	1,002563	1,000706	0,999593	0,999593
25	0,992467	0,992512	0,991842	0,990466	0,988422	0,985781	0,982638	0,979112	0,975336	0,97145	0,967595	0,963904	0,960495	0,957468	0,954896	0,952826	0,952826
45	0,952293	0,950945	0,949068	0,946676	0,943799	0,940487	0,936808	0,932839	0,92867	0,924393	0,920103	0,915885	0,911819	0,90797	0,904388	0,901102	0,901102
65	0,909966	0,907216	0,904091	0,900602	0,896768	0,89262	0,888196	0,883543	0,878709	0,873749	0,868714	0,863653	0,85861	0,853622	0,848717	0,843911	0,843911
85	0,867482	0,863205	0,858619	0,853727	0,848542	0,84308	0,837365	0,831422	0,825283	0,818978	0,812538	0,805993	0,79937	0,792689	0,785968	0,779216	0,779216
105	0,821953	0,816009	0,809806	0,80334	0,796612	0,789622	0,782377	0,774881	0,767144	0,759174	0,750982	0,742577	0,733966	0,725159	0,71616	0,706971	0,706971
115	0,800443	0,793588	0,786486	0,77913	0,771512	0,763627	0,755471	0,747041	0,738333	0,729346	0,72008	0,710534	0,700708	0,690602	0,680217	0,669552	0,669552
225	0,702084	0,672886	0,640699	0,605282	0,566378	0,523709	0,476973	0,425835	0,36993	0,308846	0,242126	0,169251	0,08964	0,002634	-0,09251	-0,19664	-0,19664

Figure 4.44: Fraction $\frac{\sigma_{xx,Analytical}}{\sigma_{xx,Numerical}}$ of CW1

4.3. Results

From the analysis in this chapter it was found that the analytical stress distribution did not equal the numerical stress distribution at some parts of the prestressed concrete beams. This was the case in the socalled "disturbed areas". These areas are located near concentrated loads, so around supports and external concentrated loads. After analysis it was found that the analytical stress distribution concerning the principal tensile

stress σ_1 was too high. After analysis of the different stress components σ_x, σ_y and τ_{xy}, it was found that components σ_y and τ_{xy} are the cause of the disruption of the in the "disturbed areas". The stress component σ_x is compared to the other components less disturbed. Further, it turned out that a change of σ_y and τ_{xy} have more impact on the magnitude σ_1, then a change of σ_x. This also appeared from the conducted pre-analysis using the cirkel of Mohr, see section 2.3. The change of σ_x has more impact on the principal compressive stress σ_2. Further, it appeared that the Poisson's ratio had a low neglectable influence.

5

Suitability of the uniaxial tensile strength and accuracy of models

In this chapter attention is paid to an accurate model which predicts the first Shear crack in the web. Furthermore, the strength criterion, to which the model is tested, will be considered. As described in section 1.3 there will be considered 6 models, 5 analytical models and 1 numerical model. As for the strength criteria there will be considered 3 criteria. The chapter is divided into various sections, in which each beam collection is being considered separately.

5.1. Choulli

5.1.1. Pre-analysis

This paragraph will form a short introduction and an outline of the this topic. First some things will be explained, for example the choices made are explained. Further a clear overview of the analysis is given.

Considered strength criterions

For the uniaxial concrete tensile strength there will be made use of the f_{ctm} according to the Eurocode. For the different Choulli beams this parameter is calculated, see section 4.1.2. For the biaxial concrete tensile strength there will be made use of the methods of Mohr-Coulomb and Huber, see section 2.7. In formula 5.1 the failure model for the compression/tension region according to Mohr-Coulomb.

$$f_{ctm,eff} = \left(1 + \frac{\sigma_2}{f_{cm}}\right) f_{ctm} \tag{5.1}$$

where:

$f_{ctm,eff}$ = the effective mean concrete tensile strength
f_{ctm} = the mean concrete tensile strength
f_{cm} = the mean concrete compressive strength
σ_2 = the present principal compressive stress

In formula 5.2 the failure model for the compression/tension region according to Huber.

$$f_{ctm,eff} = \left(1,6 - 0,2 f_{cm}^{\frac{1}{3}} + 0,6 \frac{\sigma_2}{f_{cm}}\right) f_{ctm} \tag{5.2}$$

where:

$f_{ctm,eff}$ = the effective mean concrete tensile strength
f_{ctm} = the mean concrete tensile strength
f_{cm} = the mean concrete compressive strength
σ_2 = the present principal compressive stress

In section 2.7 also the failure criterions of Kupfer et all and Lee et all were described. The disadvantage, however, is that no real models are described in these studies. In fact, it remains the presentation of the experimental results and the observation that biaxial behavior plays a role in determining strength parameters. Because of this, it was decided not to use Kupfer et all and Lee et all in the analysis in this study.

Considered models

In this section the models to be considered are explained. In figure 5.1 the considered points per model in the web of the "East" beams.

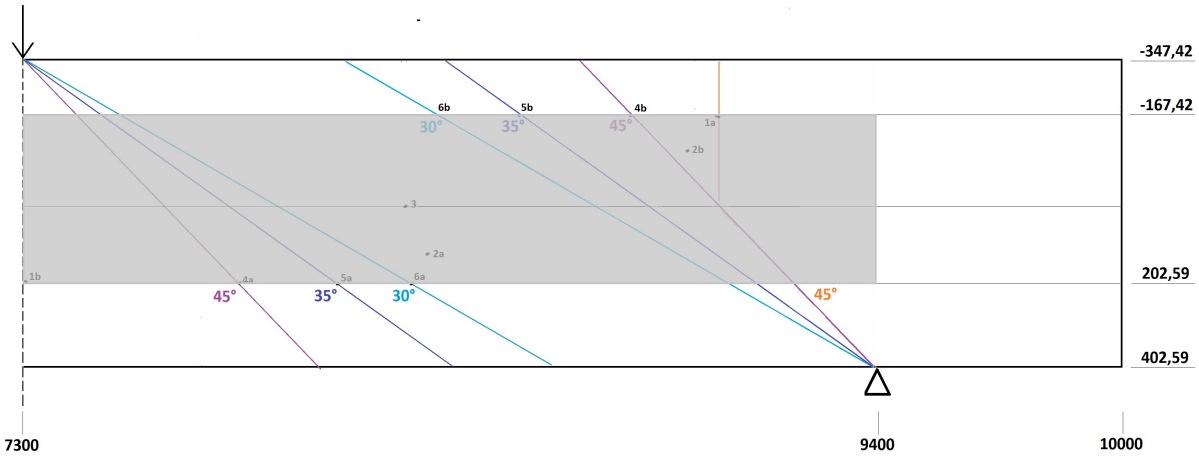

Figure 5.1: The considered points of the Choulli "East" beams, distance and height in mm

Figure 5.1 is on the interval of 7300 mm to 10000 mm, from the start of the beam. The grey area of the figure represents the coverage of the tables of the "East" beams in appendix "Choulli: Fraction $\frac{\sigma_1}{f_{ctm,eff}}$ according to Mohr-Coulomb" of the appendix report. These tables contain data about the fraction $\frac{\sigma_1}{f_{ctm,eff}}$, the $f_{ctm,eff}$ is determined according to the method Mohr-Coulomb. Point 1a and 1b are the points considered in model 1 as stated in the Eurocode, point 1a is located straight under the external load at the transition point of web to flange and point 1b is located straight above the intersection point of the 45°line and the line of the neutral axis. The 45°line starts from the support. Model 1 is considered with the analytical model. The Eurocode states that in case there is a changing width over the height, then σ_1 should be considered in more horizontal axes parallel to the neutral axis. From the analysis done in chapter 4 it was already known that the highest σ_1 was situated in these points. Point 2a and 2b from model 2 can be seen as "free" points. Point 2a is the point which consideres the greatest value of σ_1 starting from the virtual vertical line through the external point load. Point 2b is the point which consideres the greatest value of σ_1 starting from the virtual vertical line through the support. Model 2 is considered with the numerical model. As concluded out of the numerical analysis in chapter 4 both around the external load and the support the value of σ_1 is disturbed. As a result, the maximum value of σ_1 will not be found directly around respectively the external force and the support. The nearest location of the maximum value of σ_1 is considered. Point 3 of model 3 is considered at the neutral axis of the beam, located in the middle between the external load and the support, model 3 is considered with the analytical model. The reason for consideration is that the study of Choulli indicates that the first shear crack starts around this point, see section 3.1.2. The points of model 4, 5 and 6 can be found at the intersection point of respectively the 30°, 35°and the 45°line with the socalled horizontal transition line of the web to flange. The 30°, 35°and the 45°line starts from both the external force and the support. By comparing the values of σ_1 of these points, something can be said about the development of σ_1 related to $f_{ctm}/f_{ctm,eff}$. Model 4, 5 and 6 are considered with both the analytical and numerical model. All the models are considered uniaxial and biaxal. In figure 5.2 the the considered points per model in the web of the "West" beams. Figure 5.2 is on the interval of 0 mm to 2700 mm, from the start of the beam. The grey area of the figure represents the coverage of the tables of the "West" beams in appendix "Choulli: Fraction $\frac{\sigma_1}{f_{ctm,eff}}$ according to Mohr-Coulomb" of the appendix report. These tables also contain data about the fraction $\frac{\sigma_1}{f_{ctm,eff}}$, the $f_{ctm,eff}$ is determined also according to the method Mohr-Coulomb.

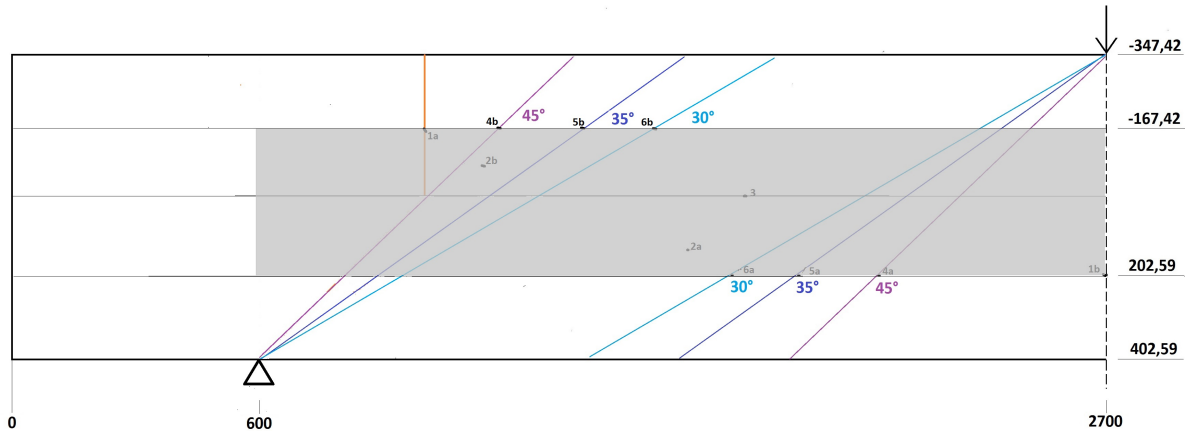

Figure 5.2: The considered points of the Choulli "West" beams, distance and height in mm

5.1.2. Analysis of models and strength criterion

In this section the results of beam HAP1E will be discussed. This is done with reference to respectively figure 5.1 and 5.2. The results of the remaining beams will be summarized. Thereafter, an attempt is made to make a link between the experiments and the models. Finally, a more practical situation is being considered.

HAP1E

In the strength analysis there is made use of f_{ctm} = 5,06 N/mm^2. As described in the pre-analysis points 1a and 1b of model 1 are considered as stated in the Eurocode. The analytical model uncertainty $\frac{\sigma_{1,anal.}}{f_{ctm}}$ of 1a gives $\frac{4,44}{5,06}$ = 0,88. The analytical model uncertainty $\frac{\sigma_{1,anal.}}{f_{ctm}}$ of 1b gives $\frac{5,11}{5,06}$ = 1,00. Without accounting for both biaxial behavior and the disturbed behavior observed in the numerical analysis this would mean that point 1b could be a critical point. The location of point 2a is 7950 mm from start of the beam and 202 mm relative to the neutral axis. The location of point 2b is 8700 mm from start of the beam and -122 mm relative to the neutral axis. The numerical uniaxial model uncertainty $\frac{\sigma_{1,num.}}{f_{ctm}}$ of 2a gives $\frac{3,98}{5,06}$ = 0,79. The numerical uniaxial model uncertainty $\frac{\sigma_{1,num.}}{f_{ctm}}$ of 2b gives $\frac{4,19}{5,06}$ = 0,83. The numerical biaxial model uncertainty $\frac{\sigma_{1,num.}}{f_{ctm,eff,mc}}$ of 2a gives $\frac{3,98}{4,86}$ = 0,82. The numerical biaxial model uncertainty $\frac{\sigma_{1,num.}}{f_{ctm,eff,mc}}$ of 2b gives $\frac{4,19}{4,41}$ = 0,95. Without accounting for biaxial behavior points 2a and 2b would not be classified as critical points. The numerical biaxial model uncertainty with Huber gives the model uncertainty $\frac{\sigma_{1,anal.}}{f_{ctm,eff,hub}}$ of 2a gives $\frac{3,98}{3,04}$ = 1,31. The model uncertainty $\frac{\sigma_{1,anal.}}{f_{ctm,eff,hub}}$ of 2b gives $\frac{4,19}{3,03}$ = 1,39. As described point 3 is the critical point according to the Choulli study. In figure 5.3 the table of $\sigma_{1,Num.}$ on the interval of 8125 mm to 8525 mm, from start of the beam. In figure 5.4 the table of θ_p also on the interval of 8125 mm to 8525 mm, from start of the beam. The θ_p represents the angle of the principal stress, in this case σ_2. Only the values of θ_p in case $\sigma_1 > 3,9$ N/mm^2 are presented, so in case $\sigma_1 < 3,9$ N/mm^2 then $\theta_p = 0$. Note that in fact it does not matter whether the analytical or the numerical results for point 3 are presented, because point 3 is not in the disturbed area, see also the fraction $\frac{\sigma_{1,anal.}}{\sigma_{1,num.}}$ in appendix "Choulli: Numerical results" of the appendix report. The numerical biaxial model uncertainty $\frac{\sigma_{1,num.}}{f_{ctm,eff,mc}}$ of 3 gives $\frac{4,02}{4,35}$ = 0,92. As it can be seen from figure 5.3 around point 3 the σ_1 equals at least 4 N/mm^2, so there is a significant area in which it is possible to get a crack. In figure 5.4 it can be seen that all these stresses have a angle of more or less 62°(-28+90). So possible cracks could start under an angle of 28°. In figure 5.3 the bold values form the shear crack line in the web, this can be compared with the crack line of figure 3.5, in section 3.1.2. The line is drawn, starting from the point of model 3. It can be seen that it is likely that the crack is initiated in the neutral axis, because the highest principal tensile stress σ_1 in the crack appears at this location. The numerical biaxial model uncertainty according to Huber $\frac{\sigma_{1,num.}}{f_{ctm,eff,hub}}$ of 3 gives $\frac{4,02}{2,99}$ = 1,35.

	Plaats n	8125	8150	8175	8200	8225	8250	8275	8300	8325	8350	8375	8400	8425	8450	8475	8500	8525
	-347,41	-0,00679	-0,00557	-0,00427	-0,0029	-0,00144	8,28E-05	0,001678	0,003339	0,005066	0,006856	0,00871	0,010626	0,012606	0,014651	0,016761	0,01894	0,02119
	-167,41	3,02116	3,059273	3,097228	3,135157	3,173168	3,211341	3,249736	3,288389	3,327312	3,366493	3,40589	3,445432	3,485013	3,524488	3,563671	3,602329	3,640174
	-147,41	3,26303	3,300401	3,337196	3,373618	3,409832	3,445963	3,482106	3,51832	3,554634	3,591042	3,627504	3,66394	3,700234	3,736221	3,771692	3,806385	3,839979
	-122,41	3,558488	3,594102	3,628821	3,662881	3,696473	3,729746	3,76281	3,795735	3,828557	3,861271	3,893836	3,926166	3,958136	3,989571	4,020247	4,049885	4,078147
	-97,412	3,661269	**3,693446**	**3,724405**	3,754416	3,7837	3,812432	3,840741	3,868714	3,896398	3,923798	3,950878	3,977558	4,003712	4,029168	4,0537	4,07703	4,09882
	-72,412	3,751382	3,779848	**3,806774**	**3,832468**	3,857183	3,88112	3,904432	3,927226	3,949564	3,971466	3,992905	4,013811	4,034067	4,053504	4,071906	4,088998	4,104449
	-47,412	3,828474	3,852948	3,875577	**3,896703**	**3,916614**	**3,935537**	**3,953651**	3,971084	3,98792	4,004193	4,019892	4,034959	4,04929	4,062727	4,075065	4,08604	4,095333
σ1	-22,412	3,892266	3,912461	3,930531	3,946854	3,961746	**3,975465**	**3,988216**	**4,00015**	4,011371	4,021932	4,03184	4,041054	4,049483	4,056987	4,063374	4,068396	4,071751
σxx	2,58783	3,942533	3,958156	3,971409	3,982702	3,992382	4,000735	4,007989	**4,014322**	**4,019856**	**4,024666**	**4,028779**	4,032169	4,034765	4,036444	4,037032	4,0363	4,033966
τxy	27,5878	3,979087	3,989838	3,99802	4,004071	4,008365	4,011214	4,01287	4,013533	**4,013348**	**4,012409**	**4,010762**	**4,0084**	4,005271	4,001272	3,996247	3,98999	3,98224
σyy	52,5878	4,001755	4,007337	4,0102	4,01081	4,009565	4,006798	4,002787	3,997749	3,991849	3,985202	3,97787	**3,969868**	**3,96116**	**3,951662**	3,941242	3,929714	3,916843
	77,5878	4,01037	4,010485	4,007794	4,002783	3,99587	3,987409	3,977693	3,96696	3,955391	3,943117	3,930217	3,916723	**3,902618**	**3,887837**	**3,872268**	**3,855749**	3,838066
	102,587	4,004746	3,999111	3,99065	3,979863	3,967184	3,952982	3,937565	3,921183	3,904032	3,886255	3,867946	3,849152	3,829871	3,810055	**3,789613**	**3,768403**	**3,746238**
	127,587	3,984671	3,973023	3,958602	3,941918	3,923414	3,903468	3,882397	3,86046	3,837862	3,814755	3,791242	3,767382	3,743186	3,718622	3,693612	3,668039	**3,641735**
	152,587	3,949892	3,932001	3,911469	3,888809	3,864468	3,838827	3,812203	3,78486	3,757005	3,728793	3,700335	3,671693	3,642888	3,613898	3,584663	3,555079	3,525001
	177,587	3,900105	3,875787	3,849045	3,820388	3,790259	3,759031	3,72702	3,694483	3,661624	3,628595	3,595506	3,562421	3,529363	3,496319	3,463236	3,430025	3,396559
	202,587	3,871195	3,840508	3,807803	3,773546	3,738141	3,701929	3,665194	3,628168	3,591036	3,553936	3,51697	3,480201	3,443657	3,407338	3,371213	3,335221	3,299277
	402,587	0,016893	0,01442	0,012023	0,009699	0,007446	0,005261	0,003142	0,001088	-0,0009	-0,00283	-0,0047	-0,0065	-0,00824	-0,00992	-0,01153	-0,01307	-0,01454

Figure 5.3: The $\sigma_{1,Num}$ around point 3 of HAP1E

	Plaats n	8125	8150	8175	8200	8225	8250	8275	8300	8325	8350	8375	8400	8425	8450	8475	8500	8525
	-347,41	0	0	0	0	0	0	0	0	0	0	0	0	0	0	0	0	0
	-167,41	0	0	0	0	0	0	0	0	0	0	0	0	0	0	0	0	0
	-147,41	0	0	0	0	0	0	0	0	0	0	0	0	0	0	0	0	0
	-122,41	0	0	0	0	0	0	0	0	0	0	0	-27,9714	-28,1229	-28,2718	-28,4182	-28,5622	-28,7039
	-97,412	0	0	0	0	0	0	0	0	0	0	-27,6878	-27,8151	-27,9397	-28,0615	-28,1806	-28,2971	-28,4112	-28,523
	-72,412	0	0	0	0	0	0	-27,3809	-27,4867	-27,5905	-27,6917	-27,7902	-27,8859	-27,9788	-28,0688	-28,1563	-28,2413	-28,3244
	-47,412	0	0	0	0	-27,287	-27,3679	-27,4475	-27,5254	-27,6009	-27,6738	-27,744	-27,8112	-27,8756	-27,9372	-27,9963	-28,0532	-28,1083
	-22,412	0	-27,227	-27,2796	-27,3333	-27,3873	-27,4406	-27,4925	-27,5425	-27,59	-27,6349	-27,677	-27,7162	-27,7525	-27,7861	-27,8174	-27,8467	-27,8745
θp	2,58783	-27,3629	-27,3868	-27,4127	-27,4394	-27,4662	-27,492	-27,5163	-27,5385	-27,5583	-27,5754	-27,5896	-27,601	-27,6096	-27,6156	-27,6195	-27,6216	-27,6226
	27,5878	-27,5271	-27,525	-27,5244	-27,5243	-27,5239	-27,5223	-27,5191	-27,5137	-27,5058	-27,4952	-27,4818	-27,4655	-27,4466	-27,4254	-27,4021	-27,3774	-27,3518
	52,5878	-27,67	-27,6419	-27,6149	-27,588	-27,5604	-27,5315	-27,5007	-27,4678	-27,4322	-27,394	-27,353	-27,3093	-27,2631	-27,2148	-27,1646	-27,1132	-27,0614
	77,5878	-27,7918	-27,7377	-27,6842	-27,6303	-27,5754	-27,5191	-27,4607	-27,4001	-27,3369	-27,2711	-27,2026	-27,1316	-27,0582	0	0	0	0
	102,587	-27,8927	-27,8123	-27,7319	-27,6508	-27,5684	-27,4844	-27,3983	-27,3098	-27,2189	0	0	0	0	0	0	0	0
	127,587	-27,9725	-27,8653	-27,7575	-27,6487	-27,5384	-27,4262	0	0	0	0	0	0	0	0	0	0	0
	152,587	-28,0309	-27,896	-27,76	0	0	0	0	0	0	0	0	0	0	0	0	0	0
	177,587	-28,067	0	0	0	0	0	0	0	0	0	0	0	0	0	0	0	0
	202,587	0	0	0	0	0	0	0	0	0	0	0	0	0	0	0	0	0
	402,587	0	0	0	0	0	0	0	0	0	0	0	0	0	0	0	0	0

Figure 5.4: The θ_p around point 3 of HAP1E

Points 4a, 5a and 6a are not in the numerical disturbed area. The analytical model uncertainty $\frac{\sigma_{1,anal.}}{f_{ctm}}$ of 4a gives $\frac{4,05}{5,06} = 0,80$ and $\frac{\sigma_{1,anal.}}{f_{ctm,eff,mc}}$ gives $\frac{4,05}{4,49} = 0,90$. The analytical model uncertainty $\frac{\sigma_{1,anal.}}{f_{ctm}}$ of 5a gives $\frac{3,71}{5,06} = 0,73$ and $\frac{\sigma_{1,anal.}}{f_{ctm,eff,mc}}$ gives $\frac{3,71}{4,44} = 0,84$. The analytical model uncertainty $\frac{\sigma_{1,anal.}}{f_{ctm}}$ of 6a gives $\frac{3,48}{5,06} = 0,69$ and $\frac{\sigma_{1,anal.}}{f_{ctm,eff,mc}}$ gives $\frac{3,48}{4,39} = 0,79$. The analytical model uncertainty $\frac{\sigma_{1,anal.}}{f_{ctm}}$ of 4b gives $\frac{4,22}{5,06} = 0,83$ and $\frac{\sigma_{1,anal.}}{f_{ctm,eff,mc}}$ gives $\frac{4,22}{4,47} = 0,94$. The analytical model uncertainty $\frac{\sigma_{1,anal.}}{f_{ctm}}$ of 5b gives $\frac{3,86}{5,06} = 0,76$ and $\frac{\sigma_{1,anal.}}{f_{ctm,eff,mc}}$ gives $\frac{3,86}{4,42} = 0,87$. The analytical model uncertainty $\frac{\sigma_{1,anal.}}{f_{ctm}}$ of 6b gives $\frac{3,66}{5,06} = 0,72$ and $\frac{\sigma_{1,anal.}}{f_{ctm,eff,mc}}$ gives $\frac{3,66}{4,39} = 0,83$. In table 5.1 and 5.2 a summary of the results.

Point	**Location Distance [mm]**	**Location Height [mm]**	σ_1 **Anal.**	σ_1 **Num.**	$\mathbf{f}_{ctm,eff}$ **MC Anal.**	$\mathbf{f}_{ctm,eff}$ **MC Num.**	$\mathbf{f}_{ctm,eff}$ **Hub Anal.**	$\mathbf{f}_{ctm,eff}$ **Hub Num.**
1a	8950	-167,41	4,44	3,56	4,49	4,50	3,07	3,08
1b	7300	202,59	5,11	-0,54	4,62	4,69	3,15	3,19
2a	7950	202,59	-	3,98	-	4,86	-	3,04
2b	8700	-122,41	-	4,19	-	4,41	-	3,03
3	8350	2,59	3,97	4,03	4,37	4,35	3,0	2,99
4a	7900	202,59	4,05	3,94	4,49	4,44	3,07	3,04
5a	8150	202,59	3,71	3,84	4,44	4,40	3,04	3,02
6a	8325	202,59	3,48	3,59	4,39	4,36	3,01	3,0
4b	8800	-167,41	4,22	3,86	4,47	4,47	3,06	3,07
5b	8525	-167,41	3,86	3,64	4,42	4,44	3,03	3,04
6b	8350	-167,41	3,66	3,37	4,39	4,41	3,01	3,03

* all stress parameters $\left[\frac{N}{mm^2}\right]$

Table 5.1: Stress and strength results HAP1E

Point	**Location Distance [mm]**	**Location Height [mm]**	$\frac{\sigma_{1,anal.}}{\mathbf{f}_{ctm}}$ [-]	$\frac{\sigma_{1,num.}}{\mathbf{f}_{ctm}}$ [-]	$\frac{\sigma_{1,anal.}}{\mathbf{f}_{ctm,eff,mc}}$ [-]	$\frac{\sigma_{1,num.}}{\mathbf{f}_{ctm,eff,mc}}$ [-]	$\frac{\sigma_{1,anal.}}{\mathbf{f}_{ctm,eff,hb}}$ [-]	$\frac{\sigma_{1,num.}}{\mathbf{f}_{ctm,eff,hb}}$ [-]
1a	8950	-167,41	0,88	0,70	-	0,79	-	1,15
1b	7300	202,59	1,00	-0,11	-	-0,12	-	-0,17
2a	7950	202,59	-	0,79	-	0,82	-	1,31
2b	8700	-122,41	-	0,83	-	0,95	-	1,39
3	8350	2,59	0,79	0,80	0,91	0,92	1,32	1,35
4a	7900	202,59	0,80	0,78	0,90	0,89	1,32	1,30
5a	8150	202,59	0,73	0,76	0,84	0,87	1,22	1,27
6a	8325	202,59	0,69	0,71	0,79	0,82	1,16	1,20
4b	8800	-167,41	0,83	0,76	0,94	0,86	1,38	1,26
5b	8525	-167,41	0,76	0,72	0,87	0,82	1,27	1,20
6b	8350	-167,41	0,72	0,67	0,83	0,76	1,22	1,11

Table 5.2: Results model uncertainty of HAP1E

Other results

In this section the other results will be presented. In table 5.3 and 5.4 the results of HAP1TE, f_{ctm} = 4,9 N/mm^2. In table 5.5 and 5.6 the results of HAP2E, f_{ctm} = 5 N/mm^2. In table 5.7 and 5.8 the results of HAP2TE, f_{ctm} = 5 N/mm^2. In table 5.9 and 5.10 the results of HCP1TE, f_{ctm} = 4,7 N/mm^2. In table 5.11 and 5.12 the results of HCP2TE, f_{ctm} = 4,9 N/mm^2. In table 5.13 and 5.14 the results of HAP1TW, f_{ctm} = 4,9 N/mm^2. In table 5.15 and 5.16 the results of HAP1W, f_{ctm} = 5,06 N/mm^2. In table 5.17 and 5.18 the results of HAP2TW, f_{ctm} = 5 N/mm^2. In table 5.19 and 5.20 the results of HAP2W, f_{ctm} = 5 N/mm^2. In table 5.21 and 5.22 the results of HCP1TW, f_{ctm} = 4,7 N/mm^2. In table 5.23 and 5.24 the results of HCP2TW, f_{ctm} = 4,9 N/mm^2.

Point	**Location Distance [mm]**	**Location Height [mm]**	σ_1 **Anal.**	σ_1 **Num.**	$\mathbf{f}_{ctm,eff}$ **MC Anal.**	$\mathbf{f}_{ctm,eff}$ **MC Num.**	$\mathbf{f}_{ctm,eff}$ **HB Anal.**	$\mathbf{f}_{ctm,eff}$ **HB Num.**
1a	8950	-167,41	4,33	3,46	4,32	4,32	3,08	3,08
1b	7300	202,59	4,90	-0,57	4,43	4,50	3,15	3,19
2a	8000	202,59	-	3,83	-	4,23	-	3,03
2b	8700	-122,41	-	4,09	-	4,23	-	3,03
3	8350	2,59	3,86	3,91	4,18	4,16	3,0	2,99
4a	7900	202,59	3,89	3,80	4,30	4,24	3,07	3,04
5a	8150	202,59	3,56	3,70	4,24	4,20	3,04	3,01
6a	8325	202,59	3,36	3,46	4,20	4,17	3,01	2,99
4b	8800	-167,41	4,12	3,76	4,29	4,30	3,06	3,07
5b	8525	-167,41	3,77	3,55	4,24	4,26	3,03	3,04
6b	8350	-167,41	3,57	3,29	4,20	4,23	3,01	3,03

* all stress parameters $\left[\frac{N}{mm^2}\right]$

Table 5.3: Stress and strength results HAP1TE

Point	**Location Distance [mm]**	**Location Height [mm]**	$\frac{\sigma_{1,anal.}}{\mathbf{f}_{ctm}}$ **[-]**	$\frac{\sigma_{1,num.}}{\mathbf{f}_{ctm}}$ **[-]**	$\frac{\sigma_{1,anal.}}{\mathbf{f}_{ctm,eff,mc}}$ **[-]**	$\frac{\sigma_{1,num.}}{\mathbf{f}_{ctm,eff,mc}}$ **[-]**	$\frac{\sigma_{1,anal.}}{\mathbf{f}_{ctm,eff,hb}}$ **[-]**	$\frac{\sigma_{1,num.}}{\mathbf{f}_{ctm,eff,hb}}$ **[-]**
1a	8950	-167,41	0,88	0,71	-	0,80	-	1,12
1b	7300	202,59	1,00	-0,12	-	-0,13	-	-0,18
2a	8000	202,59	-	0,79	-	0,91	-	1,26
2b	8700	-122,41	-	0,83	-	0,97	-	1,35
3	8350	2,59	0,78	0,80	0,92	0,94	1,29	1,31
4a	7900	202,59	0,79	0,77	0,91	0,89	1,27	1,25
5a	8150	202,59	0,73	0,76	0,84	0,88	1,17	1,23
6a	8325	202,59	0,69	0,71	0,80	0,83	1,11	1,16
4b	8800	-167,41	0,84	0,77	0,96	0,88	1,34	1,23
5b	8525	-167,41	0,77	0,73	0,89	0,84	1,24	1,17
6b	8350	-167,41	0,73	0,67	0,85	0,78	1,19	1,09

Table 5.4: Results model uncertainty of HAP1TE

Point	**Location Distance [mm]**	**Location Height [mm]**	σ_1 **Anal.**	σ_1 **Num.**	$\mathbf{f}_{ctm,eff}$ **MC Anal.**	$\mathbf{f}_{ctm,eff}$ **MC Num.**	$\mathbf{f}_{ctm,eff}$ **HB Anal.**	$\mathbf{f}_{ctm,eff}$ **HB Num.**
1a	8950	-167,41	3,79	3,08	4,54	4,55	3,15	3,15
1b	7300	202,59	5,47	0,43	4,72	4,81	3,25	3,31
2a	7950	202,59	-	4,13	-	4,59	-	3,17
2b	8700	-97,41	-	3,68	-	4,48	-	3,11
3	8350	2,59	3,66	3,69	4,48	4,47	3,11	3,11
4a	7900	202,59	4,27	4,12	4,63	4,59	3,20	3,18
5a	8150	202,59	3,86	3,94	4,59	4,56	3,17	3,16
6a	8325	202,59	3,61	3,67	4,56	4,54	3,15	3,14
4b	8800	-167,41	3,60	3,32	4,52	4,53	3,14	3,14
5b	8525	-167,41	3,29	3,11	4,48	4,50	3,11	3,12
6b	8350	-167,41	3,11	2,87	4,45	4,48	3,09	3,11

* all stress parameters $\left[\frac{N}{mm^2}\right]$

Table 5.5: Stress and strength results HAP2E

Point	**Location Distance [mm]**	**Location Height [mm]**	$\frac{\sigma_{1,anal.}}{\mathbf{f}_{ctm}}$ [-]	$\frac{\sigma_{1,num.}}{\mathbf{f}_{ctm}}$ [-]	$\frac{\sigma_{1,anal.}}{\mathbf{f}_{ctm,eff,mc}}$ [-]	$\frac{\sigma_{1,num.}}{\mathbf{f}_{ctm,eff,mc}}$ [-]	$\frac{\sigma_{1,anal.}}{\mathbf{f}_{ctm,eff,hb}}$ [-]	$\frac{\sigma_{1,num.}}{\mathbf{f}_{ctm,eff,hb}}$ [-]
1a	8950	-167,41	0,76	0,62	-	0,68	-	0,98
1b	7300	202,59	1,09	0,09	-	0,09	-	0,13
2a	7950	202,59	-	0,83	-	0,90	-	1,30
2b	8700	-97,41	-	0,74	-	0,82	-	1,18
3	8350	2,59	0,73	0,74	0,82	0,83	1,18	1,19
4a	7900	202,59	0,85	0,82	0,92	0,89	1,33	1,30
5a	8150	202,59	0,77	0,79	0,84	0,86	1,22	1,25
6a	8325	202,59	0,72	0,73	0,79	0,81	1,14	1,17
4b	8800	-167,41	0,72	0,66	0,80	0,73	1,15	1,06
5b	8525	-167,41	0,66	0,62	0,73	0,69	1,06	1,00
6b	8350	-167,41	0,62	0,57	0,70	0,64	1,01	0,92

Table 5.6: Results model uncertainty of HAP2E

Point	**Location Distance [mm]**	**Location Height [mm]**	σ_1 **Anal.**	σ_1 **Num.**	$\mathbf{f}_{ctm,eff}$ **MC Anal.**	$\mathbf{f}_{ctm,eff}$ **MC Num.**	$\mathbf{f}_{ctm,eff}$ **HB Anal.**	$\mathbf{f}_{ctm,eff}$ **HB Num.**
1a	8950	-167,41	4,02	3,28	4,53	4,53	3,14	3,14
1b	7300	202,59	6,0	0,67	4,71	4,81	3,25	3,31
2a	7925	202,59	-	4,50	-	4,59	-	3,17
2b	8775	-122,41	-	3,88	-	4,47	-	3,11
3	8350	2,59	3,93	3,96	4,47	4,46	3,10	3,10
4a	7900	202,59	4,67	4,50	4,63	4,59	3,20	3,17
5a	8150	202,59	4,22	4,29	4,58	4,56	3,17	3,16
6a	8325	202,59	3,94	3,99	4,55	4,53	3,15	3,14
4b	8800	-167,41	3,82	3,52	4,51	4,51	3,12	3,13
5b	8525	-167,41	3,49	3,30	4,46	4,48	3,10	3,11
6b	8350	-167,41	3,30	3,04	4,43	4,47	3,08	3,10

* all stress parameters $\left[\frac{N}{mm^2}\right]$

Table 5.7: Stress and strength results HAP2TE

Point	**Location Distance [mm]**	**Location Height [mm]**	$\frac{\sigma_{1,anal.}}{\mathbf{f}_{ctm}}$ [-]	$\frac{\sigma_{1,num.}}{\mathbf{f}_{ctm}}$ [-]	$\frac{\sigma_{1,anal.}}{\mathbf{f}_{ctm,eff,mc}}$ [-]	$\frac{\sigma_{1,num.}}{\mathbf{f}_{ctm,eff,mc}}$ [-]	$\frac{\sigma_{1,anal.}}{\mathbf{f}_{ctm,eff,hb}}$ [-]	$\frac{\sigma_{1,num.}}{\mathbf{f}_{ctm,eff,hb}}$ [-]
1a	8950	-167,41	0,80	0,66	-	0,72	-	1,04
1b	7300	202,59	1,20	0,13	-	0,14	-	0,20
2a	7925	202,59	-	0,90	-	0,98	-	1,42
2b	8775	-122,41	-	0,78	-	0,87	-	1,25
3	8350	2,59	0,79	0,79	0,88	0,89	1,27	1,28
4a	7900	202,59	0,93	0,90	1,00	0,98	1,46	1,42
5a	8150	202,59	0,84	0,86	0,92	0,94	1,33	1,36
6a	8325	202,59	0,79	0,80	0,87	0,88	1,25	1,27
4b	8800	-167,41	0,76	0,70	0,85	0,78	1,22	1,13
5b	8525	-167,41	0,70	0,66	0,78	0,74	1,13	1,06
6b	8350	-167,41	0,66	0,61	0,74	0,68	1,07	0,98

Table 5.8: Results model uncertainty of HAP2TE

Point	**Location Distance [mm]**	**Location Height [mm]**	σ_1 **Anal.**	σ_1 **Num.**	$\mathbf{f}_{ctm,eff}$ **MC Anal.**	$\mathbf{f}_{ctm,eff}$ **MC Num.**	$\mathbf{f}_{ctm,eff}$ **HB Anal.**	$\mathbf{f}_{ctm,eff}$ **HB Num.**
1a	8950	-167,41	5,54	4,51	3,98	3,98	3,02	3,02
1b	7300	202,59	7,40	0,03	4,20	4,34	3,15	3,23
2a	7950	202,59	-	5,60	-	3,97	-	3,02
2b	8750	-122,41	-	5,29	-	3,88	-	2,96
3	8350	2,59	5,20	5,24	3,84	3,83	2,94	2,93
4a	7900	202,59	5,77	5,57	4,05	3,99	3,07	3,02
5a	8150	202,59	5,23	5,38	3,98	3,93	3,02	2,99
6a	8325	202,59	4,89	5,02	3,93	3,90	2,99	2,97
4b	8800	-167,41	5,27	4,83	3,94	3,95	3,0	3,0
5b	8525	-167,41	4,82	4,54	3,87	3,90	2,96	2,97
6b	8350	-167,41	4,56	4,19	3,83	3,86	2,93	2,95

* all stress parameters $\left[\frac{N}{mm^2}\right]$

Table 5.9: Stress and strength results HCP1TE

Point	**Location Distance [mm]**	**Location Height [mm]**	$\frac{\sigma_{1,anal.}}{\mathbf{f}_{ctm}}$ **[-]**	$\frac{\sigma_{1,num.}}{\mathbf{f}_{ctm}}$ **[-]**	$\frac{\sigma_{1,anal.}}{\mathbf{f}_{ctm,eff,mc}}$ **[-]**	$\frac{\sigma_{1,num.}}{\mathbf{f}_{ctm,eff,mc}}$ **[-]**	$\frac{\sigma_{1,anal.}}{\mathbf{f}_{ctm,eff,hb}}$ **[-]**	$\frac{\sigma_{1,num.}}{\mathbf{f}_{ctm,eff,hb}}$ **[-]**
1a	8950	-167,41	1,18	0,96	-	1,13	-	1,49
1b	7300	202,59	1,57	0,01	-	0,01	-	0,01
2a	7950	202,59	-	1,19	-	1,41	-	1,86
2b	8750	-122,41	-	1,12	-	1,36	-	1,79
3	8350	2,59	1,11	1,12	1,35	1,37	1,77	1,79
4a	7900	202,59	1,23	1,19	1,42	1,40	1,88	1,84
5a	8150	202,59	1,11	1,14	1,31	1,37	1,73	1,80
6a	8325	202,59	1,04	1,07	1,24	1,29	1,63	1,69
4b	8800	-167,41	1,12	1,03	1,34	1,22	1,76	1,61
5b	8525	-167,41	1,02	0,97	1,24	1,16	1,63	1,53
6b	8350	-167,41	0,97	0,89	1,19	1,09	1,56	1,42

Table 5.10: Results model uncertainty of HCP1TE

Point	**Location Distance [mm]**	**Location Height [mm]**	σ_1 **Anal.**	σ_1 **Num.**	$\mathbf{f}_{ctm,eff}$ **MC Anal.**	$\mathbf{f}_{ctm,eff}$ **MC Num.**	$\mathbf{f}_{ctm,eff}$ **HB Anal.**	$\mathbf{f}_{ctm,eff}$ **HB Num.**
1a	8950	-167,41	5,40	4,50	4,30	4,31	3,09	3,09
1b	7300	202,59	9,29	2,53	4,58	4,71	3,26	3,34
2a	7900	202,59	-	6,93	-	4,44	-	3,17
2b	8700	-47,41	-	5,45	-	4,23	-	3,05
3	8350	2,59	5,55	5,56	4,26	4,25	3,06	3,06
4a	7900	202,59	7,21	6,93	4,49	4,44	3,20	3,17
5a	8150	202,59	6,49	6,53	4,44	4,41	3,17	3,15
6a	8325	202,59	6,03	6,04	4,40	4,38	3,15	3,14
4b	8800	-167,41	5,13	4,77	4,27	4,28	3,07	3,08
5b	8525	-167,41	4,69	4,43	4,22	4,24	3,04	3,05
6b	8350	-167,41	4,43	4,09	4,18	4,21	3,02	3,03

* all stress parameters $\left[\frac{N}{mm^2}\right]$

Table 5.11: Stress and strength results HCP2TE

Point	**Location Distance [mm]**	**Location Height [mm]**	$\frac{\sigma_{1,anal.}}{\mathbf{f}_{ctm}}$ [-]	$\frac{\sigma_{1,num.}}{\mathbf{f}_{ctm}}$ [-]	$\frac{\sigma_{1,anal.}}{\mathbf{f}_{ctm,eff,mc}}$ [-]	$\frac{\sigma_{1,num.}}{\mathbf{f}_{ctm,eff,mc}}$ [-]	$\frac{\sigma_{1,anal.}}{\mathbf{f}_{ctm,eff,hb}}$ [-]	$\frac{\sigma_{1,num.}}{\mathbf{f}_{ctm,eff,hb}}$ [-]
1a	8950	-167,41	1,10	0,92	-	1,05	-	1,46
1b	7300	202,59	1,89	0,52	-	0,54	-	0,76
2a	7900	202,59	-	1,36	-	1,54	-	2,18
2b	8700	-47,41	-	1,11	-	1,28	-	1,79
3	8350	2,59	1,13	1,13	1,30	1,31	1,81	1,82
4a	7900	202,59	1,47	1,41	1,61	1,56	2,25	2,18
5a	8150	202,59	1,32	1,33	1,46	1,48	2,05	2,07
6a	8325	202,59	1,23	1,23	1,37	1,38	1,92	1,93
4b	8800	-167,41	1,05	0,97	1,20	1,11	1,67	1,55
5b	8525	-167,41	0,96	0,90	1,11	1,05	1,54	1,45
6b	8350	-167,41	0,90	0,83	1,06	0,97	1,47	1,35

Table 5.12: Results model uncertainty of HCP2TE

Point	**Location Distance [mm]**	**Location Height [mm]**	σ_1 **Anal.**	σ_1 **Num.**	$\mathbf{f}_{ctm,eff}$ **MC Anal.**	$\mathbf{f}_{ctm,eff}$ **MC Num.**	$\mathbf{f}_{ctm,eff}$ **HB Anal.**	$\mathbf{f}_{ctm,eff}$ **HB Num.**
1a	1050	-167,41	4,53	3,53	4,30	4,32	3,07	3,08
1b	2700	202,59	5,30	-1,44	4,43	4,52	3,15	3,20
2a	2025	202,59	-	3,98	-	4,23	-	3,03
2b	1300	-122,41	-	4,17	-	4,22	-	3,02
3	1650	2,59	4,1	4,0	4,17	4,16	2,99	2,99
4a	2100	202,59	4,19	3,93	4,30	4,24	3,07	3,04
5a	1850	202,59	3,83	3,84	4,24	4,20	3,04	3,01
6a	1675	202,59	3,60	3,58	4,20	4,17	3,01	2,99
4b	1200	-167,41	4,31	3,83	4,27	4,29	3,06	3,06
5b	1475	-167,41	3,95	3,62	4,22	4,25	3,02	3,04
6b	1650	-167,41	3,74	3,34	4,18	4,22	3,00	3,02

* all stress parameters $\left[\frac{N}{mm^2}\right]$

Table 5.13: Stress and strength results HAP1TW

Point	**Location Distance [mm]**	**Location Height [mm]**	$\frac{\sigma_{1,anal.}}{\mathbf{f}_{ctm}}$ [-]	$\frac{\sigma_{1,num.}}{\mathbf{f}_{ctm}}$ [-]	$\frac{\sigma_{1,anal.}}{\mathbf{f}_{ctm,eff,mc}}$ [-]	$\frac{\sigma_{1,num.}}{\mathbf{f}_{ctm,eff,mc}}$ [-]	$\frac{\sigma_{1,anal.}}{\mathbf{f}_{ctm,eff,hb}}$ [-]	$\frac{\sigma_{1,num.}}{\mathbf{f}_{ctm,eff,hb}}$ [-]
1a	1050	-167,41	0,93	0,72	-	0,82	-	1,15
1b	2700	202,59	1,08	-0,29	-	-0,31	-	-0,45
2a	2025	202,59	-	0,81	-	0,94	-	1,31
2b	1300	-122,41	-	0,85	-	0,99	-	1,38
3	1650	2,59	0,83	0,82	0,98	0,97	1,36	1,34
4a	2100	202,59	0,86	0,80	0,97	0,93	1,36	1,29
5a	1850	202,59	0,78	0,78	0,90	0,92	1,26	1,28
6a	1675	202,59	0,74	0,73	0,86	0,86	1,20	1,20
4b	1200	-167,41	0,88	0,78	1,00	0,89	1,41	1,25
5b	1475	-167,41	0,81	0,74	0,94	0,85	1,31	1,19
6b	1650	-167,41	0,76	0,68	0,89	0,79	1,25	1,11

Table 5.14: Results model uncertainty of HAP1TW

Point	**Location Distance [mm]**	**Location Height [mm]**	σ_1 **Anal.**	σ_1 **Num.**	$\mathbf{f}_{ctm,eff}$ **MC Anal.**	$\mathbf{f}_{ctm,eff}$ **MC Num.**	$\mathbf{f}_{ctm,eff}$ **HB Anal.**	$\mathbf{f}_{ctm,eff}$ **HB Num.**
1a	1050	-167,41	4,26	3,41	4,51	4,52	3,09	3,09
1b	2700	202,59	4,77	-1,43	4,61	4,69	3,15	3,19
2a	2025	202,59	-	3,78	-	4,42	-	3,03
2b	1300	-122,41	-	4,02	-	4,43	-	3,03
3	1650	2,59	3,78	3,85	4,38	4,36	3,0	3,0
4a	2100	202,59	3,79	3,73	4,49	4,43	3,07	3,04
5a	1850	202,59	3,47	3,66	4,44	4,39	3,04	3,02
6a	1675	202,59	3,28	3,41	4,39	4,36	3,02	3,0
4b	1200	-167,41	4,06	3,70	4,49	4,49	3,07	3,07
5b	1475	-167,41	3,71	3,50	4,44	4,45	3,04	3,05
6b	1650	-167,41	3,52	3,24	4,41	4,42	3,02	3,03

* all stress parameters $\left[\frac{N}{mm^2}\right]$

Table 5.15: Stress and strength results HAP1W

Point	**Location Distance [mm]**	**Location Height [mm]**	$\frac{\sigma_{1,anal.}}{\mathbf{f}_{ctm}}$ **[-]**	$\frac{\sigma_{1,num.}}{\mathbf{f}_{ctm}}$ **[-]**	$\frac{\sigma_{1,anal.}}{\mathbf{f}_{ctm,eff,mc}}$ **[-]**	$\frac{\sigma_{1,num.}}{\mathbf{f}_{ctm,eff,mc}}$ **[-]**	$\frac{\sigma_{1,anal.}}{\mathbf{f}_{ctm,eff,hb}}$ **[-]**	$\frac{\sigma_{1,num.}}{\mathbf{f}_{ctm,eff,hb}}$ **[-]**
1a	1050	-167,41	0,84	0,67	-	0,75	-	1,10
1b	2700	202,59	0,94	-0,28	-	-0,31	-	-0,45
2a	2025	202,59	-	0,75	-	0,85	-	1,25
2b	1300	-122,41	-	0,80	-	0,91	-	1,33
3	1650	2,59	0,75	0,76	0,86	0,88	1,26	1,29
4a	2100	202,59	0,75	0,74	0,84	0,84	1,23	1,23
5a	1850	202,59	0,69	0,72	0,78	0,83	1,14	1,21
6a	1675	202,59	0,65	0,67	0,75	0,78	1,09	1,14
4b	1200	-167,41	0,80	0,73	0,90	0,83	1,32	1,21
5b	1475	-167,41	0,73	0,69	0,84	0,79	1,22	1,15
6b	1650	-167,41	0,70	0,64	0,80	0,73	1,16	1,07

Table 5.16: Results model uncertainty of HAP1W

Point	**Location Distance [mm]**	**Location Height [mm]**	σ_1 **Anal.**	σ_1 **Num.**	$\mathbf{f}_{ctm,eff}$ **MC Anal.**	$\mathbf{f}_{ctm,eff}$ **MC Num.**	$\mathbf{f}_{ctm,eff}$ **HB Anal.**	$\mathbf{f}_{ctm,eff}$ **HB Num.**
1a	1050	-167,41	3,98	3,26	4,53	4,53	3,14	3,14
1b	2700	202,59	5,91	-0,37	4,71	4,84	3,25	3,32
2a	2025	202,59	-	4,47	-	4,58	-	3,17
2b	1300	-122,41	-	3,87	-	4,47	-	3,10
3	1650	2,59	3,89	3,92	4,47	4,46	3,10	3,10
4a	2100	202,59	4,60	4,46	4,63	4,59	3,20	3,17
5a	1850	202,59	4,16	4,27	4,58	4,56	3,17	3,16
6a	1675	202,59	3,89	3,95	4,55	4,53	3,15	3,14
4b	1200	-167,41	3,78	3,50	4,51	4,51	3,13	3,13
5b	1475	-167,41	3,46	3,27	4,47	4,48	3,10	3,11
6b	1650	-167,41	3,27	3,02	4,44	4,46	3,08	3,09

* all stress parameters $\left[\frac{N}{mm^2}\right]$

Table 5.17: Stress and strength results HAP2TW

Point	**Location Distance [mm]**	**Location Height [mm]**	$\frac{\sigma_{1,anal.}}{\mathbf{f}_{ctm}}$ [-]	$\frac{\sigma_{1,num.}}{\mathbf{f}_{ctm}}$ [-]	$\frac{\sigma_{1,anal.}}{\mathbf{f}_{ctm,eff,mc}}$ [-]	$\frac{\sigma_{1,num.}}{\mathbf{f}_{ctm,eff,mc}}$ [-]	$\frac{\sigma_{1,anal.}}{\mathbf{f}_{ctm,eff,hb}}$ [-]	$\frac{\sigma_{1,num.}}{\mathbf{f}_{ctm,eff,hb}}$ [-]
1a	1050	-167,41	0,80	0,65	-	0,72	-	1,04
1b	2700	202,59	1,18	-0,07	-	-0,08	-	-0,11
2a	2025	202,59	-	0,89	-	0,98	-	1,41
2b	1300	-122,41	-	0,77	-	0,87	-	1,25
3	1650	2,59	0,78	0,78	0,87	0,88	1,25	1,27
4a	2100	202,59	0,92	0,89	1,00	0,97	1,44	1,41
5a	1850	202,59	0,83	0,85	0,91	0,94	1,31	1,35
6a	1675	202,59	0,78	0,79	0,85	0,87	1,23	1,26
4b	1200	-167,41	0,76	0,70	0,84	0,78	1,21	1,12
5b	1475	-167,41	0,69	0,65	0,77	0,73	1,11	1,05
6b	1650	-167,41	0,65	0,60	0,74	0,68	1,06	0,97

Table 5.18: Results model uncertainty of HAP2TW

Point	**Location Distance [mm]**	**Location Height [mm]**	σ_1 **Anal.**	σ_1 **Num.**	$\mathbf{f}_{ctm,eff}$ **MC Anal.**	$\mathbf{f}_{ctm,eff}$ **MC Num.**	$\mathbf{f}_{ctm,eff}$ **HB Anal.**	$\mathbf{f}_{ctm,eff}$ **HB Num.**
1a	1050	-167,41	3,85	3,15	4,54	4,54	3,15	3,15
1b	2700	202,59	5,62	-0,49	4,71	4,83	3,25	3,32
2a	2025	202,59	-	4,26	-	4,58	-	3,17
2b	1275	-97,41	-	3,75	-	4,48	-	3,11
3	1650	2,59	3,74	3,78	4,48	4,47	3,11	3,10
4a	2100	202,59	4,38	4,25	4,63	4,59	3,20	3,17
5a	1850	202,59	3,96	4,07	4,59	4,56	3,17	3,16
6a	1675	202,59	3,70	3,76	4,56	4,54	3,15	3,14
4b	1200	-167,41	3,66	3,39	4,52	4,52	3,13	3,13
5b	1475	-167,41	3,34	3,17	4,48	4,49	3,11	3,11
6b	1650	-167,41	3,16	2,92	4,45	4,47	3,09	3,10

* all stress parameters $\left[\frac{N}{mm^2}\right]$

Table 5.19: Stress and strength results HAP2W

Point	**Location Distance [mm]**	**Location Height [mm]**	$\frac{\sigma_{1,anal.}}{\mathbf{f}_{ctm}}$ [-]	$\frac{\sigma_{1,num.}}{\mathbf{f}_{ctm}}$ [-]	$\frac{\sigma_{1,anal.}}{\mathbf{f}_{ctm,eff,mc}}$ [-]	$\frac{\sigma_{1,num.}}{\mathbf{f}_{ctm,eff,mc}}$ [-]	$\frac{\sigma_{1,anal.}}{\mathbf{f}_{ctm,eff,hb}}$ [-]	$\frac{\sigma_{1,num.}}{\mathbf{f}_{ctm,eff,hb}}$ [-]
1a	1050	-167,41	0,77	0,63	-	0,69	-	1,00
1b	2700	202,59	1,12	-0,10	-	-0,10	-	-0,14
2a	2025	202,59	-	0,85	-	0,93	-	1,34
2b	1275	-97,41	-	0,75	-	0,84	-	1,21
3	1650	2,59	0,75	0,76	0,83	0,84	1,20	1,22
4a	2100	202,59	0,88	0,85	0,95	0,93	1,37	1,34
5a	1850	202,59	0,79	0,81	0,86	0,89	1,25	1,29
6a	1675	202,59	0,74	0,75	0,81	0,83	1,17	1,20
4b	1200	-167,41	0,73	0,68	0,81	0,75	1,17	1,08
5b	1475	-167,41	0,67	0,63	0,75	0,71	1,08	1,02
6b	1650	-167,41	0,63	0,58	0,71	0,65	1,02	0,94

Table 5.20: Results model uncertainty of HAP2W

Point	**Location Distance [mm]**	**Location Height [mm]**	σ_1 **Anal.**	σ_1 **Num.**	$\mathbf{f}_{ctm,eff}$ **MC Anal.**	$\mathbf{f}_{ctm,eff}$ **MC Num.**	$\mathbf{f}_{ctm,eff}$ **HB Anal.**	$\mathbf{f}_{ctm,eff}$ **HB Num.**
1a	1050	-167,41	4,37	3,51	4,07	4,07	3,07	3,08
1b	2700	202,59	4,98	-1,09	4,20	4,29	3,15	3,21
2a	2025	202,59	-	3,95	-	3,98	-	3,02
2b	1275	-122,41	-	4,14	-	3,97	-	3,0
3	1650	2,59	3,90	3,99	3,92	3,90	2,98	2,98
4a	2100	202,59	3,95	3,90	4,06	3,99	3,07	3,03
5a	1850	202,59	3,61	3,83	3,99	3,95	3,03	3,0
6a	1675	202,59	3,40	3,58	3,94	3,91	3,0	2,98
4b	1200	-167,41	4,16	3,81	4,04	4,04	3,06	3,06
5b	1475	-167,41	3,81	3,60	3,98	4,0	3,02	3,03
6b	1650	-167,41	3,60	3,33	3,95	3,97	3,0	3,01

* all stress parameters $\left[\frac{N}{mm^2}\right]$

Table 5.21: Stress and strength results HCP1TW

Point	**Location Distance [mm]**	**Location Height [mm]**	$\frac{\sigma_{1,anal.}}{\mathbf{f}_{ctm}}$ **[-]**	$\frac{\sigma_{1,num.}}{\mathbf{f}_{ctm}}$ **[-]**	$\frac{\sigma_{1,anal.}}{\mathbf{f}_{ctm,eff,mc}}$ **[-]**	$\frac{\sigma_{1,num.}}{\mathbf{f}_{ctm,eff,mc}}$ **[-]**	$\frac{\sigma_{1,anal.}}{\mathbf{f}_{ctm,eff,hb}}$ **[-]**	$\frac{\sigma_{1,num.}}{\mathbf{f}_{ctm,eff,hb}}$ **[-]**
1a	1050	-167,41	0,93	0,75	-	0,86	-	1,14
1b	2700	202,59	1,06	-0,23	-	-0,25	-	-0,34
2a	2025	202,59	-	0,84	-	0,99	-	1,31
2b	1275	-122,41	-	0,88	-	1,04	-	1,38
3	1650	2,59	0,83	0,85	0,99	1,02	1,31	1,34
4a	2100	202,59	0,84	0,83	0,97	0,98	1,29	1,29
5a	1850	202,59	0,77	0,81	0,90	0,97	1,19	1,27
6a	1675	202,59	0,72	0,76	0,86	0,91	1,13	1,20
4b	1200	-167,41	0,88	0,81	1,03	0,94	1,36	1,25
5b	1475	-167,41	0,81	0,77	0,96	0,90	1,26	1,19
6b	1650	-167,41	0,77	0,71	0,91	0,84	1,20	1,10

Table 5.22: Results model uncertainty of HCP1TW

Point	**Location Distance [mm]**	**Location Height [mm]**	σ_1 **Anal.**	σ_1 **Num.**	$\mathbf{f}_{ctm,eff}$ **MC Anal.**	$\mathbf{f}_{ctm,eff}$ **MC Num.**	$\mathbf{f}_{ctm,eff}$ **HB Anal.**	$\mathbf{f}_{ctm,eff}$ **HB Num.**
1a	1050	-167,41	4,42	3,64	4,38	4,38	3,13	3,14
1b	2700	202,59	6,94	0,09	4,60	4,74	3,27	3,35
2a	2075	202,59	-	5,22	-	4,46	-	3,18
2b	1300	-72,41	-	4,37	-	4,30	-	3,09
3	1650	2,59	4,40	4,43	4,32	4,31	3,10	3,09
4a	2100	202,59	5,39	5,22	4,50	4,46	3,21	3,18
5a	1850	202,59	4,86	4,96	4,46	4,43	3,18	3,16
6a	1675	202,59	4,53	4,59	4,42	4,40	3,16	3,15
4b	1200	-167,41	4,20	3,89	4,35	4,35	3,12	3,12
5b	1475	-167,41	3,84	3,63	4,30	4,32	3,09	3,10
6b	1650	-167,41	3,63	3,35	4,27	4,29	3,07	3,08

* all stress parameters $\left[\frac{N}{mm^2}\right]$

Table 5.23: Stress and strength results HCP2TW

Point	**Location Distance [mm]**	**Location Height [mm]**	$\frac{\sigma_{1,anal.}}{\mathbf{f}_{ctm}}$ [-]	$\frac{\sigma_{1,num.}}{\mathbf{f}_{ctm}}$ [-]	$\frac{\sigma_{1,anal.}}{\mathbf{f}_{ctm,eff,mc}}$ [-]	$\frac{\sigma_{1,num.}}{\mathbf{f}_{ctm,eff,mc}}$ [-]	$\frac{\sigma_{1,anal.}}{\mathbf{f}_{ctm,eff,hb}}$ [-]	$\frac{\sigma_{1,num.}}{\mathbf{f}_{ctm,eff,hb}}$ [-]
1a	1050	-167,41	0,90	0,74	-	0,83	-	1,16
1b	2700	202,59	1,42	0,02	-	0,02	-	0,03
2a	2075	202,59	-	1,07	-	1,17	-	1,64
2b	1300	-72,41	-	0,89	-	1,02	-	1,41
3	1650	2,59	0,90	0,90	1,02	1,03	1,42	1,43
4a	2100	202,59	1,10	1,06	1,20	1,17	1,68	1,64
5a	1850	202,59	0,99	1,01	1,09	1,12	1,53	1,57
6a	1675	202,59	0,93	0,94	1,02	1,04	1,43	1,46
4b	1200	-167,41	0,86	0,79	0,97	0,89	1,35	1,25
5b	1475	-167,41	0,78	0,74	0,89	0,84	1,24	1,17
6b	1650	-167,41	0,74	0,68	0,85	0,78	1,18	1,09

Table 5.24: Results model uncertainty of HCP2TW

5.2. Elzanaty

5.2.1. Pre-analysis

This paragraph will form a short introduction and an outline of the this topic. First some things will be explained, for example the choices made are explained. Further a clear overview of the analysis is given.

Considered strength criterions

For the uniaxial concrete tensile strength there will be made use of the f_{ctm} according to the Eurocode. For the different Elzanaty beams this parameter is calculated, see section 4.2.2. For the biaxial concrete tensile strength there will be made use of the methods of Mohr-Coulomb and Huber, see section 2.7. In formula 5.3 the failure model for the compression/tension region according to Mohr-Coulomb.

$$f_{ctm,eff} = \left(1 + \frac{\sigma_2}{f_{cm}}\right) f_{ctm} \tag{5.3}$$

where:

$f_{ctm,eff}$ = the effective mean concrete tensile strength
f_{ctm} = the mean concrete tensile strength
f_{cm} = the mean concrete compressive strength
σ_2 = the present principal compressive stress

In formula 5.4 the failure model for the compression/tension region according to Huber.

$$f_{ctm,eff} = \left(1,6 - 0,2 f_{cm}^{\frac{1}{3}} + 0,6 \frac{\sigma_2}{f_{cm}}\right) f_{ctm} \tag{5.4}$$

where:

$f_{ctm,eff}$ = the effective mean concrete tensile strength
f_{ctm} = the mean concrete tensile strength
f_{cm} = the mean concrete compressive strength
σ_2 = the present principal compressive stress

In section 2.7 also the failure criterions of Kupfer et all and Lee et all were described. The disadvantage, however, is that no real models are described in these studies. In fact, it remains the presentation of the experimental results and the observation that biaxial behavior plays a role in determining strength parameters. Because of this, it was decided not to use Kupfer et all and Lee et all in the analysis in this study.

Considered models

In this section the points to be considered in the web are explained. Use will be made of both the analytical and numerical models. In figure 5.5 the considered points/parts in the web of the beams.

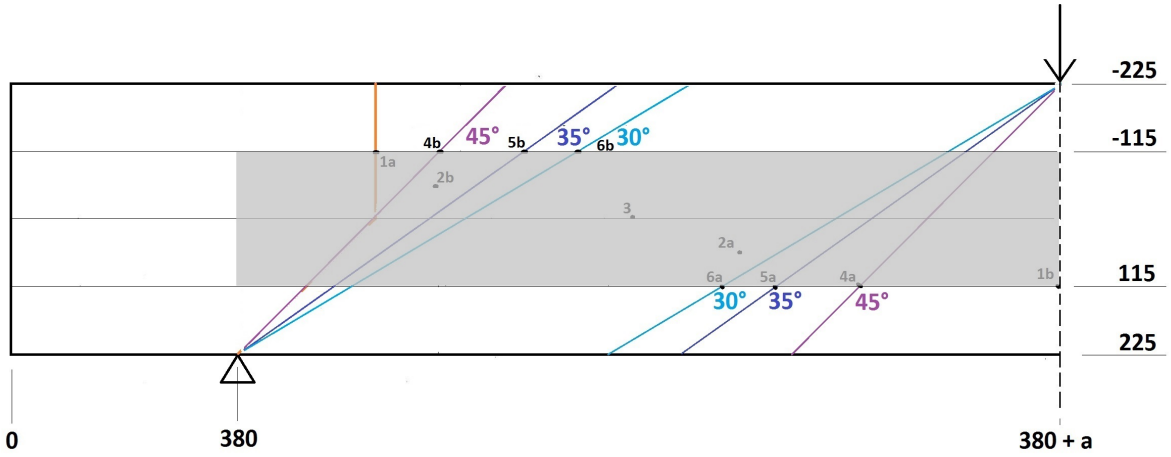

Figure 5.5: The considered points of the Elzanaty beams, distance and height in mm

Figure 5.5 is on the interval of 0 mm to 380 + a mm, from the start of the beam. The grey area of the figure represents the coverage of the tables of the beams in appendix "Elzanaty: Fraction $\frac{\sigma_1}{f_{ctm,eff}}$ according to Mohr-Coulomb" of the appendix report. These tables contain data about the fraction $\frac{\sigma_1}{f_{ctm,eff}}$, the $f_{ctm,eff}$ is determined according to the method Mohr-Coulomb. Point 1a and 1b are the points considered in model 1 as stated in the Eurocode, point 1b is located straight under the external load at the transition point of web to flange and point 1a is located straight above the intersection point of the 45°line and the line of the neutral axis. The 45°line starts from the support. Model 1 is considered with the analytical model. The Eurocode states that in case there is a changing width over the height, then σ_1 should be considered in more horizontal axes parallel to the neutral axis. From the analysis done in chapter 4 it was already known that the highest σ_1 was situated in these points. Point 2a and 2b from model 2 can be seen as "free" points. Point 2a is the point which consideres the greatest value of σ_1 starting from the virtual vertical line through the external point load. Point 2b is the point which consideres the greatest value of σ_1 starting from the virtual vertical line through the support. Model 2 is considered with the numerical model. As concluded out of the numerical analysis in chapter 4 both around the external load and the support the value of σ_1 is disturbed. As a result, the maximum value of σ_1 will not be found directly around respectively the external force and the support. The nearest location of the maximum value of σ_1 is considered. Point 3 of model 3 is considered at the neutral axis of the beam, located in the middle between the external load and the support, model 3 is considered with the analytical model. The reason for consideration is that the study of Elzanaty indicates that the first shear crack starts around this point, see section 3.2.2. The points of model 4, 5 and 6 can be found at the intersection point of respectively the 30°, 35°and the 45°line with the socalled horizontal transition line of the web to flange. The 30°, 35°and the 45°line starts from both the external force and the support. By comparing the values of σ_1 of these points, something can be said about the development of σ_1 related to $f_{ctm}/f_{ctm,eff}$. Model 4, 5 and 6 are considered with both the analytical and numerical model. All the points are considered uniaxial and biaxal.

5.2.2. Analysis of models and strength criterion

In this section the results of beam CW5 will be discussed. This is done with reference to figure 5.5. The results of the remaining beams will be summarized. Thereafter, an attempt is made to make a link between the experiments and the models. Finally, a more practical situation is being considered.

CW5

In the strength analysis there is made use of f_{ctm} = 4,6 N/mm^2. As described in the pre-analysis points 1a and 1b are considered as stated in the Eurocode. The analytical model uncertainty $\frac{\sigma_{1,anal.}}{f_{ctm}}$ of 1a gives $\frac{4,08}{4,6}$ = 0,89. The analytical model uncertainty $\frac{\sigma_{1,anal.}}{f_{ctm}}$ of 1b gives $\frac{5,10}{4,6}$ = 1,11. Without accounting for both biaxial behavior and the disturbed behavior observed in the numerical analysis this would mean that point 1b could be a critical point. The location of point 2a is 1280 mm from start of the beam and 65 mm relative to the neutral axis. The location of point 2b is 770 mm from start of the beam and -115 mm relative to the neutral axis. The numerical uniaxial model uncertainty $\frac{\sigma_{1,num.}}{f_{ctm}}$ of 2a gives $\frac{3,50}{4,6}$ = 0,76. The numerical uniaxial model

uncertainty $\frac{\sigma_{1,num.}}{f_{ctm}}$ of 2b gives $\frac{3,68}{4,6}$ = 0,80. The numerical biaxial model uncertainty $\frac{\sigma_{1,num.}}{f_{ctm,eff,mc}}$ of 2a gives $\frac{3,50}{3,73}$ = 0,94. The numerical biaxial model uncertainty $\frac{\sigma_{1,num.}}{f_{ctm,eff,mc}}$ of 2b gives $\frac{3,68}{3,86}$ = 0,95. Without accounting for biaxial behavior points 2a and 2b would not be classified as critical points. As described point 3 is the critical point according to the Elzanaty study. In figure 5.6 the table of $\sigma_{1,Num.}$ on the interval of 1000 mm to 1160 mm, from start of the beam. In figure 5.7 the table of θ_p also on the interval of 1000 mm to 1160 mm, from start of the beam. The θ_p represents the angle of the principal stress, in this case σ_2. Only the values of θ_p in case $\sigma_1 >$ 3,4 N/mm^2 are presented, so in case $\sigma_1 <$ 3,4 N/mm^2 then $\theta_p = 0$. Note that in fact it does not matter whether the analytical or the numerical results for point 3 are presented, because point 3 is not in the disturbed area, see also the fraction $\frac{\sigma_{1,anal.}}{\sigma_{1,num.}}$ in appendix "Elzanaty: Numerical results" of the appendix report. The numerical biaxial model uncertainty $\frac{\sigma_{1,num.}}{f_{ctm,eff,mc}}$ of 3 gives $\frac{3,61}{3,67}$ = 0,98. As it can be seen from figure 5.6 around point 3 the σ_1 equals at least 3,55 N/mm^2, so there is a significant area in which it is possible to get a crack. In figure 5.7 it can be seen that all these stresses have a angle of more or less -64°(26-90). So possible cracks could start under an angle of 26°.

σ1 σxx τxy σyy	Plaats n	1000	1010	1020	1030	1040	1050	1060	1070	1080	1090	1100	1110	1120	1130	1140	1150	1160
	-225	0,008731	0,007711	0,006704	0,00571	0,004729	0,00376	0,002803	0,001859	0,000928	8,99E-06	-0,0009	-0,00179	-0,00267	-0,00354	-0,0044	-0,00524	-0,00607
	-115	3,28126	3,256591	3,231945	3,207354	3,182841	3,158429	3,134131	3,10996	3,085922	3,062021	3,038255	3,014621	2,991109	2,967709	2,944405	2,921178	2,898006
	-95	3,384924	3,364194	3,343331	3,32237	3,301342	3,280267	3,259162	3,238038	3,216897	3,195739	3,174557	3,153336	3,132059	3,110701	3,089232	3,067614	3,045805
	-75	3,489733	3,473142	3,456306	3,43926	3,422033	3,404648	3,38712	3,36946	3,351669	3,333744	3,315676	3,297447	3,279037	3,260415	3,241546	3,222388	3,20289
	-55	3,565308	3,552999	3,540358	3,527421	3,514214	3,500758	3,487067	3,473147	3,458997	3,444611	3,429974	3,415067	3,399861	3,384322	3,368407	3,352069	**3,335249**
	-35	3,611643	3,603668	3,595304	3,586583	3,577529	3,56816	3,558483	3,548502	3,538213	3,527602	3,516652	3,505335	**3,493619**	**3,481463**	**3,468817**	**3,455626**	**3,441825**
	-15	3,628858	3,625195	3,621115	3,616645	3,611805	3,606606	3,601054	**3,595146**	**3,588871**	**3,582213**	**3,575147**	**3,56764**	**3,559653**	3,551139	3,542042	3,532298	3,521836
	5	3,617189	3,617753	3,6179	3,617651	3,61702	**3,616015**	**3,614635**	**3,612871**	**3,610709**	**3,608125**	3,60509	3,601564	3,597503	3,592852	3,587551	3,581527	3,574704
	25	3,576992	**3,581642**	**3,585901**	**3,589783**	**3,593299**	**3,59645**	**3,59923**	3,601626	3,603618	3,605177	3,606268	3,606847	3,606863	3,606258	3,604962	3,602902	3,599993
	45	**3,50876**	**3,5173**	3,525497	3,533364	3,540903	3,548113	3,554983	3,561495	3,567624	3,573338	3,578596	3,583351	3,587548	3,591122	3,594003	3,59611	3,597355
	65	3,390293	3,402588	3,414619	3,426391	3,437904	3,449149	3,460109	3,470763	3,481081	3,491025	3,500552	3,509608	3,518134	3,526061	3,533315	3,539809	3,545451
	85	3,229858	3,245646	3,261272	3,276737	3,292032	3,307146	3,322057	3,336739	3,351158	3,365273	3,379035	3,39239	3,405272	3,41761	3,429325	3,440329	3,450523
	105	3,082217	3,100944	3,119617	3,138235	3,156789	3,175267	3,193648	3,211905	3,230008	3,247915	3,265581	3,282952	3,299966	3,316555	3,332641	3,348138	3,362952
	115	3,021798	3,041726	3,061689	3,081681	3,101692	3,121706	3,141703	3,161659	3,181544	3,201322	3,220952	3,240386	3,25957	3,278444	3,296938	3,314978	3,33248
	225	-0,00578	-0,00486	-0,00392	-0,00298	-0,00202	-0,00106	-7,8E-05	0,000913	0,001915	0,002929	0,003955	0,004993	0,006043	0,007105	0,00818	0,009267	0,010366

Figure 5.6: The $\sigma_{1,Num}$ around point 3 of CW5

θ Principal stress		1000	1010	1020	1030	1040	1050	1060	1070	1080	1090	1100	1110	1120	1130	1140	1150	1160
	-225																	
	-115	0	0	0	0	0	0	0	0	0	0	0	0	0	0	0	0	0
	-95	0	0	0	0	0	0	0	0	0	0	0	0	0	0	0	0	0
	-75	25,42399	25,32574	25,22742	25,12909	25,03078	24,93254	0	0	0	0	0	0	0	0	0	0	0
	-55	25,46877	25,39559	25,32224	25,24873	25,17509	25,10136	25,0276	24,95387	24,88025	24,80682	24,73371	24,66103	0	0	0	0	0
	-35	25,45137	25,4025	25,35341	25,30409	25,25456	25,20485	25,15499	25,10503	25,05506	25,00514	24,95538	24,90589	24,85679	24,80824	24,7604	24,71345	24,66759
	-15	25,37448	25,34929	25,32388	25,29824	25,27234	25,24622	25,21988	25,19338	25,16675	25,14008	25,11344	25,08694	25,06068	25,0348	25,00945	24,98477	24,96097
	5	25,2393	25,23731	25,23514	25,23276	25,23013	25,22726	25,22416	25,22084	25,21735	25,21373	25,21006	25,2064	25,20286	25,19955	25,19658	25,1941	25,19227
	25	25,04578	25,06661	25,08734	25,10791	25,12828	25,14844	25,16837	25,18808	25,20759	25,22693	25,24614	25,2653	25,28446	25,30372	25,32316	25,34292	25,3631
	45	24,79264	24,83601	24,87938	24,92268	24,96587	25,00891	25,05177	25,09445	25,13693	25,17924	25,22141	25,26346	25,30545	25,34744	25,38949	25,43169	25,47412
	65	0	24,48483	24,55115	24,61755	24,68396	24,75033	24,81662	24,88279	24,94883	25,01472	25,08046	25,14608	25,21157	25,27698	25,34234	25,40768	25,47307
	85	0	0	0	0	0	0	0	0	0	0	0	0	25,01574	25,10521	25,19451	25,28364	25,3726
	105	0	0	0	0	0	0	0	0	0	0	0	0	0	0	0	0	0
	115	0	0	0	0	0	0	0	0	0	0	0	0	0	0	0	0	0
	225																	

Figure 5.7: The θ_p around point 3 of CW5

Points 4a, 5a and 6a are not in the numerical disturbed area. The analytical model uncertainty $\frac{\sigma_{1,anal.}}{f_{ctm}}$ of 4a gives $\frac{3,87}{4,6}$ = 0,84 and $\frac{\sigma_{1,anal.}}{f_{ctm,eff,mc}}$ gives $\frac{3,87}{3,91}$ = 0,99. The analytical model uncertainty $\frac{\sigma_{1,anal.}}{f_{ctm}}$ of 5a gives $\frac{3,46}{4,6}$ = 0,75 and $\frac{\sigma_{1,anal.}}{f_{ctm,eff,mc}}$ gives $\frac{3,46}{3,82}$ = 0,91. The analytical model uncertainty $\frac{\sigma_{1,anal.}}{f_{ctm}}$ of 6a gives $\frac{3,23}{4,6}$ = 0,70 and $\frac{\sigma_{1,anal.}}{f_{ctm,eff,mc}}$ gives $\frac{3,23}{3,76}$ = 0,86. The analytical model uncertainty $\frac{\sigma_{1,anal.}}{f_{ctm}}$ of 4b gives $\frac{3,78}{4,6}$ = 0,82 and $\frac{\sigma_{1,anal.}}{f_{ctm,eff,mc}}$ gives $\frac{3,78}{3,88}$ = 0,97. The analytical model uncertainty $\frac{\sigma_{1,anal.}}{f_{ctm}}$ of 5b gives $\frac{3,38}{4,6}$ = 0,74 and $\frac{\sigma_{1,anal.}}{f_{ctm,eff,mc}}$ gives $\frac{3,38}{3,80}$ = 0,89. The analytical model uncertainty $\frac{\sigma_{1,anal.}}{f_{ctm}}$ of 6b gives $\frac{3,13}{4,6}$ = 0,68 and $\frac{\sigma_{1,anal.}}{f_{ctm,eff,mc}}$ gives $\frac{3,13}{3,74}$ = 0,84. In table 5.25 and 5.26 a summary of the results.

Point	**Location Distance [mm]**	**Location Height [mm]**	σ_1 **Anal.**	σ_1 **Num.**	$\mathbf{f}_{ctm,eff}$ **MC Anal.**	$\mathbf{f}_{ctm,eff}$ **MC Num.**	$\mathbf{f}_{ctm,eff}$ **HB Anal.**	$\mathbf{f}_{ctm,eff}$ **HB Num.**
1a	650	-115	4,08	3,41	3,93	3,93	3,03	3,03
1b	1760	115	5,10	1,21	4,08	4,12	3,12	3,14
2a	1280	65	-	3,50	-	3,73	-	2,91
2b	770	-115	-	3,68	-	3,86	-	2,99
3	1070	5	3,61	3,61	3,71	3,67	2,89	2,88
4a	1380	115	3,87	3,31	3,91	3,84	3,01	2,97
5a	1220	115	3,46	3,41	3,82	3,76	2,96	2,93
6a	1100	115	3,23	3,22	3,76	3,71	2,93	2,90
4b	760	-115	3,78	3,68	3,88	3,86	3,0	2,99
5b	920	-115	3,38	3,47	3,80	3,79	2,95	2,94
6b	1040	-115	3,13	3,18	3,74	3,73	2,91	2,91

* all stress parameters $\left[\frac{N}{mm^2}\right]$

Table 5.25: Stress and strength results CW5

Point	**Location Distance [mm]**	**Location Height [mm]**	$\frac{\sigma_{1,anal.}}{\mathbf{f}_{ctm}}$ [-]	$\frac{\sigma_{1,num.}}{\mathbf{f}_{ctm}}$ [-]	$\frac{\sigma_{1,anal.}}{\mathbf{f}_{ctm,eff,mc}}$ [-]	$\frac{\sigma_{1,num.}}{\mathbf{f}_{ctm,eff,mc}}$ [-]	$\frac{\sigma_{1,anal.}}{\mathbf{f}_{ctm,eff,hb}}$ [-]	$\frac{\sigma_{1,num.}}{\mathbf{f}_{ctm,eff,hb}}$ [-]
1a	650	-115	0,89	0,74	-	0,87	-	1,13
1b	1760	115	1,11	0,26	-	0,29	-	0,38
2a	1280	65	-	0,76	-	0,94	-	1,20
2b	770	-115	-	0,80	-	0,95	-	1,23
3	1070	5	0,78	0,79	0,97	0,98	1,25	1,26
4a	1380	115	0,84	0,72	0,99	0,86	1,28	1,11
5a	1220	115	0,75	0,74	0,91	0,91	1,17	1,16
6a	1100	115	0,70	0,70	0,86	0,87	1,10	1,11
4b	760	-115	0,82	0,80	0,97	0,95	1,26	1,23
5b	920	-115	0,74	0,76	0,89	0,92	1,15	1,18
6b	1040	-115	0,68	0,69	0,84	0,85	1,08	1,10

Table 5.26: Results model uncertainty of CW5

Other results

In this section the other results will be presented. In table 5.27 and 5.28 the results of CW1, f_{ctm} = 4,65 N/mm^2. In table 5.29 and 5.30 the results of CW2, f_{ctm} = 4,6 N/mm^2. In table 5.31 and 5.32 the results of CW3, f_{ctm} = 4,6 N/mm^2. In table 5.33 and 5.34 the results of CW4, f_{ctm} = 4,6 N/mm^2. In table 5.35 and 5.36 the results of CW6, f_{ctm} = 4,6 N/mm^2. In table 5.37 and 5.38 the results of CW7, f_{ctm} = 4,6 N/mm^2. In table 5.39 and 5.40 the results of CW8, f_{ctm} = 3,35 N/mm^2. In table 5.41 and 5.42 the results of CW9, f_{ctm} = 4,2 N/mm^2. In table 5.43 and 5.44 the results of CW10, f_{ctm} = 4,5 N/mm^2. In table 5.45 and 5.46 the results of CW11, f_{ctm} = 4,0 N/mm^2. In table 5.47 and 5.48 the results of CW12, f_{ctm} = 3,3 N/mm^2. In table 5.49 and 5.50 the results of CW13, f_{ctm} = 4,5 N/mm^2. In table 5.51 and 5.52 the results of CW14, f_{ctm} = 4,5 N/mm^2. In table 5.53 and 5.54 the results of CW15, f_{ctm} = 4,4 N/mm^2. In table 5.55 and 5.56 the results of CW16, f_{ctm} = 4,5 N/mm^2. In table 5.57 and 5.58 the results of CW17, f_{ctm} = 4,5 N/mm^2.

Point	**Location Distance [mm]**	**Location Height [mm]**	σ_1 **Anal.**	σ_1 **Num.**	$\mathbf{f}_{ctm,eff}$ **MC Anal.**	$\mathbf{f}_{ctm,eff}$ **MC Num.**	$\mathbf{f}_{ctm,eff}$ **HB Anal.**	$\mathbf{f}_{ctm,eff}$ **HB Num.**
1a	650	-115	4,71	4,03	3,91	3,91	3,05	3,05
1b	1450	115	5,33	1,13	4,0	4,08	3,11	3,15
2a	-	-	-	-	-	-	-	-
2b	760	-115	-	4,27	-	3,84	-	3,0
3	910	5	4,36	4,33	3,70	3,67	2,92	2,90
4a	1070	115	4,07	3,72	3,80	3,76	2,98	2,96
5a	900	115	3,67	3,7	3,71	3,67	2,93	2,91
6a	790	115	3,42	3,37	3,64	3,60	2,88	2,86
4b	760	-115	4,35	4,27	3,85	3,84	3,01	3,0
5b	920	-115	3,89	3,93	3,76	3,75	2,96	2,95
6b	1040	-115	3,60	3,47	3,69	3,67	2,92	2,90

* all stress parameters $\left[\frac{N}{mm^2}\right]$

Table 5.27: Stress and strength results CW1

Point	**Location Distance [mm]**	**Location Height [mm]**	$\frac{\sigma_{1,anal.}}{\mathbf{f}_{ctm}}$ **[-]**	$\frac{\sigma_{1,num.}}{\mathbf{f}_{ctm}}$ **[-]**	$\frac{\sigma_{1,anal.}}{\mathbf{f}_{ctm,eff,mc}}$ **[-]**	$\frac{\sigma_{1,num.}}{\mathbf{f}_{ctm,eff,mc}}$ **[-]**	$\frac{\sigma_{1,anal.}}{\mathbf{f}_{ctm,eff,hb}}$ **[-]**	$\frac{\sigma_{1,num.}}{\mathbf{f}_{ctm,eff,hb}}$ **[-]**
1a	650	-115	1,01	0,87	-	1,03	-	1,32
1b	1450	115	1,15	0,24	-	0,28	-	0,36
2a	1270	65	-	-	-	-	-	-
2b	770	-115	-	0,92	-	1,11	-	1,42
3	910	5	0,94	0,93	1,18	1,18	1,49	1,49
4a	1070	115	0,88	0,80	1,07	0,99	1,36	1,26
5a	900	115	0,79	0,80	0,99	1,00	1,26	1,27
6a	790	115	0,73	0,73	0,94	0,94	1,18	1,18
4b	760	-115	0,93	0,92	1,13	1,11	1,44	1,42
5b	920	-115	0,84	0,85	1,03	1,05	1,32	1,33
6b	1040	-115	0,77	0,75	0,97	0,95	1,23	1,20

Table 5.28: Results model uncertainty of CW1

Point	**Location Distance [mm]**	**Location Height [mm]**	σ_1 **Anal.**	σ_1 **Num.**	$\mathbf{f}_{ctm,eff}$ **MC Anal.**	$\mathbf{f}_{ctm,eff}$ **MC Num.**	$\mathbf{f}_{ctm,eff}$ **HB Anal.**	$\mathbf{f}_{ctm,eff}$ **HB Num.**
1a	650	-115	4,14	3,49	3,92	3,92	3,05	3,05
1b	1760	115	5,35	1,37	4,09	4,15	3,15	3,19
2a	1290	115	-	3,65	-	3,82	-	2,99
2b	770	-115	-	3,75	-	3,85	-	3,0
3	1070	5	3,70	3,73	3,71	3,68	2,92	2,90
4a	1380	115	4,04	3,52	3,92	3,86	3,05	3,01
5a	1220	115	3,60	3,59	3,83	3,78	2,99	2,96
6a	1100	115	3,36	3,39	3,78	3,74	2,96	2,94
4b	760	-115	3,82	3,75	3,87	3,86	3,02	3,0
5b	920	-115	3,42	3,53	3,79	3,79	2,97	2,96
6b	1040	-115	3,17	3,23	3,73	3,72	2,93	2,92

* all stress parameters $\left[\frac{N}{mm^2}\right]$

Table 5.29: Stress and strength results CW2

Point	**Location Distance [mm]**	**Location Height [mm]**	$\frac{\sigma_{1,anal.}}{\mathbf{f}_{ctm}}$ [-]	$\frac{\sigma_{1,num.}}{\mathbf{f}_{ctm}}$ [-]	$\frac{\sigma_{1,anal.}}{\mathbf{f}_{ctm,eff,mc}}$ [-]	$\frac{\sigma_{1,num.}}{\mathbf{f}_{ctm,eff,mc}}$ [-]	$\frac{\sigma_{1,anal.}}{\mathbf{f}_{ctm,eff,hb}}$ [-]	$\frac{\sigma_{1,num.}}{\mathbf{f}_{ctm,eff,hb}}$ [-]
1a	650	-115	0,90	0,76	-	0,89	-	1,15
1b	1760	115	1,16	0,30	-	0,33	-	0,43
2a	1290	115	-	0,79	-	0,96	-	1,22
2b	770	-115	-	0,82	-	0,97	-	1,25
3	1070	5	0,80	0,81	1,00	1,01	1,27	1,28
4a	1380	115	0,88	0,77	1,03	0,91	1,33	1,17
5a	1220	115	0,78	0,78	0,94	0,95	1,20	1,21
6a	1100	115	0,73	0,74	0,89	0,91	1,14	1,15
4b	760	-115	0,83	0,82	0,99	0,97	1,27	1,25
5b	920	-115	0,74	0,77	0,90	0,93	1,15	1,19
6b	1040	-115	0,69	0,70	0,85	0,87	1,08	1,10

Table 5.30: Results model uncertainty of CW2

Point	**Location Distance [mm]**	**Location Height [mm]**	σ_1 **Anal.**	σ_1 **Num.**	$\mathbf{f}_{ctm,eff}$ **MC Anal.**	$\mathbf{f}_{ctm,eff}$ **MC Num.**	$\mathbf{f}_{ctm,eff}$ **HB Anal.**	$\mathbf{f}_{ctm,eff}$ **HB Num.**
1a	650	-115	3,82	3,20	3,95	3,95	3,07	3,06
1b	2220	115	6,64	-0,10	4,24	4,43	3,24	3,35
2a	1710	115	-	4,20	-	3,99	-	3,09
2b	770	-115	-	3,46	-	3,88	-	3,02
3	1300	5	3,35	3,31	3,73	3,71	2,93	2,92
4a	1840	115	4,92	3,77	4,11	4,04	3,16	3,12
5a	1680	115	4,36	4,18	4,05	3,98	3,12	3,08
6a	1560	115	3,99	3,93	3,99	3,93	3,09	3,05
4b	760	-115	3,54	3,45	3,90	3,89	3,04	3,03
5b	920	-115	3,17	3,27	3,83	3,81	2,99	2,98
6b	1040	-115	2,93	3,0	3,77	3,76	2,95	2,95

* all stress parameters $\left[\frac{N}{mm^2}\right]$

Table 5.31: Stress and strength results CW3

Point	**Location Distance [mm]**	**Location Height [mm]**	$\frac{\sigma_{1,anal.}}{\mathbf{f}_{ctm}}$ [-]	$\frac{\sigma_{1,num.}}{\mathbf{f}_{ctm}}$ [-]	$\frac{\sigma_{1,anal.}}{\mathbf{f}_{ctm,eff,mc}}$ [-]	$\frac{\sigma_{1,num.}}{\mathbf{f}_{ctm,eff,mc}}$ [-]	$\frac{\sigma_{1,anal.}}{\mathbf{f}_{ctm,eff,hb}}$ [-]	$\frac{\sigma_{1,num.}}{\mathbf{f}_{ctm,eff,hb}}$ [-]
1a	650	-115	0,83	0,70	-	0,81	-	1,04
1b	2220	115	1,44	-0,02	-	-0,02	-	-0,03
2a	1710	115	-	0,91	-	1,05	-	1,36
2b	770	-115	-	0,75	-	0,89	-	1,14
3	1300	5	0,73	0,72	0,90	0,89	1,14	1,14
4a	1840	115	1,07	0,82	1,20	0,93	1,56	1,21
5a	1680	115	0,95	0,91	1,08	1,05	1,40	1,36
6a	1560	115	0,87	0,85	1,00	1,00	1,29	1,29
4b	760	-115	0,77	0,75	0,91	0,89	1,16	1,14
5b	920	-115	0,69	0,71	0,83	0,86	1,06	1,10
6b	1040	-115	0,64	0,65	0,78	0,80	0,99	1,02

Table 5.32: Results model uncertainty of CW3

Point	**Location Distance [mm]**	**Location Height [mm]**	σ_1 **Anal.**	σ_1 **Num.**	$\mathbf{f}_{ctm,eff}$ **MC Anal.**	$\mathbf{f}_{ctm,eff}$ **MC Num.**	$\mathbf{f}_{ctm,eff}$ **HB Anal.**	$\mathbf{f}_{ctm,eff}$ **HB Num.**
1a	650	-115	4,20	3,53	3,92	3,91	3,01	3,01
1b	1760	115	5,31	1,32	4,08	4,14	3,11	3,14
2a	1280	65	-	3,68	-	3,73	-	2,90
2b	770	-115	-	3,80	-	3,85	-	2,97
3	1070	5	3,73	3,76	3,70	3,67	2,88	2,86
4a	1380	115	4,02	3,50	3,91	3,85	3,0	2,97
5a	1220	115	3,59	3,58	3,82	3,77	2,95	2,92
6a	1100	115	3,35	3,38	3,76	3,72	2,92	2,89
4b	760	-115	3,88	3,80	3,87	3,86	2,98	2,97
5b	920	-115	3,48	3,58	3,79	3,78	2,93	2,93
6b	1040	-115	3,22	3,28	3,73	3,72	2,89	2,89

* all stress parameters $\left[\frac{N}{mm^2}\right]$

Table 5.33: Stress and strength results CW4

Point	**Location Distance [mm]**	**Location Height [mm]**	$\frac{\sigma_{1,anal.}}{\mathbf{f}_{ctm}}$ **[-]**	$\frac{\sigma_{1,num.}}{\mathbf{f}_{ctm}}$ **[-]**	$\frac{\sigma_{1,anal.}}{\mathbf{f}_{ctm,eff,mc}}$ **[-]**	$\frac{\sigma_{1,num.}}{\mathbf{f}_{ctm,eff,mc}}$ **[-]**	$\frac{\sigma_{1,anal.}}{\mathbf{f}_{ctm,eff,hb}}$ **[-]**	$\frac{\sigma_{1,num.}}{\mathbf{f}_{ctm,eff,hb}}$ **[-]**
1a	650	-115	0,91	0,77	-	0,90	-	1,17
1b	1760	115	1,15	0,29	-	0,32	-	0,42
2a	1280	65	-	0,80	-	0,99	-	1,27
2b	770	-115	-	0,83	-	0,99	-	1,28
3	1070	5	0,81	0,82	1,00	1,02	1,29	1,31
4a	1380	115	0,87	0,76	1,03	0,91	1,34	1,18
5a	1220	115	0,78	0,78	0,94	0,95	1,22	1,23
6a	1100	115	0,73	0,74	0,89	0,91	1,15	1,17
4b	760	-115	0,84	0,83	1,0	0,99	1,30	1,28
5b	920	-115	0,76	0,78	0,92	0,95	1,19	1,22
6b	1040	-115	0,70	0,71	0,86	0,88	1,11	1,14

Table 5.34: Results model uncertainty of CW4

Point	**Location Distance [mm]**	**Location Height [mm]**	σ_1 **Anal.**	σ_1 **Num.**	$\mathbf{f}_{ctm,eff}$ **MC Anal.**	$\mathbf{f}_{ctm,eff}$ **MC Num.**	$\mathbf{f}_{ctm,eff}$ **HB Anal.**	$\mathbf{f}_{ctm,eff}$ **HB Num.**
1a	650	-115	3,88	3,32	4,02	4,02	3,08	3,08
1b	1760	115	5,82	1,72	4,23	4,30	3,21	3,25
2a	1280	115	-	3,79	-	3,92	-	3,02
2b	770	-75	-	3,53	-	3,91	-	3,04
3	1070	5	3,65	3,62	3,88	3,85	3,0	2,98
4a	1380	115	4,34	3,70	4,09	4,04	3,13	3,09
5a	1220	115	3,83	3,71	4,02	3,97	3,09	3,05
6a	1100	115	3,55	3,48	3,98	3,93	3,06	3,03
4b	760	-115	3,58	3,52	3,98	3,96	3,06	3,05
5b	920	-115	3,20	3,28	3,91	3,89	3,01	3,0
6b	1040	-115	2,95	2,99	3,85	3,84	2,98	2,98

* all stress parameters $\left[\frac{N}{mm^2}\right]$

Table 5.35: Stress and strength results CW6

Point	**Location Distance [mm]**	**Location Height [mm]**	$\frac{\sigma_{1,anal.}}{\mathbf{f}_{ctm}}$ [-]	$\frac{\sigma_{1,num.}}{\mathbf{f}_{ctm}}$ [-]	$\frac{\sigma_{1,anal.}}{\mathbf{f}_{ctm,eff,mc}}$ [-]	$\frac{\sigma_{1,num.}}{\mathbf{f}_{ctm,eff,mc}}$ [-]	$\frac{\sigma_{1,anal.}}{\mathbf{f}_{ctm,eff,hb}}$ [-]	$\frac{\sigma_{1,num.}}{\mathbf{f}_{ctm,eff,hb}}$ [-]
1a	650	-115	0,84	0,72	-	0,83	-	1,08
1b	1760	115	1,27	0,37	-	0,40	-	0,53
2a	1280	115	-	0,82	-	0,97	-	1,25
2b	770	-75	-	0,77	-	0,90	-	1,16
3	1070	5	0,79	0,79	0,94	0,94	1,22	1,22
4a	1380	115	0,94	0,80	1,06	0,92	1,39	1,20
5a	1220	115	0,83	0,81	0,95	0,93	1,24	1,21
6a	1100	115	0,77	0,76	0,89	0,89	1,16	1,15
4b	760	-115	0,78	0,77	0,90	0,89	1,17	1,15
5b	920	-115	0,69	0,71	0,82	0,84	1,06	1,09
6b	1040	-115	0,64	0,65	0,77	0,78	0,99	1,0

Table 5.36: Results model uncertainty of CW6

Point	**Location Distance [mm]**	**Location Height [mm]**	σ_1 **Anal.**	σ_1 **Num.**	$\mathbf{f}_{ctm,eff}$ **MC Anal.**	$\mathbf{f}_{ctm,eff}$ **MC Num.**	$\mathbf{f}_{ctm,eff}$ **HB Anal.**	$\mathbf{f}_{ctm,eff}$ **HB Num.**
1a	650	-115	3,64	3,11	4,05	4,04	3,11	3,10
1b	1760	115	5,30	1,60	4,23	4,31	3,21	3,26
2a	1300	115	-	3,53	-	4,03	-	3,09
2b	760	-115	-	3,31	-	3,99	-	3,07
3	1070	5	3,39	3,39	3,90	3,88	3,02	3,00
4a	1380	115	3,95	3,45	4,10	4,06	3,14	3,11
5a	1220	115	3,50	3,45	4,03	4,0	3,10	3,07
6a	1100	115	3,25	3,23	3,99	3,95	3,07	3,05
4b	760	-115	3,36	3,31	4,0	3,99	3,08	3,07
5b	920	-115	3,0	3,09	3,94	3,93	3,04	3,03
6b	1040	-115	2,77	2,82	3,88	3,88	3,01	3,0

* all stress parameters $\left[\frac{N}{mm^2}\right]$

Table 5.37: Stress and strength results CW7

Point	**Location Distance [mm]**	**Location Height [mm]**	$\frac{\sigma_{1,anal.}}{\mathbf{f}_{ctm}}$ [-]	$\frac{\sigma_{1,num.}}{\mathbf{f}_{ctm}}$ [-]	$\frac{\sigma_{1,anal.}}{\mathbf{f}_{ctm,eff,mc}}$ [-]	$\frac{\sigma_{1,num.}}{\mathbf{f}_{ctm,eff,mc}}$ [-]	$\frac{\sigma_{1,anal.}}{\mathbf{f}_{ctm,eff,hb}}$ [-]	$\frac{\sigma_{1,num.}}{\mathbf{f}_{ctm,eff,hb}}$ [-]
1a	650	-115	0,79	0,67	-	0,77	-	1,00
1b	1760	115	1,15	0,35	-	0,37	-	0,49
2a	1300	115	-	0,77	-	0,88	-	1,14
2b	760	-115	-	0,72	-	0,83	-	1,08
3	1070	5	0,74	0,74	0,87	0,87	1,12	1,13
4a	1380	115	0,86	0,75	0,96	0,85	1,26	1,11
5a	1220	115	0,76	0,75	0,87	0,86	1,13	1,12
6a	1100	115	0,71	0,70	0,81	0,82	1,06	1,06
4b	760	-115	0,73	0,72	0,84	0,83	1,09	1,08
5b	920	-115	0,65	0,67	0,76	0,79	0,99	1,02
6b	1040	-115	0,60	0,61	0,71	0,73	0,92	0,94

Table 5.38: Results model uncertainty of CW7

Point	**Location Distance [mm]**	**Location Height [mm]**	σ_1 **Anal.**	σ_1 **Num.**	$\mathbf{f}_{ctm,eff}$ **MC Anal.**	$\mathbf{f}_{ctm,eff}$ **MC Num.**	$\mathbf{f}_{ctm,eff}$ **HB Anal.**	$\mathbf{f}_{ctm,eff}$ **HB Num.**
1a	650	-115	2,95	2,44	2,68	2,67	2,64	2,63
1b	1760	115	3,54	0,80	2,81	2,84	2,72	2,73
2a	1280	65	-	2,46	-	2,45	-	2,50
2b	780	-115	-	2,65	-	2,60	-	2,59
3	1070	5	2,57	2,57	2,44	2,40	2,50	2,48
4a	1380	115	2,70	2,30	2,63	2,56	2,61	2,57
5a	1220	115	2,43	2,38	2,54	2,48	2,56	2,52
6a	1100	115	2,27	2,25	2,49	2,43	2,52	2,49
4b	760	-115	2,73	2,65	2,62	2,61	2,61	2,60
5b	920	-115	2,44	2,51	2,54	2,53	2,56	2,55
6b	1040	-115	2,26	2,30	2,48	2,47	2,52	2,52

* all stress parameters $\left[\frac{N}{mm^2}\right]$

Table 5.39: Stress and strength results CW8

Point	**Location Distance [mm]**	**Location Height [mm]**	$\frac{\sigma_{1,anal.}}{\mathbf{f}_{ctm}}$ **[-]**	$\frac{\sigma_{1,num.}}{\mathbf{f}_{ctm}}$ **[-]**	$\frac{\sigma_{1,anal.}}{\mathbf{f}_{ctm,eff,mc}}$ **[-]**	$\frac{\sigma_{1,num.}}{\mathbf{f}_{ctm,eff,mc}}$ **[-]**	$\frac{\sigma_{1,anal.}}{\mathbf{f}_{ctm,eff,hb}}$ **[-]**	$\frac{\sigma_{1,num.}}{\mathbf{f}_{ctm,eff,hb}}$ **[-]**
1a	650	-115	0,88	0,73	-	0,92	-	0,93
1b	1760	115	1,05	0,24	-	0,28	-	0,29
2a	1280	65	-	0,73	-	1,00	-	0,98
2b	780	-115	-	0,79	-	1,02	-	1,02
3	1070	5	0,77	0,77	1,05	1,06	1,03	1,04
4a	1380	115	0,81	0,69	1,02	0,90	1,04	0,89
5a	1220	115	0,72	0,71	0,95	0,96	0,95	0,94
6a	1100	115	0,68	0,67	0,91	0,93	0,90	0,91
4b	760	-115	0,81	0,79	1,04	1,02	1,05	1,02
5b	920	-115	0,73	0,75	0,96	0,99	0,95	0,98
6b	1040	-115	0,67	0,69	0,91	0,93	0,90	0,91

Table 5.40: Results model uncertainty of CW8

Point	**Location Distance [mm]**	**Location Height [mm]**	σ_1 **Anal.**	σ_1 **Num.**	$\mathbf{f}_{ctm,eff}$ **MC Anal.**	$\mathbf{f}_{ctm,eff}$ **MC Num.**	$\mathbf{f}_{ctm,eff}$ **HB Anal.**	$\mathbf{f}_{ctm,eff}$ **HB Num.**
1a	650	-115	3,41	2,88	3,58	3,57	3,04	3,04
1b	1760	115	4,63	1,20	3,76	3,81	3,15	3,18
2a	1290	115	-	3,07	-	3,50	-	2,99
2b	770	-115	-	3,08	-	3,51	-	3,0
3	1070	5	3,10	3,08	3,39	3,36	2,93	2,91
4a	1380	115	3,48	2,96	3,60	3,54	3,05	3,02
5a	1220	115	3,09	3,01	3,52	3,46	3,01	2,97
6a	1100	115	2,88	2,84	3,47	3,42	2,98	2,94
4b	760	-115	3,15	3,08	3,53	3,51	3,01	3,0
5b	920	-115	2,82	2,89	3,45	3,44	2,96	2,96
6b	1040	-115	2,60	2,64	3,39	3,38	2,93	2,92

* all stress parameters $\left[\frac{N}{mm^2}\right]$

Table 5.41: Stress and strength results CW9

Point	**Location Distance [mm]**	**Location Height [mm]**	$\frac{\sigma_{1,anal.}}{\mathbf{f}_{ctm}}$ [-]	$\frac{\sigma_{1,num.}}{\mathbf{f}_{ctm}}$ [-]	$\frac{\sigma_{1,anal.}}{\mathbf{f}_{ctm,eff,mc}}$ [-]	$\frac{\sigma_{1,num.}}{\mathbf{f}_{ctm,eff,mc}}$ [-]	$\frac{\sigma_{1,anal.}}{\mathbf{f}_{ctm,eff,hb}}$ [-]	$\frac{\sigma_{1,num.}}{\mathbf{f}_{ctm,eff,hb}}$ [-]
1a	650	-115	0,81	0,69	-	0,81	-	0,95
1b	1760	115	1,10	0,29	-	0,32	-	0,38
2a	1290	115	-	0,73	-	0,88	-	1,03
2b	770	-115	-	0,73	-	0,88	-	1,03
3	1070	5	0,74	0,73	0,91	0,92	1,06	1,06
4a	1380	115	0,83	0,71	0,97	0,84	1,14	0,98
5a	1220	115	0,74	0,72	0,88	0,87	1,03	1,01
6a	1100	115	0,69	0,68	0,83	0,83	0,97	0,96
4b	760	-115	0,75	0,73	0,89	0,88	1,05	1,03
5b	920	-115	0,67	0,69	0,82	0,84	0,95	0,98
6b	1040	-115	0,62	0,63	0,77	0,78	0,89	0,90

Table 5.42: Results model uncertainty of CW9

Point	**Location Distance [mm]**	**Location Height [mm]**	σ_1 **Anal.**	σ_1 **Num.**	$\mathbf{f}_{ctm,eff}$ **MC Anal.**	$\mathbf{f}_{ctm,eff}$ **MC Num.**	$\mathbf{f}_{ctm,eff}$ **HB Anal.**	$\mathbf{f}_{ctm,eff}$ **HB Num.**
1a	650	-115	3,76	3,22	3,92	3,91	3,09	3,08
1b	1780	115	5,75	1,72	4,13	4,20	3,22	3,26
2a	1320	115	-	3,72	-	3,91	-	3,08
2b	780	-75	-	3,43	-	3,80	-	3,02
3	1080	5	3,54	3,51	3,77	3,74	3,0	2,98
4a	1400	115	4,28	3,63	4,0	3,94	3,14	3,10
5a	1240	115	3,80	3,65	3,93	3,88	3,10	3,06
6a	1120	115	3,49	3,41	3,88	3,83	3,07	3,04
4b	760	-115	3,47	3,41	3,87	3,86	3,06	3,05
5b	920	-115	3,10	3,18	3,80	3,79	3,02	3,0
6b	1040	-115	2,86	2,90	3,74	3,73	2,98	2,98

* all stress parameters $\left[\frac{N}{mm^2}\right]$

Table 5.43: Stress and strength results CW10

Point	**Location Distance [mm]**	**Location Height [mm]**	$\frac{\sigma_{1,anal.}}{\mathbf{f}_{ctm}}$ [-]	$\frac{\sigma_{1,num.}}{\mathbf{f}_{ctm}}$ [-]	$\frac{\sigma_{1,anal.}}{\mathbf{f}_{ctm,eff,mc}}$ [-]	$\frac{\sigma_{1,num.}}{\mathbf{f}_{ctm,eff,mc}}$ [-]	$\frac{\sigma_{1,anal.}}{\mathbf{f}_{ctm,eff,hb}}$ [-]	$\frac{\sigma_{1,num.}}{\mathbf{f}_{ctm,eff,hb}}$ [-]
1a	650	-115	0,84	0,72	-	0,82	-	1,04
1b	1780	115	1,28	0,38	-	0,41	-	0,53
2a	1320	115	-	0,83	-	0,95	-	1,21
2b	780	-75	-	0,76	-	0,90	-	1,14
3	1080	5	0,79	0,78	0,94	0,94	1,18	1,18
4a	1400	115	0,95	0,81	1,07	0,92	1,36	1,17
5a	1240	115	0,84	0,81	0,97	0,94	1,23	1,19
6a	1120	115	0,78	0,76	0,90	0,89	1,14	1,12
4b	760	-115	0,77	0,76	0,90	0,89	1,13	1,12
5b	920	-115	0,69	0,71	0,82	0,84	1,03	1,06
6b	1040	-115	0,64	0,65	0,76	0,78	0,96	0,98

Table 5.44: Results model uncertainty of CW10

Point	**Location Distance [mm]**	**Location Height [mm]**	σ_1 **Anal.**	σ_1 **Num.**	$\mathbf{f}_{ctm,eff}$ **MC Anal.**	$\mathbf{f}_{ctm,eff}$ **MC Num.**	$\mathbf{f}_{ctm,eff}$ **HB Anal.**	$\mathbf{f}_{ctm,eff}$ **HB Num.**
1a	650	-115	3,24	2,74	3,39	3,38	2,97	2,97
1b	1780	115	4,49	1,20	3,57	3,63	3,08	3,12
2a	1310	115	-	2,96	-	3,32	-	2,93
2b	780	-115	-	2,93	-	3,31	-	2,93
3	1080	5	2,95	2,93	3,21	3,17	2,87	2,85
4a	1400	115	3,37	2,86	3,42	3,36	3,0	2,96
5a	1240	115	3,01	2,91	3,35	3,29	2,94	2,91
6a	1120	115	2,78	2,74	3,30	3,24	2,92	2,89
4b	760	-115	2,99	2,93	3,34	3,32	2,95	2,94
5b	920	-115	2,68	2,75	3,26	3,25	2,90	2,89
6b	1040	-115	2,47	2,51	3,21	3,20	2,87	2,86

* all stress parameters $\left[\frac{N}{mm^2}\right]$

Table 5.45: Stress and strength results CW11

Point	**Location Distance [mm]**	**Location Height [mm]**	$\frac{\sigma_{1,anal.}}{\mathbf{f}_{ctm}}$ **[-]**	$\frac{\sigma_{1,num.}}{\mathbf{f}_{ctm}}$ **[-]**	$\frac{\sigma_{1,anal.}}{\mathbf{f}_{ctm,eff,mc}}$ **[-]**	$\frac{\sigma_{1,num.}}{\mathbf{f}_{ctm,eff,mc}}$ **[-]**	$\frac{\sigma_{1,anal.}}{\mathbf{f}_{ctm,eff,hb}}$ **[-]**	$\frac{\sigma_{1,num.}}{\mathbf{f}_{ctm,eff,hb}}$ **[-]**
1a	650	-115	0,81	0,68	-	0,81	-	0,92
1b	1780	115	1,12	0,30	-	0,33	-	0,38
2a	1310	115	-	0,74	-	0,89	-	1,01
2b	780	-115	-	0,73	-	0,88	-	1,00
3	1080	5	0,74	0,73	0,92	0,92	1,03	1,03
4a	1400	115	0,84	0,72	0,98	0,85	1,12	0,97
5a	1240	115	0,75	0,73	0,90	0,89	1,02	1,00
6a	1120	115	0,70	0,69	0,84	0,84	0,95	0,95
4b	760	-115	0,75	0,73	0,90	0,88	1,02	1,0
5b	920	-115	0,67	0,69	0,82	0,84	0,92	0,95
6b	1040	-115	0,62	0,63	0,77	0,79	0,86	0,88

Table 5.46: Results model uncertainty of CW11

Point	**Location Distance [mm]**	**Location Height [mm]**	σ_1 **Anal.**	σ_1 **Num.**	$\mathbf{f}_{ctm,eff}$ **MC Anal.**	$\mathbf{f}_{ctm,eff}$ **MC Num.**	$\mathbf{f}_{ctm,eff}$ **HB Anal.**	$\mathbf{f}_{ctm,eff}$ **HB Num.**
1a	650	-115	2,82	2,34	2,65	2,64	2,63	2,63
1b	1780	115	3,46	0,81	2,79	2,82	2,72	2,74
2a	1300	65	-	2,37	-	2,44	-	2,51
2b	780	-115	-	2,53	-	2,57	-	2,59
3	1080	5	2,46	2,46	2,42	2,39	2,50	2,48
4a	1400	115	2,64	2,24	2,62	2,55	2,62	2,57
5a	1240	115	2,38	2,32	2,54	2,48	2,56	2,53
6a	1120	115	2,21	2,19	2,48	2,43	2,53	2,50
4b	760	-115	2,60	2,53	2,60	2,58	2,60	2,59
5b	920	-115	2,33	2,39	2,52	2,51	2,56	2,55
6b	1040	-115	2,16	2,19	2,46	2,45	2,52	2,51

* all stress parameters $\left[\frac{N}{mm^2}\right]$

Table 5.47: Stress and strength results CW12

Point	**Location Distance [mm]**	**Location Height [mm]**	$\frac{\sigma_{1,anal.}}{\mathbf{f}_{ctm}}$ [-]	$\frac{\sigma_{1,num.}}{\mathbf{f}_{ctm}}$ [-]	$\frac{\sigma_{1,anal.}}{\mathbf{f}_{ctm,eff,mc}}$ [-]	$\frac{\sigma_{1,num.}}{\mathbf{f}_{ctm,eff,mc}}$ [-]	$\frac{\sigma_{1,anal.}}{\mathbf{f}_{ctm,eff,hb}}$ [-]	$\frac{\sigma_{1,num.}}{\mathbf{f}_{ctm,eff,hb}}$ [-]
1a	650	-115	0,85	0,71	-	0,89	-	0,89
1b	1780	115	1,05	0,24	-	0,29	-	0,30
2a	1300	65	-	0,72	-	0,97	-	0,95
2b	780	-115	-	0,77	-	0,98	-	0,98
3	1080	5	0,75	0,74	1,02	1,03	0,99	0,99
4a	1400	115	0,80	0,68	1,00	0,88	1,00	0,87
5a	1240	115	0,72	0,70	0,93	0,94	0,93	0,92
6a	1120	115	0,67	0,66	0,89	0,90	0,87	0,88
4b	760	-115	0,79	0,77	1,0	0,98	1,0	0,98
5b	920	-115	0,71	0,72	0,92	0,95	0,91	0,94
6b	1040	-115	0,65	0,66	0,88	0,89	0,86	0,87

Table 5.48: Results model uncertainty of CW12

Point	**Location Distance [mm]**	**Location Height [mm]**	σ_1 **Anal.**	σ_1 **Num.**	$\mathbf{f}_{ctm,eff}$ **MC Anal.**	$\mathbf{f}_{ctm,eff}$ **MC Num.**	$\mathbf{f}_{ctm,eff}$ **HB Anal.**	$\mathbf{f}_{ctm,eff}$ **HB Num.**
1a	650	-115	4,03	3,37	3,80	3,80	3,03	3,03
1b	1780	115	5,07	1,23	3,96	4,01	3,12	3,16
2a	1290	65	-	3,49	-	3,59	-	2,91
2b	770	-115	-	3,64	-	3,73	-	2,99
3	1080	5	3,55	3,57	3,56	3,54	2,89	2,87
4a	1400	115	3,85	3,31	3,78	3,72	3,02	2,98
5a	1240	115	3,46	3,42	3,70	3,64	2,95	2,93
6a	1120	115	3,21	3,22	3,63	3,58	2,93	2,90
4b	760	-115	3,73	3,64	3,75	3,73	3,0	2,99
5b	920	-115	3,34	3,44	3,66	3,65	2,95	2,94
6b	1040	-115	3,09	3,15	3,60	3,59	2,91	2,90

* all stress parameters $\left[\frac{N}{mm^2}\right]$

Table 5.49: Stress and strength results CW13

Point	**Location Distance [mm]**	**Location Height [mm]**	$\frac{\sigma_{1,anal.}}{\mathbf{f}_{ctm}}$ [-]	$\frac{\sigma_{1,num.}}{\mathbf{f}_{ctm}}$ [-]	$\frac{\sigma_{1,anal.}}{\mathbf{f}_{ctm,eff,mc}}$ [-]	$\frac{\sigma_{1,num.}}{\mathbf{f}_{ctm,eff,mc}}$ [-]	$\frac{\sigma_{1,anal.}}{\mathbf{f}_{ctm,eff,hb}}$ [-]	$\frac{\sigma_{1,num.}}{\mathbf{f}_{ctm,eff,hb}}$ [-]
1a	650	-115	0,90	0,75	-	0,89	-	1,11
1b	1780	115	1,13	0,27	-	0,31	-	0,39
2a	1290	65	-	0,78	-	0,97	-	1,20
2b	770	-115	-	0,81	-	0,98	-	1,22
3	1080	5	0,79	0,79	1,00	1,01	1,23	1,24
4a	1400	115	0,85	0,74	1,02	0,89	1,27	1,11
5a	1240	115	0,77	0,76	0,94	0,94	1,17	1,17
6a	1120	115	0,71	0,72	0,88	0,90	1,09	1,11
4b	760	-115	0,83	0,81	0,99	0,97	1,24	1,22
5b	920	-115	0,74	0,76	0,91	0,94	1,13	1,17
6b	1040	-115	0,69	0,70	0,86	0,88	1,06	1,08

Table 5.50: Results model uncertainty of CW13

Point	**Location Distance [mm]**	**Location Height [mm]**	σ_1 **Anal.**	σ_1 **Num.**	$\mathbf{f}_{ctm,eff}$ **MC Anal.**	$\mathbf{f}_{ctm,eff}$ **MC Num.**	$\mathbf{f}_{ctm,eff}$ **HB Anal.**	$\mathbf{f}_{ctm,eff}$ **HB Num.**
1a	650	-115	4,06	3,40	3,81	3,81	3,01	3,0
1b	1780	115	5,08	1,24	3,96	4,02	3,10	3,13
2a	1290	65	-	3,51	-	3,60	-	2,89
2b	770	-115	-	3,66	-	3,74	-	2,97
3	1080	5	3,57	3,59	3,57	3,55	2,87	2,85
4a	1400	115	3,86	3,33	3,79	3,73	3,0	2,96
5a	1240	115	3,47	3,44	3,70	3,65	2,94	2,91
6a	1120	115	3,22	3,24	3,64	3,59	2,91	2,88
4b	760	-115	3,75	3,66	3,76	3,74	2,98	2,97
5b	920	-115	3,36	3,46	3,67	3,66	2,93	2,92
6b	1040	-115	3,11	3,17	3,61	3,60	2,89	2,89

* all stress parameters $\left[\frac{N}{mm^2}\right]$

Table 5.51: Stress and strength results CW14

Point	**Location Distance [mm]**	**Location Height [mm]**	$\frac{\sigma_{1,anal.}}{\mathbf{f}_{ctm}}$ **[-]**	$\frac{\sigma_{1,num.}}{\mathbf{f}_{ctm}}$ **[-]**	$\frac{\sigma_{1,anal.}}{\mathbf{f}_{ctm,eff,mc}}$ **[-]**	$\frac{\sigma_{1,num.}}{\mathbf{f}_{ctm,eff,mc}}$ **[-]**	$\frac{\sigma_{1,anal.}}{\mathbf{f}_{ctm,eff,hb}}$ **[-]**	$\frac{\sigma_{1,num.}}{\mathbf{f}_{ctm,eff,hb}}$ **[-]**
1a	650	-115	0,90	0,75	-	0,89	-	1,13
1b	1780	115	1,13	0,28	-	0,31	-	0,40
2a	1290	65	-	0,78	-	0,97	-	1,22
2b	770	-115	-	0,81	-	0,98	-	1,24
3	1080	5	0,79	0,80	1,00	1,01	1,24	1,26
4a	1400	115	0,86	0,74	1,02	0,89	1,29	1,12
5a	1240	115	0,77	0,76	0,94	0,94	1,18	1,18
6a	1120	115	0,72	0,72	0,88	0,90	1,11	1,12
4b	760	-115	0,83	0,81	1,0	0,98	1,26	1,23
5b	920	-115	0,75	0,77	0,92	0,94	1,15	1,18
6b	1040	-115	0,69	0,70	0,86	0,88	1,08	1,10

Table 5.52: Results model uncertainty of CW14

Point	**Location Distance [mm]**	**Location Height [mm]**	σ_1 **Anal.**	σ_1 **Num.**	$\mathbf{f}_{ctm,eff}$ **MC Anal.**	$\mathbf{f}_{ctm,eff}$ **MC Num.**	$\mathbf{f}_{ctm,eff}$ **HB Anal.**	$\mathbf{f}_{ctm,eff}$ **HB Num.**
1a	650	-115	3,43	2,93	3,84	3,84	3,07	3,07
1b	1780	115	4,94	1,48	4,02	4,10	3,18	3,23
2a	1320	115	-	3,31	-	3,82	-	3,06
2b	770	-115	-	3,12	-	3,78	-	3,04
3	1080	5	3,17	3,17	3,69	3,67	2,98	2,97
4a	1400	115	3,70	3,23	3,89	3,85	3,10	3,08
5a	1240	115	3,30	3,25	3,83	3,79	3,06	3,03
6a	1120	115	3,04	3,04	3,78	3,75	3,04	3,02
4b	760	-115	3,17	3,12	3,80	3,79	3,05	3,04
5b	920	-115	2,83	2,92	3,73	3,72	3,01	3,0
6b	1040	-115	2,62	2,67	3,68	3,67	2,97	2,97

* all stress parameters $\left[\frac{N}{mm^2}\right]$

Table 5.53: Stress and strength results CW15

Point	**Location Distance [mm]**	**Location Height [mm]**	$\frac{\sigma_{1,anal.}}{\mathbf{f}_{ctm}}$ [-]	$\frac{\sigma_{1,num.}}{\mathbf{f}_{ctm}}$ [-]	$\frac{\sigma_{1,anal.}}{\mathbf{f}_{ctm,eff,mc}}$ [-]	$\frac{\sigma_{1,num.}}{\mathbf{f}_{ctm,eff,mc}}$ [-]	$\frac{\sigma_{1,anal.}}{\mathbf{f}_{ctm,eff,hb}}$ [-]	$\frac{\sigma_{1,num.}}{\mathbf{f}_{ctm,eff,hb}}$ [-]
1a	650	-115	0,78	0,67	-	0,76	-	0,95
1b	1780	115	1,12	0,34	-	0,36	-	0,46
2a	1320	115	-	0,75	-	0,87	-	1,08
2b	770	-115	-	0,71	-	0,83	-	1,03
3	1080	5	0,72	0,72	0,86	0,87	1,06	1,07
4a	1400	115	0,84	0,73	0,95	0,84	1,19	1,05
5a	1240	115	0,75	0,74	0,86	0,86	1,08	1,07
6a	1120	115	0,69	0,69	0,80	0,81	1,00	1,01
4b	760	-115	0,72	0,71	0,83	0,83	1,04	1,03
5b	920	-115	0,64	0,66	0,76	0,79	0,94	0,97
6b	1040	-115	0,59	0,61	0,71	0,73	0,88	0,90

Table 5.54: Results model uncertainty of CW15

Point	**Location Distance [mm]**	**Location Height [mm]**	σ_1 **Anal.**	σ_1 **Num.**	$\mathbf{f}_{ctm,eff}$ **MC Anal.**	$\mathbf{f}_{ctm,eff}$ **MC Num.**	$\mathbf{f}_{ctm,eff}$ **HB Anal.**	$\mathbf{f}_{ctm,eff}$ **HB Num.**
1a	650	-115	4,00	3,35	3,81	3,80	3,02	3,02
1b	1780	115	5,0	1,21	3,96	4,0	3,11	3,14
2a	1300	65	-	3,44	-	3,60	-	2,90
2b	770	-115	-	3,62	-	3,74	-	2,98
3	1080	5	3,52	3,54	3,57	3,54	2,88	2,86
4a	1400	115	3,79	3,27	3,78	3,72	3,01	2,97
5a	1240	115	3,41	3,38	3,70	3,64	2,94	2,92
6a	1120	115	3,17	3,18	3,64	3,59	2,91	2,89
4b	760	-115	3,71	3,62	3,76	3,74	2,99	2,98
5b	920	-115	3,32	3,42	3,67	3,66	2,94	2,93
6b	1040	-115	3,08	3,13	3,61	3,60	2,90	2,90

* all stress parameters $\left[\frac{N}{mm^2}\right]$

Table 5.55: Stress and strength results CW16

Point	**Location Distance [mm]**	**Location Height [mm]**	$\frac{\sigma_{1,anal.}}{\mathbf{f}_{ctm}}$ [-]	$\frac{\sigma_{1,num.}}{\mathbf{f}_{ctm}}$ [-]	$\frac{\sigma_{1,anal.}}{\mathbf{f}_{ctm,eff,mc}}$ [-]	$\frac{\sigma_{1,num.}}{\mathbf{f}_{ctm,eff,mc}}$ [-]	$\frac{\sigma_{1,anal.}}{\mathbf{f}_{ctm,eff,hb}}$ [-]	$\frac{\sigma_{1,num.}}{\mathbf{f}_{ctm,eff,hb}}$ [-]
1a	650	-115	0,89	0,74	-	0,88	-	1,11
1b	1780	115	1,11	0,27	-	0,30	-	0,38
2a	1300	65	-	0,76	-	0,95	-	1,19
2b	770	-115	-	0,80	-	0,97	-	1,22
3	1080	5	0,78	0,79	0,99	1,00	1,22	1,24
4a	1400	115	0,84	0,73	1,00	0,88	1,26	1,10
5a	1240	115	0,76	0,75	0,92	0,93	1,16	1,16
6a	1120	115	0,70	0,71	0,87	0,89	1,09	1,10
4b	760	-115	0,82	0,80	0,99	0,97	1,24	1,21
5b	920	-115	0,74	0,76	0,90	0,93	1,13	1,16
6b	1040	-115	0,68	0,70	0,85	0,87	1,06	1,08

Table 5.56: Results model uncertainty of CW16

Point	**Location Distance [mm]**	**Location Height [mm]**	σ_1 **Anal.**	σ_1 **Num.**	$\mathbf{f}_{ctm,eff}$ **MC Anal.**	$\mathbf{f}_{ctm,eff}$ **MC Num.**	$\mathbf{f}_{ctm,eff}$ **HB Anal.**	$\mathbf{f}_{ctm,eff}$ **HB Num.**
1a	650	-115	4,04	3,38	3,77	3,77	3,06	3,06
1b	1780	115	5,07	1,24	3,93	3,99	3,16	3,19
2a	1290	65	-	3,50	-	3,56	-	2,93
2b	770	-115	-	3,65	-	3,69	-	3,01
3	1080	5	3,56	3,58	3,52	3,49	2,91	2,89
4a	1400	115	3,85	3,32	3,75	3,68	3,05	3,01
5a	1240	115	3,46	3,43	3,66	3,60	2,98	2,96
6a	1120	115	3,21	3,23	3,59	3,54	2,95	2,92
4b	760	-115	3,74	3,65	3,72	3,70	3,03	3,02
5b	920	-115	3,35	3,45	3,63	3,61	2,97	2,97
6b	1040	-115	3,10	3,16	3,56	3,55	2,93	2,93

* all stress parameters $\left[\frac{N}{mm^2}\right]$

Table 5.57: Stress and strength results CW17

Point	**Location Distance [mm]**	**Location Height [mm]**	$\frac{\sigma_{1,anal.}}{\mathbf{f}_{ctm}}$ [-]	$\frac{\sigma_{1,num.}}{\mathbf{f}_{ctm}}$ [-]	$\frac{\sigma_{1,anal.}}{\mathbf{f}_{ctm,eff,mc}}$ [-]	$\frac{\sigma_{1,num.}}{\mathbf{f}_{ctm,eff,mc}}$ [-]	$\frac{\sigma_{1,anal.}}{\mathbf{f}_{ctm,eff,hb}}$ [-]	$\frac{\sigma_{1,num.}}{\mathbf{f}_{ctm,eff,hb}}$ [-]
1a	650	-115	0,90	0,75	-	0,90	-	1,11
1b	1780	115	1,13	0,28	-	0,31	-	0,39
2a	1290	65	-	0,78	-	0,99	-	1,20
2b	770	-115	-	0,81	-	0,99	-	1,21
3	1080	5	0,79	0,80	1,01	1,03	1,22	1,24
4a	1400	115	0,85	0,74	1,03	0,90	1,26	1,10
5a	1240	115	0,77	0,76	0,94	0,95	1,16	1,16
6a	1120	115	0,71	0,72	0,89	0,91	1,09	1,10
4b	760	-115	0,83	0,81	1,0	0,99	1,24	1,21
5b	920	-115	0,74	0,77	0,92	0,95	1,13	1,16
6b	1040	-115	0,69	0,70	0,87	0,89	1,06	1,08

Table 5.58: Results model uncertainty of CW17

5.3. Results

In this section the results wil be discussed. As described in chapter 1, the results of the model uncertainties per model, per strength criterion of the Choulli and Elzanaty experiments will be combined, from which the mean and the variation coefficient are determined. The results are based on one important feature: the results are based on both the complete set of experiments and on the the set of experiments where no flexural cracks have been observed. In case of the set of experiments where no flexural cracks have been observed, also the experiments where the tensile stress in the ultimate fiber does not exceed the uniaxial tensile strength f_{ctm} are considered. In table 5.59 the mean results of the model uncertainties are given. In table 5.60 the variance of the model uncertainties. In table 5.61 the mean results of the model uncertainties of the experiments without flexural cracks are given. In table 5.62 the variance of the model uncertainties of the experiments without flexural cracks are given. As described in section 5.1.1, model 1 in table 5.59 and 5.60 represents the analytical model according to the Eurocode, model 2 represents the numerical model, model 3 represents the "midheight" model around the neutral axis, model 4,5 and 6 represents respectively the 45°, the 35°and the 30°model. Further 3 strength criterions will be considered: the uniaxial tensile strength f_{ctm}, the biaxial tensile strength according to "Mohr-Coulomb" and the biaxial tensile strength according to "Huber".

5.3.1. Consideration of complete set of Chouli and Elzanaty experiments

The analytical "midheight" model around the neutral axis shows the highest consistency according to table 5.60, this holds true when both the uniaxial and biaxial tensile strength are considered. Based on table 5.59 it can be seen that the resistance of the model is overestimated with 20%. Based on the fact that there is little difference in consistency between the model with uniaxial tensile strength and the model which accounts for biaxial tensile strength, it is preferable for practice to apply a reduced uniaxial tensile strength, the reduction factor in this case equals 0,8.

For model 1 in the tables the highest principal tensile stress σ_1 is taken of the area to be considered. Compared to the other models the model according to the Eurocode is consistent. However, in table 5.59 it can be seen that the stress distribution is overrated, this is caused by the fact that some of the considered points of model 1 are situated in the disturbed area. The value of the model uncertainty is determined on one hand by a too high stress distribution and on the other hand by an overrated tensile strength f_{ctm}. So the value looks favorable, but one should keep in mind the before described phenomena.

Also for model 2 the highest principal tensile stress σ_1 is taken of the area to be considered. In case the biaxial tensile strength of "Mohr-Coulomb" is taken into account this gives the most consistent variant, compared to the uniaxial tensile strength and the biaxial tensile strength according to "Huber". It can be seen that model 2 was not more consistent compared to the other models. Based on table 5.59 it can be seen that the resistance of the model is overestimated with 14%.

For model 4, 5 and 6 also the maximum principal tensile stress σ_1 is taken. Compared to the analytical "midheight" model these models are less consistent. It also can be seen from table 5.59 that the points of model 4 are situated in the disturbed area. The points of model 5 and 6 are not situated in the disturbed area. It can be seen that the stress distribution of the points 5 of model 5 equals the mean stress of point 3 of model 3. If biaxiality is taken into account it can be seen that the model uncertainty of both Mohr-Coulomb and Huber is slightly higher, this is caused by the fact that the principal compressive stress σ_2 is higher in model 3 compared to model 5.

The "midheight" model around the neutral axis offers the best consistency, according to table 5.60. Out of analysis it was found that the area around the point of model 3 contains stresses that more or less equals the stresses of the point of model 3, so it is not a single point peak stress, see also chapter 4. In chapter 5 a stress analysis of HAP1E and CW5 was made for the crack in the web. It appeared out of analysis that the stress initiated the crack could be located in the neutral axis, because of the fact that the principal stress σ_1 was highest there. For the experiments CW1, CW6, CW7, CW8, CW17 and HAP1W there was also made a stress analysis of the crack, see appendix "Choulli and Elzanaty: σ_1 over crack" of the appendix report. The present crack was the first crack. From CW3 and HAP2E it is known that the first crack was not situated exactly in the middle between the support and the external load.

Model	$\frac{\sigma_{1,anal.}}{\mathbf{f}_{ctm}}$ [-]	$\frac{\sigma_{1,num.}}{\mathbf{f}_{ctm}}$ [-]	$\frac{\sigma_{1,anal.}}{\mathbf{f}_{ctm,eff,mc}}$ [-]	$\frac{\sigma_{1,num.}}{\mathbf{f}_{ctm,eff,mc}}$ [-]	$\frac{\sigma_{1,anal.}}{\mathbf{f}_{ctm,eff,hb}}$ [-]	$\frac{\sigma_{1,num.}}{\mathbf{f}_{ctm,eff,hb}}$ [-]
1	1,18	0,73	-	0,85	-	1,10
2	-	0,86	-	1,01	-	1,31
3	0,81	0,81	0,98	0,99	1,26	1,27
4	0,91	0,85	1,05	0,99	1,37	1,29
5	0,82	0,82	0,96	0,97	1,25	1,26
6	0,77	0,76	0,91	0,91	1,18	1,18

* the results are based on the 12 Choulli and 17 Elzanaty experiments

Table 5.59: Mean results of the model uncertainties

Model	$\frac{\sigma_{1,anal.}}{\mathbf{f}_{ctm}}$ [-]	$\frac{\sigma_{1,num.}}{\mathbf{f}_{ctm}}$ [-]	$\frac{\sigma_{1,anal.}}{\mathbf{f}_{ctm,eff,mc}}$ [-]	$\frac{\sigma_{1,num.}}{\mathbf{f}_{ctm,eff,mc}}$ [-]	$\frac{\sigma_{1,anal.}}{\mathbf{f}_{ctm,eff,hb}}$ [-]	$\frac{\sigma_{1,num.}}{\mathbf{f}_{ctm,eff,hb}}$ [-]
1	0,16	0,10	-	0,12	-	0,13
2	-	0,16	-	0,15	-	0,19
3	0,12	0,12	0,13	0,13	0,15	0,15
4	0,16	0,17	0,14	0,16	0,18	0,19
5	0,16	0,16	0,14	0,15	0,18	0,18
6	0,16	0,16	0,14	0,14	0,18	0,18

* the results are based on the 12 Choulli and 17 Elzanaty experiments

Table 5.60: Variation coefficients of the mean model uncertainties

Model	$\frac{\sigma_{1,anal.}}{\mathbf{f}_{ctm}}$ [-]	$\frac{\sigma_{1,num.}}{\mathbf{f}_{ctm}}$ [-]	$\frac{\sigma_{1,anal.}}{\mathbf{f}_{ctm,eff,mc}}$ [-]	$\frac{\sigma_{1,num.}}{\mathbf{f}_{ctm,eff,mc}}$ [-]	$\frac{\sigma_{1,anal.}}{\mathbf{f}_{ctm,eff,hb}}$ [-]	$\frac{\sigma_{1,num.}}{\mathbf{f}_{ctm,eff,hb}}$ [-]
1	1,09	0,74	-	0,87	-	1,10
2	-	0,81	-	0,98	-	1,23
3	0,79	0,79	0,99	1,0	1,23	1,24
4	0,85	0,79	1,0	0,96	1,27	1,20
5	0,76	0,76	0,92	0,93	1,16	1,16
6	0,71	0,71	0,88	0,88	1,09	1,09

* the results are based on 3 Choulli and 11 Elzanaty experiments, the results of HCP2TW, HAP2E, HAP2W, HAP1TW, HAP2TE, HAP2TW, HCP1TE, HCP1TW, HCP2TE, CW3, CW6, CW7, CW10, CW11 and CW15 are left out

Table 5.61: Mean results of the model uncertainties, without flexural cracked experiments

Model	$\frac{\sigma_{1,anal.}}{\mathbf{f}_{ctm}}$ [-]	$\frac{\sigma_{1,num.}}{\mathbf{f}_{ctm}}$ [-]	$\frac{\sigma_{1,anal.}}{\mathbf{f}_{ctm,eff,mc}}$ [-]	$\frac{\sigma_{1,num.}}{\mathbf{f}_{ctm,eff,mc}}$ [-]	$\frac{\sigma_{1,anal.}}{\mathbf{f}_{ctm,eff,hb}}$ [-]	$\frac{\sigma_{1,num.}}{\mathbf{f}_{ctm,eff,hb}}$ [-]
1	0,06	0,06	-	0,08	-	0,10
2	-	0,05	-	0,05	-	0,11
3	0,06	0,06	0,08	0,07	0,10	0,11
4	0,04	0,06	0,05	0,07	0,10	0,10
5	0,04	0,04	0,05	0,06	0,09	0,10
6	0,04	0,04	0,05	0,05	0,10	0,09

* the results are based on 3 Choulli and 11 Elzanaty experiments, the results of HCP2TW, HAP2E, HAP2W, HAP1TW, HAP2TE, HAP2TW, HCP1TE, HCP1TW, HCP2TE, CW3, CW6, CW7, CW10, CW11 and CW15 are left out

Table 5.62: Variation coefficients of the mean model uncertainties, without flexural cracked experiments

5.3.2. Consideration of Chouli and Elzanaty experiments without flexural cracks

In case only the experiments without flexural cracks and without exceeding of the uniaxial tensile strength $f_{ctm,fl}$ in the ultimate fiber are taken into account, then clear differences can be noticed. In table 5.63 an overview of all experiments of Choulli and Elzanaty. In the column "Flexural cracks observed" is indicated whether there are observed flexural cracks before the first shear crack was observed, this is based on the reports of Choulli[8] and Elzanaty[9], see also section 3.1.2 and 3.2.2. In the column "Analytical σ_x" the σ_x in the ultimate fiber according to the analytical stress distribution. In the column "Numerical σ_x" the σ_x in the ultimate fiber according to the numerical stress distribution. The σ_x of the Choulli experiments is considered under the external load and the σ_x of the Elzanaty experiments is considered in the middle of the beam. Despite the fact that σ_x of the Choulli beams is located in the disturbed area, the greatest value is present here. The σ_x of the Elzanaty beams is not located in the disturbed area, nevertheless there is a difference in the magnitude of σ_x in case both the analytical and numerical stress distribution is considered, this is also noted in section 4.2.1. In addition to the observations of bending cracks, also the experiments at which the $\frac{Analytical\sigma_x}{f_{ctm,fl}} > 1{,}0$ are left out. Based on this HCP2TW, HAP2E, HAP2W, HAP1TW, HAP2TE, HAP2TW, HCP1TE, HCP1TW, HCP2TE, CW3, CW6, CW7, CW10, CW11 and CW15 are left out. From tables 5.59 and 5.61 it can be seen that the "means" of the models are lower. From tables 5.60 and 5.62 it can be seen that the models without experiments accounting for flexural cracks and without exceeding of the uniaxial tensile strength f_{ctm} in the ultimate fiber are more consistent. From table 5.61 it can be seen that in case the experiments with flexural cracks are left out that both the uniaxial tensile strength f_{ctm} and the tensile strength according to Mohr-Coulomb are overestimated.

Experiment	**Flexural cracks observed**	**Analytical** σ_x	**Numerical** σ_x	$\mathbf{f}_{ctm,fl}$	**Analytical** $\frac{\sigma_x}{\mathbf{f}_{ctm,fl}}$ [-]
CW1		0,55	0,06	5,267	0,10
CW2		4,6	3,05	5,267	0,87
CW3		11,99	6,08	5,267	2,28
CW4		4,13	2,54	5,29	0,78
CW5		3,74	1,86	5,29	0,71
CW6	x	7,34	5,53	5,30	1,38
CW7		6,33	5,17	5,29	1,20
CW8		2,12	0,61	3,83	0,55
CW9		4,73	3,07	4,83	0,98
CW10		7,53	5,76	5,29	1,42
CW11		4,92	3,38	4,6	1,07
CW12		2,49	1,09	3,80	0,66
CW13		3,92	2,25	5,18	0,76
CW14		3,88	2,23	5,18	0,75
CW15		5,87	4,87	5,06	1,16
CW16		3,7	2,05	5,18	0,71
CW17		3,87	2,25	5,06	0,76
HAP1E		2,34	0,52	5,06	0,46
HAP1TE		1,88	0,1	4,9	0,38
HAP1TW	x	2,76	0,46	4,9	0,56
HAP1W		1,58	-0,12	5,06	0,31
HAP2E		6,23	4,51	5	1,25
HAP2TE	x	7,22	5,87	5	1,44
HAP2TW	x	7,06	5,83	5	1,41
HAP2W		6,51	5,34	5	1,30
HCP1TE	x	6,47	5,14	4,7	1,38
HCP1TW	x	2,04	0,35	4,7	0,43
HCP2TE	x	13,1	11,49	4,9	2,67
HCP2TW		8,95	7,62	4,9	1,83

[1] all stress parameters $\left[\frac{N}{mm^2}\right]$

[2] the tensile stresses in the ultimate fiber of the Choulli experiments are located near the external load

[3] the tensile stresses in the ultimate fiber of the Elzanaty experiments are located in the middle of the beam

[4] based on the table the experiments HCP2TW, HAP2E, HAP2W, HAP1TW, HAP2TE, HAP2TW, HCP1TE, HCP1TW, HCP2TE, CW3, CW6, CW7, CW10, CW11 and CW15 are left out

Table 5.63: Overview of the observed flexural cracks and tensile stresses in the ultimate fiber

For model 3 the biaxial behavior is considered graphically in figure 5.8, this figure is based on the data of table 5.64. The blue points and the blue linear line from figure 5.8 represent the Moh-Coulomb strength criterion, this is the part of the strength criterion model in the compression/tension quadrant. The blue points are the graphical respresentation of the data in colomn "$\frac{\sigma_{2,anal.}}{f_{cm}}$" and the calculated $\frac{\sigma_{1,anal.}}{f_{ctm}}$ using the formula of the Mohr-Coulomb strength criterion, formula 5.1. The orange points from figure 5.8 represent the data of columns "$\frac{\sigma_{1,anal.}}{f_{ctm}}$" and "$\frac{\sigma_{2,anal.}}{f_{cm}}$". The orange linear line represent the trend line of the orange points. The formula of this trend line can be seen as a formula of a hypothetical model for -0,25 < $\frac{\sigma_2}{f_{cm}}$ < -0,125, after all, there were for example no experiments where $\frac{\sigma_2}{f_{cm}}$ was around -0,80. Because the experiments all have a $\frac{\sigma_2}{f_{cm}}$ around -0.20, it is not possible to speak of a possible strength criterion. The mean result of colomn "$\frac{\sigma_{1,anal.}}{f_{ctm,eff,mc}}$" is 0,98 and the variation coefficient is 0,08, which corresponds to the values of the tables 5.61 and 5.62. In case the hypothetical model is used, colomn "$\frac{\sigma_{1,anal.}}{f_{ctm,eff,model}}$", the mean result is 1,0 and the variation coefficient is 0,06.

Experiment	$\frac{\sigma_{1,anal.}}{\mathbf{f}_{ctm}}$ [-]	$\frac{\sigma_{2,anal.}}{\mathbf{f}_{cm}}$ [-]	$\frac{\sigma_{1,anal.}}{\mathbf{f}_{ctm,eff,model}}$ [-]	$\frac{\sigma_{1,anal.}}{\mathbf{f}_{ctm,eff,mc}}$ [-]
CW1	0,94	-0,20	1,20	1,18
CW2	0,80	-0,19	1,03	0,99
CW4	0,81	-0,20	1,04	1,01
CW5	0,78	-0,19	1,0	0,97
CW8	0,77	-0,27	0,96	1,06
CW9	0,74	-0,19	0,95	0,92
CW12	0,75	-0,27	0,94	0,92
CW13	0,79	-0,21	1,01	1,0
CW14	0,79	-0,21	1,01	1,0
CW16	0,78	-0,21	1,0	0,98
CW17	0,79	-0,22	1,01	1,01
HAP1E	0,79	-0,14	1,03	0,91
HAP1TE	0,78	-0,15	1,01	0,91
HAP1W	0,75	-0,13	0,98	0,87

Table 5.64: Biaxial behavior of model 3, without experiments with flexural cracks

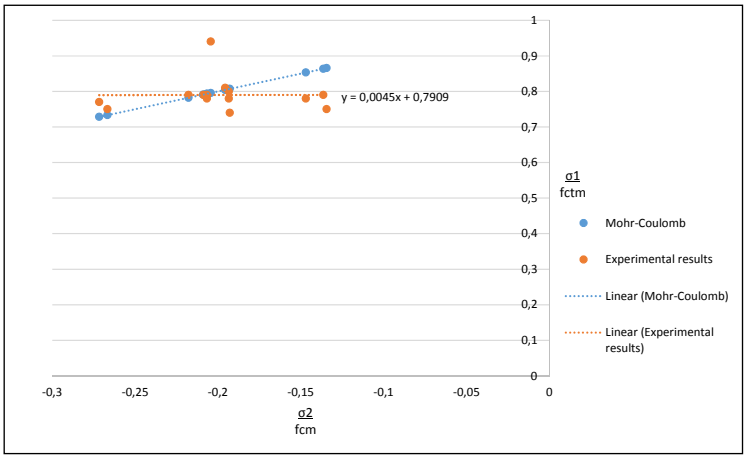

Figure 5.8: Biaxial behavior of model 3, without experiments with flexural cracks

6

Conclusions

In this chapter the conclusions will be discussed regarding the experimentally found shear tension behavior of prestressed concrete beams. The central main question was: “What model determines the resistance with respect to the formation of shear tension cracks most accurate?” In order to answer this question in total 29 experimentally tested prestressed concrete beams, by researchers Choulli[8] and Elzanaty[9], were evaluated. The loads in these experiments were exclusively concentrated loads. The experiments were both modeled analytically and numerically. As described there were considered 6 models and 3 strength criterions.

- From the analysis of the results in chapter 4 it was found that the analyical stress distribution did not equal the numerical stress distribution. This was the case in the described “disturbed” areas. These areas are located near the concentrated loads, so around supports and external concentrated loads. After evaluation of the results it was found that the analytical stress distribution concerning the principal tensile stress σ_1 was too high. The stress distribution is overestimated. It was found that the components σ_y and τ_{xy} are mainly the cause of the disruption. Further, it was found that the Poisson’s ratio had a low neglectable influence.

- From tables 5.60 and 5.62 it can be seen that there is a significant effect on the consistency of the models in case only the experiments without flexural cracks are considered. It can be seen that in case the experiments that show flexural cracks are left out the models are more accurate. From tables 5.59 and 5.61 it can be seen that the mean model uncertanties are lower, in case the experiments that show flexural cracks are left out. It can be seen that the reduction in model 3 is the least. It appears that the tension cracks have more influence on the stress distribution at locations outside the neutral axis, closer to the middle of the beam.

- The analytical model 3, the “midheight” model around the neutral axis, shows the highest consistency based on the consideration of the complete set of experiments, this holds true when both the uniaxial and biaxial tensile strength are considered. This model is proposed as the analytical model. The proposal about the strength criterion is to apply 80% of the uniaxial strength f_{ctm} to predict diagonal tension cracking. This is only valid for concentrated loads.

- For model 1, the “Eurocode” model, the highest principal tensile stress σ_1 is taken in the area to be considered. Compared to the other models the model according to the Eurocode is consistent. However, it was found that the principal tensile stress is located in the “disturbed” area. The analytical stress distribution is overestimated in these parts of the prestressed beams. Further, it was found that the uniaxial tensile strength f_{ctm} is overestimated. It is not recommended to use the Eurocode model, because it gives conservative results. This is only valid for concentrated loads. The Eurocode model is suitable for new constructions, but less suitable for existing buildings.

- For model 2, the “LE-FEA” model, also the highest principal tensile stress σ_1 is taken in the area to be considered. It was found that model 2 was not more consistent compared to the other models, for example to model 3. In case only the experiments without flexural cracks are considered, it was found that the model was much more consistent, even slightly more then model 3. This means that the presence of flexural cracks can be of important influence.

- There were considered three strength criterions, the uniaxial tensile strength f_{ctm}, the biaxial tensile strength according to Mohr-Coulomb and the biaxial tensile strength according to Huber. It was found that both the biaxial tensile strength according to Mohr-Coulomb and the biaxial tensile strength according to Huber does not contribute significantly to the accuracy of the models, so there was not found a significant higher consistency. It was found that, in case the complete set of experiments is considered, the uniaxial tensilde strength f_{ctm} is overestimated and the biaxial tensile strength according to Mohr-Coulomb is reasonable well estimated and the biaxial strengh criterion according to Huber is underestimated. In case the set of experiments without flexural cracks is considered, both the uniaxial tensilde strength f_{ctm} and the biaxial tensile strength criterion according to Mohr-Coulomb is overestimated and the biaxial strengh criterion according to Huber is underestimated.

For future research it is recommended to investigate the influence of present flexural cracks on the stress distribution, what will be the influence on the way of predicting diagonal tension cracking. From the results in this study it can be seen that the presence of flexural cracks can have significant influence on the consistency of the models. Further, it is also important for future research to consider distributed loads in addition to concentrated loads, because in practice there will be always present a significant distributed load. Finally, in the case of the strength criterion, it is also essential to consider experiments with a varying $\frac{\sigma_2}{f_{cm}}$.

Bibliography

[1] Hoeveel bruggen beheert rijkswaterstaat. URL `https://www.rijkswaterstaat.nl/wegen/wegbeheer/bruggen/veelgestelde-vragen.aspx`.

[2] Onderzoek borging constructieve veiligheid bruggen en viaducten. Technical report, Ministerie van Volkshuisvesting, Ruimtelijke Ordening en Milieubeheer, 2009.

[3] Proefelementen TU Delft 1601740. Technical report, Spanbeton, 2016.

[4] P. D. Arthur. The shear strength of pre-tensioned i beams with unreinforced webs. *Magazine of Concrete Research*, 17(53):199–210, 1965.

[5] D. E. Beskos. Fracture of plain concrete under biaxial stresses. *Cement and concrete research*, 4(1):979–985, 1974.

[6] J. Blaauwendraad. *Plate analyses, theory and application.* TU Delft, Delft, The Netherlands, 2006.

[7] C. R. Braam and P. Lagendijk. *Constructieleer Gewapend Beton.* Aeneas, Boxtel, The Netherlands, 2011.

[8] Y. Choulli. *Shear behavior of prestressed I-beams made with High-Strength self compacting concrete.* PhD thesis, Universitat Politecnica De Catalunya, 2005.

[9] A. Elzanaty. *Shear critical High-strength.* PhD thesis, Cornell University, 1985.

[10] A. Elzanaty, A. Nilson, and F. Slate. Shear capacity of prestressed concrete beams using high-strength concrete. *ACI journal*, (83):359–368, 1986.

[11] A. Ghali, A. M. Neville, and T. G. Brown. *Structural Analyses.* Spon Press, Abingdon, UK, 2003.

[12] C. Hartsuijker. *Mechanica: Spanningen, vervormingen en verplaatsingen.* Boom uitgevers Amsterdam, Amsterdam, The Netherlands, 2000.

[13] C. Hartsuijker and J. W. Welleman. *Spanningsleer en Bezwijkmodellen.* TU Delft, Delft, The Netherlands, 2013.

[14] R. C. Hibbeler. *Statica.* Pearson Benelux, Amsterdam, The Netherlands, 2010.

[15] R. C. Hibbeler. *Sterkteleer.* Pearson Benelux, Amsterdam, The Netherlands, 2013.

[16] P. Huber, B. Kromoser, T. Huber, and J. Kolleger. Berechnungsansatz zur ermittlung der schubtragfahigkeit bestehender spannbetonbruckentrager mit geringem querkraftbewehrungsgrad. *Bauingenieur*, 6(1):36–47, 2016.

[17] B. S. Institution. *Eurocode 2: Design of Concrete Structures: Part 1-1: General Rules and Rules for Buildings.* 2004.

[18] B. Jena and F. N. Pannell. The diagonal cracking strength of continuous prestressed concrete beams. *Magazine of concrete research*, 24(78):3–14, 1972.

[19] H. Kupfer, H. Hilsdorf, and H. Rush. Behavior of concrete under biaxial stresses. *ACI Journal*, 66(52): 656–666, 1969.

[20] S. K. Lee, Y. C. Song, and S. H. Han. Biaxial behavior of plain concrete of nuclear containment building. *Nuclear Engineering and Design*, 227(1):143–153, 2004.

[21] L. J. M. Nelissen. Biaxial testing of normal concrete. *Heron*, 18(1):3–29, 1972.

[22] A. Simone. *An introduction to the analyses of slender structures.* TU Delft, Delft, The Netherlands, 2007.

[23] J. C. Walraven. Background document for prenv 1992-1-1:2002. 2002.

[24] J. C. Walraven and C. R. Braam. *Prestressed concrete.* TU Delft, Delft, The Netherlands, 2015.